The In Situ Generation of Liquid Crystalline Polymer

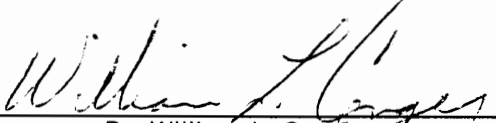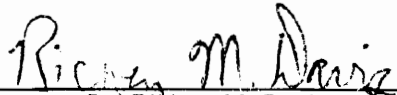**Reinforcements in Thermoplastics**
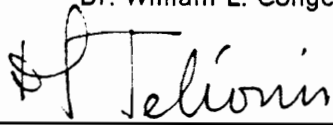
by

Ashish Mahendra Sukhadia

Dissertation submitted to the Faculty of the

Virginia Polytechnic Institute and State University

in partial fulfillment of the requirements for the degree of

Doctor of Philosophy

in

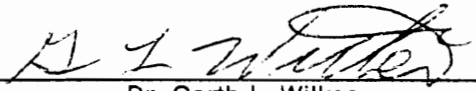Department of Chemical Engineering

APPROVED:

_____
. Dr. Donald G. Baird

_____   _____
Dr. William L. Conger   Dr. Richey M. Davis

_____   _____
Dr. Demetrios P. Telionis   Dr. Garth L. Wilkes

April 4, 1991

Blacksburg, Virginia

The In Situ Generation of Liquid Crystalline Polymer

Reinforcements in Thermoplastics

by

Ashish Mahendra Sukhadia

Dr. Donald G. Baird. Chairman

Department of Chemical Engineering

(ABSTRACT)

The overall objective of this work was to enhance the mechanical properties of thermoplastics by blending with liquid crystalline polymers (LCPs). Injection molding and sheet extrusion studies of blends of poly(ethylene terephthalate) (PET) with several LCPs were conducted with an emphasis on blends containing 50 wt % or less of the LCP. It was seen that significant enhancements (50-350%) in the tensile and flex moduli of PET were achieved by blending with 0-50 wt % LCPs via injection molding. The level of property enhancements was lower in the case of-sheet extrusion due largely to processing limitations which made it difficult to obtain high draw ratios.

Since thermotropic LCPs typically have high melting temperatures it is difficult to blend several thermoplastics such as polypropylene (PP) with these LCPs in the same extruder or molding unit. Thus a blending method (hereon referred to as the dual-extruder mixing method) was developed to overcome this limitation. In this method, the matrix and LCP polymers were plasticated in two separate extruders, subsequently mixed downstream in a static mixer (Kenics) and the melt blend than passed through an appropriate capillary or sheet die to generate strands or sheets, respectively. Using this method, blends of PET and PP with several LCPs were extruded into strands and sheets. In some cases, for example PP and Vectra A900 (LCP), the difference in their normal processing temperatures was in excess of 100°C.

Strands of PET/Vectra A900 70/30 composition ratio were observed to have higher moduli than a blend of the same composition extruded using a single extruder at all the draw ratios tested. This was determined to be due to the different LCP fibrillar morphology in the two

cases. In the case of the dual-extruder mixing method, the LCP fibrils were continuous, running the length of the extrudate, and further devoid of any skin-core structure. In contrast, the single-screw extruder blend had a distinct skin-core fibril-droplet type of structure and the LCP fibrils were not continuous. On the basis of other independent experiments, it was confirmed that the LCP fibrils in the dual-extruder mixing method were generated in the static mixer itself whereas the LCP fibrils in the case of single-screw extrusion were generated in the converging section of the die and/or by drawing at the die exit. This difference in the mode of LCP fibril generation in the two cases was attributed to the distributive mixing mechanism of the static mixer compared to the dispersive mixing in the extruder. Strands of PP/LCP and PET/LCP had significantly enhanced tensile moduli compared to the corresponding matrix tensile modulus. Enhancements of 10-20 times that of the pure matrix were achieved when blends containing about 20-30 wt % of the LCP were extruded from the dual-extruder mixing method. The tensile moduli of sheets of PET/LCP and PP/LCP blends were not much higher than that of the corresponding matrix polymer and this was attributed to the low molecular orientation achieved in the sheets due to low draw ratios. The tensile strengths of the majority of the blends were not enhanced to any appreciable degree and poor wetting and adhesion between the thermoplastic-LCP polymers was believed to be the cause.

Comparison of some of the mechanical properties (tensile modulus, tensile strength, flexural modulus) of the thermoplastic/LCP blends generated in this study with data from the literature on thermoplastic/inorganic filler composites showed that when compared on the basis of equal wt % of the reinforcement in the blend, the LCP composites can yield mechanical properties which are in the same range as those obtained using inorganic fillers.

to my family

Acknowledgements

The author wishes to express his sincere appreciation to Professor Donald G. Baird for all his help in providing guidance, suggestions and criticisms necessary to complete this work. Many thanks are also due to Prof. Baird for his (hidden) love, understanding and respect that the author had the benefit of during his tenure. The author believes most sincerely that he could not have got any better preparation and training for starting his career as he has working with Prof. Baird. The author also wishes to thank Professor Garth L. Wilkes for the use of his laboratory facilities which was crucial for much of the characterization studies required during the course of this work. Thanks are also due him for his assistance in explaining and interpreting some of the morphology and x-ray scattering data. In addition, thanks go to Professors Conger, Davis and Telionis for serving on the advisory committee.

The author would also like to thank the following:

- Dr. Arindam Datta for his help in the processing and characterization of most of the PP/LCP studies conducted here and also for the frequent suggestions, comments and discussions that always helped. Arindam has been a good friend of the author for the duration of his stay in Blacksburg and thanks are due to him also for all those wonderful parties that provided a break from the otherwise monotonous life of a graduate student.

- Dr. Ravi Ramanathan for helping the author settle down at VPI&SU during the author's initial months here and also for his guidance in "how not to upset Dr. Baird".

- Dr. Tong Sun, who it was a privilege to work with and who was always there to discuss all those "chemistry things" that were often beyond the grasp of the author.

- Paulo DSouza for all his help with the injection-molding and for that memorable trip to Virginia Beach with his family.

- Soon-to-be Dr. Tom Wilson for keeping the computers and darkroom in the laboratory "grinding" all the year round and for his friendship and sense of humor which always helped bring laughter in the laboratory.

- Soon-to-be Dr. Carl Reed for teaching the author a lot about machines and how they work and how they don't and how to fix them when they don't and for his willing company at Pizza Hut.

- All the members of Dr. Baird's research group, past and present, and in particular Randy, Jo Ellen, Margarita, Sudhir, Demetrios, John, Thanh, Alice and Beth for their help.

- Soon-to-be Dr. Joan Mullerleille for being a very good friend and an even better listener and for her help with the SEM.

- Soon-to-be Dr. David Rodrigues for his help with the WAXS, his weird sense of humor and for being a good roommate for several years.

- All the other members of Dr. Wilke's research group, past and present, and in particular to Leo, Don Brandon and Don Loveday.

- Billy Williams for providing much assistance with the machine shop.

- Wendall Brown for his help, expediency and consultations in constructing the dual-extruder blending apparatus.

- All the chemical engineering department personnel including Carol, Diane, Diane C., Sue and Sandy for their help throughout.

- Sangeeta, the author's lovely wife who was unfortunate enough to marry the author in his final year and who sacrificed all of her time in helping the author graduate. The author would like to say a very special thank-you to his wife for her tremendous love, patience

and understanding. This work would indeed have been much more difficult to finish were

it not for her presence.

- Army Research Office for providing financial support for the duration of this work.

- Anyone else whom the author may have inadvertently forgotten to mention, with apolo-

gies.

Original Contributions

The author considers the following as his original contribution:

The design and development of a blending method, hereon referred to as the dual-extruder mixing method, for blending of thermoplastic-LCP polymer pairs which do not have an overlap in their normal processing temperature regimes.

Table of Contents

List of Illustrations

List of Tables

1.0   Introduction

In view of the fact that the development and commercialization of wholly new polymeric materials to meet specific applications is often a costly and time consuming process, the concept of tailoring a polymers' properties through blending has long been recognized as a viable alternative. Consequently, the concept of composites, multilayer extrusion, lamination etc., which combine the advantages of two or more materials to achieve specific properties, has received considerable attention in recent years. In particular, fiber-reinforced polymer composites offer substantial improvement of the engineering performance of various polymers and have found tremendous application in aircraft, automotive and marine industries (1).

Until recently, composites usually referred to the fiber- reinforcement of thermoset matrices with inorganic fillers such as glass, graphite, or polyaramide fibers. However, more recently the term has also been used more loosely to define blends of two polymers in which some kind of reinforcing effect is present. Thus throughout this manuscript the terms composites and blends will be used interchangeably.

Both thermosetting and thermoplastic composites exhibit some disadvantages. For example, thermoset matrices suffer from several disadvantages such as long processing times, moisture sensitivity and brittleness. Further, they are non-recyclable. On the other hand, thermoplastic matrices reinforced with inorganic fillers leads to some processing problems

(2). The addition of these fibers to a polymer melt results in a substantial increase in viscosity, which makes processing more difficult and energy intensive. Additional problems include wear on the processing equipment due to abrasion and difficulties in compounding. For these and other reasons, it would be highly desirable to find an approach in which the reinforcing species is not actually present before the processing of the resin, but comes *into existence during* the processing. The in situ formation of the reinforcing species has led to the term in situ composite to describe materials of this type.

In order to accomplish the aforementioned goal of generating polymeric composites in situ, researchers have worked with a variety of systems in the last few years (3,4,5,6,7). In these studies, the reinforcing species is a special kind of thermoplastic - a thermotropic liquid crystalline polymer (LCP). Thermotropic LCPs (TLCPs) are long-chain organic molecules, usually fully aromatic polyesters, that possess sufficient chain stiffness to give extremely high stiffness and strength, and yet are flexible enough to melt. These materials exhibit more than a single transition in passing from the solid to the liquid state. Thus there exist one or more intermediate phases with molecular ordering, known as "mesophases", between that of a solid and that of an isotropic fluid (69). In these mesophases, the molecules show some degree of rotational order (and sometimes partial translational order also) even though the crystal lattice has been destroyed. It is a lack of this lattice structure that gives the mesophases or liquid crystals their fluidity and yet they are ordered fluid phases. It is this combination of liquid-like (fluidity) and solid-like (molecular order) character in a single phase that makes liquid crystals unique and gives rise to a host of interesting properties. More will be said about some specific LCPs and in particular about their rheological and mechanical properties in a later section.

Interest in liquid crystalline polymers has grown in recent years primarily due to their inherent stiffness and strength, high use temperatures and low melt viscosity (4). Despite an extensive flurry of research and development activities, however, established commercial markets of LCPs are relatively few. The high cost of the monomer has resulted in LCPs being much more expensive than "conventional" thermoplastics. As a consequence of this high cost

of LCPs, blending of LCPs with engineering thermoplastics offers the possibility for developing new materials with desirable properties, but at a reduced cost. In fact, one of the primary areas of research involving LCPs today is in the generation of in situ reinforced composites. The properties of such reinforced blends are similar to that of conventional short-fiber reinforced composites (2).

A fair amount of work has been done on the formation of in situ composites to date. The works thus far have been successful in establishing that certain features of these systems e.g., reduction in viscosity of the blend upon addition of LCP, enhancement in mechanical properties in the machine direction etc. are apparently common to most LCP/thermoplastic blends investigated. These will be treated in more detail later. Much of the work done in that respect has been almost repetitive without bringing forth any substantially new information. Consequently, there are still many problems and unanswered questions regarding the development of these complex systems. One of the biggest drawbacks of TLCPs is that they have high melting temperatures. This results in rather high processing temperatures, which are often near or above the thermal degradation temperatures of common thermoplastics. Also, the presence of an LCP dispersed phase frequently results in a low viscosity of the blend at processing temperatures. This in turn leads to low melt strengths, making processing difficult and any post-extrusion drawing nearly impossible for some LCP blend systems. Drawing, as will be shown later, is essential to imparting molecular orientation in the polymer and thus the inability to draw poses a major problem in obtaining high strength composites.

A lack of sufficient data in the literature, on some aspects of the formation of in situ composites, has added to the above processing complications. For example (and as will be further elucidated in the literature review), given a particular system of a thermoplastic matrix polymer and a reinforcing LCP, it is not yet well understood under what conditions the thermotropic LCPs will form a reinforcing phase. In particular, knowledge of the processing conditions by which specific fibrillation of the LCP phase can be achieved is still quite limited. Furthermore, an understanding of which factors and to what extent they influence the formation of a truly reinforced composite is still quite obscure. The effects, if any, of the "miscibility"

and interfacial surface tension of the two phases in determining the morphology and end properties of the composite system are little known at this time. A high degree of orientation of the LCP phase is imperative to the formation of high strength composites. However, even if good orientation of the LCP phase in the matrix is obtained, the question still remains as to what level of optimization of properties is possible with a given system and what has actually been attained. A better understanding of the deformation of polymer droplets, suspended in another polymer melt, is indeed of fundamental importance. Properties of polymer blends depend to a large extent on the size, shape and the degree of dispersion (i.e., morphology) obtained by different polymer processing operations. This complex interconnection between processing conditions, morphology and change in the blend (or composite) properties, remains a matter of empirical importance.

One other comment that needs to be made is the fact that all of the work on blends of in situ composites and blends reported in the literature to date have been limited to systems in which the two components have some degree of overlap of their processing temperature range. The fact that many of the LCPs of interest have quite high melting temperatures, has seriously inhibited the number of thermoplastics that can be successfully blended with LCPs.

With the above in mind, the main objectives of this research are briefly outlined as follows. An extensive discussion of the research objectives is deferred till after the literature review. The principal objectives of this work are: to design and develop a new processing or mixing method which will allow the blending of higher melting LCPs with commodity or engineering thermoplastics whose nominal processing temperatures are much lower than those of the LCP; to establish the rheological properties of the polymer melts and the design parameters (number of mixing elements, residence time, etc.) necessary to predict a priori the feasibility of blending a given polymer pair; to determine the differences, if any, in the morphology and mechanical properties of blends extruded via the mixing method described below and from single-screw extrusion; and to determine if the blends processed by the mixing method may be further processed by injection molding, solid phase forming and thermoforming without a loss in their mechanical properties.

A general description of the proposed mixing method is as follows. The process involves the extrusion of the two components in two separate extruders. The melts will then be brought together and mixed in a motionless (static) mixer and the melt blend then passed through either a flat sheet die or a capillary die to produce flat films or rods, respectively. Some prerequisites implicitly involved in this design are a thorough knowledge of the melt rheology of the two components and an analysis of the governing heat transfer processes. Much of the rheological data will be generated as part of this study. Two matrix materials will be used in this study, poly(ethylene terephthalate) (PET) and polypropylene (PP). Several different LCPs will be used to varying degrees in this study. A wholly aromatic copolyester of p-hydroxybenzoic acid (PHB or HBA) and hydroxynaphthoic (HNA) in the molar ratio of 73/27 HBA/HNA, commercially known as VECTRA A900 and marketed by Hoechst-Celanese is one of the main LCPs that will be used. Further, two copolyesters of PET and hydroxybenzoic acid (HBA or PHB) in the composition ratios of 40/60 mole % and 20/80 mole % will also be used extensively.

As was mentioned earlier, the biggest motivation in making in situ composites is to produce high strength materials. Thus the measurement of the mechanical properties of both the flat films and rods will form an integral part of this study. Of particular interest are the tensile strengths and the shear and tensile moduli of the films and rods. Also, the correlation of processing variables with orientation, morphology and properties in each case will be undertaken.

As will be shown later, both LCPs and their blends tend to have good mechanical properties in the machine direction but poor properties in the transverse direction. This limitation might be overcome if the as extruded sheets are treated as prepregs so that a number of sheets may be consolidated together to form a 'composite' whose properties are strong in all directions. Having an in situ composite whose matrix has a lower melting temperature than the reinforcement should offer a special advantage in such a process. Consequently, the potential of the unidirectionally reinforced as extruded sheets to form composites by consolidation of several sheets under pressure will be tested. Mechanical properties as well as

morphological studies will also be carried out. One other process that can take advantage of the special feature of these in situ composites is thermoforming. Further processing of the as extruded films would appear to be possible without significant loss of orientation and structure of the reinforcement (LCP phase). Thus thermoforming studies on the extruded films will also be carried out to test the validity of this conjecture.

A brief introduction to the subject of in situ composites was presented in this chapter. Also, a preliminary introduction to liquid crystalline polymers was also given. Some of the findings of the literature were briefly outlined and the main research objectives of this study were given. In the following chapter, an attempt will be made to present the literature as it pertains to the current research. It is hoped that the literature review will be successful in bringing the research goals into proper perspective. On the basis of the findings of the literature review, the proposed research is developed and presented at the end of Chapter 2.

2.0 Literature Review

It is clear that the field of polymer composites and blends has expanded greatly in the last twenty or so years. Much of the increased activity in this area can be attributed to the fact that polymer blends offer unique materials with the desirable features of its constituents. As a result of the active research pursued in this field, the literature has been literally flooded with publications from both the theoretical and experimental viewpoint. Thus no exhaustive review of polymer blends is attempted. Rather, appropriate references are given where deemed necessary.

To gain any kind of an understanding of the development of in-situ composites, it becomes necessary to examine several different aspects of polymer blends. Most of the subjects reviewed later are directly related to the process of specific fibrillation of one polymer in another. Thus this chapter is divided into several sections. Section 2.1 gives a brief review of the general area of polymer blends along with a discussion of some of the terminology currently employed. In Section 2.2, the fundamental aspects of drop deformation are reviewed. Both experimental and theoretical work from the literature is presented in order to establish the current status of this very pertinent phenomena. Although no study of the drop deformation phenomena per se is proposed, it is felt that a review of the subject is nevertheless necessary in understanding the development of in-situ composites. Section 2.3 is a brief

discussion on the stability of the elongated domains formed by the deformation of droplets. Condition under which the thread-like entities (i.e., fibrils) are unstable and break up into droplets are outlined. The development of morphology in two-phase polymer blends with an emphasis on the specific fibrillation process is discussed in Section 2.4. Following that, Section 2.5 is devoted to a discussion of some features of liquid crystalline polymers (LCPs) that are necessary towards the further understanding of this work. A general introduction to liquid crystals is followed by a review of the rheology of thermotropic LCPs. In particular, the viscosity behavior, the shear and temperature history dependence, and the processing of LCPs is discussed. In Section 2.6, specific studies on the generation of in-situ composites are discussed. The literature is examined critically in order to highlight the areas that are deficient in any respect. Finally, in Section 2.7 some preliminary results of this author are presented, leading up to the proposed research at the end of Chapter 2.

2.1 Polymer Blends-Some General Considerations

2.1.1 Polymer-Polymer miscibility

Polymer blends may be defined as an intimate mixtures of two (or more) kinds of polymers, with no covalent bonds between them (8). After blending together, polymer pairs may be qualitatively considered immiscible, partially miscible or miscible depending on whether two distinct phases remain, partial mixing of the two polymers takes place at the molecular level, or a single thermodynamically stable phase is formed.

It is probably appropriate at this stage to digress a little, and distinguish between miscibility and compatibility since these terms have often been used quite interchangeably in the literature. "Compatibility" has been used by many investigators of polymer blend behavior

to describe systems that are homogeneous to the eye and have enhanced physical properties. Included in this definition of compatible systems are also those systems exhibiting good interphase adhesion between the constituents and those that provide ease of blending. Miscibility, on the other hand connotes polymer blend systems with behavior similar to that expected of a single-phase system (9). The term miscibility implies ideal molecular mixing and suggests that the level of mixing is adequate to yield macroscopic properties expected of a single-phase material (14).

As mentioned earlier, when dealing with blends of polymers, one may encounter two extreme situations: a gross phase separation, or an inhomogeneous mixture at the molecular level. It it important to realize, however, that in reality the situation is much more complex and a host of intermediate cases are possible. For example, one may see increasing separation at the molecular level alone, formation of a co-continuous morphology, or phase separation into dispersed heterogeneous morphologies of increasing phase size (63, 64). Clearly, then, one must be aware of the size-scale probed by a particular method before definite conclusions may be made.

The final macroscopic properties of homogeneous or miscible blends is often times limited to being intermediate to those of the corresponding homopolymers. Although this mediation of properties does possess limitations to the gamut of properties displayed by polymer blends, it does offer an interesting way to broaden the "processing window" of a given system, and also to generate a continuous range of properties between those of the homopolymers (63). Blending of immiscible polymers is more attractive, however, because these systems offer the advantage of additivity of properties of the homopolymers (64).

It is important to make some comments regarding immiscible blends since they are the blends of particular interest to this study. The phase structure or morphology of immiscible blends is a function of processing history. Further, the mechanical behavior of the blend is also likely related to the morphology. This then suggests that a given immiscible blend would give rise to different properties depending on its processing history (134). Thus a careful selection of parameters and a thorough knowledge of the rheology of the two components is

critical to produce a blend with desired properties. Later discussion on in-situ composites will clarify this point further.

In the next section a discussion of the thermodynamic factors that govern whether a system will be miscible, immiscible or partially miscible are briefly discussed.

2.1.2 Thermodynamics of Polymer Blends

The major factor affecting the thermodynamics of polymer blends is the large molecular weight of both components. As a result of the large molecular weights of the polymers involved, the number of moles of each polymer in the blend is small resulting in a low entropy of mixing in the free energy of mixing expression shown below:

$$\Delta G_m \; = \; \Delta H_m - T\Delta S_m \tag{1}$$

The heat of mixing ΔH_m is generally thought to be positive, at least for relatively nonpolar systems. Therefore, even though the sign of the combinatorial entropy favors mixing, the entropy term is too small to negate the overall free energy. Further, $\Delta G_m < 0$ is a necessary but not sufficient condition for miscibility. The other condition that must be satisfied for miscibility is (10)

$$\left(\frac{\partial^2 \Delta G_m}{\partial \phi_2^2} \right)_{T,p} > 0 \tag{2}$$

The theory of polymer solutions was extended to mixtures of polymers by Scott (11) and obtained the following expression for the Gibb's free energy of mixing:

$$\Delta G_m \; = \; (RTV/V_r)[(\phi_A/x_A) \ln \phi_A + (\phi_B/x_B) \ln \phi_B + \chi_{AB}\phi_A\phi_B] \tag{3}$$

where V_r is the reference volume which is taken as close to the molar volume of the smallest repeat unit as possible, ϕ_A and ϕ_B are the volume fractions of polymers A and B respectively, x_A and x_B are the degrees of polymerization of polymer A and polymer B in terms of the reference volume V_r, respectively, and χ_{AB} is related to the enthalpy of interaction of the polymer repeat units. The interaction parameter, χ_{AB}, between molecules of comparable size is often written in terms of the Hilderbrand solubility parameters (12,13) as

$$\chi_{AB} = (V_r/RT)(\delta_A - \delta_B)^2 \qquad [4]$$

where δ_A and δ_B are the Hilderbrand solubility parameters for A and B, respectively. Experimental methods for the determination of solubility parameters have been found to be tedious and largely dependent on the nature of the solvent used (14). To overcome this limitation, several methods have been offered to predict the solubility parameters. One such method is the one proposed by Hoy (15) based on the group molar attraction constants. Each group or repeat unit is given a molar attraction value, Fi, which are then summed as:

$$\delta = \frac{\rho \sum F_i}{M} \qquad [5]$$

where ρ is the density of the polymer at the temperature of interest and M is the molecular weight of the repeat unit. One can use the estimated value of the solubility parameter to calculate the interaction parameter. If complete miscibility of the two polymers is desired, this calculated value of the interaction parameter must not exceed it's critical value, $(\chi_{AB})_{CR}$, calculated from the equation

$$(\chi_{AB})_{CR} = 1/2[1/x_A^{1/2} + 1/x_B^{1/2}]^2 \qquad [6]$$

where x_A and x_B are as defined earlier (14). It should be noted that the procedure used above in determining the miscibility of a system of two polymers is only approximate.

Some thermodynamic considerations regarding the miscibility behavior of blends were reviewed in this section. It was seen that experimental determination of the solubility parameter is difficult and several predictive methods have been proposed. In the next section, the phenomena of drop deformation and break-up is reviewed. A study of the dynamics of deformation of a small drop of fluid suspended in another fluid is critical in understanding the morphology development in polymer blends. The thermodynamic miscibility criteria along with the drop deformation phenomena determine to a large extent the final phase morphologies of two phase polymer blend systems.

2.2 Drop Deformation and Burst

The dynamics of a small isolated drop of fluid of viscosity μ_d freely suspended in a second fluid of viscosity μ_m which is caused to move in a prescribed manner have been the subject of several investigations (17-24), starting with the pioneering work of Taylor in 1934 (16). At vanishingly small Reynolds number the drop is able to translate with the same velocity as the local applied flow. However, due to the effects of surface and interfacial tension and the unequal viscosities, the drop can neither freely deform in the local shear nor in general remain spherical. From experimental and theoretical analysis of the phenomena, it has become clear that the process is governed by two competing forces: viscous shearing and/or elongational stresses leading to the droplet deformation, and interfacial forces which oppose the shape change. The drop continues to elongate and will eventually break up, when the viscous normal stress tending to elongate and disrupt the drop exceeds the interfacial forces resisting this deformation (17).

An understanding of the droplet deformation and breakup phenomena is of fundamental importance when dealing with two-phase systems. Taylor's experiments revealed most of the

qualitative aspects of the drop deformation and burst phenomena and have been summarized in a recent work by Bentley and Leal (18) as follows:

1. At low flow strengths, drops of all viscosity ratios deform into prolate spheroids with the longest axis of the drop aligned with the principal axis of strain, for both extensional (also referred to as irrotational) as well as simple shear flows.

2. When the drop viscosity is low compared with that of the suspending fluid (i.e., $\mu_d << \mu_m$), the drops assumes highly deformed but steady shapes with pointed ends, and the shear rate required for burst becomes quite large.

3. The behavior of the drop, in the case where the drop viscosity is much larger compared to the suspending medium or matrix viscosity (i.e., $\mu_d >> \mu_m$), is completely different for the extensional and simple shear flows cases. In extensional flows, the burst is seen to occur at low strain rates. In simple shear flows, however, the drops assume slightly deformed shapes which are unaffected by further increases in shear rate, and no drop burst is observed, regardless of the shear rate, beyond a certain critical viscosity ratio.

The droplet deformation and breakup process has also been examined theoretically. Typically, for small deformations perturbation techniques have been used, slender body theory for large deformations and numerical methods for intermediate deformations. Taylor (16) has shown that in steady uniform shearing flow, the droplet deforms into a spheroid, and the shape of the droplet depends on the viscosity ratio of the droplet to medium phase and the ratio of the product of the local stress and the droplet radius to the interfacial tension, often referred to as the Weber or Capillary number. The deformation of the drop is thus related to the physical properties of the fluid by the following equation:

$$D = We\left(\frac{19\lambda + 16}{16\lambda + 16} \right), \qquad \alpha = \pi/4 \ \text{ for We} << 1, \ \lambda = O(1) \qquad [7a]$$

$$D = \frac{5}{4\lambda}, \qquad \alpha = 0 \ \text{ for We} = O(1), \ \lambda >> 1 \qquad [7b]$$

where the Weber number, We, and the viscosity ratio, λ are defined as

$$We = \frac{\dot{\gamma}a\mu_m}{\sigma} \qquad [8]$$

and

$$\lambda = \frac{\mu_d}{\mu_m} \qquad [9]$$

and $\dot{\gamma}$ is the shear rate, a is the initial droplet radius, and σ is the interfacial tension, α is the angle between the flow direction and the major axis of the spheroid, and D is the deformation parameter given by

$$D = \frac{L - B}{L + B} \qquad [10]$$

where L and B are the major and minor axis lengths of the spheroid, respectively.

Since Taylor's pioneering studies on droplet deformation, a number of other studies began to emerge. Rumscheidt and Mason (35) studied drop deformation over a wide range of interfacial tension and viscosity ratio. Their results are shown in Figure 1. They observed four different types of deformation in uniform shear flow and two types in plane hyperbolic flow. In Figure 1, k represents the viscosity ratio and σ the interfacial tension.

Second order solutions were obtained by subsequent workers (19, 20), using D as the perturbation parameter. However, these solutions were still incapable of obtaining accurate predictions for higher deformations. Another first order solution, valid for small deformations only, was developed which could be applied to any time-dependent linear flow field (21).

Karam and Bellinger (22) conducted some experiments using silicone oil as the dispersed phase and corn syrup as the continuous phase and concluded that Taylor's theory, regarding the deformation and breakup of droplets in simple shear field, was essentially correct. They further concluded, on the basis of their experiments, that the droplets broke up most readily when the viscosity ratio, λ is between 0.2 and 1.0 and that breakup was easier at large Weber numbers.
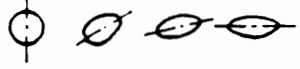
	Mode of Deformation	Range of Viscosity Ratio and Surface Tension
Uniform Shear Flow		$k < 0.14,$ $\quad \sigma < 10.$
		$0.14 < k < 0.65,\ 10 < \sigma < 20$
		$0.7 < k < 2.2,$ $\quad \sigma < 20$
		$k > 3.8,$ $\quad \sigma > 4.0$
Hyperbolic Flow		$k < 0.2,$ $\quad \sigma < 38$
		$k > 6.0,$ $\quad \sigma > 4.8$

Figure 1. Schematic showing the mode of droplet deformation in different flow fields [35].

All the work done on drop deformation so far was restricted to Newtonian drop-Newtonian medium systems. Flumerfelt (23) studied the breakup of Newtonian drops in steady and unsteady shear fields of viscoelastic fluids. The results indicated that for all the systems studied, there was a minimum drop size. a_{min}, below which breakup could not be achieved. The elasticity of the continuous phase was seen to increase both a_{min} and the critical shear rate $\dot{\gamma}_c$ required for breakup when $a > a_{min}$. Also interesting to note is the fact that again both $\dot{\gamma}_c$ and a_{min} were seen to decrease significantly under unsteady shear conditions (a step change application) as compared to the "steady" shear conditions (a gradual application of shear). Such transient and steady deformation studies were also conducted by Torza et al. (24) with similar results. Their studies indicated that the mechanism of drop burst was more dependent on the rate of increase of the velocity gradient, $\dot{\gamma}$, up to the critical value, $\dot{\gamma}_c$, than on the viscosity ratio. Further, no drop burst was observed beyond a viscosity ratio of 3.0.

Using the concepts of thermodynamics, Vanoene (25) advanced a theory on the mechanisms of two-phase formations from a mixture of two viscoelastic fluids. He pointed out that in addition to the viscosity ratio and the interfacial tension of the two liquids, elasticity of the liquids (namely, the normal stress differences) should play an important role in determining the deformability of a viscoelastic droplet suspended in a viscoelastic medium. He thus proposed that when both the components are viscoelastic, the component with the larger normal stress functions will form droplets dispersed in the other component. On the basis of his studies on extrusion of two-phase polymer blends, he concluded that since neither shear rate, residence time in the capillary nor temperature had a marked influence on the morphology of the extrudate, the various structures must arise from parameters that depend on the radial position in the capillary but are independent of the length of the capillary. He also noted that reextrusion affected only the degree of dispersion of the extrudates and did not alter the morphology in any way. Tavgac (36) and Lee (37) reported contrasting results on the effect of fluid elasticity on the extent of drop deformation in shear and extensional flow fields. In Couette (simple shear) flow, Tavgac observed differences in deformability between Newtonian and viscoelastic droplets and further claimed that the effect of fluid elasticity varied with the

viscosity ratio. Lee, on the other hand, reported no perceptible differences in deformability of Newtonian and viscoelastic droplets in plane hyperbolic flow.

Studies of droplet deformation in pressure-driven flows through converging and uniform channels were conducted by Han and Funatsu (26). They observed that at wall shear rates of a suspending medium below a certain critical value, the initially spherical droplets, elongated very much at the die entrance and then recoiled to some extent in the fully developed region downstream of the channel. However, when the shear rate was higher than a critical value, the deformed droplet broke up into several smaller droplets. Chin and Han (27) presented one of the few theoretical analyses for the deformation of a viscoelastic drop in an viscoelastic medium in a steady extensional flow field. They used a Coleman-Noll, second order fluid constitutive equation and a first-order perturbation. They found that the medium elasticity played a much smaller role than medium viscosity in affecting the deformation of the droplets. In another study on the stability of a liquid cylinder in nonuniform shear (or Poiseuille) flow (28), the authors concluded that an increase in any one of the three parameters: medium elasticity, droplet phase elasticity and interfacial tension led to an increase in the rate of growth of the disturbances whereas an increase in the medium viscosity stabilized the liquid cylinder.

Elmendorp and Maalcke (29,30) experimented with Newtonian systems and viscoelastic solutions and found that the elasticity in the dispersed phase tends to stabilize droplets whereas elasticity in the medium phase tends to destabilize them. They were unsuccessful, however, in predicting droplet deformation in viscoelastic systems by substituting the shear dependent viscosities in the the equations for Newtonian droplet deformation and further by correcting for fluid elasticity by substituting an apparent interfacial tension as suggested by Vanoene (25).

It was observed experimentally in many studies of droplet deformation and breakup that the droplets assumed long and slender shapes upon deformation at high strain rates, specifically when the viscosity ratio was small. Taylor (31) was the first to propose that the behavior of these long droplets could be described qualitatively by the slender-body theory. His analy-

sis was made more rigorous by Buckmaster (32, 33), who found that there were many steady shapes of the droplet possible. Acrivos and Lo (34) showed all of these steady shapes but one to be unstable.

More recently (18), a more sophisticated experimental setup than that of previous investigators, was used to study the drop deformation and breakup phenomena. Their work in noteworthy in two respects. Firstly, the authors studied a range of flow types between the simple shear and hyperbolic extension limits. Secondly, they compared a number of asymptotic deformation and burst theories to their experimental data showing the range of validity and limitations of each. Some of their results are as follows. In most cases, the theories agreed well with their experimental observations. For viscosity ratios less than unity, the Capillary number (or We) required for burst and the deformation at the point of burst both decreased with increasing viscosity ratio for all strong flows (i.e., flows in which the magnitude of the strain rate exceeds that of the vorticity). In the case of irrotational (or extensional) flows, the critical value of the Capillary number reached a constant value with further increases in the viscosity ratio. Finally, for the case of simple shear flow, it was observed that the critical Capillary number goes through a minimum at a viscosity ratio of about 1.0 and there exists an upper limit to the viscosity ratio beyond which no burst is possible.

A study of the rheological and interfacial effects on the dispersion process during melt extrusion of polymer/rubber blends in a co-rotating twin screw extruder was carried out quite recently by Wu (38). For the various blend systems studied, he observed that all the data points fell on a single master curve of Weber number versus the viscosity ratio. He also noted that the particle size of the dispersed phase was directly proportional to the interfacial tension. Other factors being equal, the smallest particle size was seen to occur at a viscosity ratio of unity. Lastly, he observed breakup of viscoelastic drops at viscosity ratios higher than 4.0, which was attributed to the elastic effects, the presence of an elongational field and the complex viscosity-temperature profile along the extruder barrel. Figure 2 is a summary of the range of viscosity ratios within which drop deformation is possible for the various systems studied. Similar results were observed for blends of polypropylene/polycarbonate in which

deformation of the minor phase was found to be significant at viscosity ratios as high as 17 (39). This was again attributed to the elasticities of the two components.

It is clear from the numerous results cited above (which are not exhaustive in themselves) that the type of flow field and the viscosity ratio are critical in determining the mode of droplet deformation and burst. The experimental results and some of the general "ground rules" established thus far for droplet deformation and breakup in Newtonian systems may be summarized as follows.

In simple shear flows, three separate regimes of viscosity ratio were determined which governed the deformation and breakup. For viscosity ratios greater than about 4.5, no burst was possible regardless of We. The droplets show a small but stable deformation and the critical Weber number for burst, We_c approaches infinity. If the viscosity ratio is around unity, the deformation behavior is dominated (24,26) by the rate of increase of the shear rate i.e., $d\dot{\gamma}/dt$. If the critical conditions are imposed suddenly from the quiescent state or from conditions of low We, the drop bursts by emitting thin tails from both ends. In contrast, if the shear rate is increases slowly so that there is a gradual transition from subcritical to critical conditions, the drop is pulled to a great length before it develops a neck around the center causing it to burst and giving rise to larger satellite drops. For viscosity ratios less than one, the droplet bursts by a phenomenon which has come to be called as "tip streaming" (18) ejecting small droplets from both ends. Interestingly enough, the lower the viscosity ratio was below unity, the greater was the sustainable steady deformation and the higher the critical We number required for burst.

In extensional flow, for viscosity ratios less than 0.2, droplets develop pointed ends and when We > We_c the droplet bursts by "tip streaming". For viscosity ratios greater than 0.2, the droplets burst by emitting thin long tails which are continuously pulled out of the droplets in a thread-like fashion from both ends. If the flow is instantaneously stopped, the thread immediately breaks up into larger drops. Tomotika (40,41) studied the problem of thread breakup and concluded that breakup is a surface tension driven effect balanced by viscous forces. He showed from his analyses that if the ratio of the viscosities of the two fluids is neither zero
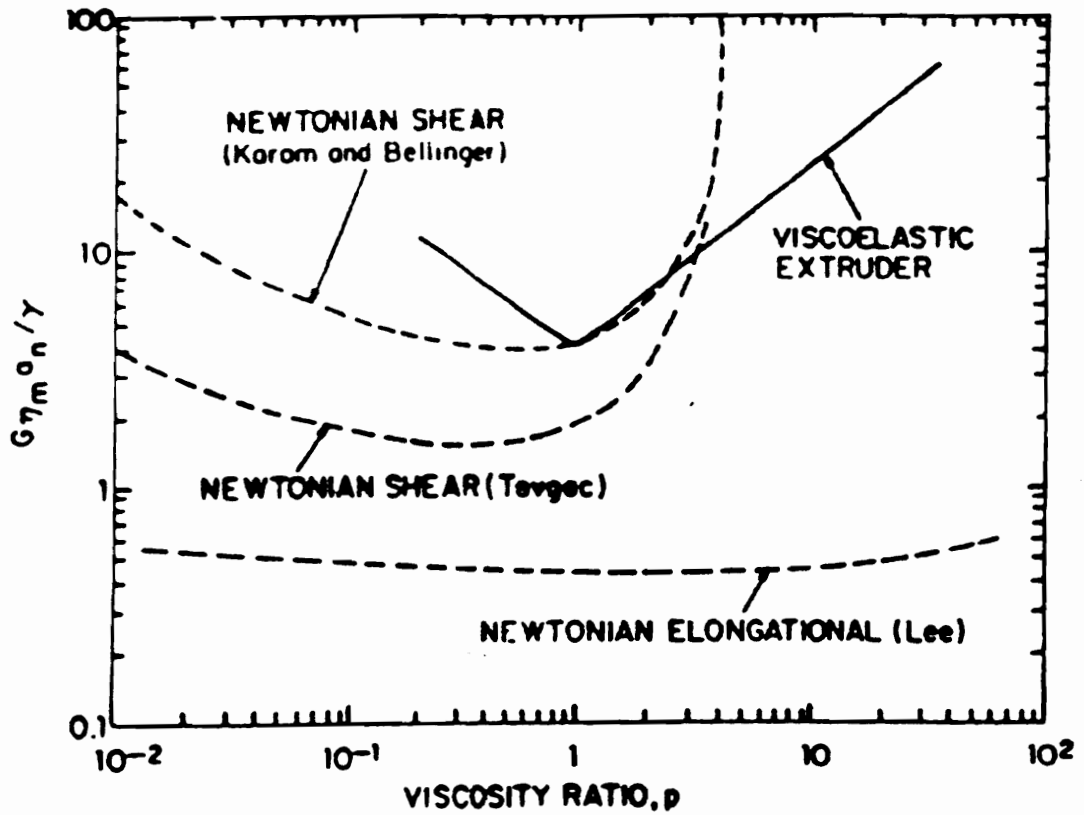
Figure 2. Master curves for viscoelastic blends in a co-rotating twin screw extruder with those for Newtonian liquids in steady shear and elongational flow. Weber number vs viscosity ratio [38].

nor infinity, then the droplet breakup always occurs at a certain definite value of the wavelength of the initial disturbance.

In the above section, the parameters that govern the deformation and breakup of drops of one polymer suspended in another were discussed. The importance of both the Weber number and the viscosity ratio in the deformation process was established. It was seen that in the case where the viscosity of the dispersed phase was much lower than that of the matrix, i.e. for low viscosity ratios, the drops were able to achieve highly deformed but stable entities. The situation for viscosity ratios greater than about 3 is different in that although no burst is possible, it also becomes increasingly difficult to deform the droplets to any appreciable extent. Further, it was also observed that in shear flow there exists both an upper and lower limit on the viscosity ratio beyond which no drop burst is possible. Drop breakup in extensional flow fields is possible over a much wider range of viscosity ratios showing that extensional flow fields are more effective than uniform shearing flow fields in breaking up droplets.

2.3 Domain Stability

The morphology of a polymer blend of incompatible polymers is governed not only by the deformation and breakup of the dispersed phase but also by capillary instabilities of the thread-like particles and by coalescence of the dispersed phase (65). Drop deformation and breakup has been discussed in the previous section This section deals with the stability of the fibrils, a phenomenon, which plays an important role in determining the final morphology. Some of the experimental work on the development of the morphology of polymer blends, with emphasis to fibril formation will be reviewed in the next section.

It is known that a liquid cylinder is thermodynamically unstable because of an unfavorable ratio of the surface to the volume (45). It has also been noted that when the ratio of the length of the liquid cylinder to its diameter reached 4.5, the lateral surface of the cylinder be-

comes equal to the surface of two spheres with the total volume being equal to the volume of the initial cylinder. Any further increase in the length of the cylinder is energetically unfavorable and it splits into drops, the driving-force for this breakup being the interfacial tension (45,65). A liquid stream or thread with an aspect ratio greater than 4.5 is thus a nonequilibrium system, and its fracture will then be determined by the local conditions of flow, coupled with the rheological and interfacial properties of the fluid mixture (45).

The breakup of capillaries for inviscid jets in air was first described by Lord Rayleigh in 1878 (66). The growth of capillary instabilities on a Newtonian thread suspended in a Newtonian fluid was examined theoretically by Tomotika (40,41) who considered a sinusoidally distorted thread

$$R(z) = \bar{R} + \alpha \sin(2\pi \frac{z}{\Lambda})$$ [11]

where $\bar{R}$ is the average thread radius, α is the distortion radius, Λ is the distortion wavelength and z is the coordinate along the thread. It has been noted (30) that when $\Lambda > 2\pi R$, the interfacial area decreases with increase in distortion amplitude. Consequently, a liquid thread is unstable to distortions of wavelength larger than the circumference of the thread. Tomotika's theory shows that when $\Lambda > 2\pi R$, the distortion amplitude α grows exponentially with time as

$$\alpha = \alpha_0 \exp(qt)$$ [12]

where α_0 is the distortion at time zero and

$$q = \frac{\sigma}{2\eta_c R_0} \Omega(\Lambda, \lambda)$$ [13]

where σ is the interfacial tension, η_c is the matrix viscosity, and λ is the viscosity ratio (dispersed/matrix). The value of the growth rate of the disturbance, $\Omega(\Lambda, \lambda)$, is found to have a maximum for a certain value of the distortion wavelength, Λ_m, which is dependent on the viscosity ratio, λ (30). Thus assuming that the thread contains all wavelengths with equal initial

amplitudes at the time of creation, the distortion wavelength at which the growth rate is maximum is expected to lead to thread break-up (30).

Breakup of the thread will take place when the distortion amplitude equals the average thread radius (65), i.e. when $\alpha = \overline{R}$. The time needed to convert the thread-like particles to a number of small droplets can then be calculated to give

$$t_b = \frac{1}{q} \ln(\frac{0.8R_0}{\alpha_0})$$ [14]

Thus if the time for thread breakup exceeds the droplet deformation time, then one can expect cylindrical bodies to be present in the matrix polymer. Freezing in this intermediate morphology would then yield the reinforcing fibers instead of a disperse phase that consists of essentially droplets.

Elmendorp (30) and Tsebrenko et al. (45) have studied this problem of thread breakup experimentally. Elmendorp studied both Newtonian and viscoelastic thread breakup in a Newtonian medium. In the case of Newtonian thread breakup in a Newtonian medium, it was observed that good agreement of data with Tomotika's theory was obtained. The wavelength dependence of the $\Omega(\Lambda, \lambda)$ function for a viscosity ratio, λ, of 13 is shown in Fig. 4, where, in-spite of some scatter, the agreement is good. Further, as expected from theory, the breakup time of the threads decreased with an increase in the magnitude of the relative initial distortion. For different conditions, the breakup time varied from a few seconds to a few hours. The data of high molecular weight model viscoelastic threads in a Newtonian medium, however, did not fit the theory too well. In contrast, experiments with molten polymers using polypropylene and polystyrene in polyethylene showed good agreement with theory. These results were explained by the fact that calculation of the elongation rate from the diminishing radii of the waists of the breaking threads yielded rates of that order of 10^{-5} s^{-1} to 10^{-3} s^{-1}, a Newtonian region for most polymer melts.

Tsebrenko et al. (45) conducted some extensive experiments to determine the conditions under which fracture of ultrafine fibers in the flow of mixtures of Non-Newtonian polymer melts
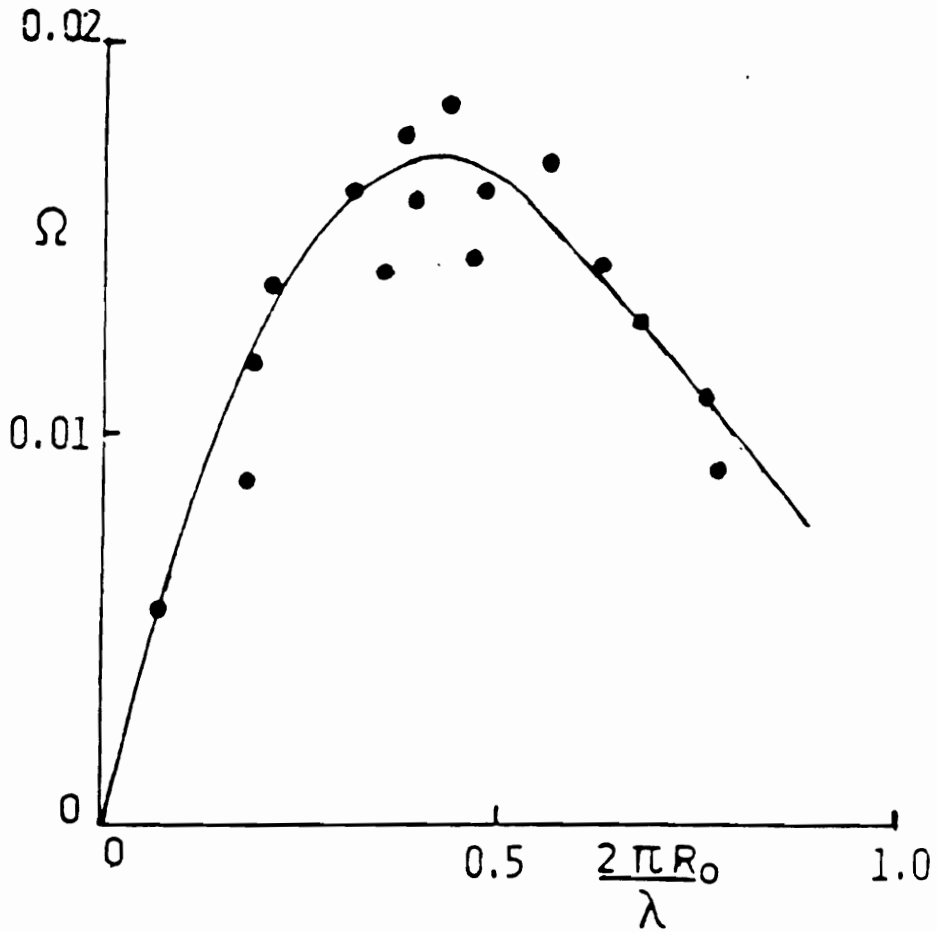
Figure 3. Wavelength dependence of the Ω (λ, p) function for a viscosity ratio, p = 13. Solid points - experimental; drawn curve - calculated from Tomotika's theory [30].

takes place. Their results are of great importance to the current work and are as follows. They concluded that the same parameters that control drop deformation (viscosity ratio and Weber number) also determine the critical conditions for fracture of the resulting liquid cylinder. However, the agreement of the experimental data for viscoelastic liquids with the theories developed for Newtonian fluids is only qualitative. This conclusion was based on the following facts. It was found that the disturbance wavelength and the size of the resulting drops are greater for the polymer systems than for Newtonian liquids. The growth of amplitude of the destructive wave slows down at the final stages of fracture. Theoretically and experimentally determined values of the lifetime of a polymer stream, that is time to break, differ by 2-3 orders of magnitude. All other things being equal, the time to break or burst of a polymer stream is determined by the viscosity of the medium, for the same value of the viscosity ratio. This latter effect is shown in Figure 4 where the reduced lifetime of the liquid cylinder, t_B/R, is plotted against the logarithm of the viscosity ratio, K. The authors attribute these observed differences to the non-Newtonian effects arising due to the elasticity of the polymer melts. Another important result from their studies is that a mixture of polymers, one of which forms fibers in the other, is maximally unstable if the viscosity ratio of the melts is close to unity. Further, when the viscosity ratio is less than unity, the enhanced elasticity of the matrix polymer stabilizes liquid streams of the disperse phase (i.e. the time to break grows). One last result of interest is the fact that fracture of the fibers was seen to be possible only at temperatures greater than the melting point of the fiber forming polymer. However, this was seen to be a necessary but not sufficient condition for breakup. The other condition that had to be satisfied is that the temperature should also be greater than the melting point of the matrix polymer before breakup can be achieved.

Study of domain stability has also been reported by Jorgensen et al. (66,67,68) during capillary flow of well dispersed two phase polymer blends. Blends of polystyrene (PS) and polymethylmethacrylate (PMMA) were used in their experimental investigation. Their results indicate that the domains are stable when the viscosity ratio (dispersed/matrix) is greater than one. To explain the experimental results, a hypothesis was developed for the stability of
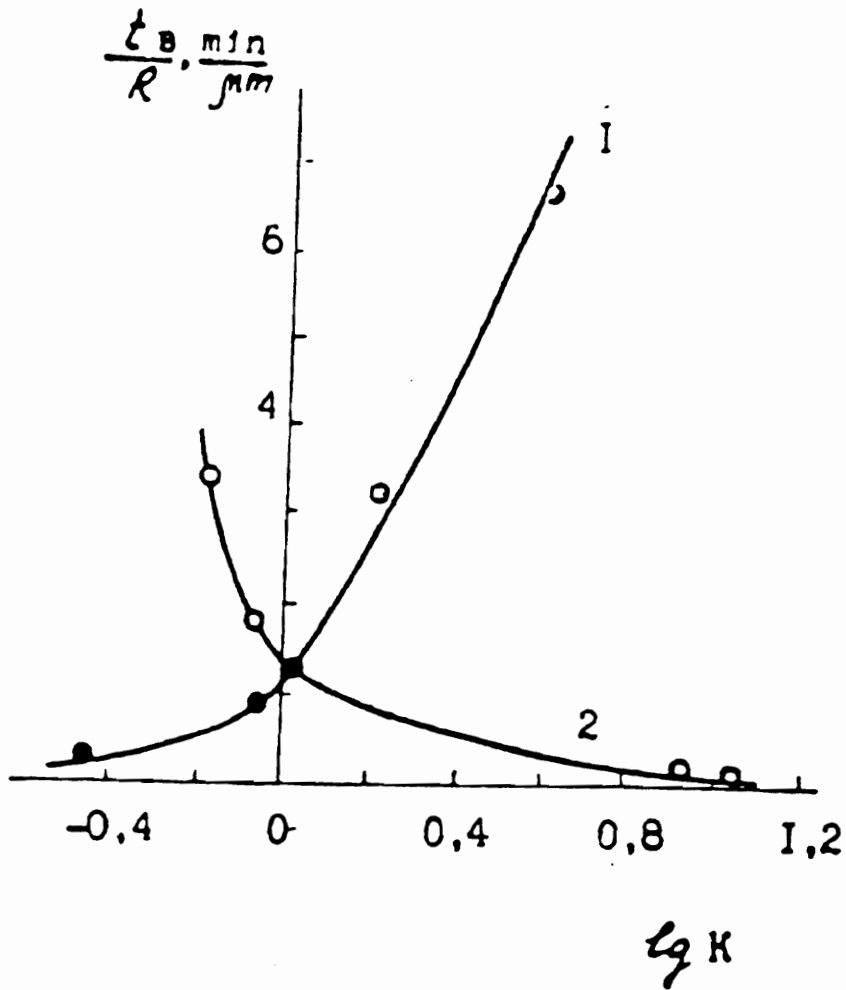
Figure 4. Dependence of the reduced lifetime of the liquid cylinder on the viscosity ratio of the phases for (1) η_{CEVA} = const. and (2) η_{POM} = const. [45].

viscoelastic domains in a viscoelastic medium, which was applicable in the inlet region and the beginning region of the capillary die. If the ratio between the relaxation time of the domains to that of the matrix phase is greater or equal to one, then it is postulated that the domain is stable. This hypothesis was seen to agree well with experimental data on the PS/PMMA system studied.

The purpose of this section was to briefly review the literature on the stability phenomena of thread-like particles of one polymer suspended in another. Experimental results show that again the Weber number and viscosity ratio are important in determining whether the thread will remain stable or breakup into drops. Thus it is important to realize that even though appropriate processing conditions for the deformation of a drop into a fibril may be achieved, the final morphology will still depend on whether the fibril is stable or not.

2.4 Morphology of Polymer Blends

In microheterogeneous (multiphase) polymer blends the identity of the components is retained and hence processability and ultimate performance characteristics of the blend will depend on the sizes and shapes (i.e. morphology) of the individual phases (42). An important consequence of the above observation is that the morphology-melt rheology dependence on the mixing process and shear is quite often more pronounced than the dependence on composition. It is the intent of this section to present some of the work done on two-phase polymer blends in an effort to bring to attention some of the parameters that control the resultant morphology of immiscible two-phase blends.

In general, three basic morphologies are possible (42): dispersed, stratified (lamellar, sandwich) and co-continuous. The dispersed morphology (which is the type of morphology of greatest interest to this research) can be further divided into droplet and rod (or fibril) in matrix type. The morphology of a blend, formed from immiscible polymers, is governed by a

multitude of factors. Among them are the composition, viscosities, elastic and interfacial properties of both the components, the magnitude of the shear and elongational flow fields prevalent in the mixer, time scale of mixing (residence time), and post-processing i.e., further processing after the mixing stage. Furthermore, special features of the components, for e.g. the presence of yield stresses or strain-induced crystallization, could also result in different morphologies with unusual properties.

The work of Tsebrenko (43, 44, 45), Vinogradov (46), and Ablazova (47) dealt with the phenomenon of specific fibrillation from melts of polymer mixtures wherein thousands of ultrafine fibrils oriented along the extrusion axis were obtained as a result of extrusion through a single orifice i.e., capillary die. Although a number of systems were studied by the above authors, the most significant results were obtained on mixtures of polyoxymethylene (POM) with copolyamides (CPA). Upon extraction of the CPA with a solvent, the POM remained as a bundle of fine fibrils less than 1 μm in diameter. The authors conclude that fibrillation in the system was achieved, not after the melt leaves the die, but in the inlet zone of the capillary. Further, a viscosity ratio, of dispersed to matrix phase, of unity was found to be optimal for fibrillation in terms of obtaining long fibers of small diameter. A rather interesting setup with a dismountable capillary was used by Tsebrenko (43) to determine where the fibrillation takes place. The capillary die, after equilibration of flow, was quickly removed and immersed in liquid nitrogen. Examination of these chilled samples proved conclusively that the fibrillation indeed occurred in the entrance zone of the capillary. In Fig. 5 is shown the photomicrographs of longitudinal sections of a frozen sample of POM fibrils in a CPA matrix. On the basis of these results, the authors proposed a qualitative mechanism by which fibrillation takes place. This is shown in Fig. 6. The authors propose that under the effect of tensile stresses acting in the direction of the stream the stretching and coalescence of the droplets takes place in the entrance zone (Fig. 6, A). Close to the entrance to the duct the stream narrows sharply (Fig. 6, B) and at a definite distance down the entrance (Fig. 6, C) the influence of its walls becomes manifest, leading to intensive development of shear and retardation of the stream. The shrinkage (enlargement of diameters) and loss of parallelism of fibrils seen from microphoto-

graphs gave support to this argument. In the zone of shear (Fig. 6, D) the fibrils become parallel once again.

Vinogradov and coworkers (72) studied extrusion of blends of PE/PS through a capillary die to determine the conditions under which fibril formation occurred. The viscosity ratio, mixture preparation conditions and the stress level were the variables in the study. It was observed that method of preparation of the blends did not influence the fiber formation process. However, it was established that the fiber formation occurred within a definite range of shear stresses, dependent on the viscosity ratio. A critical stress level was calculated beyond which extremely long fibers were formed. Further, an upper limit to this stress level was also determined beyond which no fiber formation was observed due to unsteady high elastic turbulent flow. These results are shown in Fig. 7. The authors also noted that formation of fibrils was impossible, regardless of the shear stress, for viscosity ratios greater than 10.

It is important to point out that the fibril formation process has been observed to occur in shear fields also (48,49). Both these studies were conducted on PE/PS blends in a rotary viscometer of the cone and plate type and showed that fibrillation in incompatible polymer melts under uniform shear fields is possible. Berger et al. (54) found in blends of polyethylene terephthalate with polyamide- 6 that a fibril in matrix structure by pure shearing and without draw was possible only when the dispersed phase had a higher viscosity than the matrix phase. These results are in contrast to those predicted by the drop deformation theory. However, when draw was imposed on the extruded melt, fibril-in-matrix structures were observed for all viscosity ratios examined. However, Dreval (48) concluded that the range of shear stresses where fibrillation was found to occur was narrower in the case of uniform shear fields (Figure 8) than in the case of flow through capillaries. Further, in the systems that they studied, it was seen that the viscosity ratio varied by several orders of magnitude whereas the elasticity ratio did not vary more than an order of magnitude. On the basis of these observations the authors concluded that the viscosity ratio must play a more dominant role in the fibrillation process. Both coalescence and extensional flow were thought to be responsible for the formation of fibers in capillary flows.
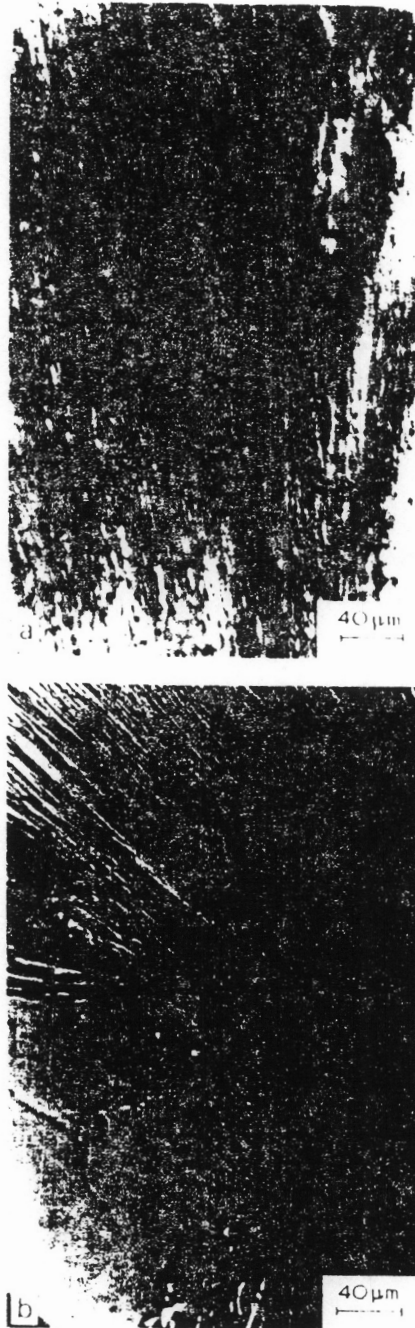
Figure 5. Microphotographs of longitudinal sections illustrating the formation of funnel in entrance zone (a) along the stream axis; (b) parallel to the axis at a distance of 0.5 mm from it [43].
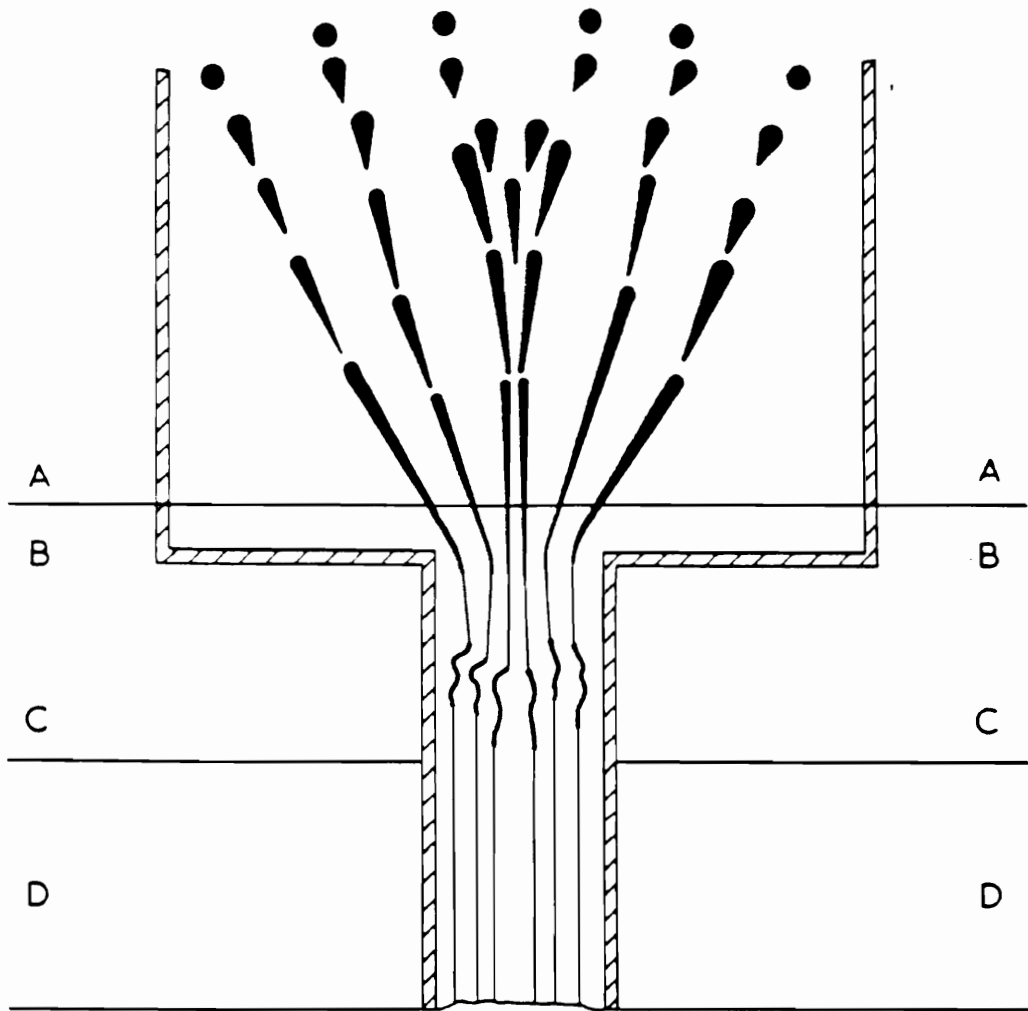
Figure 6. Representation of the fibrillation process in the entrance zone and in the ducts [43].
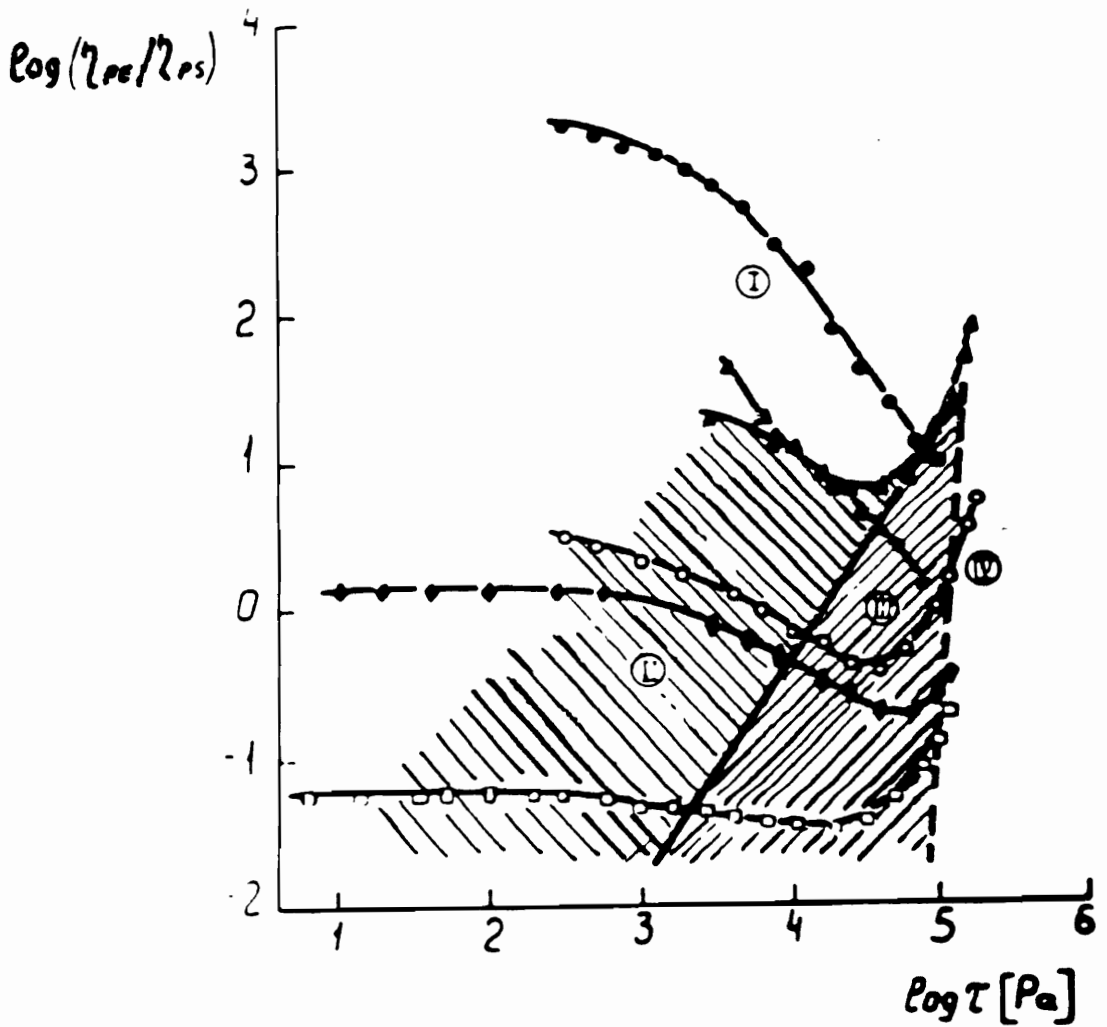
Figure 7. Viscosity ratio versus shear stress for PE/PS blends. Region I, no fibers; Region II, imperfect PE fibers; Region III, perfect PE fibers; Region IV, disintegrated fibers. Boundaries of pronounced fiber formation region: thick line, τ_{cr}; dashed line, τ_{lim} [72].
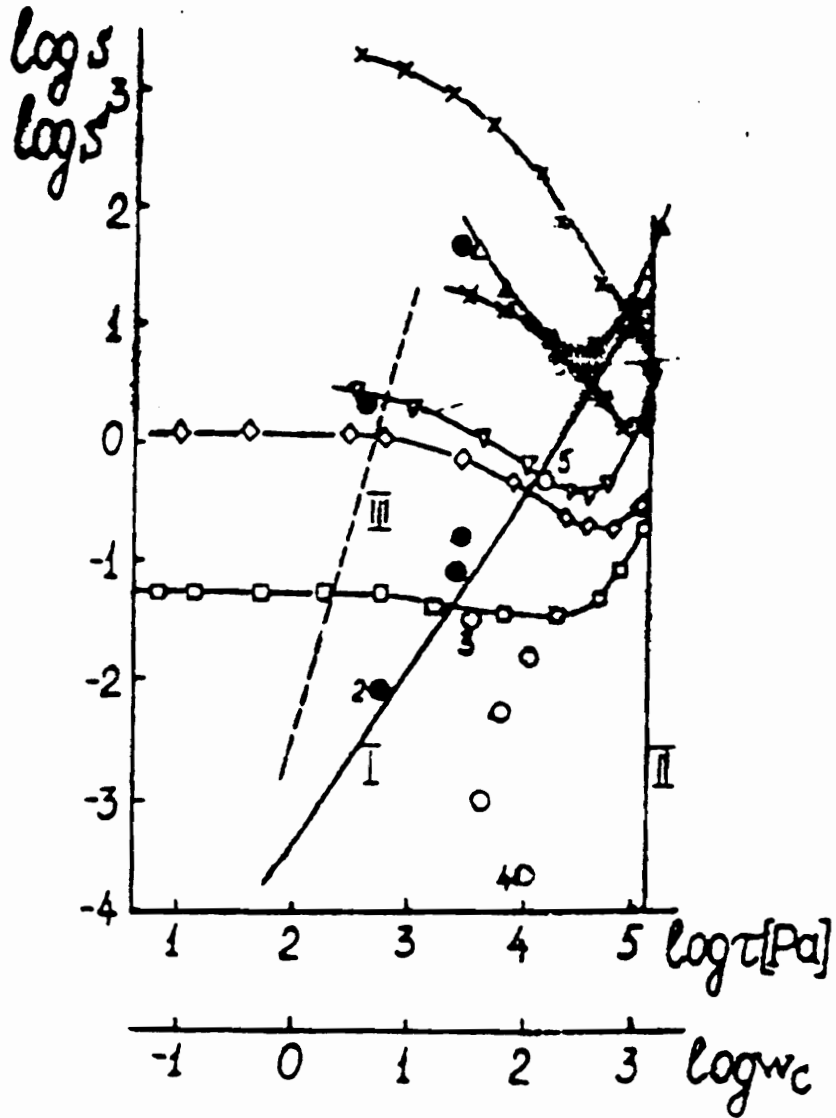
Figure 8. Viscosity ratio versus shear stress for PE/PS blends. Circles represent rotary viscometer data; open circles - fibril formation; closed circles - no fibril formation. Other symbols from capillary results (Fig. 7) [48].

Danesi and Porter (50) find in comparing blends of different polyethylenes and ethylene propylene terpolymer that the best dispersion occurs when the two phases have the same viscosity. Heikens et al. (51) report that in their study of polyethylene-polypropylene blends, the finest disperse phase morphology is attained when the matrix phase has a higher viscosity. A study (52) on the blending of polypropylene (PP) and polystryrene (PS) in a single-screw Brabender extruder with a Koch static mixer placed between the capillary and extruder was carried out to determine the influence of various parameters on the phase structure, i.e. morphology. The authors report that the viscoelastic properties of the individual phases do affect the morphology of the blends. Their experimental results were seen to be consistent with Vanoene's theory. In another study of PP dispersed in PS (55) extruded through capillary dies, it was observed that conditions that provided fewer possibilities of re-laxation (low ambient temperature at the outflow of the melt from the capillary, decrease in L/D ratio for constant D, increase in shear strain) all led to thinner PP fibrils arranged in the PS matrix.

Min et al. (53) report results on the development of phase morphology in incompatible polymer melt blends of polyethylene/polystyrene (PE/PS), polyethylene/polycarbonate (PE/PC) and polyethylene/nylon-6 (PE/N6). The blends were extruded through a 3/4-inch Brabender extruder with a Koch static mixer. Several results were obtained. The blends did not seem to corroborate Vanoene's argument, in that the first normal stress difference-shear stress re-lationships, N_1 vs. σ_{12}, did not show any specific correlation to either the coarseness of the morphology or the droplet-fibril transitions for the blend systems. It was also observed that fibrillar morphology of the dispersed phase was possible only if it had a lower viscosity than the medium phase. Further, the coarseness of the blends of N6, PC, and PS in PE were in the order N6 > PC > PS. This was attributed to the fact that the interfacial tension of PE/N6 > PE/PC > PE/PS. Figure 9 shows a schematic view of the longitudinal phase morphologies at various viscosity ratios.

Han et al. (56) studied the effect of mixing on the state of dispersion of PP/PS blends using a single screw extruder, with and without a static mixer (Kenics Corp. Thermogenizer) and a
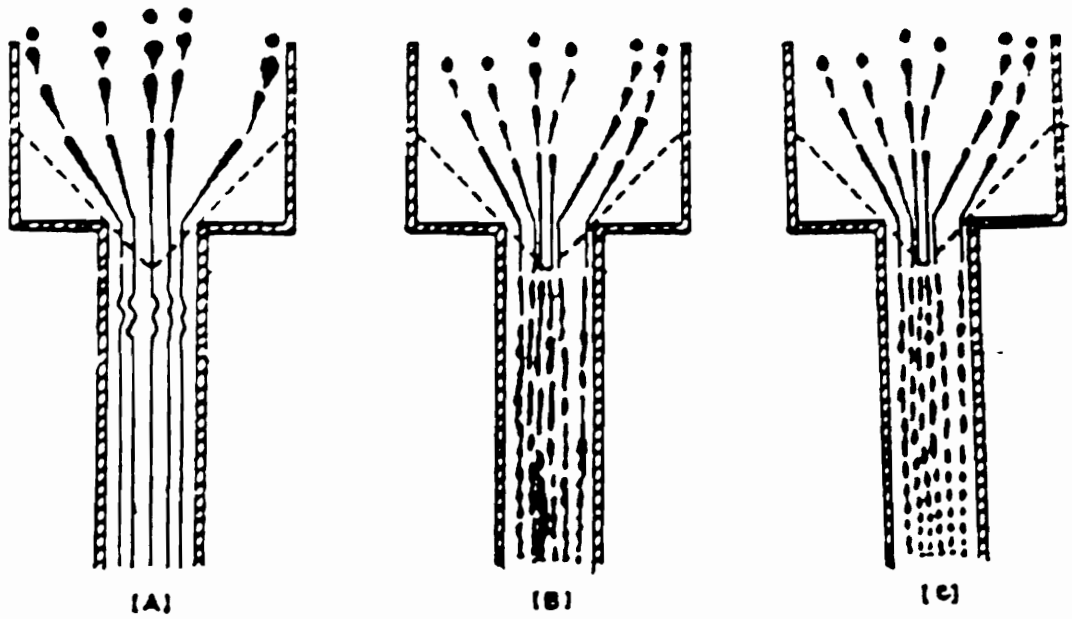
Figure 9. Schematic view of the longitudinal phase morphologies at various viscosity ratios (a) $\lambda < 0.7$ (b) $0.7 < \lambda < 1.7$ and (c) $\lambda > 2.2$ [53].

twin screw extruder. The extrudate was passed through a capillary die and the morphology examined. It was seen that the static mixer and twin screw extruder yielded droplets of PS in PP, whereas the single screw gave long fibrils of PS in PP. The droplets were attributed to the breakup of long fibrils of PS into smaller particles as the melt mixture passed through the static mixing elements. However, this would imply that fibrils of the PS were created not in the capillary die, but upon exit from the extruder. No clarification or speculation regarding this point was made. A more likely explanation for the observed results is that the high degree of mixing in the static mixer may have resulted in a very fine dispersion of the minor phase in the matrix. Deformation of these smaller drops to form fibrils is more difficult due to a lower Weber number and thus the minor phase remained as droplets in the final morphology.

A series of studies, more germane to this research, have been conducted by McHugh et al. (57, 58, 59) on fiber formation of crystallizable blends upon flow through capillary and slit dies. In their more recent study (57), the authors examined the rheological, morphological and thermal behavior of low concentration crystallizable binary blends in capillary flow under processing conditions conducive to the crystallization of the minor phase. Several HDPEs of different molecular weight and a standard grade PP were used as the minor or dispersed phase with a LLDPE as the matrix phase. The authors conclude that the most desirable matrix phase should have a lower melting point than that of the fibrillating component, and hence remain molten during extrusion. Further, the production of extended chain, and potentially reinforcing fibrils in capillary flow was observed to be enhanced by extrusion temperatures near the minor phase normal melting point and at flow rates below the onset of stratified radial morphology development. At temperatures well below the melting point of the dispersed phase, undistorted particles of the minor phase dominate the morphology as would be expected. However, at temperatures well above the melting point of the minor phase also, it was seen that spherical particles dominated the morphology and this was attributed to the retraction of the fully amorphous minor phase caused by relaxation of stresses upon exit from the die. It should also be mentioned that the authors had little success in correlating the observed morphologies with the rheological properties of the blends, and could not gain any

information regarding either the mechanism or kinetics of the fibril formation nor predict the presence or absence of fibrils from the rheological data. In a study of extrusion of the same polymer blend systems through a slit die (59), the authors note that formation of slender filaments of the minor phase occurs when the two phases have an interfacial tension approaching zero, thereby promoting high Weber numbers and thus high deformation. In contrast to other studies, however, the authors claim that for flow induced crystallization of the minor phase under shearing flow to occur, its viscosity must be greater than that of the carrier phase at the given shear rate conditions. For a lower minor phase viscosity, flow induced crystallization was seen to occur only in the converging section of the die, which was attributed to the large extensional component of the rate-of-strain tensor.

Several researchers have observed the phenomena of migration and encapsulation when dealing with two phase blends. Lee and White (60), for example, studied blends of PS with low density polyethylene (LDPE) and high density polyethylene (HDPE) extruded through capillaries, and concluded that in all cases there was a definite tendency of the low viscosity component to migrate towards the surface region. Berger et al. (54) report that the phenomenon of encapsulation is a consequence of the differences in elasticity (first normal stress difference) of the two phases. They observed that when the droplet phase is more elastic than the matrix, no inclusions are see. But when the droplet phase is less elastic than the matrix phase, inclusion of the more elastic matrix are observed in the droplet phase. Han (61), on the basis of his experimental studies of PS/HDPE blends, concluded that the interface shape was more strongly influenced by the viscosity difference rather than the elasticity difference of the two phases.

In a more recent study by Hobbs et al. (62), it is postulated that the morphology of multiphase blends can be predicted from the calculation of spreading coefficients which may be determined from a knowledge of surface and interfacial energies of the different phases. The results of their studies on a number of three and four component systems indicated that the morphologies are dominated by the relative abilities of the blend components to spread on one another. The authors, however, caution that the results be treated as preliminary due to

the fact that a number of approximations were involved in determining the surface and interfacial tensions.

2.5 Liquid Crystalline Polymers (LCPs)

A brief mention of LCPs was made in Chapter 1. However, it is crucial to review several important characteristics of LCPs in more detail, in order to bring the research goals into proper perspective. The forthcoming sections are, therefore, devoted to a discussion of LCPs and their unique properties.

2.5.1 Introduction to Liquid Crystals

The term liquid crystal signifies a state of aggregation that is intermediate between the crystalline solid and the amorphous or isotropic liquid. Liquid crystalline materials differ from other materials in that they exhibit more than a single transition in going from the solid to liquid state. These intermediate phases or "mesophases" possess a high degree of order, and yet do not have the periodic molecular three-dimensional lattice structure of crystalline solids. Instead the liquid crystals have only one or two dimensional order. It is due to this ordering in the liquid state that the liquid crystals exhibit anisotropy or direction dependent properties unlike isotropic fluids whose properties are the same in all directions.

Two types of liquid crystal (LC) mesophases are known to exist, viz. thermotropic and lyotropic. When transitions from the solid, through to the intermediate phases to the isotropic state are brought about by thermal processes then the LC is said to be a thermotropic LC (TLCP). If, however, the transitions are induced by changes in concentration and temperature then the LC is called a lyotropic LC. In the case of lyotropic LCPs, at very low concentrations,

the polymer solution is isotropic. As the concentration in increased, the viscosity increases

and goes through a maximum. The concentration at the maximum indicates the onset of liquid

crystallinity and the solution exhibits birefringence. Much of the activity is shifting towards

thermotropic systems due to some advantages outlined in the coming sections. Thus the re-

view that follows is directed with greater attention to thermotropic LCPs. Further, in this re-

search, only thermotropic LCPs will be considered.

Both thermotropic and lyotropic mesophases can be further classified, based primarily

upon their symmetry, into three major groups-the nematic, the cholesteric and the smectic

(70). Schematic representation of the above three groups is illustrated in Fig. 10 and described

below. The molecular order of nematic LCs is characterized by two distinct features; there is

long range orientational order, i.e., the molecules tend to align parallel to each other and

secondly there is no long range correlation of the molecular center of mass positions. Con-

sequently, the nematic mesophases possess only one dimensional order. They have a high

degree of mobility and are easily oriented by a variety of forces (71)- electric and magnetic

fields, mechanical stresses, temperature gradients and surface forces to cite a few.

In the case of cholesteric liquid crystals, as in the nematic phase, lack of long range

translational order imparts fluidity to the phase. On a local scale, the ordering of the nematic

and cholesteric phases is very similar. However, on a larger scale, the structure of the

cholesteric phase appears to be formed by twisting a series of parallel nematic layers, re-

sulting in periodic helical structure. The axis of the helix is perpendicular to the molecular axis

within each layer. When the distance between two planes with the same orientation direction

is comparable to optical wavelengths, the periodicity results in strong Bragg scattering of light

(69). If the wavelength of the scattered light is in the visible region of the electromagnetic

spectrum, the cholesteric phase appears brightly colored.

Smectic liquid crystals have stratified structures and a great variety of molecular ar-

rangements are possible within each stratification (70). Their molecular ordering is typified

by the fact that the molecules are oriented in one direction but with the centers of gravity of

the molecules arranged in distinct layers. The resultant two dimensional order of the smectic

A) SMECTIC

B) NEMATIC
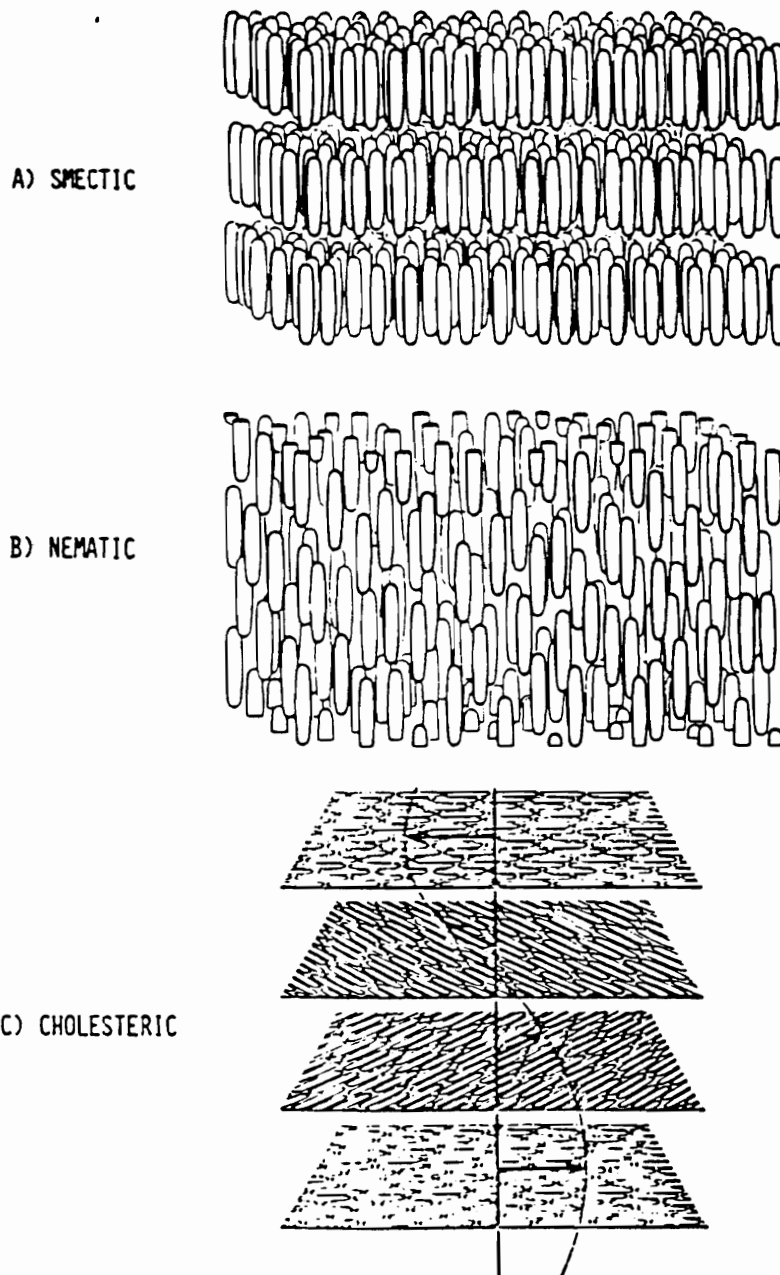
C) CHOLESTERIC

Figure 10.   Schematic of types of liquid crystal mesophase structures [108].

mesophase hinders molecular motion and is thus more viscous than either the nematic or cholesteric phases.

A variety of chemical structural units may result in the formation of a mesophase. An essential requirement for the formation of a mesophase is that the molecule be highly geometrically anisotropic, usually long and relatively narrow (i.e., high aspect ratio) (70). LCPs can be classified into four basic groups: rigid rod-like molecules, helical molecules and block-like molecules which may be either comb-like molecules or semi-flexible linear molecules. In the case of comb-like polymers, the mesogen appears as a pendant side chain attached to the main chain by flexible links. In the semi-flexible linear polymers, the mesogen appears as part of the main chain or backbone, the mesogenic units being linked by flexible spacers. The term "mesogenic unit" refers to the rigid chain segments in the backbone or side groups which determine whether or not the polymer will form a liquid crystal.

2.5.2 Rheology of Liquid Crystalline Polymers

The anisotropic structure of LCPs has led to anomalous rheological behavior, which is not yet completely understood. The rheological behavior of these systems is quantitatively and qualitatively different from that of their isotropic analogs (76). The quantitative difference is primarily evident as a low viscosity and long relaxation time compared to those of an isotropic polymer of comparable molecular weight and distribution. Qualitatively, LCPs exhibit several unusual phenomena. These include shear thinning at low shear rates, little or no extrudate swell despite high elasticity observed in small amplitude oscillatory deformation, transient negative normal stress difference and dependence of flow behavior on thermal and mechanical history (76).

The dependence of the rheology of LCPs on the deformation and temperature history leads to complicated microstructures during processing (73). The interdependence between material properties and morphology, in turn, results in properties that are often unpredictable.

Inspite of these apparent disadvantages, the interest in LCPs has spurred a tremendous amount of research in determining their rheological properties.

The purpose of this section is to bring forth some aspects of the rheological behavior of LCPs. Further, a review of the rheology with particular attention to the shear and temperature history dependencies will be presented. Once again much of the discussion will be limited to thermotropic LCPs as they are of direct interest to this research.

2.5.2.1   *General Flow Behavior of Liquid Crystal Polymers*

Although most discussions on the rheology of LCPs are centered around a three-region flow curve proposed by Onagi and Asada (74) as shown in Fig. 11, experimental evidence to support this hypothesis as being common to all LCPs is lacking. However, a brief discussion of the model is included for completeness. The flow curve consists of a shear thinning region at low shear rates (Region I) followed by a "pseudo-Newtonian plateau" region (Region II) and a second region of shear thinning (Region III). The existence of Region I flow behavior differentiates the rheology of these materials from that of random-coil, flexible polymers (73). The presence of a polydomain structure (Fig. 12), which gave rise to yield stresses when deformed at low shear rates, was believed responsible for the occurrence of Region I. As the shear rate is increased, it was proposed that this polydomain structure begins to break, forming a more uniform monodomain structure. The flow becomes shear rate independent corresponding to Region II. Further breakup of the monodomain at still higher shear rates leads to shear thinning in Region III. Although one or more of these regions have been identified for different LCP systems, a fair amount of controversey is still ongoing as to the existence of the three region flow curve and possible reasons for its occurrence. This is discussed by Wissburn (71) and Baird (75) for those interested in further reading.
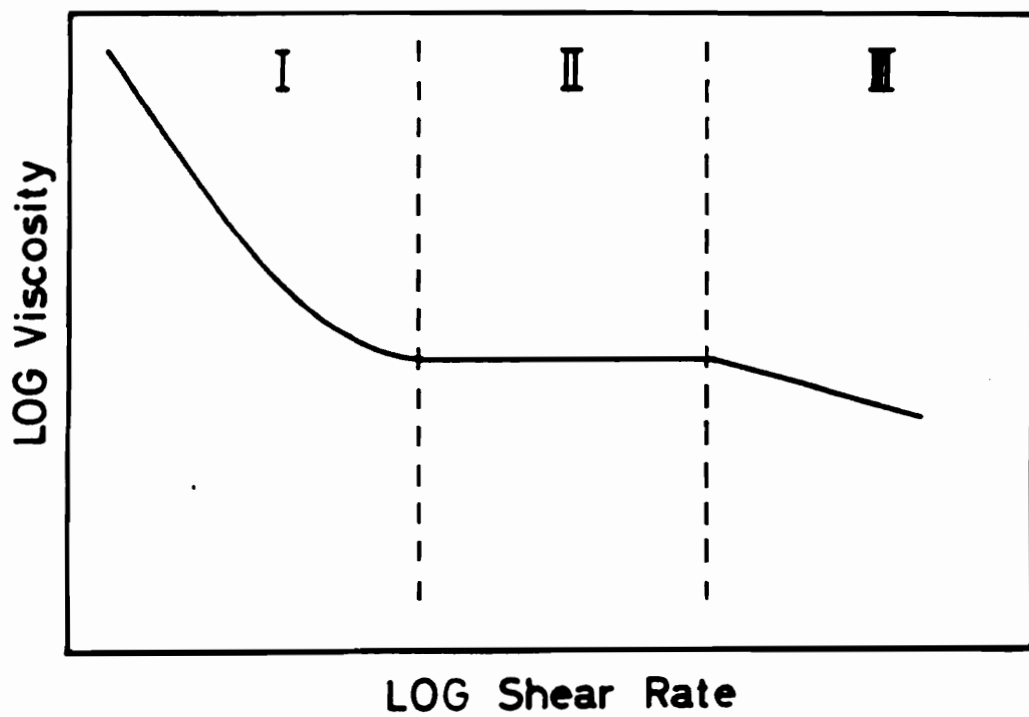
Figure 11. Three region flow curve proposed by Onogi and Asada [74].
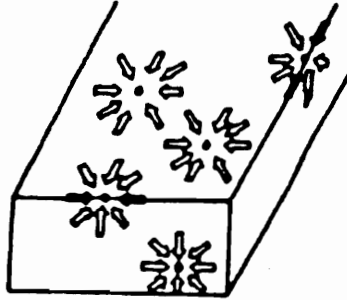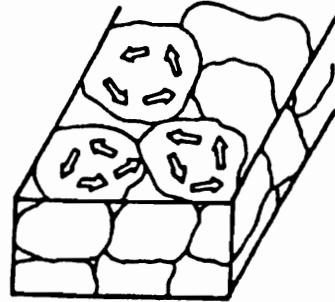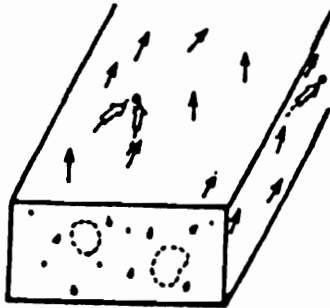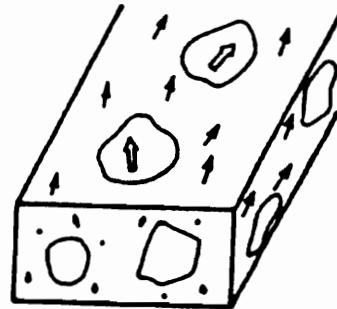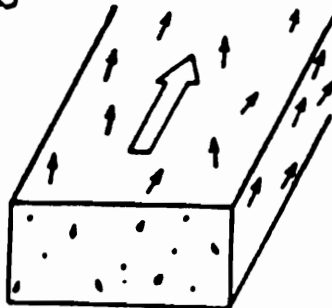
Figure 12.   Proposed structure corresponding to the three flow regions of Fig. 11 [74].

2.5.2.2 Viscosity Dependence on Shear-Rate

As mentioned earlier, rheological behavior of LCPs has been observed to be markedly different from flexible chain polymers in several respects (75,76). In particular, it has been observed that the viscosity of LCPs is dependent on the shear-rate over many orders of magnitude of the shear rate (71,73,75,76,77,78). An important consequence of the latter result is that at processing conditions, the viscosity of the LCP is likely to be several orders of magnitude lower than that of flexible chain isotropic systems (75). Several different systems have been reported to exhibit this shear thinning behavior; a copolyester of hydroxybenzoic acid (HBA) and poly(ethylene terephthalate) (PET) with a molar composition of 60/40 (75); a copolymer of HBA and 2,6-hydroxynaphthoic acid (HNA) in 73/27 molar ratio (76); a copolymer of terephthaloyl chloride and isophthaloyl chloride in stoichiometric ratios 0.75/0.25 and 0.9/0.1 (73) to cite a few. An example of this shear-thinning behavior for a 60 mol % PHB/PET copolyester is shown in Figure 13 [75]. Clearly, the viscosity decreases with increasing shear rate over nearly 5 orders of magnitude, starting from a shear rate of 1/sec. In the high shear rate range, the viscosity appears to reach a limiting value called the infinite shear viscosity, η_∞, of about 0.6 Pa.s.

The shear rate at which a polymer begins to exhibit shear-thinning behavior is related to a characteristic relaxation time for flexible chain polymers (81). Onset of shear-thinning behavior at low shear rates indicates long relaxation times. Baird (75) has shown for the 60 mol % PHB/PET copolyester that although the stresses relax in a matter of few seconds, the orientation and texture take long times (order of minutes) to relax. Wissburn (71) has reported that the relaxation time of the 60/40 PHB/PET copolyester at 280°C is about 1000 times that of homopolymeric PET (which is isotropic). A comparison of relaxation times of a rigid rod- like LCP and a flexible chain polymer such as PET may not be very meaningful. A more suitable comparison would, of course, be the relaxation times of an LCP in its anisotropic and isotropic melt states. However, such a comparison is made difficult by the fact that very few thermotropic LCPs to date have a nematic-isotropic transition temperature for which the
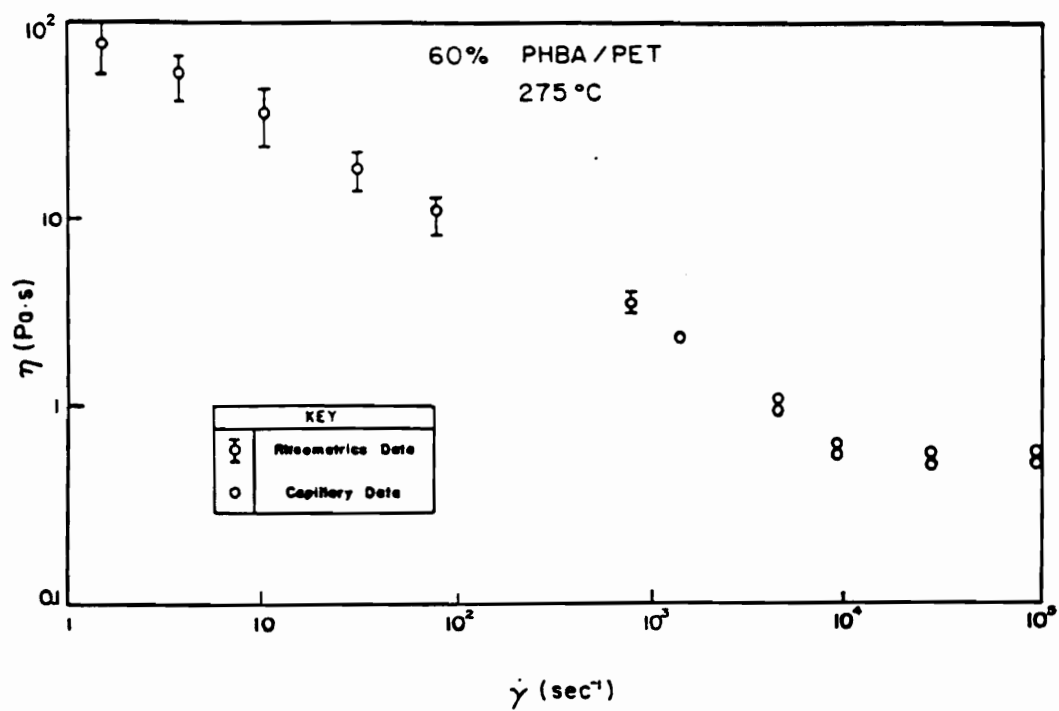
Figure 13. Viscosity versus shear rate for 60 mol % PHB/PET obtained from cone-and-plate and capillary rheometers [75].

isotropic state is thermally stable. It is important to realize that the consequence of a large relaxation time of orientation and texture is that orientation of the LCP that is developed during melt processing, may be retained in the solid state upon cooling provided that the relaxation time is longer than the processing time scale involved. This is an inherent advantage associated with the processing of LCPs.

Tuttle et al. (73) report for a copolymer of terthaloyl chloride and isophthaloyl chloride in stochiometric ratio of 0.75/0.25, that the isotropic melt showed mainly Newtonian behavior whereas the nematic state shear thinned. Similar results on some low melting polyesters have been reported by Wissburn and Griffin (82). Blumstein and coworkers (83) found that although both the nematic and isotropic melts shear thinned in the range of shear rates studied, the nematic melt showed a greater degree of shear thinning behavior than the isotropic melt.

2.5.2.3 Plateau viscosity

Another interesting phenomena in the rheology of most thermotropic and lyotropic LCPs is that the viscosity of the liquid crystalline material is lower than that of the corresponding isotropic melt or solution (71). In the case of lyotropic LCPs, the viscosity does not increase monotonically with concentration, but goes through a maximum. The concentration at the maximum corresponds to a change from the isotropic to the anisotropic phase. This behavior, for example, has been observed in solutions of poly-p-phenylene terephthalamide (PPT) (79) and poly-p-benzamide (PBA) (80), and is considered to be a general trend in lyotropic LCPs.

In the case of thermotropic LCPs, the transitions between different phases are a consequence of changes in the temperature. Only a limited number of studies of thermotropic LCP (TLCP) systems via rheological techniques appears in the published literature . However, it is generally observed that as the TLCP goes from the nematic to isotropic transition, it's viscosity increases, leading to a maximum, as the viscosity again decreases with temperature

in the isotropic melt (84). Usually, the nematic to isotropic transition in polymeric liquid crys-
tals occurs over a wide temperature range and this is attributed to the distribution of molec-
ular weights and the fact that a variety of structural possibilities with long-range order exist
(84). It is interesting to note that such a maxima in viscosity versus temperature has not been
observed with all systems. For example, Bickel (85) reported no increase in viscosity at the
nematic to isotropic transition. It is likely that the increase in viscosity at the nematic-isotropic
transition was offset by a decrease in viscosity with increased temperature. White and Fellers
(86) on the other hand, observed that TLCP melts of hydroxypropyl cellulose (HPC) decreased
in viscosity from 160 C to 190°C. then increased between 190°C and 210°C, which corresponded
to the onset of the isotropic phase as determined by a loss of birefringence in that temperature
range. Simoff and Porter (87) also report a similar decrease in viscosity from their studies of
poly(bisphenol E isopthalate-co- naphthalate) BPE/I/N copolyester with a composition of
50/40/10. The semicrystalline-nematic transition occurred around 284°C. The viscosity was
seen to decrease with increasing temperature till 310 C and then increased with further in-
crease in temperature. This is shown in Figure 14. Again, the increase in viscosity was attri-
buted to a gradual transition from the nematic to isotropic state. Kiss (84) has reported an
anomalous temperature dependence of viscosity in a copolymer of hydroxybenzoic acid (HBA
or PHB), isopthalic acid (IA) and hydroquinone (HQ) in that the lower melting compositions
exhibit viscosity increase with temperature over a wide range of temperatures, starting from
the melting point of the polymer. This anomaly was suggested to be due to the existence of
a biphasic melt consisting of both isotropic and anisotropic states.

It is clear from the above findings that LCPs exhibit a shear rate dependent viscosity over
several orders of magnitude of the shear rate. Further, they appear to possess longer relax-
ation times of orientation and texture than comparable isotropic polymers. An important con-
sequence of a long relaxation time is that the orientation developed during flow can be
retained upon solidification. Also, the time for stresses to relax is much faster than would be
expected on the basis of a relaxation time determined from the flow curve or the time for re-
laxation of orientation. Some thermotropic LCP systems have also been shown to exhibit a

maximum in the viscosity versus temperature relationship. This maximum in viscosity occurs at the nematic to isotropic transition temperature. It was mentioned earlier that the rheology of LCPs is history dependent. Thus a discussion of this behavior is presented in the following section.

2.5.3   History Dependence

To understand the rheological behavior of LCPs more completely, it is imperative to study both the shear and temperature history dependencies in detail. The relative importance of this history dependence is apparent from the fact that a number of researchers in the past few years have devoted considerable time and effort towards achieving a more robust understanding of this phenomena (78,88,89,92). It is important that one appreciates the ramifications of the effects of thermal and deformation histories on the rheology and morphology of the LCP. Once again no exhaustive review of the subject is contemplated. However, some unique properties of the LCPs, which lend a certain direction to their processing possibilities, will be discussed in depth. This section is broken up into two major sections, one dealing with the thermal history and the second with the deformation history dependence.

2.5.3.1   Thermal History Dependence

Some extensive studies on this subject have been conducted by Done (88) and Done and Baird (89) who studied thermal and deformation history effects on three different LCP systems; a copolyester of 60/40 PHB/PET, a copolyester of 80/20 PHB/PET and a copolyester of PHB (or HBA) and 2- hydroxy-6-naphthoic acid (HNA) commercially known as LCP2000. All the above materials were subjected to small amplitude dynamic shear, steady shear and transient experiments using the cone-and-plate geometry mode of the Rheometrics Mechanical
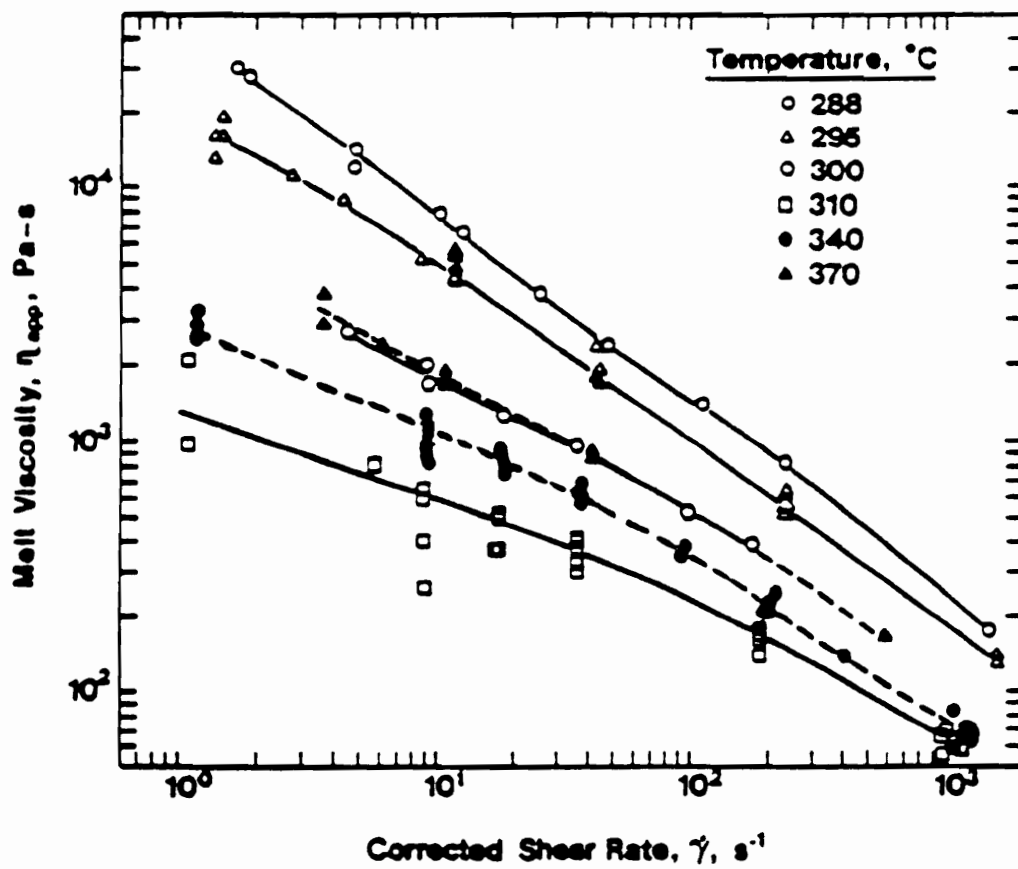
Figure 14. Viscosity versus shear rate at different temperatures for BPE/I/N copolyester [87].

Spectrometer (RMS). Two different thermal histories were used; one was to heat the pellets from room temperature to the desired test temperature and the other was to heat pellets to a higher (preheat) temperature and then drop the temperature rapidly to lower test temperatures. The dynamic viscosity of the melt preheated to a higher temperature was observed to decrease significantly as compared to the dynamic viscosity at the same test temperature but without preheating to the higher temperature, although by different extents, for all the three materials tested. Figure 15 shows a representative example of the results of this test for the 60/40 PHB/PET material. Isothermal time sweeps were also conducted on all the materials at their preheat temperatures. The possibility of degradation leading to a drop in viscosity after preheating was ruled out because the storage modulus, G', remained essentially unchanged after about 20 minutes. It was thus concluded that the decrease in rheological properties upon cooling the melt from higher temperatures was not due to degradation but more likely due to "supercooling" of the nematic state.

Another important test performed was to measure the small strain dynamic properties of the melt upon cooling from a temperature much higher than the normal melting point. Figure 16 shows the storage modulus, G', plotted against temperature during cooling from temperatures higher than the flow temperatures for the three materials mentioned earlier. It is observed that the value of G' is nearly constant for the 60/40 PHB/PET and 80/20 PHB/PET down to temperatures of about 200°C and 275°C, respectively. The LCP2000, however, showed a continuous rise in G', rising more abruptly around 220°C. These results demonstrate that it is possible to deform the melts at temperatures as much as 50°C below the normal melting point.

Done and Baird (158) in a more recent paper report on a fairly comprehensive investigation on the solidification behavior and recovery kinetics of three LCPs, 60/40 PHB/PET, 80/20 PHB/PET and Vectra A900. Their findings are particularly germane to this study. Cooling tests at a rate of 5°C/min as described above for the three materials were conducted from 330°C. It was observed that the way in which G' increased with decreasing temperature for the three LCPs was quite different. The 60/40 PHB/PET polymer showed G' increasing very gradually
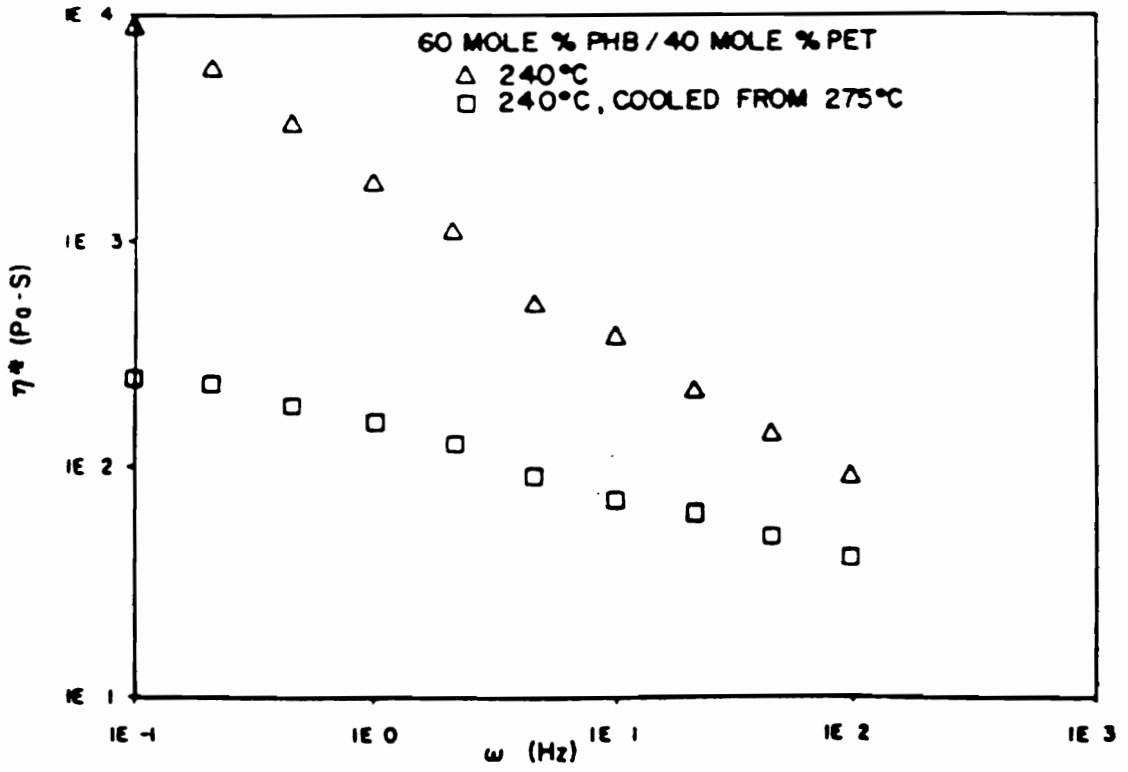
Figure 15. Dynamic viscosity vs. frequency for the 60/40 PHB/PET samples with different thermal histories [89].
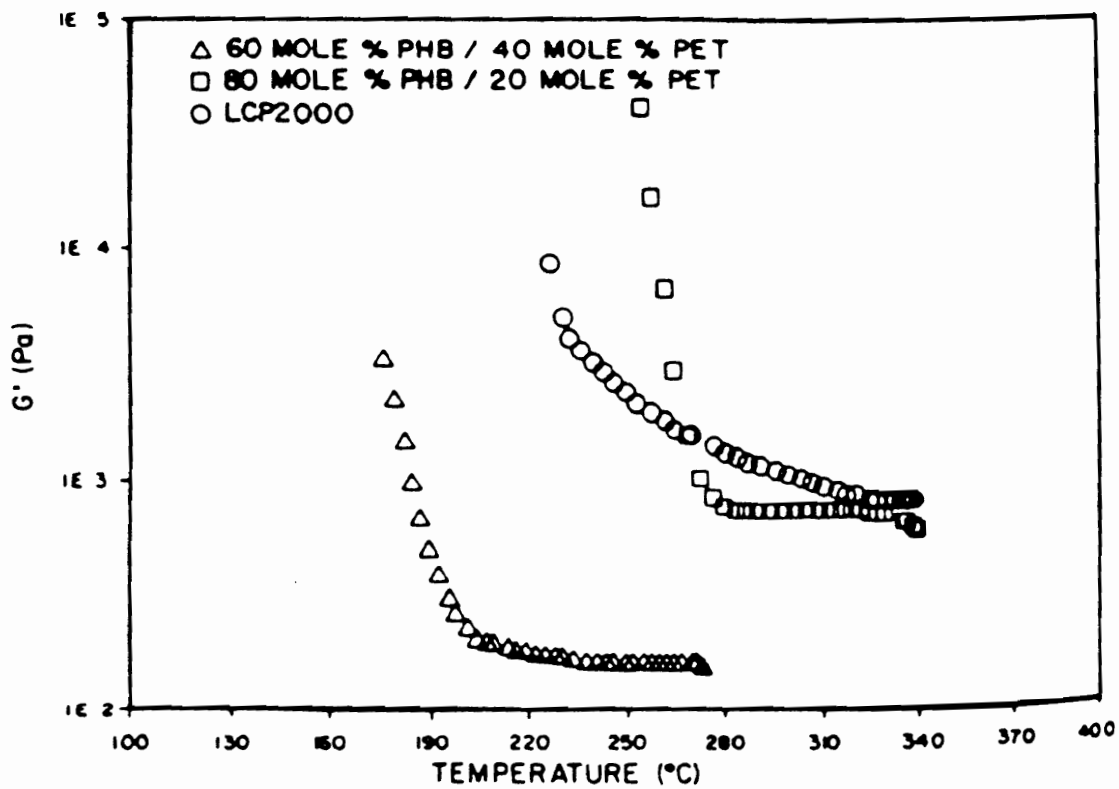
Figure 16. Storage modulus, G', vs. temperature during cooling from temperatures higher than flow temperatures, measured at strain amplitude of 5 percent [89].

until 210°C and then a more rapid rise at temperatures below that. The 80/20 PHB/PET on the other hand exhibited G′ that was unchanged at high temperatures and then increased very rapidly as the solidification temperatures was approached. For Vectra A900, G′ increased continuously until the solidification point was reached. The degree of supercooling for the above LCPs was 85°C, 20°C and 50°C, respectively. From isothermal time sweeps conducted at various temperatures below the respective melting temperatures, it was observed that induction periods during crystallization were present for only the 60/40 PHB/PET and Vectra A900 polymers. The lack of an induction period with the 80/20 PHB/PET was attributed to the rapid crystallization of the PHB-rich phase. The authors further note that the solidification in each of the cases was due to both crystallization as well as freezing of the mesophase. The degree of crystallinity in each case was low, less than 5 % as measured by DSC. Finally, the authors conclude that from a processing standpoint, the 60/40 PHB/PET and Vectra A900 are more suitable in processes such as blow molding and film blowing than the 80/20 PHB/PET system.

A study conducted by Wissburn (78) on the 60/40 PHB/PET copolyester (prepared in his laboratory by the method of Jackson et al. (99)) also found significant effects of thermal history on the viscosity behavior of the polymer. The polymer, in these experiments, was melted in the capillary rheometer at high temperatures (240°C and 300°C) and then cooled to 210°C. which took about 15 minutes. The results of the experiments are shown in Figure 17. Preheating to 240°C lowers the viscosity considerably relative to the viscosity measured at 210°C directly without any prior preheating. However, on preheating to 300°C, one observes that there is a quantitative and qualitative change in the flow curve. The shape of the flow curve changes from solid-like at 210°C to a typical viscoelastic one upon preheating to 300°C. Degradation being responsible for this behavior was ruled out by the fact that the inherent viscosities (IV) of the samples measured after the heat treatment were relatively unchanged. The presence of a small degree of PHB crystallinity in the case of no preheating, and the relative absence of crystallinity (as determined by WAXS and DSC) in the preheated samples led the author to believe that crystallinity may have been responsible for the observed behavior.
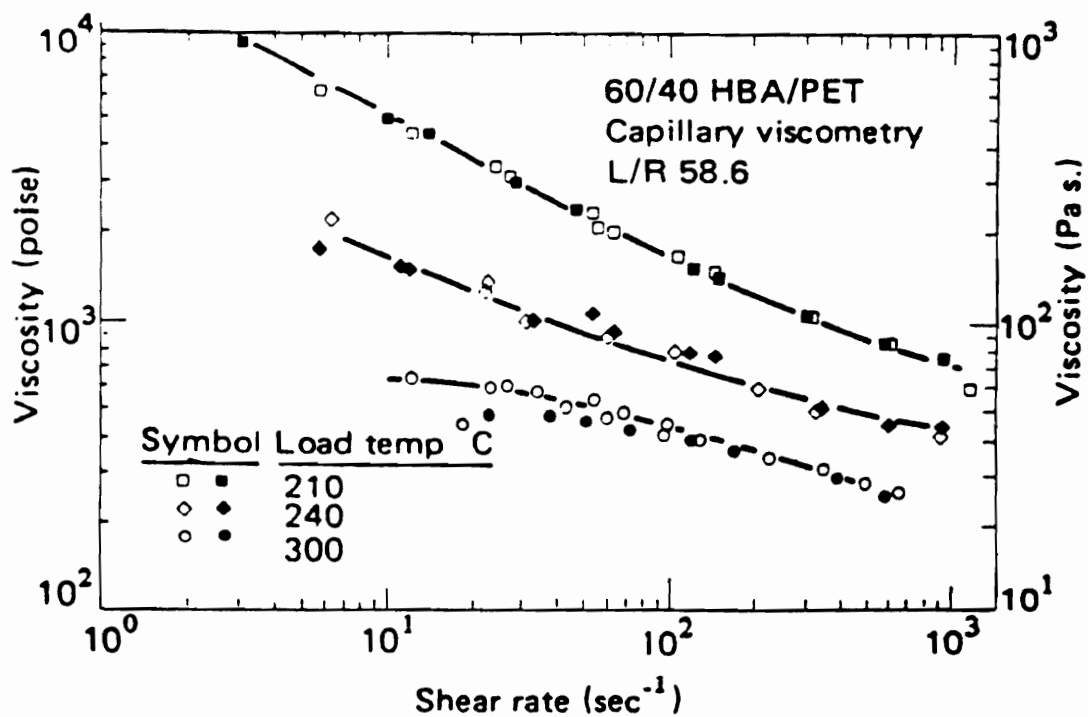
Figure 17.   Effect of preheating on the viscosity of 60/40 PHB/PET copolyester [78].

Lin and Winter (92) also report on effects of crystallinity on the rheology for a copolyester of HBA/HNA 73/27 (commercially known as Vectra A900). Isothermal time sweeps at different temperatures indicated a rise in storage modulus with time. WAXS and Differential Scanning Calorimetry (DSC) results indicated that this behavior was due to the presence of HBA crystallinity. Furthermore, the authors observed that after preheating to 320°C, the melt of Vectra A900 shows relatively stable rheological properties over long times at temperatures above the melting temperature. However, if the same polymer was annealed at temperatures slightly above the melting point without any prior heating to elevated temperatures, a notable growth in the complex modulus and relative elasticity were observed. This latter observation was attributed to the formation of high melting crystals with improved order which was confirmed by WAXS and DSC experiments. It is of interest to note that the stabilizing effect of preheating to 320°C was attributed to the melting of all residual crystallites which were otherwise believed to play the role of nuclei of the crystallization above the melting temperature. The authors conclude that the crystallization of Vectra A900 under these conditions is likely by a two step mechanism, nucleation and growth. The nucleation rate is lower than the growth rate. After preheating to 320°C, the crystallization process was believed to be inhibited by the lack of nuclei. The increase in the value of G' with time could be reversed by increasing the temperature above the melting point of the high melting HBA crystallites which further gave support to the fact that the observed phenomena was due to physical and not chemical changes in the LCP. Wissburn (82) similarly observed that heating a thermotropic LCP above its nematic-isotropic transition temperature erased all previous shear history effects.

A very similar study as conducted by Lin and Winter above was reported recently on LCP80 (155) yielding qualitatively similar results as those seen for Vectra A900 above. Again, isothermal time sweeps conducted at 300°C, 310°C and 320°C showed a rapid rise in the complex viscosity at 300°C but much slower rise at 310°C and even slower rise at 320°C. Furthermore, after 2 hours at 300°C. the entire observed increase in the rheological parameters were erased by briefly heating the material to 320°C. However, upon returning to 300°C, the material once again exhibited strongly increasing rheological parameters with time unlike the Vectra

A900 case discussed above. This behavior was explained by the presence of crystallites of pure PHB which persist to temperatures above 320°C. In fact, these crystallites were observed to melt completely only above 328°C (106). The authors rightly note in their conclusion that although the transients associated with crystalline aging are unlikely to be of any consequence over the flow times characteristic of typical processing operations, the kinetics of the crystalline melting could still be relevant (155). For example, Lin and Winter (156,157) in another series of studies with Vectra A900 in the supercooled liquid state point out that the degree of molecular orientation that may be retained in a sheared sample depends largely on the competition between the ability to induce molecular orientation and the rate of structural relaxation, both of which in turn are restricted by crystallization in the supercooled melt. The authors thus observed that at temperatures above or slightly below the melting temperature, the sample deforms quite readily but this strain-induced orientation also relaxes quite rapidly (tens of seconds). However, as the degree of supercooling (Tm-T) was increased, the sample could only deform during the initial time period although a higher degree of molecular orientation could be retained due to the fact that rapid crystallization hindered the structural relaxation in the supercooled nematic liquid state. In another study, Cogswell (90) reported that the flow behavior of a thermotropic polyester changed from that of a paste- like solid at 223 °C to that of a viscoelastic liquid upon preheating to 240°C. Further, the preheated sample exhibited a highly oriented fibrillar morphology upon extrusion. This was attributed to the supercooling effect of the nematic state.

Viola et al. (91) studied the effects of thermal history on the viscosity, die swell and morphology of the 60/40 PHB/PET copolyester. A capillary rheometer was used in their experiments and two different conditions were investigated. In one case, both the barrel and the capillary were held at the same temperature and in the other case the barrel was held at a higher temperature than the capillary. Thus the melt upon extrusion (shearing) was being cooled in the second case. It was observed that the viscosity was lower in the first case and was attributed to the possible formation of a nematic state at the higher barrel temperature.

It was further observed that shearing while cooling (second case) changed the morphology of the sample and yielded a more fibrous texture than the first case.

In summary, several important points regarding the effects of thermal history need to emphasized. It is obvious from the above that thermal history can have a pronounced effect on the rheology and morphology of thermotropic LCPs. The supercooling phenomena has been shown to occur for a number of systems and lends itself as a powerful tool in processing a LCP at temperatures below the melting or solidification temperatures. The presence of crystallinity was also shown to have a drastic effect on the melt rheology. Preheating LCP melts to temperatures much above their melting points results in relatively stable rheological behavior for several hours. However, if the sample is just melted and kept a little above its melting temperature, without prior heating to an elevated temperature, the melt displays a severe increase in the complex modulus (92). Lastly, it is possible to remove all prior thermal history of a LCP sample by heating it to a temperature above its liquid crystalline-isotropic state transition temperature.

2.5.3.2   Shear History Dependence

Several workers have studied the effects of shear history on the rheology of LCPs. Wissburn and Griffin (82), for example, report a substantial decrease in the complex viscosity of a thermotropic LCP with increase in preshear rate as shown in Figure 18. This depend- ence of viscosity on the shear history was explained by the polydomain assumption proposed by Onogi and Asada (74). Similar studies by Cogswell (90) on a 20 weight percent solution of poly-p- phenylene terephthalamide (PPT) in concentrated sulphuric acid, showed that the viscosity was reduced by several orders of magnitude upon preshearing at 200 sec^{-1}. Further, the lyotropic system changed from a paste-like state to a low viscosity state and could be readily drawn into fibers. Qualitatively similar results were also obtained for a

thermotropic polyester, in that preshear changed the extrudate from paste-like to one with uniform and high orientation.

In addition to steady shear and dynamic tests, some transient behavior studies such as stress growth and relaxation have also been reported. Cogwell (93) reported the effect of preshear on the stress growth of a thermotropic LCP. The melt was presheared at 0.04 sec^{-1} until a steady state response was reached. The flow was then stopped and the stress allowed to relax below 200 Pa, which took a few minutes, and then shearing restarted at the same shear rate. The stress was seen to climb back immediately to its previous equilibrium value. However, if a much higher preshear rate of 1.14 sec^{-1} was applied, and the procedure repeated, it was observed that there was significant initial overshoot of the stress before returning to the prior equilibrium value. The difference in the stress growth behavior was attributed to the reorganization of texture due to the two different preshear rates. Cogswell explained that relaxation to an equilibrium domain structure was fast enough after shearing at the higher rate that this structure had to broken up again upon startup, resulting in the overshoot peak. The transient shear tests by Baird (135) have indeed shown that relaxation is faster upon cessation of shear with an increase in shear rate. Cogswell thus suggested that a range of rheological responses at a given shear rate are possible, depending on the shear history of the material.

In summary, it is seen in general that preshearing reduces the viscosity of the material, the magnitude of reduction increasing with an increase in the rate of preshearing. Although some of this behavior may be explained in terms of a change in the orientation and texture of the LCPs, the presence of residual crystallinity in the materials is very likely to add to the complexities making any definitive conclusions improper.
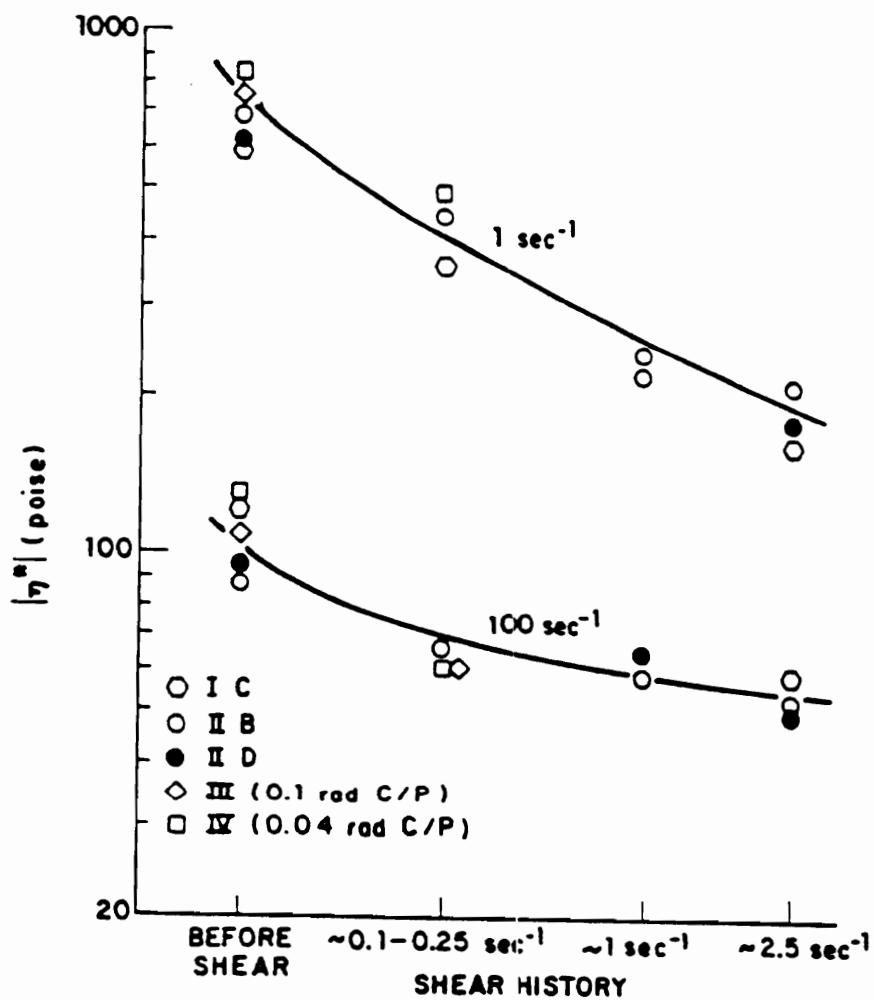
Figure 18. Effect of preshear on the dynamic viscosity of a thermotropic LCP [82].

2.5.4 Processing of Liquid Crystalline Polymers

LCPs are claimed to be one of the most promising class of polymeric materials due to the unique combination of properties they offer to the end user (94). An impressive list of such advantages includes low melt viscosity, fast cycle times, very low mold shrinkage/warpage/sinking, excellent mechanical properties, good solvent resistance, low flammability, high continuous use temperatures, low thermal expansion, excellent barrier properties and low water absorption (93,100). Attention in recent years has shifted from lyotropic to thermotropic LCPs mainly because thermotropic LCPs offer some processing advantages over lyotropic LCPs. Processing of lyotropic LCPs typically involves the use of toxic or corrosive solvents. Further, their processing has been limited to producing spun fibers. On the other hand, thermotropic LCPs can be processed without the use of secondary agents with the added advantage that they can be processed by other methods such as injection molding, film blowing, melt spinning etc. Some examples of processing of LCPs are given below with a view to highlight the properties that may be attained and also to emphasize the processing parameters involved.

Much of the potential of LCPs, both thermotropic and lyotropic, has so far been realized only in the formation of highly oriented fibers of ultra-high modulus and strength (95). This has been possible because of the fact that LCPs can be very highly oriented during flow and much of this orientation is retained in the solid state. Similar superiority of mechanical properties is also possible from solid-state or solution processing of flexible polymers such as polyethylene (PE), which do not form mesophases (95). Their processing from LCPs differs in that significant draw of the fiber is needed and the ultra-drawing methods are more complex. Table 1 shows a comparison of fiber strengths and moduli of some typical high performance fibers (105). The SPECTRA 900 fibers are the extended chain PE fibers manufactured by Allied-Signal using a specialized spinning process, whereas the SNIA fibers are also PE fibers made by Celanese using a special drawing process Although the method by which the LCP

fibers were prepared was not specified, it is clear that the properties of LCP fibers are quite comparable to those of PE made by rather elaborate and complex methods.

The effect of processing variables on orientation and mechanical properties of melt spun thermotropic LCPs has been studied by several authors (77,95,98,101,102,103). Muramatsu and Krigbaum (102) report their results on fiber spinning of the 60/40 PHB/PET copolyester from the melt. The orientation (as determined by Wide angle X-ray diffraction or WAXS) was observed to be better in the crystalline phase when the fibers were spun at a temperature of 260 °C or higher, where essentially no PHB crystallites remained. In another study by the same authors (103), the authors found that the initial modulus increased with increasing temperature, for a given spin-draw ratio. This is illustrated in Figure 19.

Zachariades and Logan (106) investigated the orientation and mechanical properties of 80/20 PHB/PET copolyester films prepared by rotational molding and fibers prepared by melt drawing. The molded films were prepared by forming a melt between a plate-plate rheometer, compressing the melt to a given thickness in the 120-160 μm range and finally shearing the melt as it was being cooled. It was observed that the mechanical properties for both the films and fibers varied considerably with respect to the molding or extrusion temperatures. Results from these experiments are summarized in Table 2 Clearly, there is a significant enhancement in properties of both the films and fibers processed at 330°C as compared to those processed at lower temperatures. This difference was explained on the basis of the fact that above 328°C, the domains broke down under shear or elongational flow to form uniform fibrillar structures. Below this temperature only physical alignment of the unmelted and undeformed PHB rich domains was believed to occur resulting in lower properties.

Sugiyama et al. (77) reported on the melt spinning of the 60/40 PHB/PET copolyester. Without belaboring on too many experimental details, they found that the orientation (measured by WAXS and determined by Herman's orientation function, f_H) increased with increase in temperature from 230°C to 280°C with no draw. Since no draw was imposed, the authors concluded that all the orientation was developed in the capillary itself. In contrast, Acierno et al. (95) found that for the same system, the tensile modulus decreased with temperature.

Table 1. Comparison of fiber strengths and moduli of some typical high performance fibers [105].

	SPECTRA 900	SNIA‡	ARAMID	LPC‡‡
Tenacity (G/D)	30	13	22	22
Tensile Strength (10 × 3 psi)	375	163	400	358
Tensile Strength (GPa)	2.6	1.2	2.8	2.5

‡ Special drawing of PE.
‡‡ Vectran liquid crystal fiber.

	SPECTRA 900	SNIA	ARAMID	LPC
Tensile Modulus (G/D)	1400	700	1000	600
Tensile Modulus (10 × 6 psi)	17	8.5	19	9.0
Tensile Modulus (GPa)	117	58	124	60
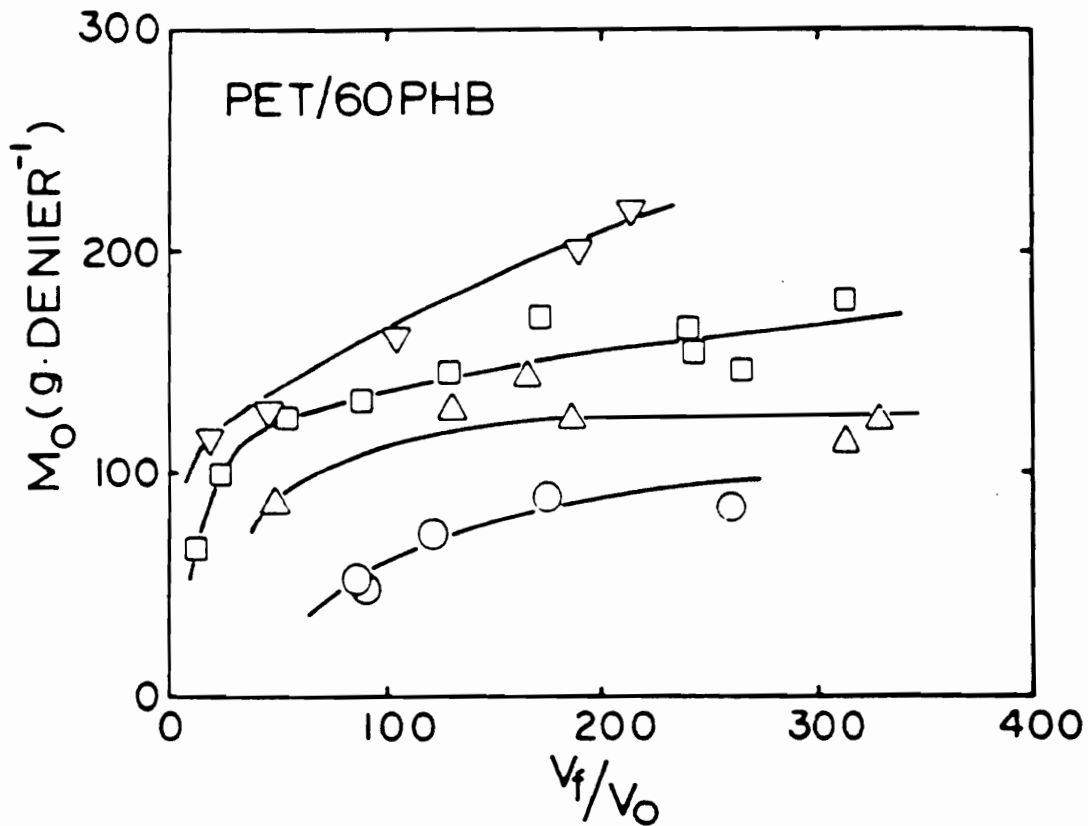
Figure 19. Young's modulus vs draw ratio for fibers spun without preheating at different temperatures: 250 C (o), 260 C (Δ), 280 C (□), and 300 C (∇) [103].

Table 2. Mechanical properties of 80/20 PHB/PET copolyester oriented films and melt drawn fibers [106].

Sample	Young Modulus (GPa)	Tensile Strength (MPa)	Elongation at Break (%)
Film oriented from melt heated at 305°C	4	104	5
Film oriented from melt heated at 330°C	19	218	9
Fiber drawn at 300°C	5	115	5
Fiber drawn at 330°C	40	225	8

Specifically, the highest value of the modulus was found at 225°C and the value at 285°C was a tenth of this. It has been suggested (104) that the contradicting results of Acierno et al. (95) with those of Sugiyama (77) and Lewis and Fellers (104) is due to the lower extrusion rate used by the former. However, for each temperature studied, they (95) reported an increase in modulus to some asymptotic value with an increase in take-up speed or draw ratio.

Chung (101). reporting results on fiber extrusion of a different system, found that only a marginal increase in f_H significantly increased the initial tensile modulus. Lewis and Fellers (104), in a recent review, concluded that the extrusion temperature was the most effective way to enhance the level of orientation. They also observed with melt spinning of 60/40 PHB/PET filaments that the level of orientation, i.e., f_H, decreased with increase in extrusion rate, at a high constant drawdown ratio, suggesting that shear flow was not very effective in the orientation of the 60/40 PHB/PET copolyester. They thus concluded that a higher orientation was possible at lower shear rates. These results are quite surprising in view of the fact that the opposite result might normally be expected. A closer inspection of their processing conditions reveals that the temperature range used by the authors was only 240°C- 270°C. It would seem then, as suggested by Zachariades and Logan earlier (106) for their own studies, that the low temperatures may not have been successful in removing the crystallinity completely which would consequently hinder the orientation of the LCP. Further, they also did not find any significant effect of the draw ratio on the Herman's orientation function, f_H. This was taken to imply that much of the orientation was developed within the die and that upon drawing, the elongational flow field outside the die, had little effect on the orientation. These results are also surprising and contrary to our expectation. Results of Muramatsu and Krigbaum (102) discussed earlier for the same system indicated that the orientation was better when the fiber spinning was carried out at 260°C or higher. This might again explain the anomalous results of Lewis and Fellers (104).

With growing awareness of the unusual properties of LCPs, two other areas have been gaining attention in recent years; injection- molding of LCPs and reinforcing of thermoplastics with LCPs. Injection-molding of thermotropic LCPs offers one avenue to attain high modulus

in the longitudinal direction in relatively thick profiles (96). However, it is often observed that the properties of injection molded plaques are anisotropic i.e., they are different in different directions. Typically the properties in the orientation or machine direction are exceptionally high but very poor in the transverse direction (99). A further problem with injection molding is the fact that often times a skin-core morphology has been observed (97,98). A high orientation in the skin layers was attributed to the fountain-flow effect at the advancing front, due to the presence of extensional flow fields. The core, on the other hand, was found to be relatively unoriented.

Although LCPs typically do exhibit superior mechanical properties relative to conventional thermoplastics, there are certain disadvantages associated with their processing. As mentioned before, LCPs are characterized by their low melt viscosities. An adverse effect of this phenomena is that LCP melts tend to have little or no melt strength making certain types of processing such as sheet and fiber extrusion and film blowing difficult. In Fig. 20 is plotted the melt strength as a function of temperature of a copolyester of 2,6 hydroxynaphthoic acid, terepthalic acid and aminophenol manufactured by Celanese and commercially known as Vectra B950 (107). It is not quite clear how the melt strength was determined. However, the units appear to be those of force (Newton). This material was characterized by DSC and it was shown that the nematic phase is formed around 290°C. Below this temperature a biphasic melt is supposed to exist and only above 300°C is the transition to nematic state complete. One observes the tremendous drop in melt strength as the polymer begins to undergo the crystal-nematic transition. At temperatures well into the nematic state, the melt strength has dropped 10 fold from the semicrystalline state. It is clear from this why processing of TLCPs alone at very high temperatures is favorable. Further, they are much more expensive than conventional thermoplastics and this reason has probably been responsible for the rather slow commercialization of LCPs. Some of the above problems have been circumvented by using LCPs to reinforce engineering thermoplastics, adding the advantages of superior properties and avoiding certain processing problems and higher costs involved with using LCPs

alone. Since blending of LCPs with thermoplastics is the main theme of this research, it will be dealt with in detail in the following section.

Some very important results may be inferred from the above studies. Firstly, the seemingly contradictory results discussed above can be better appreciated if one realizes that the degree of orientation developed in a TLCP fiber depends to a large extent on the thermal history of the sample. Specifically, for TLCPs it appears that one needs to process the material at a temperature that is well above the crystal- nematic transition temperature so that no residual crystallinity is present which seems to inhibit the formation of uniformly aligned fibrillar structures necessary for obtaining enhanced properties and orientation. Secondly, although shear flow is capable of producing some orientation of the melt, some amount of post drawing appears to be essential to maximize this orientation. Thus the importance of extensional flow fields in enhancing orientation and properties cannot be ignored. Processing of LCPs also leads to some problems. Injection molded samples have high modulus and strength in the machine direction but exhibit very poor properties in the transverse direction. Also a skin-core structure with a highly oriented skin and relatively unoriented core is often observed. The melt strength of TLCPs is seen to drop tremendously at temperatures near the crystal-nematic transition making certain kinds of processing such as sheet extrusion and film blowing difficult. The processing of TLCPs was reviewed above. In the next section the literature regarding the formation of in-situ composites in discussed. A review of this subject is critical to bring the research objectives into proper perspective.

2.6 In-Situ Composites

Much of the fundamental aspects governing the formation of in-situ composites have already been discussed in Sections 2.2 through 2.5. Specifically, the theories of drop deformation and breakup were discussed in Section 2.2. Then the phenomena of capillary instability
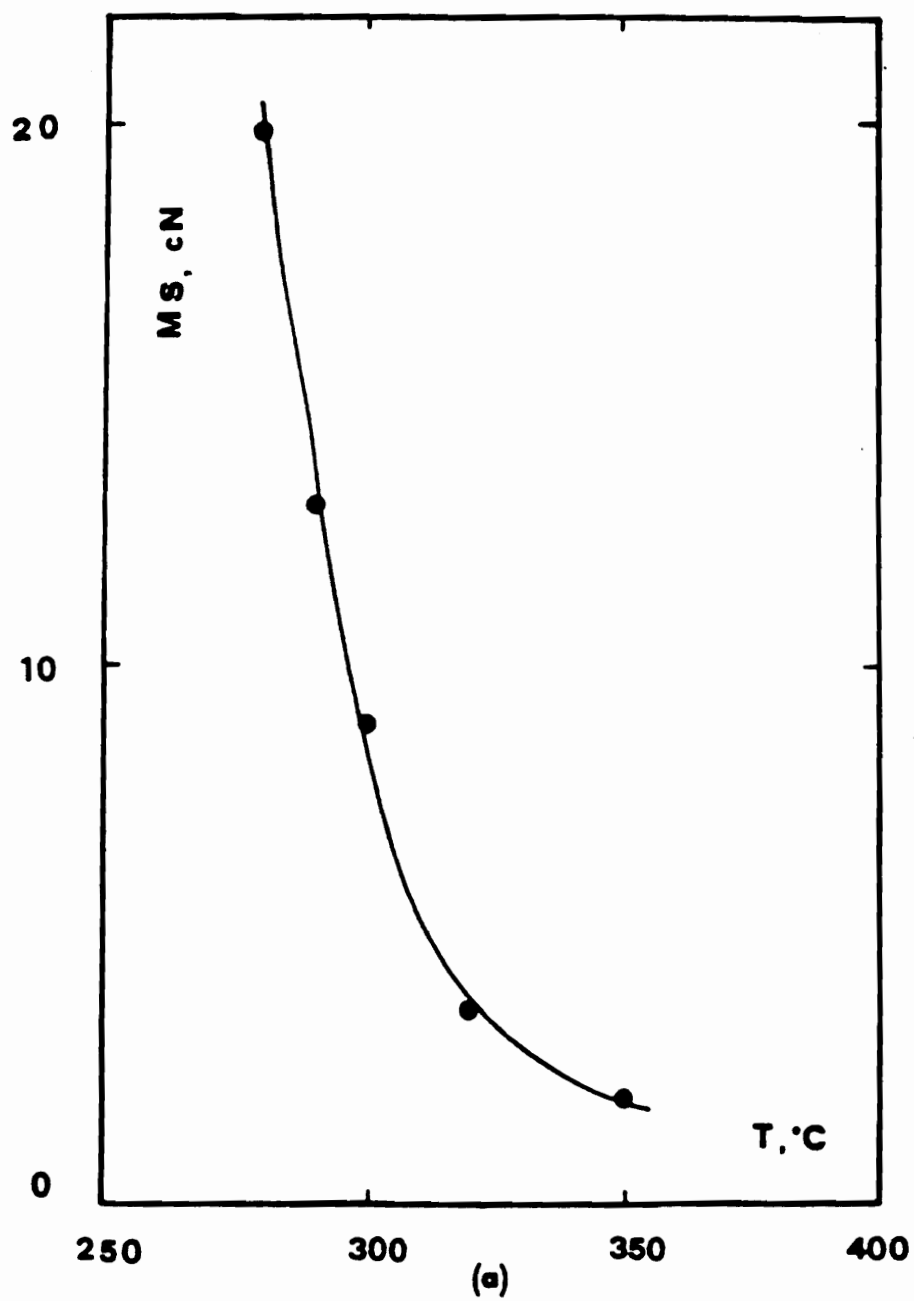
Figure 20. Melt Strength of Vectra B950 as a function of temperature [107].

and conditions under which the thread-like domains (fibrils) remained stable or broke up into drops were reviewed in Section 2.3. The morphology of two-phase blends, with a particular emphasis on the specific fibrillation process, was discussed in Section 2.4. Finally, some important aspects of the rheology and processing of LCPs were covered in Section 2.5. It is felt that at the end of this section, it should become amply clear that the literature on the subject of in- situ composites, lacks severely in several areas. Missing, in particular, are works that attempt to determine and/or alter the processing conditions which control the formation of these composites. To the best knowledge of the present author, there exists no reported data on any attempts to blend LCPs with melting temperatures (Tm) greater than that of thermoplastics. The important features of the melt rheology were established in the previous section. However, there do not appear to many works which have established definite correlations between the rheology of the components, their processing and subsequent properties. Thus in this section the literature regarding the formation of in-situ composites of flexible chain polymers by blending with thermotropic LCPs is reviewed. Herein, the emphasis will be to highlight most of the systems studied and an attempt will also be made to correlate the processing conditions with the morphology and the mechanical properties. Areas of deficiency will be brought out to pave way for the proposed research. For the sake of brevity, the 60 mole % PHB/PET copolyester will be designated as LCP60, the 80 mole % PHB/PET as LCP80, the 73/27 HBA/HNA aromatic copolyester as Vectra A900 and the 70/30 HBA/HNA as LCP-2000 through the rest of this manuscript.

2.6.1 Thermotropic LCP Blends With Flexible Chain Polymers

Siegmann et al. (109) were among the first to report on the formation of in-situ composites. Their system composed of an amorphous polyamide (PA) matrix and a HBA/HNA (the actual composition was not specified) based LCP. A significant reduction in the viscosity of the blends from that of the pure polymers was reported, with a minimum in the viscosity- com-

position curve occurring at only 5 wt % of the LCP in the blend. Similar results on Nylon 6.6/LCP (HBA/HNA) blends have been reported by Chung (110) more recently. Although a significant enhancement in the tensile modulus and strength was observed in the blends, this was accompanied by a substantial decrease in the ultimate elongation. This behavior is very characteristic of polymeric composites. A skin-core structure in injection molded samples of the blends, similar to that observed by other workers (97,98), was also noted from SEM micrographs. Of particular interest are the results wherein, as the composition of the LCP increased, a change in morphology from that of dispersed ellipsoidal LCP particles to LCP fibrils in the PA matrix were observed. At intermediate LCP compositions, both the morphologies were observed in the blends. A final note is the authors' comment that the rheological behavior was inexplicable either by the unique melt structure or by any available model and was a possible consequence of the non-uniform LCP distribution in the melt.

A recent study by Isayev and Modic (111) was conducted on blends of polycarbonate (PC) with two thermotropic LCPs (or TLCPs). The TLCPs were copolyesters of HBA/HNA in 75/25 and 70/30 molar ratios, the latter having been designated as LCP-2000 earlier. The blends were prepared either in an internal mixer with Banbury rotors or by extrusion through a Koch six-element static mixer connected to a 3/4 inch single screw extruder (Killion, Inc.). Blends consisted of the LCP ranging from 2.5 to 50 weight percent. Their results are of particular importance to the current research and are therefore discussed in some detail as follows. The rheology of both the blend systems, i.e., PC/(HBA/HNA) and PC/LCP-2000 was similar in that the viscosity of the blends at low shear rates was lower than that of the pure LCPs in each case. However, at higher shear rates, the viscosity of the blends was between those of PC and the respective LCP. Also, for the particular case of PC/(HBA/HNA) blend with 2.5 wt % of the LCP, no difference in the flow curves was observed for the blends prepared by the two mixing methods. Thus the viscous behavior was apparently not perceptible to the method of mixing. In contrast, the tensile properties and the morphology showed a very clear difference in the two methods of mixing. In Fig. 21 is shown the stress-strain behavior for the PC/(HBA/HNA) 97.5/2.5 composition blend at a shear rate of 225 sec^{-1}. Clearly, the blend mixed by the static

mixer has significantly improved properties than the one mixed in an internal mixer. This re-
sult, as verified by SEM, was a consequence of a much better dispersion of the LCP in the PC
matrix in the former case. Morphological studies using SEM gave results opposite to those
obtained by Siegmann et al. (109) i.e., fibrillar morphology was observed at LCP concen-
trations less than 10 wt % whereas at higher concentrations only large spherical LCP domains
in the PC matrix were observed. An attempt to correlate the experimentally determined me-
chanical properties with those calculated by using the composite theory, valid for
unidirectional fiber-reinforced composites, was also made. The results showed that the data
was bounded between two theoretical extremes at low concentrations, and fell below the
lower asymptote at higher concentrations.

An improvement in properties of blends made in a static mixer as compared to those
made in a corotating twin screw extruder has also been reported by Swaminathan et al. (125),
for blends of a polyetherimide (PEI) with an LCP based on an aromatic copolyester of
HBA/HNA (commercially known as Vectra A950). The LCP varying from 2.5 to 30 wt % was
blended with the PEI. The viscosity of the LCP was lower than that of the PEI in the entire shear
rate range tested. This was taken to imply that the fibrillation process for this system would
be more favorable since the viscosity ratio was greater than unity in the applicable shear rate
range. Further, the authors also report that the modulus and strength of extrudates from
capillary dies with shorter L/D ratios were higher compared to longer L/D dies. This may be
seen to be consistent with the work of Ide (113) where it was observed that as the L/D ratio
approaches zero, the tensile properties of pure LCP extrudates increase. It was shown by
morphological studies using SEM that up to 10 % of the LCP in the blend, the LCP phase re-
mained as either droplets or elongated structures. However, at 20 and 30 wt % of the LCP in
the blend, the fibrils were more perfectly formed with average diameters of 2-5 μm. This
compositional dependence of fibril formation may be explained by two effects. Firstly,
coalescence of drops to form larger drops is facilitated by the increased composition. These
larger drops are easier to deform into fibrils due to a larger Weber number as discussed in
the section on drop deformation and breakup. Also, one would expect intuitively that
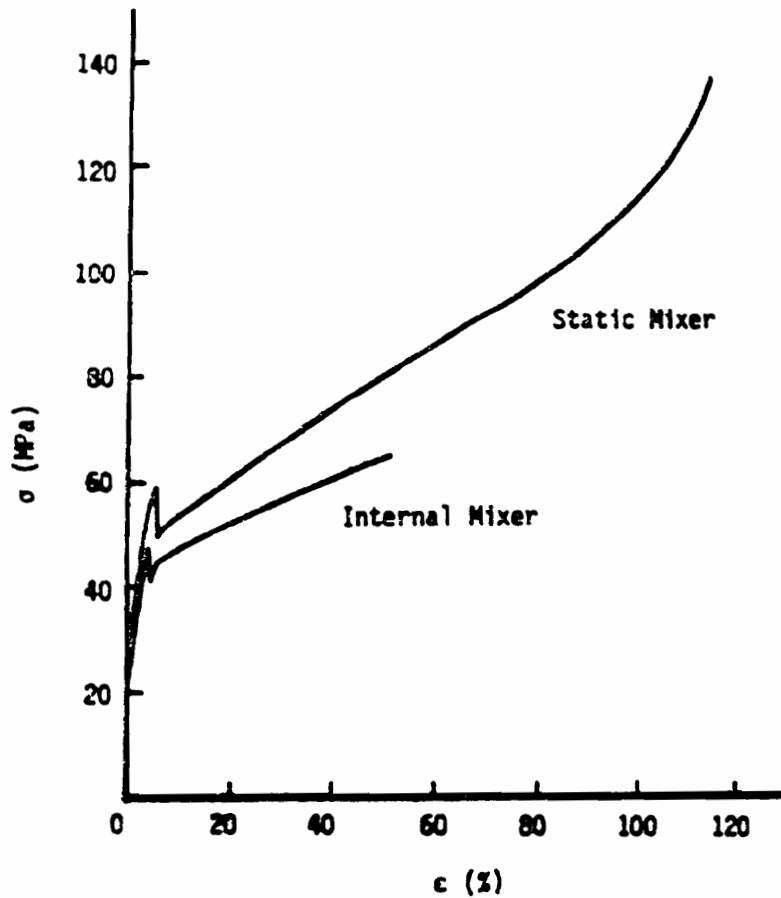
Figure 21. Stress-strain behavior for the PC/(HBA/HNA) 97.5/2.5 composition blend at a shear rate of 225 sec^{-1} [111].

connectivity between deformed droplets i.e. fibrils is easier at higher compositions leading to more perfect fibrils.

Bassett and Yee (150) described an interesting approach for forming in situ composite structures. Their approach consisted of three main steps. In the first step, blends of a thermoplastic and a LCP are spun into fibers with the LCP phase dispersed as fibrils in the thermoplastic matrix. The fibers so generated are then formed into a cloth or unidirectional tow in the second step. The third step consists of heating the tow in a mold so as to consolidate the thermoplastic matrix. It is important to mention that the molding temperature chosen is such that the thermoplastic melts without melting the LCP fibrils. Thus blends of polystyrene with Vectra B-900 (described as a wholly aromatic liquid crystal poly(ester-co-amide)) were extruded into fibers. Their experimental set up consisted of a 3/4 inch extruder, a Ross static-mixer with 6 mixing elements, an adaptor, a capillary die and a Brown filament drawing apparatus which were all connected sequentially. Several of their results are noteworthy especially in the context of this study. First, the fibers generated by the above extrusion process were observed to be less than 1 μm in diameter. in general. Secondly, although the authors fail to make this observation, no skin-core type of structure in the fibers was observed i.e. the LCP fibrils were distributed evenly through the cross-section of the fiber. The tensile modulus of the single fibers of PS/Vectra B900 60/40 blends were shown to be about 23 GPa for fibers extruded at high shear rates and maximum draw ratios of roughly 15-20. Pure PS modulus in comparison was shown to be about 3 GPa. The tensile moduli of the molded specimen was measured to be about 13 GPa. Thus quite significant enhancements in the modulus over pure PS were achieved by this method.

Blends of PC with Vectra were studied by Malik et al. (128) quite recently. The blends, with the LCP content varying from 5 to 50 wt %, were prepared in a Brabender Plasticorder at 280°C. The authors mention that a small amount of antioxident was added to prevent degradation. Films were made by compression molding and strands were extruded through a capillary die using an Instron Capillary Rheometer. It was indicated by measurement of the Young's modulus of the pure LCP that properties increased with increasing shear rate, sug-

gesting a high level of fiber orientation. However, at shear rates exceeding 150 sec^{-1} the modulus was seen to decrease. The authors were unable to explain this phenomena. The authors also report the tensile modulus and strength as a function of LCP composition in the blend. Both these properties were seen to increase sharply with addition of LCP, up to 10 wt % of the LCP. Then the properties were seen to increase less dramatically and more or less followed values predicted by the rule of mixing. The authors conclude that there exists a critical composition value beyond which the LCP does not act as a reinforcing species.

Master curves of the stress relaxation modulus, E_r, for PC, LCP and the 10 wt % LCP blend were constructed using the time-temperature superposition principles. The reinforcing effect of the LCP on the relaxation modulus of PC is shown in Fig. 22. At shorter times, the relaxation modulus is quite high for all three systems. At longer times, PC exhibits a rapid drop in modulus corresponding to the glass transition. However, it is interesting to note that the 10 wt % LCP blend shows a behavior similar to pure LCP. This is a good indication that the relaxation behavior of PC is significantly influenced by the presence of only 10 wt % LCP due to the reinforcing effect of the latter on the PC.

A wide variety of matrix polymers (both amorphous and crystalline) such as polyether sulphone (PES), polyetheramide (PEI), polyarylate, Nylon (N6), poly(butylene terephthalate) (PBT), polycarbonate (PC) and poly(etheretherketone) (PEEK) were blended with proprietary compositions of a LCP containing naphthalene moieties along the backbone by Kiss (2). Several different blending techniques were used. The author, however, reports no visible differences in the blends made by the various methods. For the large number of systems studied, the author reports that the addition of a LCP as a reinforcing additive results, in general, in a dramatic increase in the tensile and flexural moduli, an increase in the tensile and flexural strength to a lesser degree and a substantial decrease in the elongation to break. This observation is quite consistent with that of other studies. Morphologies of the various systems were found to be typical, in that elongated LCP domains in the matrix were found for all the cases reported. A reduction in the viscosity of the blends was reflected in the reductions in extruder torque, extruder melt pressure and injection pressure. Although extensive in its
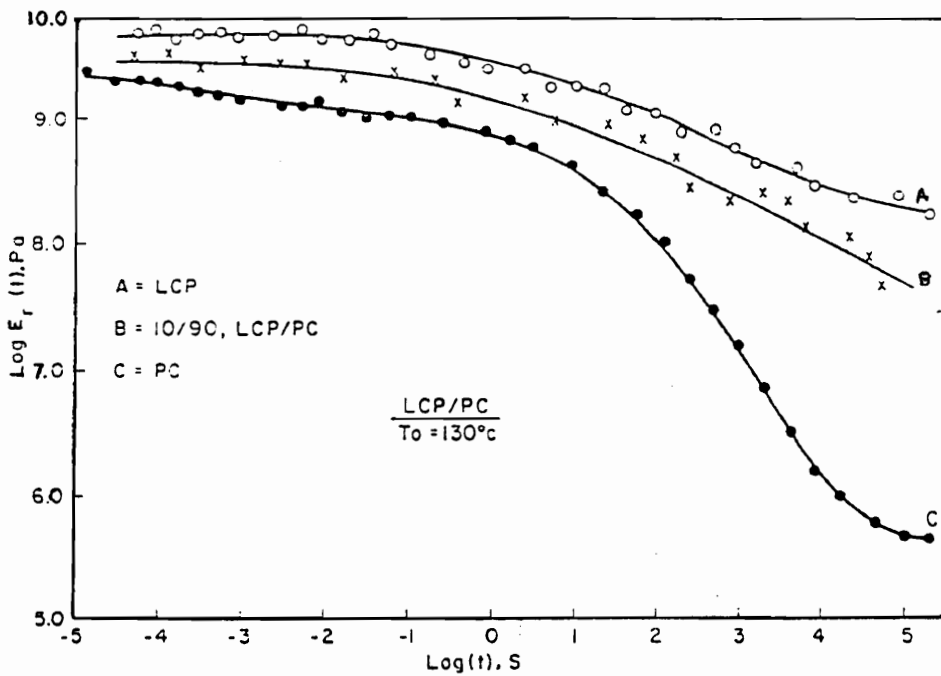
Figure 22. **Time-temperature superposition of the relaxation modulus for unblended PC, LCP and 10/90 LCP/PC blend [128].**

quantity, this study failed to discuss anything related to the structure-processing-property re-
lationships. The chemical compositions and processing conditions were not reported, and nor
were conditions for fibril formation discussed and thus any significant interpretations from this
study become difficult.

James et al. (129) report studies on blends of PES with a copolyester based on HBA/HNA.
The two components were blended in a single screw extruder and then extruded through a
capillary die to produce strands. The viscosity of the blends containing only 2 wt % of the LCP
was seen to be lower than that of pure PES by a factor of 4. This clearly shows the efficacy
of LCPs to act as processing aids for thermoplastic matrices. Similar results of reduced
viscosity of thermoplastic matrices upon addition of as low as 3 wt % of the LCP have been
reported in a patent by Cogswell (136). Reduced viscosity of thermoplastic/LCP blends com-
pared to the neat matrix phase have also been observed by other authors (2,109,110,112) and
appears to be a general observation, although at varying levels of the LCP in the blend. It was
indicated by polarized optical microscopy studies of the extruded strands that there existed
an oriented skin layer where the LCP had been stretched into fibrils and a relatively unori-
ented core where the LCP remained as spherical entities. The varying shear stress (or shear
rate) profile which is maximum at the walls and zero at the center of the capillary may account
for this skin-core effect. It should also be noted that such a skin-core structure has been ob-
served in injection-molded samples of pure LCPs as reported earlier (97,98) and was attri-
buted to the fountain-flow effect. In fact, Katoh and Schott (151) in their studies of blends of four
different ethylene vinyl alcohol copolymers (EVOH) with varying viscosities with an HBA/PET
copolyester LCP from Unitica, observed a distinct skin-core fibril-droplet structure in extruded
strands of all the blends. Furthermore, using Finite Element Method (FEM) flow analysis, the
strain that the blends experienced in the extruder was estimated to be about 3600 while the
nominal shear rate was 37 sec^{-1}. In contrast, the strain in the capillary die was estimated to
about 886 while the shear rate was 255 sec^{-1}. By increasing the screw speed in the extruder,
no perceptible change in the fibril morphology was observed. The authors thus suggest that
since the level of strain in the extruder is higher while the shear rates are higher in the

capillary die, the fibril creation may be more strongly influenced by the shear rate and not the strain which the fluid experiences.

Studies on blends of polystyrene (PS) with an LCP have been reported by Weiss et al. (127) with some interesting results. Blends of the LCP ranging from 1.54 to 10.04 wt % percent LCP were prepared on a 2-inch, 2-roll mill at a190˚C, mixing for about 8 minutes. Films of the blends were prepared by compression molding. Strands were also extruded through a capillary die using an Instron Capillary Viscometer. The LCP was seen to form a separate phase in the blend on the basis of DSC data. The Tg of PS remained almost unchanged in the blend and further the LCP clearing temperature (nematic-isotropic) was observed in all the blends. SEM of the fracture surface of extruded strands showed that the LCP existed as highly fibrillar structures in the PS matrix. Further, optical microphotographs of the fracture surfaces indicated that the LCP fibers were concentrated in the center of the specimen. This observation was seen to be a function of the extrusion rate. At lower rates, the fibers were seen to be uniformly distributed throughout the entire sample.

In an effort to further the understanding of the formation of LCP composites, with respect to the effect of the type of flow field, Blizard and Baird (112) studied blends of nylon 6,6 (N66) and PC with LCP60. Blends of N66/LCP60 and PC/LCP60 containing 10,30,50 and 70 wt % LCP were extruded through capillary dies attached to the exit of an extruder. SEM results showed distinct fibril formation for the blends containing 30 wt % or greater of the LCP phase. These results might again be explained by the coalescence phenomena discussed earlier in regards to the work of Swaminathan et al. (125). In simple shear flow generated in a cone-and-plate apparatus, no fibril formation was observed for either of the two systems (with 30 wt % LCP) for strains as high as 10,000 strain units. Also of interest are the results wherein blends of PC/LCP60 70/30 processed in the Instron Capillary Rheometer (ICR) showed fibril formation only for a capillary with L/D equal to 7.82. Tests with a capillary of L/D ratio of 21.4 showed no fibril formation. This L/D effect, which is related to the relaxation of structure in the shear field of the capillary land region, was also notably reported in a patent by Ide (112). The author claimed that processing of pure LCPs through capillary dies with a short land or preferably

no land at all, resulted in articles with high mechanical properties. Another study on Nylon 6/Vectra B950 blends extruded through capillary dies of varying L/D ratios yielded similar results (152). At nominal shear rates of 1200, blends through a die with $L/D = 40$ showed only spherical LCP morphology. In contrast, blends extruded through a die with $L/D = 0$ and at the same shear rate of 1200 sec^{-1} showed elongated fibrillar LCP morphology. Thus processing conditions wherein the LCP is subjected to some extensional flow field, as is the case in the converging section of a capillary die or post-extrusion draw, coupled with conditions that offer fewer possibilities of relaxation (such as a short L/D ratio), seem to be extremely conducive to the formation of reinforcing in-situ fibrils as suggested also by Krasnikova et al. earlier (55).

Ramanathan et al. (114) studied the extrusion of films with a melt drawing step for PC/LCP60 and PC/Vectra A900 blends. The drawing of the films outside of the film die imposes an extensional flow field, inherent to the drawing process, on the emerging film. The effects of such an extensional flow field on the orientation and properties of the blend films was studied. The authors report that for the PC/LCP60 blend films, both the tensile strength and modulus increased by a factor of two in the range of draw ratios used. For PC/Vectra A900 blends, however, the properties were not enhanced at all. A higher processing temperature in this case was believed to be responsible for this lack of improvement in properties. It should be noted that PC has a glass transition temperature of about 149°C and can be processed at around 260-280°C. However, since the Vectra A900 does not melt completely until 290-300°C, it is likely that the viscosity of PC at the processing temperatures is lower than what it would be at 260°C making fibrillation of the LCP more difficult at the prevailing conditions.

In another study by Ramanathan et al. (115) using polyphenylene sulfide (PPS) as the matrix phase and LCP60, LCP80, Vectra A900 and a 50/50 wt % blend of LCP60 and LCP80 (designated LCP60-80) as the reinforcing phases, the authors report fibrillation only for the PPS/LCP60 and PPS/LCP60-80 systems. They attribute the lack of fibrillation in the PPS/Vectra A900 system to a possible chemical reaction between PPS and Vectra A900 under the prevailing processing conditions.

The effects of miscibility of the matrix and reinforcing phases on the development of in-situ composites has been studied by Zhuang et al. (116). In their study, polystyrene (PS), poly(ethylene terephthalate) (PET) and PC were used as the matrices and LCP60 as the rein-forcing phase. Blends were prepared by both solution and melt blending. On the basis of re-sults from DSC, SEM, and dielectric thermal analysis (DETA), the authors conclude that PS was immiscible whereas both PC and PET were partially miscible with the LCP60, the PET being miscible to a higher degree than the PC. This observation was reflected in the fact that the PS/LCP60 blends had the coarsest and most distinctive phase morphologies, and the PET/LCP60 had the finest and least distinctive morphologies. Also, it was seen that for all the systems studied. there was a transition from ellipsoidal LCP particles to long LCP fibrils with increasing shear rate (or shear stress) in capillary extrudates as well as melt-spun fibers. Mechanical property enhancement of compression- molded films, extrudates and melt-spun filaments was observed for all the three blend systems. However, once again, no attempt was made to relate the morphology to the processing history.

Several other authors have also studied the effects of miscibility on different aspects of LCP reinforcement (6,117,118,119.120,121). Kyu and Zhuang (119) found that blends of PC/LCP60 form a miscible blend upon solvent casting. However, the blend undergoes phase separation during heat treatment, exhibiting a miscibility window which was reminiscent of a lower critical solution temperature (LCST). Specifically, transparent solvent cast films turned opaque upon annealing at 260°C for 10 minutes. Further, the blends showed a gross phase separation, determined by polarized light microscopy, with a high level of interconnectivity characteristic of spinodal decomposition. Iridescent colors were discernible within the phase-separated domains, which remained intact after removal of the PC phase, confirming the presence of liquid crystalline structures of the LCP60 phase.

Expecting some degree of compatibility between the pure PET and the PET/PHB copolymer (LCP60), Joseph et al. (120) and Brostow et al. (6) both studied blends of PET/LCP60. Joseph et al. mechanically mixed the two resins in a CSI-Max Mixing extruder and pressed into thin films. The LCP content was 30, 50 and 70 wt % in the blend. SEM results

show only spherical drops of the LCP at all compositions. This is probably not too surprising considering the fact that very little orientation of the LCP phase is possible in compression molding due to the lack of any significant extensional flow field. DSC studies indicated an enhancement in the rate of PET crystallization, suggesting a possible nucleating effect of the LCP. The bending (or flexural) modulus of injection molded plaques showed roughly a four fold increase, with the morphology of the plaques exhibiting a skin-core structure as noted by other workers (97,98). No comments were made, however, on any effects of the miscibility of the two phases. Brostow et al. (6) report on studies of the same system as above i.e. PET/LCP60, with less than 40 wt % of the LCP in the blends. The authors raise some interesting points in their analysis of the morphology of the blends. Blends containing 10 and 17 wt % of the LCP phase both show the existence of spherical LCP domains in the PET matrix. The authors contend that two possibilities exist regarding the nature of the LCP domains. One possibility is that the LCP domains may have two phases, a liquid crystalline and an isotropic phase, inside of each sphere. The other more likely possibility, they argue, is that the homopolymeric PET dissolves some parts of the LCP chains, mostly those that consist of PET, and thus the spherical regions would be rich in the PHB component. Mechanical properties were observed to decrease at first with the addition of a small (2-5 wt %) amount of LCP. With further addition of the LCP, the properties increase and reached a maximum before falling off again. This trend in mechanical properties is similar to that observed by Jackson and Kuhfuss (99) on injection molded samples of PHB/PET copolymers with different levels of the PHB component.

Blends of PC and PET with LCP60 (50/50 wt %) were also studied using calorimetry and microscopy by Friedrich et al. (118). The blends were obtained by co-precipitation from a common solvent with subsequent drying under reduced pressure at 100°C. Their DSC results of PC/LCP60 blend system show a decrease in the glass transition temperature, Tg, of PC which was taken to indicate partial miscibility of the LCP with PC. Upon annealing for 180 minutes at 580 K (303°C), only a single Tg was observed. Further, polarization microscopy results indicate no birefringence suggesting that the material was completely isotropic. This

effect of annealing was thought to be a consequence of a transesterification reaction. In contrast, blends of PET/LCP60 showed no significant effects of annealing on the two glass transitions observed, the lower Tg being attributed to the PET-rich phase and the higher Tg to the PHB-rich phase. Polarization microscopy results of the PET/LCP60 blend showed a phase separated melt with birefringent areas and a remarkable rectangular pattern. Upon annealing, the pattern remained almost unaltered in shape, but the birefringent areas became fewer and weaker in intensity. It is to be noted that even after annealing at 580 K (300°C) for a 100 minutes, the melt still exhibited small levels of birefringence. The authors attribute this loss of mesomorphic order also to a transesterification reaction leading to a diluted system. It is of importance to note that although for both the systems, PC/LCP60 and PET/LCP60, transesterification does appear to take place, the time scales involved for such a reaction are far longer than any typical processing times. Of particular interest are the results on the dynamic mechanical properties of the two systems. The authors find that while a reasonable reinforcing effect in blends of PC with LCP60 is seen with respect to torsion, blends of PET with LCP60 show almost no such effect. They attribute this difference to the fact that the PET and LCP60 are incompatible. The authors, however, fail to mention anything regarding the phase behavior between the homopolymeric PET and the PET- rich phase of the LCP60.

A very recent study by Nobile et al. (123) also studied the possibility of transesterification reactions using Fourier-transform infrared spectroscopy (FTIR). The system studied was PC/LCP60. Blends of PC and 10 wt % LCP60 were made in a singe-screw extruder to produce strands that were chopped into pellets. FTIR tests of the fraction of PC extracted from the PC/LCP60 90/10 blend did not reveal any absorption peaks at 1730 and 1740 cm^{-1}, typical absorption frequencies of the ester groups. Further, the inherent viscosity (IV) of the extracted PC when compared to the unfilled PC did not show any significant change. Based on these results, the authors concluded that no transesterification reaction had taken place in the processing of the PC/LCP60 blend, for the given processing conditions.

Crystallization and morphological studies on blends of PET with LCP60 (124) and with LCP80 and Vectra A900 (3) were carried out more recently. Bhattacharya et al. (124) prepared

blends of PET and LCP60 with the level of LCP varying from 3 to 20 wt % in a melt screw extruder. The authors found that the crystallization rate of PET was greatly enhanced by the addition of the LCP. This is consistent with the results of Joseph et al. (120). Of further interest are the Wide angle X-ray diffraction results whereby the presence of the LCP was seen to result in significant orientation and crystallinity during melt spinning of the blends. This was attributed to both the orientability of the LCP domains as well as to their nucleating effect. Mechanical properties of melt spun fibers of the blends showed a significant improvement in the initial modulus and the tenacity of the fibers with increase in LCP content and draw ratio. However, no correlation of the morphology or properties was made to any processing history. Sharma et al. (3) report similar results with the PET/LCP80 and the PET/Vectra A900 systems. The authors also examined the morphology using SEM of fracture surfaces of compression molded films and extruded strands of the blends. The authors report that in the case of the compression molded films, no fibrillation was seen to occur for any of the blends studied (upto 15 wt % LCP). For the PET/Vectra A900 system, the LCP particles were spherical in shape whereas the LCP80 particles were ellipsoidal indicating that the deformation of the LCP80 was higher. In the case of extruded strands, the PET/LCP80 shows the presence of short fibers of the LCP in the PET matrix while the Vectra A900 was present as nearly continuous fibers in the PET matrix. These results are a little surprising considering the fact that from the morphology of the molded films, one would have expected greater deformability (and hence longer fibers) in the PET/LCP80 system. No comment on this was made and once again no correlation of the observed morphologies to any processing variables was attempted.

A study on the shrinkage behavior of blends of amorphous polymers with LCPs was conducted more recently (117). Blends of PC and polystyrene (PS) with 10 wt % of LCP60 were prepared in a single screw extruder. Fibers of the blends were prepared by melt spinning and subsequent hot drawing. It is known that rigid fillers, such as beads or fibers, when introduced in a polymeric matrix reduce the effect of thermal shrinkage (117). This observation was put to test for the PS/LCP60 and PC/LCP60 blend systems, where the fillers were in essence replaced by the in-situ reinforced LCP fibrils. It was observed that the reinforcing effect of the

LCP60 was only observed for the PS/LCP60 system and not for the PC/LCP60 system. The authors suggest that the partial miscibility of the PC with the PET-rich phase, could be responsible for the observed results. However, it should be mentioned that SEM micrographs did show the formation of reinforcing fibrils in both systems. Sukhadia et al. (121) on studies of blends of PET with LCP60-80 (LCP60/LCP80 50/50) observed that both the dynamic and steady shear viscosity behavior of the blends containing as high as 30 wt % of the LCP. did not change much from that of pure PET behavior. This is in contrast to the observations of other systems where it is observed that upon addition of as low as 2 to 5 wt % of the LCP, a substantial reduction in the viscosity of the blends is observed (2,109,110,112). The authors (121) attribute this effect to the partial miscibility of the PET homopolymer with the PET-rich phase of the LCP.

Another interesting study using DSC and polarized optical microscopy on blends of PC/LCP60 was conducted by Jung and Kim (122). The blends were made in an internal mixer. Thermal properties investigated by DSC confirmed results obtained by other workers (118) that the glass transition of PC decreases upon addition of the LCP due to the partial mixing of the LCP with PC. However, the glass transition exhibited by the LCP remained unchanged in the blends, possibly indicating that the LCP phase excluded the PC phase. Morphology results on strands extruded through a capillary rheometer did not show any fibrillation for blends upto 30 wt % LCP60, if no draw was imposed (i.e., Draw Ratio (D.R.) = 1). However, at a D.R. of 15, extended fibrils of the LCP60 were seen for blends containing as little as 5 wt % of the LCP phase. These results once again illustrate the importance of an extensional flow field in the process of fibrillation. Polarized optical micrographs of the pure LCP60 obtained at different temperatures upon cooling from 400°C (where the LCP phase is isotropic) revealed the formation of a liquid crystalline structure at 390°C when cooled at 10°C/min after holding at 400 °C for 30 minutes. On the other hand, the optical texture of the PC/LCP60 blends containing 10 and 30 wt % LCP showed the presence of a two phase structure of the LCP phase and the PC isotropic phase. Agglomeration of the LCP phase was observed with increasing LCP content. Upon holding the melts at 300°C, the blends were seen to lose their anisotropic texture

and become isotropic after about 30 minutes. This was thought to be a result of the interfacial transesterification reaction as suggested also by Friedrich et al. (118). The mechanical properties of the blend fibers, illustrating both the importance of draw ratio and the effect due to LCP reinforcement, are shown in Figure 23.

Blizard et al. (154) have examined the morphology of extruded blends containing a TLCP via a quantitative technique to determine the percentage of LCP present as fibrils and the average domain diameter. The results and observations along with the rheological behavior of the individual components and heat transfer analysis were then used to explain the differences in the mechanical properties and morphology of three blend systems. The details of the experimentation and heat transfer analysis may be found in the manuscript itself (154). The authors draw several conclusions from their studies as follows: rheological and heat-transfer analysis of the post-die processing operations can be used to predict trends in the extrudate morphology; the tensile properties of the blends can be correlated to the composite theory; post-extrusion extensional strain i.e. drawing is critical for the formation of an optimal LCP fibrillar morphology; favorable morphology may be obtained if the extrusion temperatures are high; and the effects of the LCP composition on the morphology although not very clear, are possibly connected to both coalescence and drawing effects.

The morphology and mechanical properties of injection molded and spun fibers of blends of polystyrene (PS) with two commercial LCPs, Vectra A950 and Vectra B950, were examined more recently by Crevecoeur and Groeninckx (159). The mechanical properties obtained for the blends showed that the dispersed LCP phase possessed moderate aspect ratio fibrils in the case of the injection molded samples but nearly continuous fibrils for the spun fibers proving the importance of elongational flows. Further, the modulus and strength of the injection molded samples were observed to be below that of the rule of mixtures. However, the spun fibers were observed to obey the rule of mixtures, which is the limiting case of the Tsai-Halpin equation for continuous fibril reinforcement. Also, when the contribution of the LCP phase to the properties of the blend was back-calculated, it was seen that the LCP reached higher values in the fibers than in the injection molded plaques. This was attributed
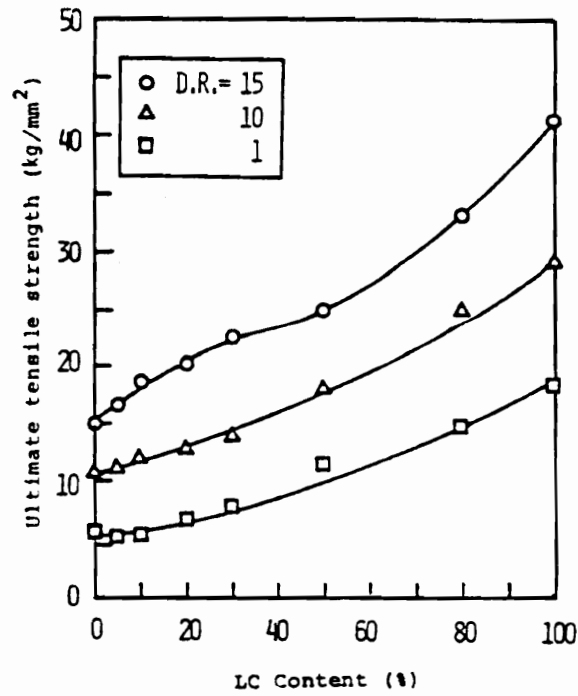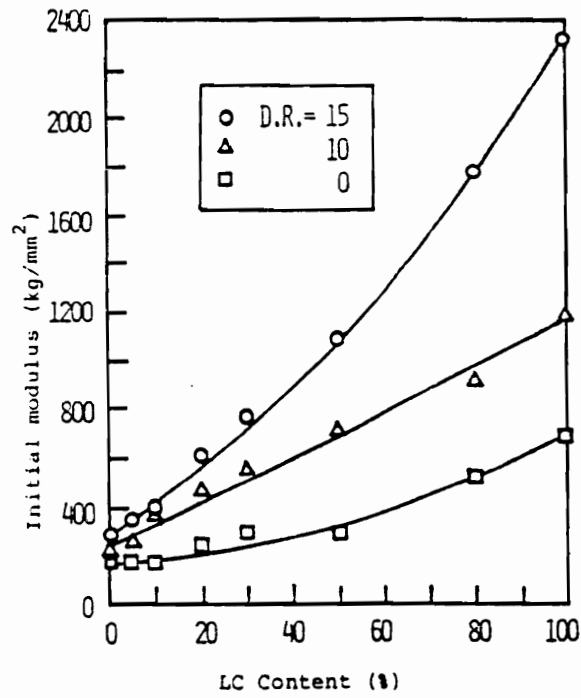
Figure 23. Effect of draw ratio and LCP content on the (a) tensile strength and (b) initial modulus of PC/LCP60 blends [122].

to both, finer morphology and higher molecular orientation (confirmed by WAXS), of the LCP phase in the fibers.

2.6.2 Effects of the Viscosity Ratio

Beery et al. (126) have looked at the formation of in-situ composites with some emphasis to the processing conditions. They studied blends of a TLCP copolyester of HBA/HNA 27/73 with PC. The LCP had a nematic-isotropic transition at 290°C. Blends were made by two consecutive passes in a screw injection molding machine at 290°C to insure good dispersion of the LCP. These blends, containing 10 and 20 wt % LCP, were then extruded through a capillary die mounted in an Instron rheometer. It should be pointed out that the apparent shear viscosity of the LCP at 13 sec^{-1} is about 14 times the PC whereas at the high shear rate region it is significantly lower than the PC (indicating a crossover of the viscosity curves at a certain shear rate). The authors observed a marked change in the morphology of the extrudates with flow conditions. This is illustrated in Fig. 24. Extrudates prepared at low shear rates contain LCP spheres or ellipsoids (Fig. 24a). Upon increasing the shear rate, the droplets elongated and turned fibrillar (Fig. 24b). Upon further increasing the shear rate, very long fibers, almost perfectly aligned in the flow direction, were observed (Fig. 24c). The droplets observed at the higher shear rates were attributed to the liquid fiber instability and breakup. A rigorous analysis of the experimental results indicated that the transition from droplet to fibrillar morphology occurred at a shear rate where the viscosities of the two blend components was approximately equal. This result is consistent with the results of Tsebrenko et al. (43-47), where maximum fibrillation was observed at a viscosity ratio of unity.

Nobile et al. (123) also addressed the effects of the viscosity ratio on fibrillation in PC/LCP60 blends containing 10 wt % of LCP60. Fibers of the blend were melt-spun by means of a Rheoscope 1000 provided with a capillary die (L/D = 10) and melt-spinning unit. The blends were melt spun at 220°C and 260°C. Both optical microscopy as well as SEM showed
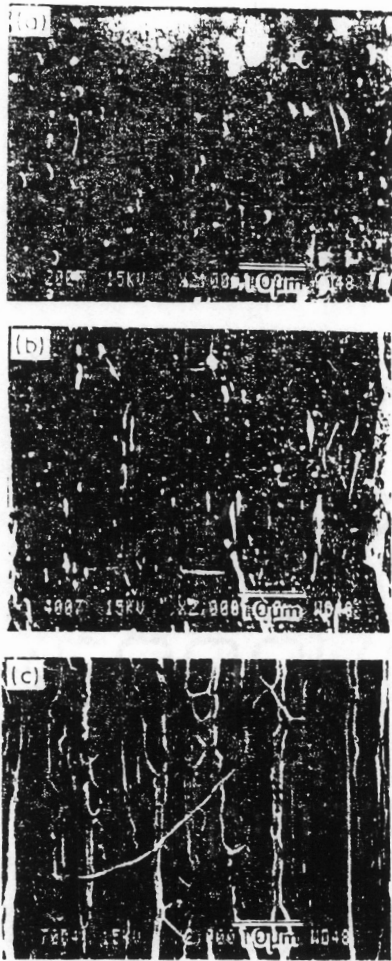
Figure 24. The microstructure of PC/LCP 90/10 blend extrudates prepared at shear rates of (a) 27, (b) 135 and (c) 5400 sec⁻¹ (selectively etched surface). The flow direction is vertical [126].

that the LCP fibrils developed only at the lower drawing temperature (220°C) whereas at 260 °C the LCP phase remained as spherical droplets. A lower viscosity of the PC at the higher temperature was thought to be incapable of deforming the LCP phase which consequently remained as droplets. Although the viscosity ratio was held responsible for the differences in the observed behavior, no quantitative evaluation was attempted. In another study cited earlier (152), it was seen that in blends of Nylon 6/Vectra extruded through a capillary die with $L/D = 0$, LCP fibrils were seen only at shear rates of 1200 sec^{-1} but absent at a lower shear rate of 6 sec^{-1}. From the flow curves presented at the extrusion temperature, it was interesting to observe that there was a possibility of crossover of the viscosities at a shear rate of about 1000 sec^{-1} where the viscosity of the LCP became lower than the matrix. Though the authors failed to give any explanation about this, the different morphologies observed could possibly be explained on the basis of this viscosity inversion.

Studies of Blizard and Baird (112) on blends of PC/CLP60 and N66/LCP60 also looked at the effect of the viscosity ratio on the morphology of blends extruded through a capillary die. The viscosity ratio of the blends varied from 0.005 for PC blends in the capillary rheometer to 0.13 for N66 blends at low shear rates in the RMS. For blends of PC/LCP60 where the LCP was present in 70 wt % (i.e. the viscosity ratio is inverted), no fibrils of the thermoplastic were seen to be present in the entire range of viscosity ratios. However, when the LCP was the minor component (30 wt %, and thus the viscosity ratio is less than unity), fibrillation was seen to occur at all values of the viscosity ratio.

Isayev and Modic (111) whose study was mentioned earlier in this section, attempted to verify the importance of the viscosity ratio for blends of PC/LCP-2000. A crossover in the flow curves of PC melt with that of LCP-2000 melts at shear rates of 6.6 sec^{-1}, 9.5 sec^{-1} and 19.5 sec^{-1}, corresponding to temperatures of 280°C, 310°C and 340°C, respectively, were noted. The crossover points can be taken as the points where the viscosities of the two melts are approximately equal. That being the case, and assuming that the postulate of Tsebrenko et al. (43-47) that maximum fibrillation occurs at a viscosity ratio of unity is correct, one would expect a maximum in mechanical properties at these conditions. It can be seen from Fig. 25 that

this is not the case for the PC/LCP-2000 system. In fact, the maximum in Young's modulus occurs for the 5 % LCP blend at 22.5 sec^{-1} and 225 sec^{-1}. A few comments regarding the above are necessary. Firstly, there is little experimental evidence directly relating the extent of fibril formation to mechanical properties to warrant such an expectation. Secondly, generation of fibrils alone in no way assures high molecular orientation or mechanical properties. Thirdly, the authors did not correlate the morphology at the three shear rates with the properties. Therefore it is very possible that the degree of fibril formation was higher for the higher shear rates, implying only that maximum fibrillation occurred not at a viscosity ratio of unity but at some value less than that.

The very potent effect of the viscosity ratio on the morphology of two phase blends was perhaps best observed by Subramaniam and Isayev (153). Blends of polyether ether ketone (PEEK) and Xydar (a LCP) were injection- molded into mini tensile bars in compositions ranging from 2.5 to 80 wt % LCP. Also, in the shear rate range of 1-100 sec^{-1}, PEEK was observed to have a lower viscosity than Xydar at 420°C. Blends containing 2.5, 5 and 10 wt % of the LCP showed only spherical or elongated LCP morphology. With 25 wt % of the LCP in the blend, the LCP fibrils about 10 μm in diameter were observed. However, with 50 and 80 wt % of the LCP in the blend, a rather stunning difference in the morphology was observed. Fibers of PEEK, roughly 2-3 μm in diameter were observed in the LCP phase (this was verified by etching). As expected, the formation of these PEEK fibers in the LCP did not serve to improve the mechanical properties. Thus the importance of having a lower viscosity LCP than the matrix during processing is noteworthy.

Thus the above findings indicate several noteworthy aspects of the generation of in-situ composites. A reduction in the viscosity of thermoplastic polymers upon addition of small amounts of LCP was observed for many systems. A better dispersion of the LCP in the matrix, as obtained for example by the use of static mixers, was shown to result in improved mechanical properties. In all cases, a certain minimum concentration of the LCP was required before fibrillation was achieved. Coalescence and ease of deformation of larger drops are likely to be responsible for this behavior. Mechanical properties of thermoplastics were ob-
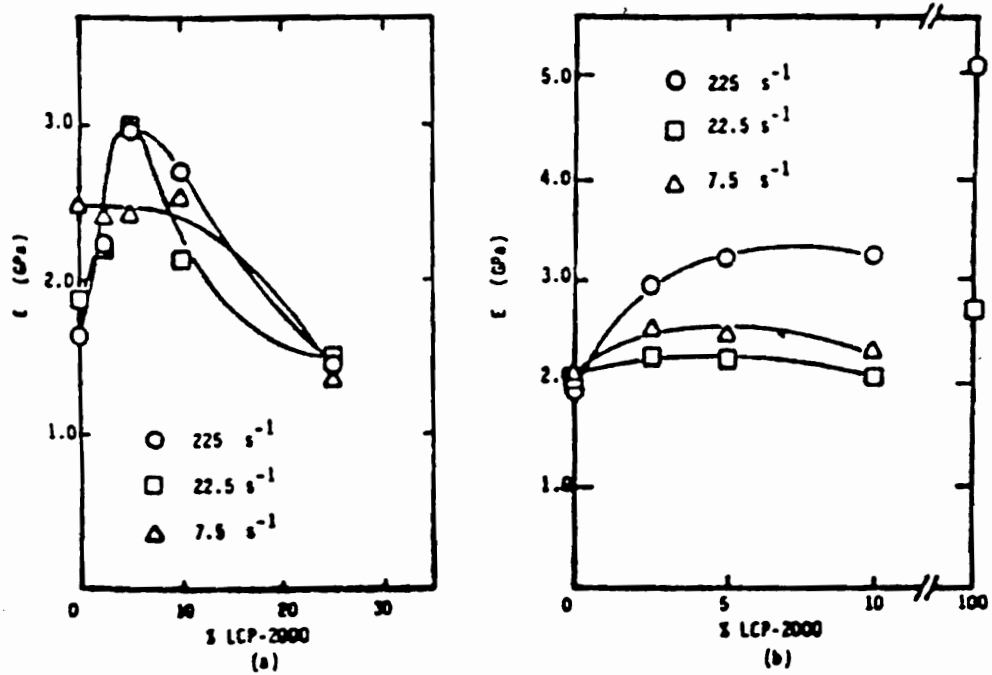
Figure 25. Young's modulus, E, as a function of LCP-2000 concentration for samples extruded at various shear rates at (a) 310°C and (b) 280°C [111].

served to be enhanced significantly upon addition of the LCP. Also, it was shown that in-

creased draw further enhanced the mechanical properties due to an increase in the

orientation. Transesterification reactions were shown to occur in some systems. However, the

time scales involved for these reactions to occur were shown to be much longer than typical

processing times. Miscibility of the matrix and LCP polymers was shown to inhibit the forma-

tion of fibrils and the reinforcing effect of the LCP that is usually observed. The viscosity ratio

was once again shown to be a controlling factor for the morphological development of these

systems. In particular, viscosity ratios of one or less were shown to be favorable for fibril for-

mation and to be able to generate a morphology in which the LCP phase forms the reinforcing

fibrils it must have a lower viscosity than the matrix at the processing conditions.

2.7   Research Objectives

The literature pertaining to the current research has been reviewed in the previous

sections. In this section the objectives of this research are given in detail after a brief dis-

cussion of the literature. This discussion in undertaken so that some of the important aspects

of the literature review which have a direct bearing on the current research may be high-

lighted and so that the statement of objectives may be better appreciated.

In the earlier sections it was seen that a fundamental understanding of the drop defor-

mation and breakup process gives us an insight into the process of specific fibrillation. In

particular, the importance of the Weber number (also known as the Capillary number) and the

viscosity ratio in determining the morphology of a two-phase polymer blend was highlighted.

Inspite of some conflict regarding the effect of the magnitude of the viscosity ratio, it is clear

that a viscosity ratio of unity or less is necessary for the formation of fibrils of the minor phase

in the matrix. Whether the optimal viscosity ratio for fibrillation is actually unity (43-47) or some

other value less than unity (16,35,53,111,112,126) is still not very certain due to the fact that experimental results supporting both arguments exist.

One of the prominent features of the rheology of LCPs is the viscosity-shear rate dependence. Specifically, the viscosity of LCPs is dependent on the shear rate over many orders of magnitude of the shear rate. Further, preheating the LCP melt to a temperature much higher than the melting temperature (as may be determined by DSC for example) and then subsequent cooling of the melt to a lower test temperature results in a much lower viscosity of the melt than if the LCP had been heated up to the test temperature directly. The magnitude of this decrease in viscosity increases with an increase in preheating temperature. This latter behavior then provides for a handy processing tool whereby the viscosity of the LCP melt may be altered by suitably changing the thermal history of the sample.

The review on blends of LCPs with flexible chain polymers also revealed some important results. Blends of LCPs with thermoplastics appeared to exhibit higher mechanical properties with an increase in the degree of dispersion of the minor phase (such as those obtained from the use of static mixers) (111,125). Further, it was also observed that processing of pure LCPs at higher temperatures led to better properties and increased orientation in many cases (77,102,103,106).

However, when blends of LCPs with thermoplastics are processed at high temperatures, it is observed that the viscosity of the matrix drops so as to increase the viscosity ratio (123), which is unfavorable for fibril formation. Also, an increase in the temperature of the melt leads to a lower viscosity, and consequently lower melt strength, of the melt blend making post-extrusion drawing more difficult for processes like sheet and rod extrusion and film-blowing. Lastly, it is clear that the melt processing temperatures of LCPs like LCP80 and Vectra A900 are higher than those of some commodity resins such as polystyrene, polycarbonate, and poly(ethylene terephthalate). For example, it is recommended that PET not be processed at higher than 301°C so as to avoid any loss in molecular weight (130).

From the discussions above and keeping in mind the information obtained from the literature review, it is proposed in the current research to:

1. To determine the extent of mechanical property enhancement of PET that can be achieved by blending with several liquid crystalline polymers, with an emphasis on blends containing 50 % or less of the LCP, using two different processing methods, viz. injection-molding and sheet extrusion.

2. To establish whether there are any advantages in both the processing and mechanical properties of the in situ reinforced LCP blends (or composites) generated in this study over inorganic fiber-filled composites (using the data available on these systems).

3. Develop a blending method which takes advantage of the supercooling behavior of some polymer melts, by plastication of the matrix and dispersed phases in two separate extruders and subsequent mixing downstream in a mixing head, to successfully generate oriented fibrillar liquid crystalline polymer reinforcements in situ in thermoplastics whose processing temperatures are lower than that of the LCP.

4. To establish the rheological properties of the melts and the design parameters (number of mixing elements, residence time, etc.) necessary to predict *a priori* the feasibility of blending a given polymer pair by the above blending method.

5. Determine the differences in the morphology and mechanical properties of strands of blends extruded from a single-screw extrusion process with those extruded using the dual-extruder blending method described above.

6. Determine the effects, if any, of varying the L/D ratio (constant D) of extrusion capillary dies on the morphology of the blends.

7. Determine if the blends made by the above method can be further processed by injection-molding, solid phase forming and thermoforming without a loss in their mechanical properties.

8. **Estimate the pressure-drop and shear-rate in the static mixer by modelling the flow as that of a power-law fluid through a packed bed.**

A review of the literature was presented in this chapter. The chapter began with a brief discussion on the miscibility and thermodynamics of polymer blends. Next, fundamentals of the drop deformation and breakup theory along with experimental results from numerous sources were discussed. Following that a discussion of the domain stability phenomenon was presented. Then the development of morphology in two phase polymer blends was discussed with particular emphasis to the fibrillation process. A brief introduction to liquid crystalline polymers was followed by a discussion of the rheological behavior. In particular, the viscosity and deformation and temperature history behavior was examined. Next, the processing of pure LCPs was reviewed and a detailed discussion on the development of in-situ composites was presented. Lastly. the research objectives were discussed. In the next chapter the methodology and experimental work required to fulfill the objectives are given.

3.0   Experimental Apparatus and Procedure

All pertinent details regarding the materials, methodology and experimental work re-

quired to reach the set goals are discussed in this chapter. In section 3.1 the polymers used

in this study are described. Following that, details of the techniques used to characterize the

structure and properties of the polymers and blends viz., rheology, morphology. mechanical

properties. molecular orientation and thermal properties, are given in section 3.2. Then in

section 3.3 information regarding the preparation of the blends using single-screw extrusion

and the new blending method developed in this study is provided. Here details of the new

blending method with regard to the design and selection of its components, assembly, start-up

and general operating procedures are also provided. Lastly, details of the post-processing

studies conducted on the blends by injection molding. solid phase forming and thermoforming

are given in section 3.4.

3.1 Materials

The matrix materials used were poly(ethylene terephthalate) (PET) and polypropylene (PP). The PET was supplied by The Goodyear Tire and Rubber Company, Akron, Ohio. The PET has a number average molecular weight (M_n) of 42,000, weight average molecular weight (M_w) of 84,000 and a melting point (T_m) of 258.5°C as specified by the manufacturer. The PET was selected due to its high molecular weight and the fact that it is believed to suitable for the extrusion of films or sheets (130). PP (Pro-Fax 6823) was obtained from Himont Company. This particular PP grade is a high temperature purging compound and has an extremely high molecular weight ($M_w \simeq 6E5$) and consequently a high viscosity (zero shear rate viscosity $\simeq$ 6E4 Pa.s at 200°C). The polydispersity index (M_w/M_n) is reported to be approximately equal to 5.

Seven thermotropic liquid crystalline polymers were used in this study. The first is a copolyester of 60 mole % parahydroxybenzoic acid (HBA or PHB) and 40 mole % poly(ethylene terephthalate) (PET) made by Tennessee Eastman Company and designated earlier as LCP60. LCP60 is believed to have number average molecular weight of roughly 20,000 and molecular weight distribution of ca. 2 which is typical of a condensation polymer (99). The second is a copolyester of the same moieites in the composition ratio of 80 mole % PHB and 20 mole % PET designated earlier as LCP80. The preparation and properties of the above two copolyesters are described in ref. (99). At the time the materials were first received from Eastman Company, they were in the experimental production stage. Subsequently, production of these materials by the company was stopped. Thus only limited quantities of the materials were available. The third LCP studied was made by blending LCP60 and LCP80 in the composition ratio of 50/50 weight percent (designated LCP60-80). The fourth is a commercial product marketed by Hoechst Celanese under the trade name of Vectra A900 and is a copolyester of 73 mole % HBA and 2-hydroxy-6-naphthoic acid (HNA). The copolyester is reported to have a relatively narrow molecular weight distribution of about 2 and a weight

average molecular weight of ca. 30,000 (76). The copolyester is thought to be completely random (131) and details of its preparation may be found in reference 131. Vectra A900 is fully aromatic and thus has a higher melting temperature as compared to LCP60. The fifth LCP also manufactured by Hoechst Celanese and known as Vectra B950 was also used in this study. Vectra B950 is described as a wholly aromatic liquid crystal polyesteramide composed of 58 mole % HNA, 21 mole % terephthalic acid (TPA) and 21 mole % 4'-hydroxy acetanilide and believed to have a molecular weight greater than 20,000 (159). The next two LCPs were used primarily due to their high processing temperatures. Thus the sixth LCP used was obtained from Du Pont Company and is known commercially as HX-4000. It is believed to be aromatic copolyester consisting of terephthalic acid. hydroquinone and phenyl hydroquinone. It's melting temperature is reported by the manufacturers to be 314°C. The last LCP used was obtained from BASF Corporation. Germany and is know as Ultrax (KR 4002). It's composition is unknown. Ultrax is reported to have a negligible tendency to crystallize and is normally processed between 280°C-330°C according to BASF.

Although many LCPs were used in this study, it is probably appropriate to mention here that the LCPs described above were used to varying degrees in this study. The extent of research done with any particular LCP was largely dictated by the polymers' properties and its use in establishing a set research objective. Some reasons for the selection of the polymers have been given above. Further comments regarding their use are deferred to the appropriate later sections.

The chemical structures of some of the LCPs is shown are Figure 26. Also, the relevant thermal transition temperatures of all the materials used in this study, where available, are summarized in Table 3.
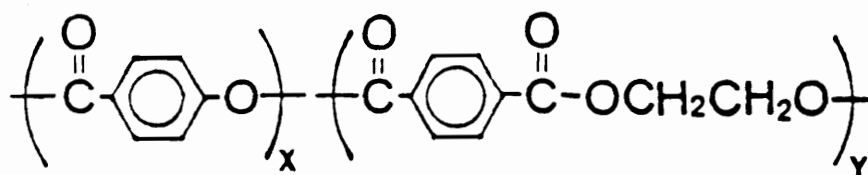
(a) 60HBA/PET (LCP60) x=0.6 y=0.4
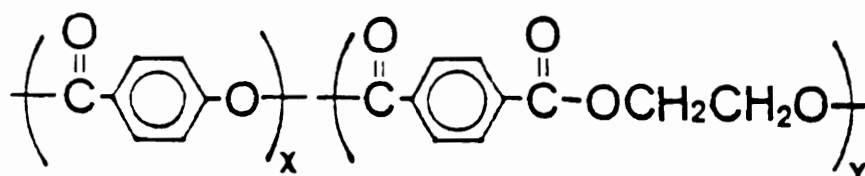
(b) 80HBA/PET (LCP80) x=0.8 y=0.2
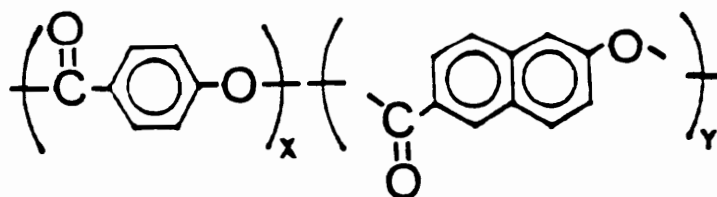
(c) HBA/HNA (Vectra A900) x=0.73 Y=0.27

Figure 26. Thermotropic LCPs used in this study (a) LCP60, (b) LCP80 and (c) Vectra A900.

Table 3. Summary of thermal transition temperatures of polymers used in this study.

MATERIAL	Tg	Tm	Tproc	Tmax
Polypropylene	-10°C	165°C	180-200°C	
PET	85°C	265°C	270-290°C	301°C
Vectra A	105°C	283°C	320-340°C	370°C
Vectra B	110°C	280°C	300-330°C	
HX4000	180°C	310°C	340-360°C	
LCP60	70°C, 143°C	252°C	270-300°C	
LCP80	70°C, 143°C	304°C	330-350°C	
LCP60-80	70°C, 143°C	293°C	310-330°C	
Ultrax			280-330°C	

3.2 Structure/Property Characterization Techniques

3.2.1 Rheology

A knowledge of the rheological behavior of polymeric materials is of critical importance from the processing and design standpoint. Data from the rheological characterization is essential to the selection of processing parameters such as temperature profiles and thermal and deformation histories the material undergoes. Most of the rheological tests were performed using the Rheometrics Mechanical Spectrometer (model RMS-800). Some of the earlier tests were done using a model RMS-605 as well. Complete descriptions of these rheometers and the various modes of operation may be found elsewhere (139). Several different rheological experiments were conducted to extract particular information about the materials behavior. These tests are outlined below. However due to the large number of materials studied and tests performed, details regarding individual test conditions will be dealt with in the appropriate sections. It may be noted that all the tests with polymer melts were performed under an inert nitrogen gas atmosphere to prevent oxidation effects.

Steady-shear viscosities were measured from 0.01 to 10.0 sec^{-1}. Beyond this region, measurements were not possible due to loss of the melt from between the plates. Further characterization of the shear properties was obtained from the oscillatory dynamic frequency sweeps. The complex viscosity ($\eta^\star$), the storage modulus (G′) and loss modulus (G″) were measured as a function of frequency from 0.01 to 100 rad/s. The above tests, i.e. steady rate sweeps or dynamic frequency sweeps were carried out using either the parallel-plate (25 mm diameter) or cone and plate (25 mm diameter, 0.1 rad) arrangements. The procedures are relatively straightforward and may be found in ref. (139). Furthermore, due to the nature of some of the tests performed, most of the tests were carried out here with the parallel-plate

arrangement since the chances of overloading the transducer are lower compared to the cone-plate arrangement, especially with a normal stress transducer.

In order to determine the solidification kinetics of the polymers at various temperatures in the melt state, isothermal time sweeps were performed. These tests were conducted in the dynamic mode. By monitoring the values of $\eta^\star$, G' and G'' as a function of time it was possible to get an indication of how long it takes the polymer before solidifying (or crystallizing) and thus get some idea of the time scales involved during processing. The polymer pellets were loaded onto the plates and heated to any desired temperature. The oven was allowed to stabilize at that temperature and after removing the excess polymer from the sides of the plates the test was begun. In some cases the experiments were conducted at temperatures lower than the preheating temperature. In these cases, the melt was cooled using the 'rapid cool' feature on the instrument to the desired lower test temperature and allowed to equilibrate which typically took a total of about 1-2 minutes. Then the test was begun with the time being measured from the beginning of the test.

When a polymer is heated to temperatures above the melting point and then allowed to cool, it is often observed that the material does not solidify at the melting point but at some temperature below that. This difference in the solidification and actual melting temperature is often referred to as the degree of supercooling. This temperature window, where the melt is in the supercooled state, represents a part of the window of processing where the polymer melt is usually viscous enough to flow and yet has the requisite melt strength to be processed. The importance of both the solidification kinetics and supercooling of polymer melts to processing operations has been discussed in ref. (140) in detail. Thus temperature sweeps on the polymer melts were performed to ascertain the degree of supercooling under different conditions. These tests were performed by heating the polymer to some temperature higher than its melting point, holding it there isothermally for 3-5 minutes, and then cooling it at a pre-programmed rate. $\eta^\star$, G' and G'' were then monitored as a function of decreasing temperature till the material approached solidification. The cooling rate for all the experiments was

an instrument program rate of 5°C/step which corresponds to a cooling rate of roughly 3°C/min.

3.2.2 Morphology

The morphology was determined by scanning electron microscopy (SEM) using a Stereoscan-S200 Instrument (Cambridge) with an accelerating voltage of 25kV. Some of the earlier SEMs were also obtained using a JEOL JSC-35C instrument. Samples for SEM were prepared by cryogenic fracture of the surface of interest after immersion in liquid nitrogen for 2-5 minutes. The samples were mounted on aluminum stubs and then coated with a thin layer of gold (100-200°A) using an SPI Sputter Coater. Finally, the sample was connected to the aluminum stub with a coating of carbon or silver conducting paint for enhanced conductivity. For the sake of brevity, scanning electron micrographs will be referred to as SEMs in the entire manuscript.

3.2.3 Mechanical Properties

In general, the tensile (Young's) modulus, tensile strength, flexural modulus and shear modulus of the materials were assessed. The tests were performed either on an Instron Mechanical Tester model-1122 or model-4204 in accordance with the ASTM standards wherever possible. In some cases the dimensions of the samples to be tested did not match those specified in the standards and in those cases appropriate modifications were used.

The tensile tests on rods (strands) were performed in accordance with ASTM 3379. The tests were performed with a constant crosshead speed of 0.5 mm/min and a gage length of at least 14 cms. All the results for the strands represent an average of at least six tests except

for draw ratios above 60 where insufficient samples were available. In these cases the data is an average of two to four tests only.

Tensile tests on sheets and injection molded bars were conducted in accordance with ASTM 638. In the case of the sheets, dog-bone samples for testing were cut using a cutting die (Type V, ASTM-638). In the case of injection molding plaques, only rectangular strips were used since it was not possible to cut dog-bone samples from the thick plaques. In most cases, the tensile tests were performed without an extensiometer. The flexural properties of the materials were determined according to standard ASTM-790 (Method-I). A three-point bending test attachment to Instron's model-1122 was used for the testing. All the above results represent an average of at least five tests.

Lastly, dynamic mechanical analysis of both, extruded sheets and injection molded plaques, was performed using the solids torsion test mode available on the RMS-800. Again the materials response to a small strain dynamic oscillatory perturbation is measured by monitoring the shear storage modulus, G′, and shear loss modulus, G″, as functions of (increasing) temperature. The values of G′ are an indication of the materials stiffness and these tests were done to compare the change in the stiffness of the blends with that of the base polymers. Also, the value of tangent delta (the ratio of G″ to G′) gives important information regarding the thermal transitions of a material (139). Thus information regarding the glass transition temperatures, side chain motions, degree of crystallinity and miscibility in blends may be extracted from these tests. Use of some of these ideas was made in this study.

3.2.4 Molecular Orientation

X-ray scattering that arises from periodic fluctuations in the electron density occurring over very small distances (1-20°A) results in Wide-Angle X-Ray Scattering (WAXS) (141). Such scattering arising from crystals in semi-crystalline polymers can be quite useful in determining the degree of crystallinity and even the size and perfection of crystals themselves. Also, the

level of molecular orientation of the crystalline polymer chains can be assessed through WAXS. In this study, the use of WAXS was made quite extensively to obtain qualitative information regarding the degree of molecular orientation present in the polymers and blends.

The experiments were conducted using a Phillips table-top X-ray generator (PW 1720) in conjunction with a standard vacuum sealed Statton (Warhus) camera. The exposure time was varied from 2 to 16 hours depending on the sample. Also, the sample to film distance was either 54.58 cm or 77.19 cm, again depending on the sample. In most cases the d-spacings were calculated so that conclusions regarding a particular diffraction pattern could be drawn with some degree of certainty.

3.2.5   Thermal Properties

Differential scanning calorimetry (DSC) was used for thermal characterization of the materials. Experiments were conducted for several different purposes. Simple heating and cooling scans were performed for polymers for which no thermal transition data was available. These scans were employed mainly to determine the glass transition temperatures (Tg), crystallization temperatures (Tc) and melting temperatures (Tm) of the neat polymers. Similar heating and cooling scans were also performed for the blends in order to study changes in the thermal transitions, if any, upon blending.

A Perkin-Elmer model DSC-2 was used for the studies. The weight of the samples varied from 5 to 12 milligrams. The heating rate was typically 20°C/min and the materials were scanned in the temperature range from 30°C to 350°C, the upper temperature limit depending on the sample.

3.3 Processing of Blends

In this section, some details regarding how the blends were processed are given. The blends were processed either by single-screw extrusion or by the blending method developed as part of this study. Thus in the first part of this section the single-screw extrusion process is described. In the second part the new blending method developed is described first. Then some information with respect to the particular design and selection of components is given. Finally, the start-up and general operating procedure are discussed in some detail.

3.3.1 Single-Screw Extrusion

Blending of different polymers was done in a laboratory size 2.54 cm (1″) single screw extruder (KL-100). The extruder has an L/D ratio of 24:1 and a compression ratio of 3:1. The extruder is equipped with three independent temperature controllers for the heaters on the barrel. The extruder is also equipped with three additional controllers for heating auxiliary equipment such as adaptors and dies. Thus a total of six independent heating zones are available.

All the materials to be extruded were dried for at least 24 hours at 120°C in a large convection oven. The dried materials were then mixed by shaking in a container in the appropriate weight ratios and fed into the hopper. Either pellets (strands) or thin films (sheets) were extruded. Appropriate dies were thus attached to the exit of the extruder by means of an adaptor. Pellets were extruded through a capillary die and the extrudate was quenched in ice-water and continuously pelletized or drawn. The sheets were extruded using a 4″ wide sheet die with a typical coathanger type feed. The extrudate was cooled with a jet of high pressure air and then taken up on a pair of highly polished chrome- plated rollers custom made by Killion Extruders, Inc.. The rollers were cooled by circulating water through them to

prevent the extrudate from sticking to the roller surface. The temperature of cooling water was between 20-23°C.

3.3.2   Dual-Extruder Mixing Method

3.3.2.1   General Description of Process

As mentioned earlier in this section, one of the prime objectives was to devise a set-up wherein a high melting LCP may be successfully blended with a thermoplastic whose processing temperature is much lower. To achieve this goal, an experimental set-up as shown schematically in Fig. 27 was designed and developed. The system consists of essentially four parts: the feed system which consists of two single-screw 1" extruders (Killion, KL-100 described earlier). a Kenics static mixer and the adaptor plus die attached to the exit of the mixer. The matrix and dispersed phases were plasticized separately in the two extruders. The melts from the two extruders were then joined at a 'T' intersection. The melt mix from here was then passed through a 0.5 inch Kenics Static Mixer and then via an adaptor to an appropriate capillary die or sheet die. It is of importance to add here that one could of course quite easily envision feeding the melt after the 'T' junction into some other type of mixing device, such as another extruder or even twin-screw extruder. The selection of the particular static mixer is discussed in the following section. The possibility of using another extruder or a twin-screw extruder instead of a static mixer will be addressed in the next chapter after appropriate results have been presented.
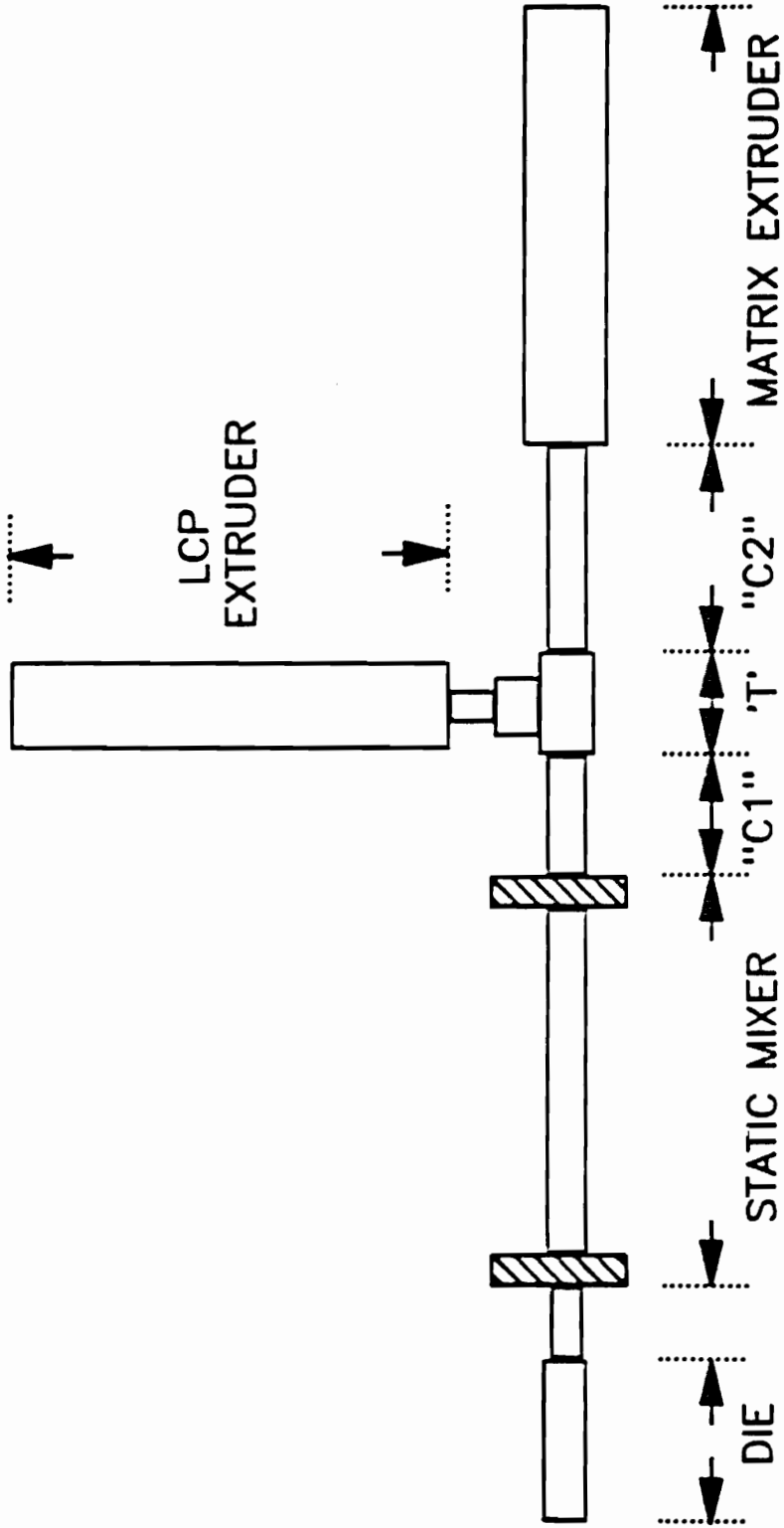
Figure 27. Schematic of the dual-extruder mixing method.

3.3.2.2 Design Criteria

Several aspects had to be taken into account to ensure that the apparatus could successfully meet the objectives of this research, i.e. to successfully generate fibrillar LCP reinforcements in matrices with lower processing temperatures than the LCP. Some of the more important considerations that went into the selection of the particular components are discussed below.

The mixer selected was a 0.5" i.d. Kenics static mixer with 18 elements which is manufactured by Chemineer, Inc.. This mixer is an in-line no-moving part, continuous mixing device (142). The unit consists of a number of short elements of right and left-hand helices. These elements are alternated and oriented such that the leading edge of one element is at 90° to the trailing edge of the one ahead. The element assembly is then enclosed within a tubular housing (empty pipe). Details of the principles of operation and mixing action of this mixer are described in (132, 142).

The selection of the mixer type and the number of elements was based on several criteria viz. the residence time in the mixer, the degree of mixing attainable and the pressure drop. There are more than 30 types of static mixers known today (143). The Kenics Static Mixer (KSM) is known to exhibit the lowest pressure drop (143,144) as well as the best homogenization (mixing) efficiency in the laminar flow regime (144) (which is the flow regime applicable in this study). Therefore it was thought to be most suitable for this work. It should also be added here that the Kenics mixer is also one of the most popular static mixers and a number of studies, both experimental and theoretical, were available as references (132,143,144,145.146). Furthermore, preliminary calculations had indicated that the residence times in the mixer containing 18 elements based on some typical flow rates were of the order of 40 seconds to 90 seconds. One concern was that the residence time not be too long (order of 4-6 minutes) to promote any significant transesterification reactions (138). Also, pressure drops were calculated to be about 350 psi, which were well within the recommended limit of 2500 psi (133), a limit beyond which the encased element assembly could be damaged. It is

worthwhile to add here that some other type of static mixer could have been used as well, due to the fact that the general operational principles of all static mixers is the same, i.e. mixing by dividing a liquid jet into layers and their subsequent recombination in geometrically different configurations (143). It is not known, and would probably remain to be established experimentally, if some other static mixer would have provided similar results to the KSM. However, due to some of the advantages involved with using the KSM. as outlined above, it was chosen for this study.

The purpose of the static mixer was two-fold. First it served as a post-extrusion mixing device for the two separately plasticized melts to yield a "homogeneous" blend. Secondly, the Kenics static mixer has been proven to be extremely efficient in removing any radial thermal gradients in the melt (132.133). Thus the second function of the mixer was to deliver melt to the die (either sheet die or capillary die) with a relatively flat temperature profile. This particular feature of the mixer becomes more important due to the fact that the two polymer streams at the inlet of the mixer have different temperatures as will be discussed later.

All the connecting sections of the piping system were cut from 0.5" i.d. stainless steel 316, schedule-80 pipe. The reducers, 'T' section and other intermediate connectors for the piping system were also made from stainless steel 316.

3.3.3 Operating Procedures

In this section the procedure to set up the apparatus is discussed with particular reference to the piping and heater bands. Following that the start-up and general operating procedures are discussed with an emphasis on some of the more common problems that were encountered during operation and steps taken to avoid them.

3.3.3.1 Assembly

The procedure that needs to be followed with respect to the assembly of the piping and heaters is best explained with the help of Figs. 27 and 28 together. In Fig. 27, the individual elements of the piping system have been designated numbers from 1 to 9 for identification. In Fig. 28, the different heating zones as they will be referred to from hereon are shown along with the approximate location of heater bands in each heating zone. The following is a step by step explanation of the assembly procedure:

1. First the LCP extruder (E2) is fixed by locking the wheels of the extruder. The height of this extruder was about 1 cm lower than the matrix extruder and thus metal sheets were placed under the wheels to elevate the extruder.

2. Next the adaptor (# 9) is fitted through the clamp ring (CR) of E2 and held in place by tightening the clamp ring. Do not clamp it too tight at this point since the adaptor will have to be rotated once the 'T' is screwed on.

3. A heater band is first slipped on to the adaptor and then the 'T' junction (# 4) is screwed on to the adaptor. It should be noted here that some kind of high temperature lubricant must be applied to the threads of each pipe section to ensure easy dismantling else there is a possibility of shearing the threads.

4. Once the 'T' is fitted tight with a wrench, it may be necessary to loosen the clamp ring and rotate # 9 to make the 'T' horizontal. Once that is done then pipe section # 3 is screwed on and the heaters for that section (Zone 'C2') are slipped on into place along with a thermocouple. Then the reducer (# 2) is threaded on and its heater slipped on.

5. Now the flange for the clamp ring corresponding to extruder E1 is first slipped onto the adaptor (# 1) along with a heater band. Then # 1 is threaded into the reducer (# 2).
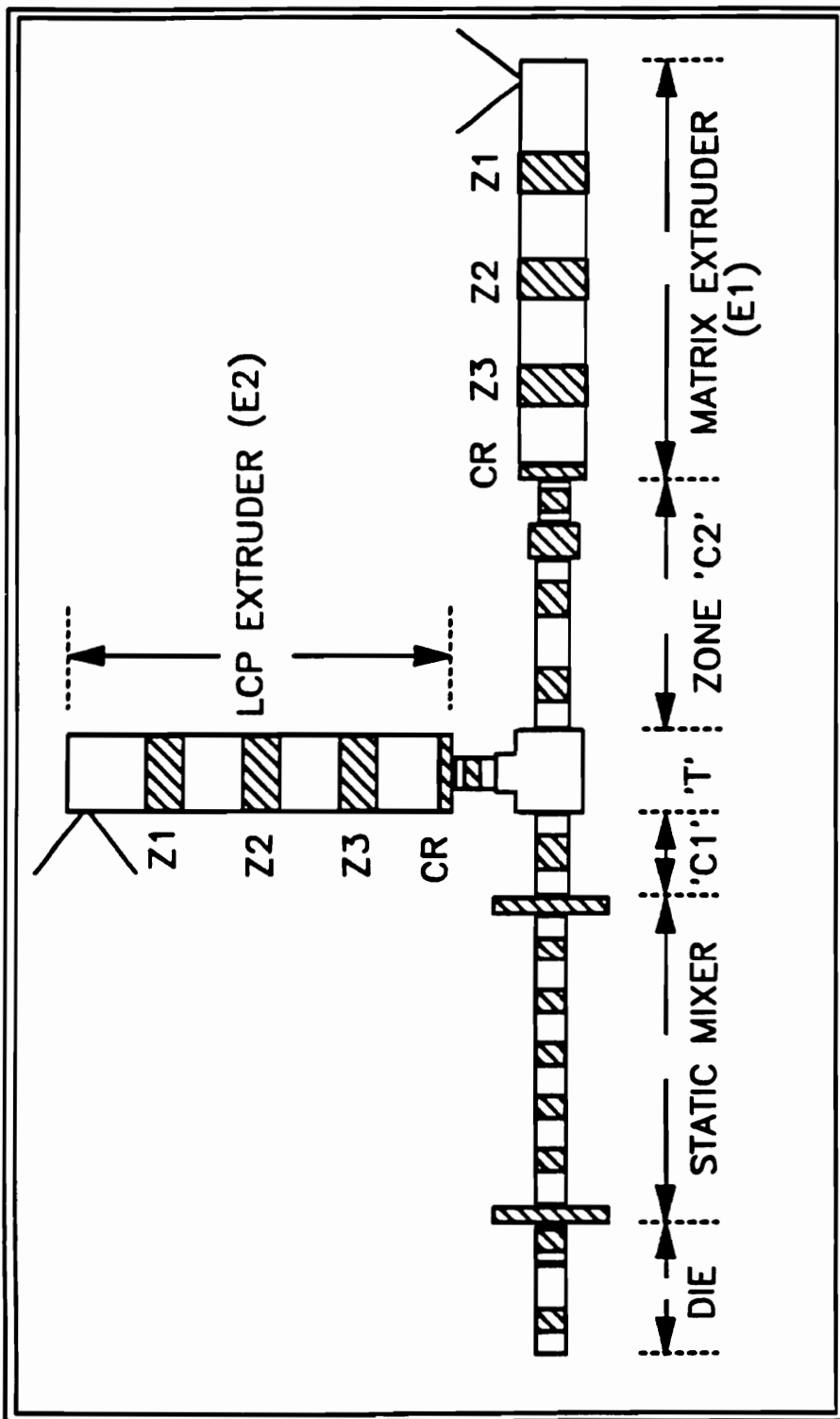
Figure 28. Schematic of the apparatus showing the different heating zones and the approximate location of the heater bands.

6. The breaker plate for E1 is then placed in its appropriate slot on the extruder and the flange is slipped onto the breaker plate and clamped shut with the help of the clamp ring (CR) of E1. A fair amount of difficulty may be encountered in completing this last step. One person may be required to push E1. another person to guide the flange onto the breaker plate and a third person to quickly clamp the ring shut. This is why it is necessary to elevate E2 before anything else is done.

7. Now the pipe section # 5 is threaded into the other side of the 'T' and a heater band and thermocouple slipped into place.

8. A reducer is then fitted on to the other end of # 5 to which a flange is fitted.

9. Now the mixer (# 6) is mounted by raising it to the required level, placing a wooden support under it and bolting the flange of the mixer to the flange attached to # 5. These bolts should not be tightened fully until the wooden support is placed under the flange (near part # 7).

10. Finally, the adaptor (# 7) to the mixer flange is threaded on and any appropriate die (# 8) attached to it. The heaters and thermocouples for parts # 7 and 8 are then slipped on and the assembly is now complete.

11. One last comment regarding the mixer needs to be made. The mixer has the flanges welded at either end. Thus the band heaters have to be carefully pried open just a little and then slipped into place on the mixer pipe. As long as care is taken not to pull the mouth of the band heaters too far apart, this method does not damage the heaters. The alternative is to invest in much more expensive 'expandable' heaters.

3.3.3.2 Start-Up/Operating Procedure

After the assembly is completed, the system is essentially ready for operation. However, due to the nature of the blending process, it is imperative that certain guidelines for the safe and successful operation be established. These are discussed below.

1. The first thing that needs to be mentioned is that due to the long sections of piping **extreme caution** needs to be exercised during start-up and shut down, especially when starting up a 'full' system (i.e. one full of polymer material from the previous run). Before the heating is started, the exit of the die should be protected by placing a box or some other obstruction in its path so that in case the pressure builds up and shoots material out of the die, no one in front of the die is injured. **This is extremely important**. To ensure a rapid rise in temperature and to prevent excessive loss of heat, the system should be insulated with an appropriate wool or fiberglass insulation. Care should be taken not to cover the heater bands with this insulation since this results in overheating and consequent shorting of the heaters.

2. In the case of starting up an empty system i.e. one in which the pipe sections are empty the heaters for the die, static mixer, zones 'C1' and 'C2' and zones Z1-Z3 and clamp-ring (CR) may all be turned on simultaneously, taking care to raise the temperature of each zone in steps of 50-75°C.

3. In the case of starting up a full system, it is good practice to start heating the system gradually from either end and working towards the center. Thus with reference to Fig. 28, the heaters for the 'Die' and zones 'Z1-Z3' of extruder E1 (matrix) should be turned on first. Once these temperatures are about 20-30°C below the melting point of the material inside, then the temperatures in these zones may be raised and the heating of the static mixer and zones 'C1' and 'C2' begun. The heating of the LCP extruder (E2) may also

be started now. The clamp rings (CR) should now be tightened fully to prevent any leakage.

4. Once all the zones have reached the set temperatures, the system should be purged for about 1C minutes with any suitable polymer to remove all the old material in the extruders and pipes that may have degraded during the heating.

5. Now the system is completely ready for operation. Typically, the matrix polymer is fed into the extruder at the desired RPM. Once the temperatures and pressures have stabilized, the LCP extruder may be started at the desired RPM. Samples should be collected only after at least 6 minutes from the time the LCP extruder is started.

6. Due to the way the polymers are fed, there is no way *'a priori'* to determine the composition of the blend. What may be done, however, is to time the disappearance of known amounts (weights) of the matrix and dispersed polymers and estimate the composition from those flow rates. The flow rates measured in this way should be averaged over at least 5 readings. As a check, the flow rate at the exit of the die may be measured and compared to the sum of the matrix and dispersed polymer flow rates.

7. After completion of a run, the purge material should be fed to each extruder and the temperatures in all the zones lowered to just above the melting (or flow) temperature of the purge material. Once the system has been thoroughly purged, the extruders should be run dry prior to shutting them down. Several different purging compounds, which have recommended use temperatures in the range of 180- 300°C., are available commercially. The compounds in the range of 250- 300°C are preferred due to higher temperatures involved in this process.

8. The drive motors on the extruders and all the heaters are then turned off. Once again the exit of the die should be covered for safety reasons.

3.3.3.3 Estimation of Blend Composition

As mentioned earlier, due to the nature of the dual-extruder mixing method, it is not possible to determine the composition of the blend in advance. Some problems in determining the blend composition were encountered in the early stages of the development of this method and therefore warrant further elaboration here. Also, steps taken to determine the composition as accurately as possible are given here.

One of the first precautions that need to be taken is to ensure that there is no leakage of polymer from any of the sections of the set-up described in Fig. 27. In particular, the problem areas were found to be at the clamp rings of the extruders, which if not sufficiently tightened after heating the extruders to the desired temperatures, were prone to substantial leakage. Therefore it is recommended that the clamp rings be tightened as much as possible and further to watch the surrounding areas of the clamp ring for 15-20 minutes after extrusion is begun for signs of leakage. In most cases, any inconsistency in the flow rates or "feeding" problems were traced back to polymer leakage. Also. the flow rates were found to be quite sensitive to the temperatures of the various sections of the mixing system. Thus it is important to maintain consistent temperature profiles from run to run. Since the flow rates were seen to vary between separate runs, it is recommended that the flow rates be monitored as frequently as possible during extrusion by measuring the disappearance of known weights of polymer so as to determine the composition more accurately. On the other hand, in cases where there was no leakage, the flow rates during any particular run were found to be quite consistent for the duration of run. Also, the total (output) flow rates should be measured during a run and compared with the sum of the matrix and dispersed polymer flow rates as a check. Again, the agreement of the total flow rate with the sum of the individual flow rates was good provided, of course, that there was no polymer leakage in the system.

3.3.4 Post-Processing of the Blends

There are some important ramifications of an in situ reinforced system having a matrix phase whose melting point is lower than the reinforcing LCP phase. As indicated by Tsebrenko et al. (45), breakup of threads (fibrils) in the matrix will only occur at temperatures greater than the melting temperature of both the matrix and dispersed phases. Thus in situ composites may provide for systems in which the matrix may be sufficiently deformable for processes like injection molding, solid phase forming and thermoforming and yet is capable of maintaining the reinforcing characteristics of the LCP phase. Thus this part of the study focussed on verifying the abovementioned hypothesis.

3.3.4.1 Injection-Molding

Injection molding of the blends was carried out in an Arburg Allrounder Model 221-55-250. The plaques were made in an end-gated mold with dimension of 1/8″ x 2.5″ x 2.5″. The injection molder is equipped with a total of 4 heating zones; zones 1-3 along the barrel of the molder and the fourth for the nozzle. Experiments were run either by tumbling the polymers in a container in the required weight ratios and then feeding the mixture to the hopper or by using pellets that were preblended using the new mixing method discussed earlier. For brevity and clarity, all blends made by the former case will be referred to as Physical Blends (PB) and all blends made by the latter method as Mixer Blends (MB).

3.3.4.2 Thermoforming

Thermoforming of sheets or plaques was done using a Hydro-Trim Corporation model Labform II-B thermoformer. The blend sheets made using the mixing apparatus were

thermoformed by preheating the sheets to some higher temperature for periods of time vary-
ing from 50 seconds to 180 seconds prior to the forming. Two different molds were used. The
shallow mold has dimensions of 0.5" x 0.75" x 1.5" while the deep mold is twice the depth i.e.
1". Due to the sample size restrictions, it was not possible to perform any mechanical property
tests on the thermoformed parts.

3.3.4.3 Solid Phase Forming

Solid phase forming of the extruded sheets was done for two reasons. First, since the
as extruded sheets are very anisotropic, the mechanical properties of these sheets is poor in
the transverse direction as compared to their properties in the machine or draw direction.
Consequently, one approach to strengthen the material is to form a composite or laminate by
stacking layers of sheets with each layer being mutually perpendicular to the adjacent one.
The second objective of this study was to observe what changes in the structure i.e.
morphology and molecular orientation might take place as a result of the solid phase forming
process.

The solid phase forming was conducted as follows. Either 4-ply or 6- ply composites with
alternate cross-stacking of the sheet layers were made by consolidating the sheets under high
pressure at elevated temperatures. The temperature of consolidation was 10-30°C above the
Tm of the matrix polymer. The edges of the four or six sheets were first soldered together
using a soldering iron to prevent them from getting misaligned during the consolidation step.
The sheets were then sprayed with a high temperature mold release agent on the top and
bottom surfaces and then enclosed in aluminum foil. This was then placed in the press (Carver
Laboratory Press. model 2696) and heated to the required temperature with a slight positive
pressure being maintained in the press. Once the melting point of the respective matrix ma-
terial was reached the pressure was increased to about 150 psi. The temperature was further
increased to the desired set point and held there for 5-10 minutes. Then the heaters were

turned off, the temperature allowed to fall to just below the melting point of the matrix material and the pressure was released. The encased composite was then pulled out of the press and inserted between a pair of steel plates which were at room temperature. Additional weight was put on top of the plates and the composite allowed to cool. It was necessary to cool the composite outside the press since it was not possible to obtain high cooling rates in the press, which in turn was necessary to prevent the composite from becoming extremely brittle due to significant crystallization.

Details of the experimental apparatus and procedure required to achieve the set objectives have been provided in this chapter. In particular, information regarding the polymers used in this study, techniques for property characterization, preparation of the blends by single-screw extrusion and the dual-extruder mixing method developed here, assembly, start-up and general operating procedures and finally the procedures for post-processing of the blends has been provided. In the following chapters the results along with analysis and discussion will be given. Also, the processing conditions for various blends and methods, which will usually be more detailed than the basic procedures described in this chapter, will also be provided in the appropriate sections.

4.0   RESULTS AND DISCUSSION

The methodology and experimental work necessary to reach the set objectives were discussed in the last chapter in detail. In this chapter the results along with the analyses and discussions will be presented. This chapter is divided into three broad sections: (i) determination of the extent of mechanical property enhancement of PET by direct blending with several LCPs (ii) results from strand and sheet extrusion using the blending method developed here and (iii) post-processing studies involving injection-molding, laminating and thermoforming of the blends. Thus in section 4.1, blends of PET with several different LCPs made by direct injection molding and sheet extrusion will be discussed. Details of the processing methods and conditions along with the mechanical properties, morphology and molecular orientation of the resultant blends will be given. In section 4.2, the melt rheology of several different polymers is discussed first so that the development of the dual-extruder mixing method may be better appreciated. Following that, details of the processing conditions for the generation of strands of several PET/LCP and PP/LCP blends by the mixing method will be discussed. This will be followed by appropriate analyses of the results of characterization tests done on the blends rods. Furthermore, results of studies aimed at comparing the mechanical properties and morphology of one blend system extruded using the blending method and the single-screw extrusion process will be presented. Following the discussion

on strand extrusion, details of the sheet extrusion process and results will be given. As mentioned in the research objectives outlined in chapter 2, one of the goals of this work was also to be able to predict a priori the feasibility of blending a given polymer pair by the blending method developed here. Thus results from the experimental work directed at answering this question along with the design and heat-transfer analysis will also be presented in this section. Then the effects of varying the L/D ratio of capillary dies (constant D) on the morphology of LCP blends will be presented. It is hoped that these studies will shed some light on the deformation and break-up of droplets and fibril stability phenomena. In section 4.3 the results of post-processing the blends by injection- molding, laminating and thermoforming will be discussed and comparisons with direct or physical blending will be made wherever possible. Finally, comparisons of the processing and mechanical properties of inorganic fiber-filled systems with the in situ LCP reinforced blends from this study will be made in section 4.4

4.1 Blends of PET with several LCPs

4.1.1 Sheet Extrusion

In an effort to examine the extent of mechanical property enhancement of PET that could be achieved by blending with LCPs, sheets of PET with two LCPs, LCP60 and LCP60-80, were extruded using a 4″ flat sheet die by the extrusion process described earlier in chapter 3. Sheets of PET/LCP60-80 blends in the composition ratios of 100/0, 98/2, 95/5, 90/10, 80/20 and 70/30 were extruded. The melts typically had low melt strength upon exiting the die. Furthermore, the amount of draw that could be imposed on the sheets was limited due to severe 'necking' of the extruded sheets. Thus the maximum draw ratios achieved were about five. It should be added here that these sheets were made using the respective preblended pellets.

The preblending prior to sheet extrusion ensured better mixing and thus a more homogeneous blend than could be achieved in a single pass through the extruder. Also, to ensure uniformity in the processing conditions, the blend pellets were extruded at 28 RPM while the sheets were extruded at 40 RPM for this set of experiments. The mass flow rates measured during sheet extrusion were of the order of 65-72 gms/min. The temperature profile for extrusion was as follows: 235°C, 295°C, 260°C, 255°C and 250°C in zones 1-3, clamp ring and sheet die, respectively.

Results of the tensile tests performed on the extruded blend sheets are shown in Fig. 29. The data along with standard deviations are provided in the appendix. One observes that on addition of a small amount of LCP60-80 (2 wt %) to PET, there is a decrease in both the tensile modulus and tensile strength from that of pure PET. Then upon further addition of the LCP the modulus and strength increase, reaching a maximum at 10 wt % of the LCP in the blend and then declining at 20 wt % and even further at 30 wt % of the LCP. The modulus and strength of the control PET were observed to be 2.8 GPa and 71.22 MPa, respectively. In comparison, the properties of the 90/10 blend were 4.4 GPa and 104 MPa representing an increase of about 57 % and 46 % in the modulus and strength of pure PET. The reasons for the initial decrease in properties at 2 wt % and the maximum at 10 wt % LCP in the blend were not obvious right away. Thus further characterization of the blends was performed to examine possible reasons for this behavior and those results are presented in the following paragraphs.

The morphology of the above sheets was examined using SEM. Scanning electron micrographs of the blends are shown in Figs. 30-31. Fig. 30a is the homopolymeric PET which shows a homogeneous but non-fibrous structure as expected. It can be seen from Figs. 30-31 that although there appears to be a tendency to form fibrils of the LCP60-80 phase in the PET matrix (indicated by the ellipsoidal LCP domains), there is no distinct fibril formation in any of these blends. Nevertheless, the LCP domains are well distributed in the PET matrix indicating that the mixing of the two components is good. The good mixing is also likely helped by the preblending step.

RESULTS AND DISCUSSION
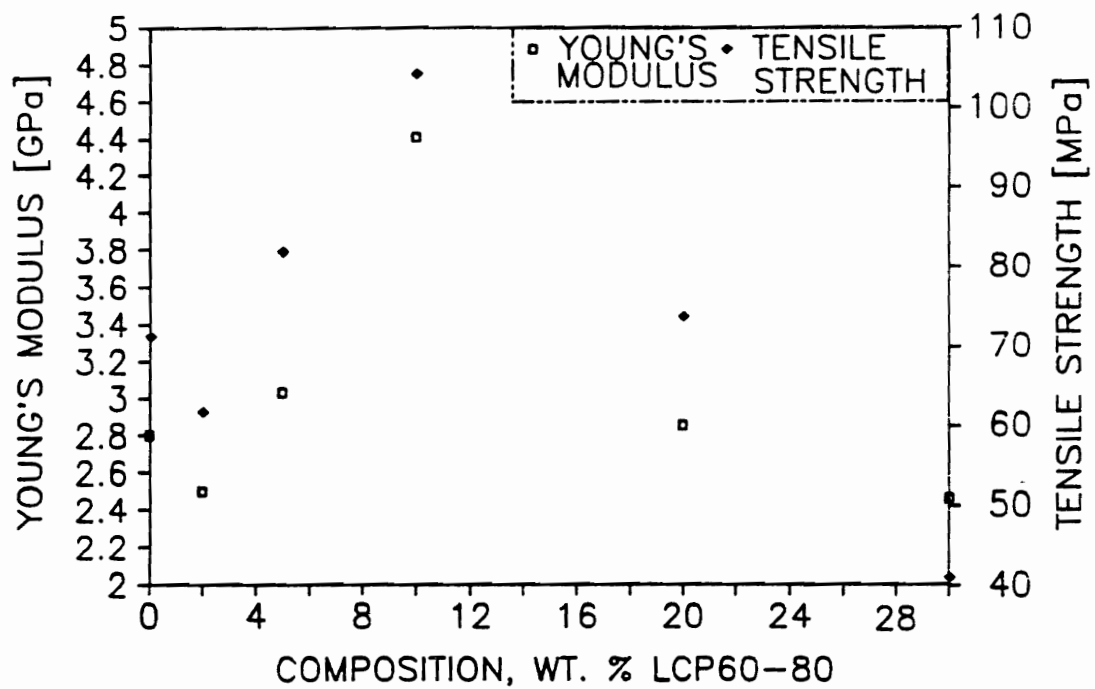
Figure 29. Tensile properties of extruded sheets of PET/LCP60-80 blends.
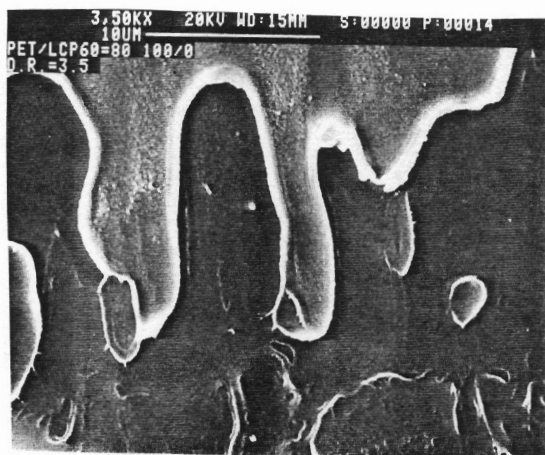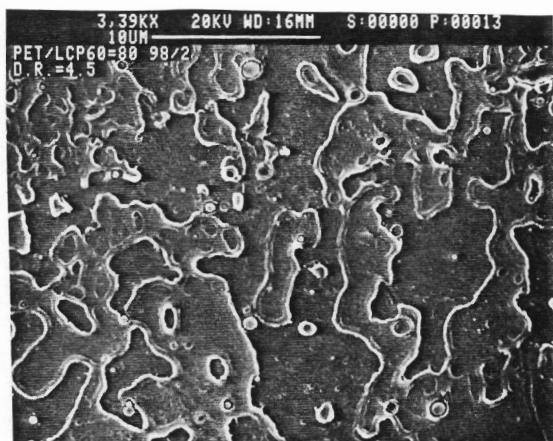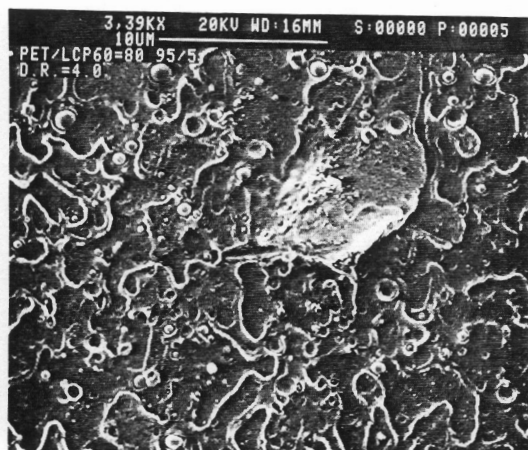
Figure 30. Scanning electron micrographs of fracture surfaces of PET/LCP60-80 blend sheets. The samples were fractured along the flow direction: (a) 100/0, (b) 98/2 and (c) 95/5.
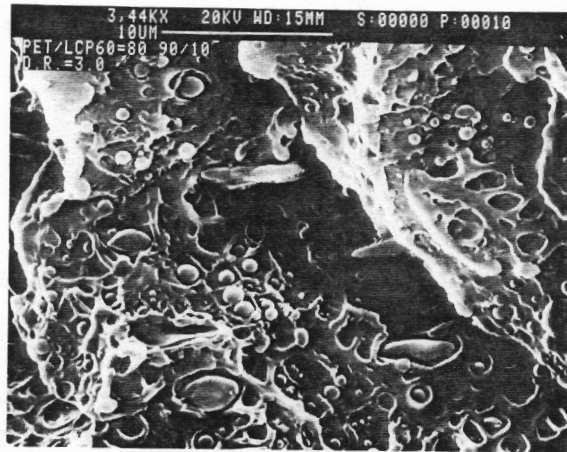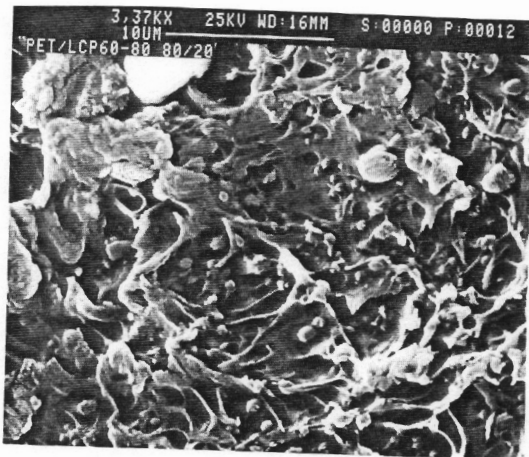
Figure 31. Scanning electron micrographs of fracture surfaces of PET/LCP60-80 blend sheets. The samples were fractured along the flow direction: (a) 90/10 (b) 80/20 and (c) 70/30.

The mechanical properties observed earlier may be explained to some extent by the morphological results. At the lower concentrations of 2 and 5 wt % LCP, the LCP phase consists largely of spherical domains which do not contribute any significant reinforcement to the PET matrix. As the concentration is increased further, the 90/10 blend shows for the first time a clear elongation of the LCP phase. This elongated LCP structure reinforces the PET matrix effectively and thus the properties of the blend are higher than pure PET. However, as the concentration of the LCP is further increased, the LCP domains in the 80/20 blend are still largely spherical but appear to have lost their bonding or adhesion with the PET matrix as evidenced by the presence of holes much larger than the LCP domain size. The morphology of the 70/30 composition blend exhibits a combination of spherical and ellipsoidal LCP domains. However, the modulus and strength of this blend are lower than even pure PET, again suggesting a loss of adhesion between the two phases. This sort of composition dependence of the properties has sometimes been seen by other researchers, although with different systems and with different levels of the LCP in the blend. For example, Brostow et al. (6) found an initial decrease and then a maximum in properties in injection-molded blends of PET/LCP60 similar to the trend seen in injection-molded samples of PET/PHB copolymers with varying levels of the PHB component by Jackson and Kuhfuss (99). In extruded filaments of PC/LCP blends, Malik et al. (128) observed drastic improvements in the tensile modulus and strength behavior up to 10 wt % LCP in the blend. Further increase in the LCP content up to 50 wt % resulted in a drop in properties which was attributed to poor wetting and a lack of adhesion between the polymers. Also, Isayev and Modic (111) reported a maximum in properties of extruded rods, compression molded sheets and injection molded disks of PC/LCP2000 blends, processed via several different conditions, at LCP levels between 0 and 10 wt % (in the 0-30 wt % LCP range studied).

Sheets of blends of PET/LCP60 were also made. However, due to the limited quantities of the LCP available, only the composition ratios 80/20 and 70/30 were made using the same processing conditions as for the PET/LCP60-80 blends. The tensile modulus and tensile strength of the 80/20 and 70/30 composition sheets with draw ratios of 4.4 were observed to

be 3.2 GPa and 58 MPa, and 4.08 GPa and 58 MPa, respectively. Thus it is obvious that the effect of increasing LCP composition on the mechanical properties is different for the two LCPs, LCP60 and LCP60-80. The morphology of the PET/LCP60 70/30 blend sheet is shown in Fig. 32 where the fracture surface of the sheet (a) along and (b) across the flow direction are shown. This morphology is quite different from the PET/LCP60-80 sheets shown earlier in that the LCP phase is seen here to be elongated into highly extended fibrils of about 1-2 μm in diameter and having aspect ratios of over 25. The reason for the differences in the LCP morphology in the two cases may be found in Fig. 33 where the complex viscosity behavior is plotted against the frequency for PET, LCP60 and LCP60-80 (preheated to 300°C) at 280°C. It is clear that the viscosity of LCP60 is lower than that of PET in the entire frequency range tested whereas the LCP60-80 has a viscosity higher than PET at low frequencies and then crosses over to become lower than PET at frequencies above 10 sec^{-1}. It was necessary to preheat the LCP60-80 to 300°C for 3 minutes to melt the polymer for the rheological test. Nevertheless, it is clear that at the processing conditions for extrusion, the PET/LCP60 has a more favorable viscosity ratio (less than unity) than the PET/LCP60-80 system. Therefore the LCP60 is capable of being deformed to a higher level as verified from the morphology in Fig. 32. This higher level of fibrillation leads to better properties at the higher LCP compositions.

A few additional comments regarding the above results are necessary. The absence of significant fibril formation of the LCP60-80 phase in the above blend sheets is believed to be due to several factors. At low levels of LCP concentration in the blend, it is intuitive to expect that coalescence of the dispersed LCP droplets will be inhibited. From the theory of drop deformation and breakup, it is known that larger drops result in higher Weber (or Capillary) numbers, which favor fibrillation (16). Thus when the concentration of the dispersed phase is low, resulting in relatively small droplets, the surface tension effects that tend to stabilize the droplets are still greater than the viscous shearing/extensional forces that tend to deform the droplets. Consequently the LCP domains remain as spherical droplets or at best ellipsoidal domains. Also, due to the low melt strength of the blends at the processing temperatures of interest, the draw ratios that could be achieved were limited. It is quite widely observed that
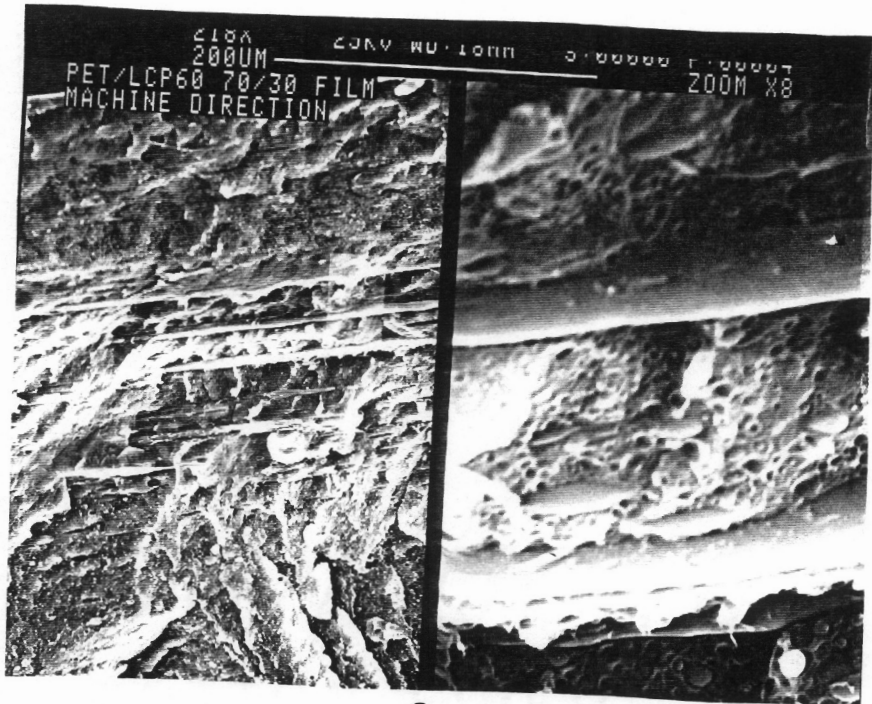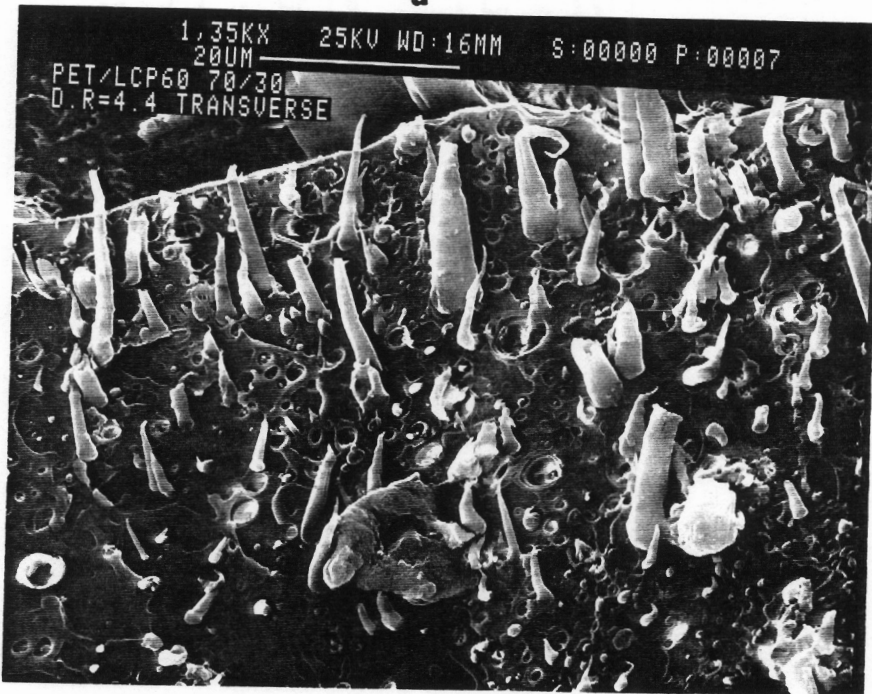
Figure 32. Scanning electron micrographs of fracture surfaces of PET/LCP60 70/30 blend sheet. The samples were fractured (a) along and (b) across the flow direction.
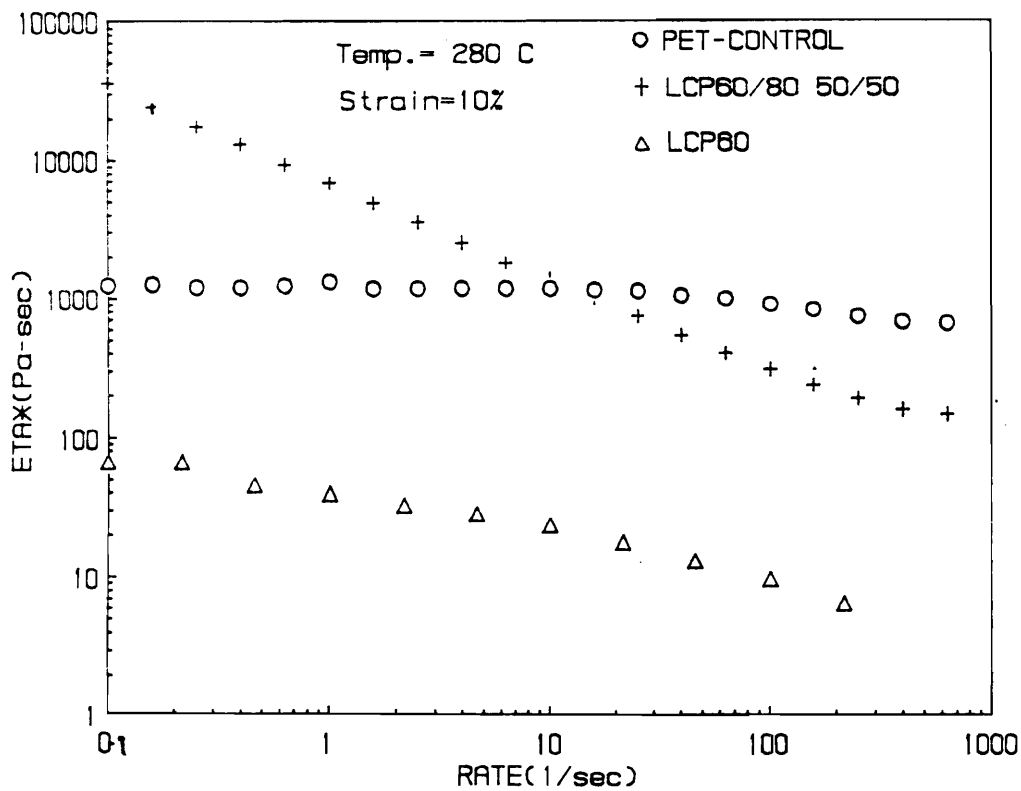
Figure 33. Complex viscosity versus frequency for pure PET, LCP60 and LCP60-80.

higher draw, which implies higher extensional force, is very effective in the fibrillation process as discussed in chapter 2. Thus the inability to reach high draw ratios, due to processing limitations, would be another possible reason for the lack of fibrillation especially at the higher LCP contents. Furthermore, the incomplete melting of the LCP60-80 crystallites is also likely due to the low processing temperatures employed in the sheet extrusion. The presence of residual crystallinity in LCPs has been shown earlier to inhibit chain alignment and formation of fibrillar structures (103.106). The low temperatures were necessary so as not to degrade the PET during the processing. Lastly, the viscosity ratio, as discussed in the previous paragraph, is greater than unity at low shear rates and is thus not favorable for fibrillation. Although, several possibilities and explanations have been discussed above, the value of these results is probably in illustrating the multitude of factors that govern the morphology of two-phase blends and in demonstrating that unless a variety of processing conditions can be optimized simultaneously, the difficulties involved in obtaining good properties by blending polymers will persist. Thus it is concluded that if the processing conditions in the sheet extrusion could be further optimized, then more significant enhancements in the mechanical properties of PET are possible by blending with LCPs. It is believed that optimization of the sheet extrusion process may be obtained by the following steps, preferably reached simultaneously: improving the melt strength to prevent the necking of the extrudate, increasing the draw ratio of the sheets and achieving a viscosity ratio less than unity under processing conditions.

4.1.2 Injection Molding

Injection-molding of several systems of PET/LCP blends in different compositions was conducted in order to determine the property enhancements of PET that could be attained. Although the emphasis here was to investigate the property enhancements in PET with relatively small amounts of the LCP (typically less than 50 wt %), some experiments were also conducted to cover the whole range of compositions i.e. 0 wt % to 100 wt % of the LCP in the

blend. It should be added here that the general procedure for injection-molding was given in the previous chapter. However, since the processing conditions associated with each system were different, they are discussed separately for each blend and/or composition as the case may be. Also, the mechanical properties of the LCP composites made in this study with be compared with data on similar inorganic fiber-filled composites available in the literature so as to get some idea about the relative magnitude of property enhancements that are possible with LCP reinforcements.

Plaques of PET/LCP blends were injection-molded using the processing conditions described below. The injection pressure in each case was 1000 psi and the injection and cooling times employed were 2 seconds and 40 seconds. respectively.

PET/LCP60-80   Temperatures - 200°C, 260°C, 320°C, 290°C and 25°C in zones 1-3, nozzle and mold, respectively

PET/VECTRA A   Temperatures - 200°C, 290°C, 310°C, 290°C and 25°C in zones 1-3, nozzle and mold, respectively

PET/HX4000   Temperatures - 245°C, 290°C, 310°C, 290°C and 25°C in zones 1-3, nozzle and mold, respectively

The tensile properties viz. the tensile modulus and tensile strength in the machine direction for the plaques processed as described above are shown in Table 4. The tensile modulus (TM) and tensile strength (TS) of pure PET were measured to be 1.87 GPa and 66.0 MPa, respectively. In comparison, the properties of the PET/LCP60-80 blends show a significant increase in the TM with increasing LCP concentration. The TM of the 90/10 composition blend is roughly 0.6 times higher than pure PET. However, with 30 and 50 wt % of the LCP60-80 in the blend, the TM of the blends increase by factors of over 2.6 and 3.4 times that of pure PET. It is of interest to point out that the TM and TS of pure LCP60-80 (LCP60/LCP80 50/50 wt % blend) injection-molded plaques processed under similar conditions are reported to be 2.19 GPa and

81.6 MPa (138). Thus, the moduli of the PET/LCP60-80 blends discussed above are actually higher than those of either of the pure components. The reasons for this observed synergism are not very obvious. However, some possibilities for this behavior will be discussed later in this section.

Before moving on to the next set of results, it seems necessary to address the fact that the LCP composition/blend properties relationship for the PET/LCP60-80 sheets and plaques show different behavior. For the sheets, a maximum in the properties was observed at 10 wt % of the LCP in the 0-30 wt % range studied whereas for the injection-molded plaques the properties increased with increase in LCP composition up to the 50 wt % LCP blend examined. One can readily infer that the degree of property enhancements as well as the level of LCP composition in the blend associated with those property enhancements are quite different for the two vastly different processing methods. Some of this seeming inconsistency may be removed if one looks closer at the processing conditions for the two processes. The maximum temperature of the blend in the case of the sheet extrusion process was 295°C. The temperature could not be increased any further due mainly to the extremely poor melt strength of the extrudate. In injection-molding, the maximum temperature was 320°C. It has been shown for several LCPs, as discussed in the literature review, that in general an increase in the processing temperatures results in an increase in the mechanical properties. Secondly, due to processing limitations, the maximum draw ratios that could be achieved in sheet extrusion were about 5. Simplified calculations using standard equations (165) for the maximum extension rates imposed on the melt during drawing of the sheets were estimated to be roughly 0.56 sec^{-1}. In contrast, the average extension rate at the advancing front in the injection molding process was estimated using equations given in ref. (174) to be of the order of 43 sec^{-1}. Thus it is clear that the injection molding process is associated with extension rates that are two orders of magnitude higher than those present in the drawing of sheets. These higher extension rates promote much higher levels of orientation as well as fibrillation. It of interest to add here that the extension rates in the drawing of extruded strands were of the order of 50 sec^{-1} which are indeed of comparable magnitude to those in the injection molding process.

Furthermore, some quick estimates of the magnitude of shear rates involved in the sheet extrusion and injection molding processes above yielded the following results. The shear rate in the extruder was estimated to be about 17 sec^{-1} whereas the shear rate in the sheet die was about 54 sec^{-1}. In comparison, the shear rate in the mold was calculated to be about 250 sec^{-1} whereas the maximum shear rate for injection molding, which normally occurs in the sprue, was estimated to be 16660 sec^{-1}. Thus even the shear rates in the injection molding process are significantly higher than those encountered in the sheet extrusion process. The SEMs of the injection molded plaques of PET/LCP60-80 90/10, 70/30 and 50/50 composition ratios all exhibited long fibrils of the LCP phase in the PET matrix. However, it is believed that it is the higher extension rates that are responsible for the formation of the fibrils in injection molding and not the higher shear rates. In fact, in an earlier study (162) conducted on the investigation of morphological development in PC/LCP60 and N6,6/LCP60 blends deformed in a uniform shearing field, it was found that shear rates of about 100 sec^{-1} and total strains up to 10,000 were not capable of forming LCP fibrils in the matrix. Thus it becomes important to realize that the processing conditions as well as the effects of the flow type can both significantly affect the morphology and hence properties of in situ LCP composites.

Blends of PET with two other LCPs, Vectra A and HX4000, were also injection-molded. The properties of PET/Vectra A and PET/HX4000, both containing 20 wt % LCP, are also shown in Table 4 from which it is clear that with the addition of the LCP, the modulus of PET is again enhanced from 1.87 GPa to 3.42 GPa and 4.71 GPa, respectively.

The morphology and degree of molecular orientation of some of these systems were examined so that the reasons for the enhancements may be established. Thus the scanning electron micrographs (SEM) of the fracture surface of the injection-molded plaques are shown in Figs. 34 and 35. Micrographs of samples fractured along (a) and across (b) the machine (or flow) direction of the plaque in the skin (Fig. 34) and core (Fig. 35) regions are shown. As can be seen from these micrographs, numerous fibrils of the Vectra A phase in the PET matrix are present in both the skin and the core of the plaque. The fibril diameters range from roughly 0.5 μm to 2 μm and have large aspect ratios. Also noteworthy is the fact that the fibrils appear

Table 4. Tensile properties of PET/LCP injection-molded plaques measured in the ma-

MATERIAL	TENSILE MODULUS* [GPa]	FLEX MODULUS* [GPa]	TENSILE STRENGTH* [MPa]
PET	1.87 (0.275)	2.44 (0.251)	66.0 (0.74)
PET/LCP60-80 90/10	3.21 (0.39)	-	60.95 (1.22)
PET/LCP60-80 70/30	4.90 (0.13)	-	67.19 (2.59)
PET/LCP60-80 50/50	6.40 (0.37)	-	72.45 (5.45)
PET/VECTRA A 80/20	3.42 (0.19)	4.55 (0.25)	103.66 (4.57)
PET/HX4000 80/20	4.71 (0.43)	4.20 (0.52)	56.99 (2.18)

*Standard deviations are given in parenthesis
PET is Poly(ethylene terphthalate)

to be well aligned along the flow direction in both the skin (Fig. 34a) and core (Fig. 35a) regions of the plaque. It should be made clear at this point that no distinct skin-core structure was readily discernible for this particular system. Thus the reference to the skin and core regions above is made to distinguish the regions of proximity to the surface and central regions of the plaque, respectively.

To determine the differences, if any, in the degree of molecular orientation attained in the skin and core regions of the plaque, the plaque was microtomed into many layers along the flow direction. Wide- angle x-ray diffraction (WAXS) patterns of the skin and core regions are shown in Fig. 36. The azimuthal dependence of the WAXS pattern in Fig. 36a, evidenced by the presence of relatively sharp arcs, is indicative of the high degree of molecular orientation present in the skin region. The d-spacing calculated from the WAXS pattern is 4.68 °A which was determined to correspond to that seen in crystalline Vectra A. In Fig. 36b there is no azimuthal dependence in the scattering pattern which implies that although there is some crystallinity in the LCP phase, there is no preferred direction of molecular orientation in the core of the plaque. The complete ring observed in Fig. 36b could be due to two possible reasons. First, it is possible that the Vectra fibrils in the core do not possess any significant orientation. Alternately, it is possible that the fibrils of the Vectra A possess a high degree of molecular orientation on an individual basis but are randomly distributed in the core leading to an unoriented core on a global scale. However, the SEMs in Fig. 35 show quite clearly that the fibrils are well aligned in the flow direction even in the core. Thus the more likely explanation is that the LCP phase in the core is itself unoriented. The lack of molecular orientation of the LCP phase in the core raises another question. Is this lack of orientation due to a rapid relaxation of orientation once attained or is it a consequence of the flow in injection-molding which is known to lead to skin/core effects? As mentioned earlier in chapter 2, LCPs have long relaxation times of orientation in the supercooled state which can be of the order of a few minutes. Furthermore, it has been observed that the orientation induced in an LCP can be retained even upon reheating into the melt for several minutes and then recooling. Thus it seems more reasonable to assume that the lack of orientation in the core is not due to thermal
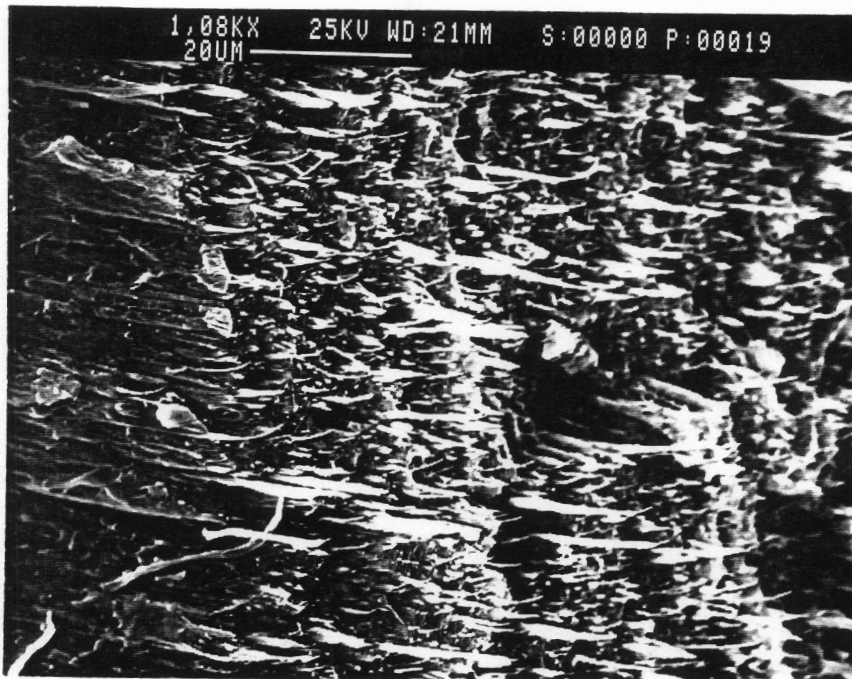
Figure 34. Scanning electron micrographs of the fracture surfaces of PET/Vectra A 80/20 injection-molded plaque in the skin region (a) along and (b) across the flow direction.
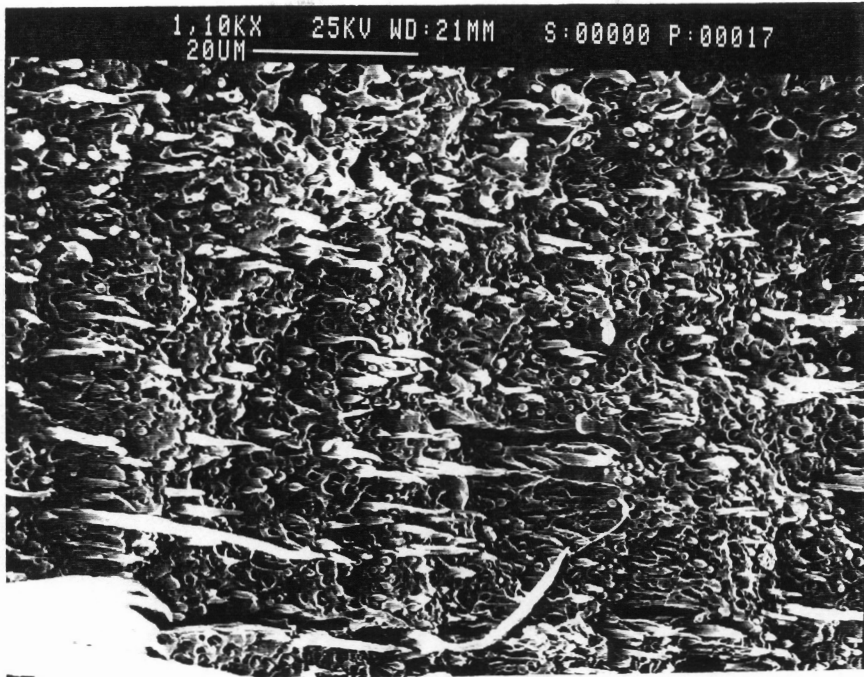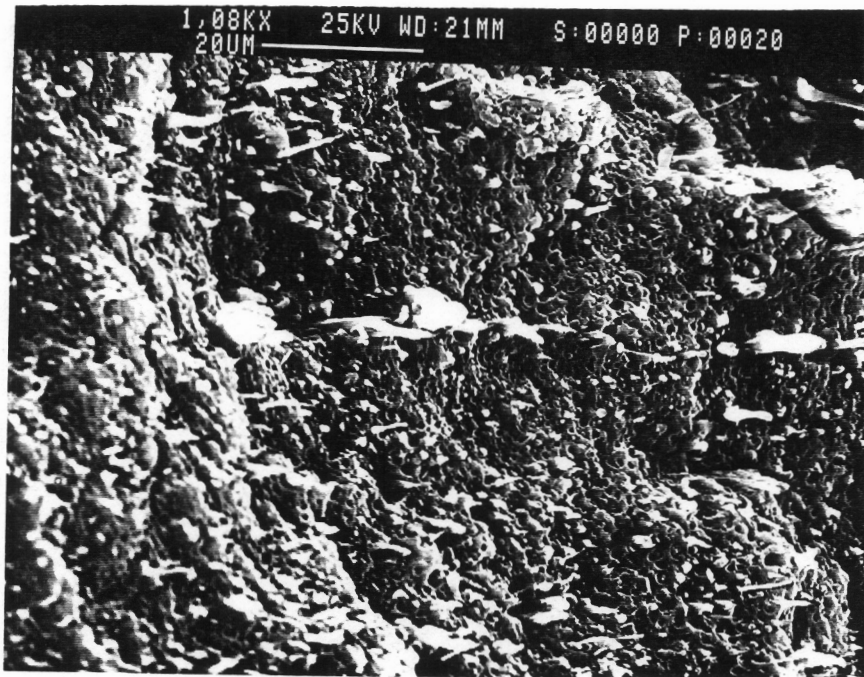
Figure 35. Scanning electron micrographs of fracture surfaces of PET/Vectra A 80/20 injection-molded plaque in the core region (a) along and (b) across the flow direction.

relaxation caused by differences in the thermal gradients but rather due to flow effects associated with injection-molding wherein the predominantly shear flow in the core is incapable of inducing any significant orientation.

In contrast to the morphology observed for the PET/Vectra A 80/20 system discussed above, the PET/HX4000 80/20 plaques exhibit a different morphology as can be seen in Fig. 37. In particular, the size of the LCP dispersed phase is much smaller than in the case of PET/Vectra A blends. Also, the white specks observed in Fig. 37a are HX4000 fibrils with the size ranging from 0.1 μm to 3 μm in diameter. They appear to have a smaller aspect ratio compared to the Vectra A fibrils. One more observation regarding the properties reported in Table 4 is mandated. Specifically, the tensile modulus and strength of HX4000 at room temperature are reported to be 21.4 GPa and 89 MPa (147) whereas the same for Vectra A are reported to be 9.6 GPa and 165 MPa (148). This trend is reflected in the properties shown in Table 4 where the modulus of the PET/HX4000 system is higher but its tensile strength lower than the PET/Vectra A blend. In fact the TM and TS of the PET/Vectra A blend is identical to that predicted by the simple law of mixtures (based on the weight fractions) whereas the TM and TS of the PET/HX4000 blend are somewhat lower than the predicted values.

As mentioned earlier, the emphasis of the above studies was on blends where the LCP was typically less than 50 wt % in the blend. However, it was also of interest to determine how the mechanical properties of the blends would be affected if the LCP was the major component in the blend. Thus blends of PET/Vectra A in the composition ratios of 100/0, 80/20, 40/60, 30/70, 20/80 and 0/100 were injection-molded. Also, PET/LCP60-80 blends in the composition ratios of 100/0, 90/10, 70/30, 50/50, 30/70, 10/90 and 0/100 were injection-molded. These two particular systems were chosen with one additional thought in mind. Several researchers (6,116,117,120) have suggested the possibility of partial miscibility between matrices such as PET and PC with LCP60 as discussed in chapter 2. Due to similarity in chemical structure, it is likely that the phase behavior of the LCP60-80 blend with PET would also show partial miscibility. On the other hand, the PET/Vectra A system is believed to be immiscible as will be shown a little later in this section. Thus it was hoped that by comparing the mechanical
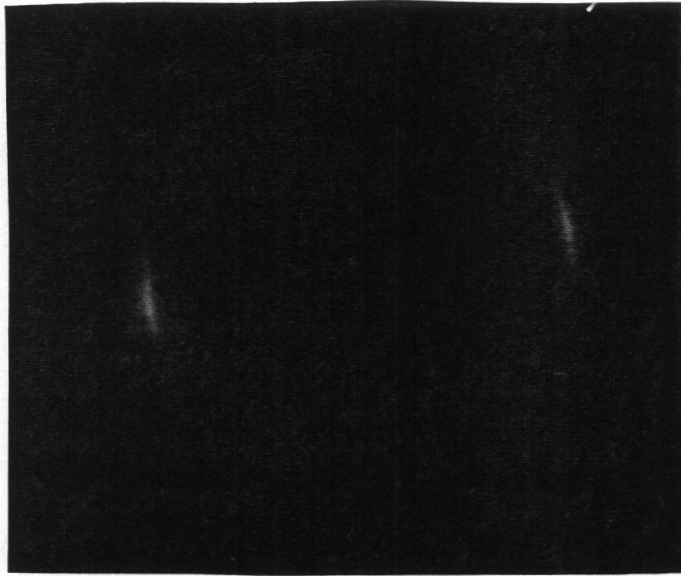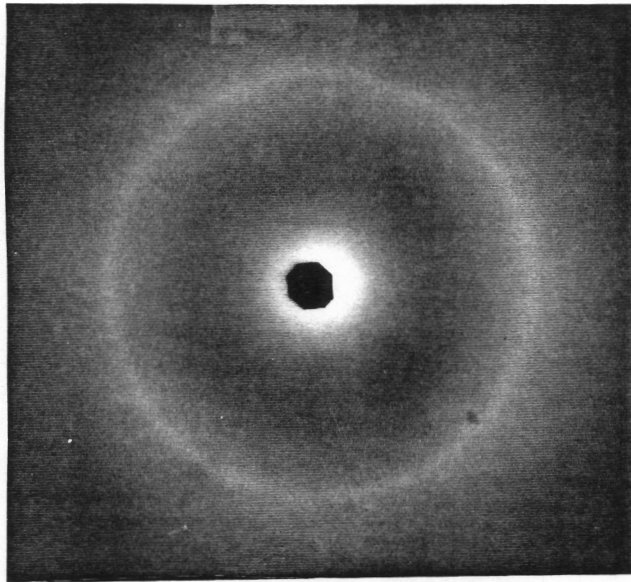
Figure 36. Wide-angle x-ray diffraction pattern of a PET/Vectra A 80/20 injection-molded plaque (a) skin and (b) core.
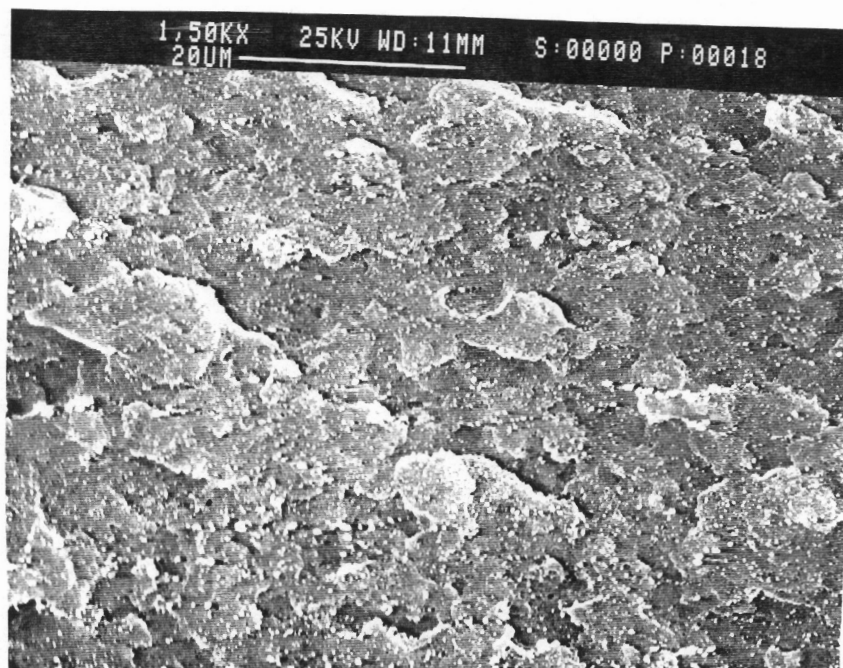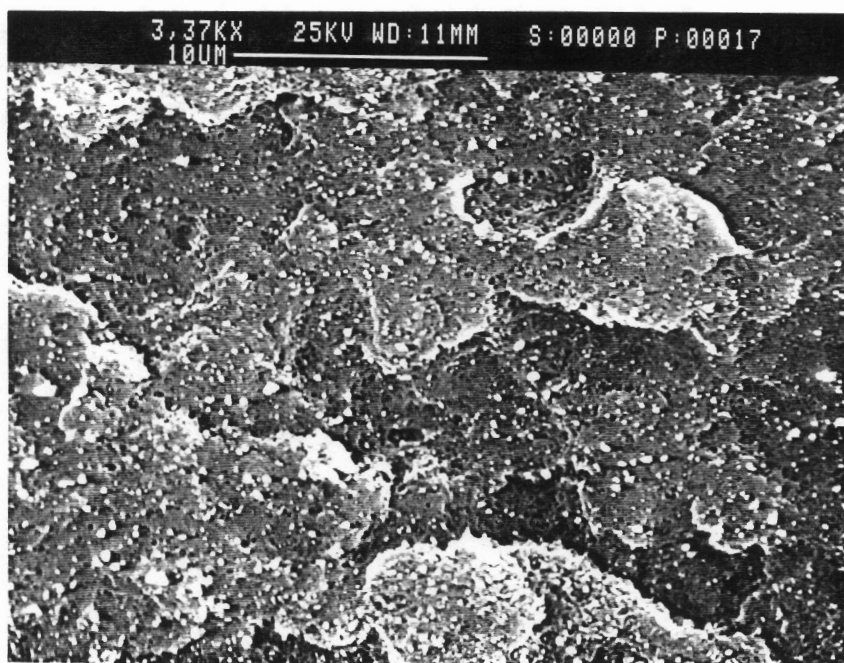
Figure 37. Scanning electron micrographs of fracture surfaces of PET/HX4000 80/20 injection-molded plaque along the flow direction: (a) low and (b) high magnifications.

property behavior, and in particular the dynamic torsional moduli of the PET/Vectra A and PET/LCP60-80 blends, some more information regarding the effects of partial miscibility might come to light.

Results from the flexural modulus tests of blends of PET/Vectra A injection-molded plaques are summarized in Fig. 38. The plaques were annealed at 200°C for 30 minutes prior to testing. The flexural moduli of pure PET and pure Vectra A900 were measured to be 2.2 GPa and 12.66 GPa, respectively. In comparison the flexural moduli of the PET/Vectra blends in the compositions ratios 80/20, 40/60, 30/70 and 20/80 by weight were measured to be 4.55 GPa, 12.41 GPa, 15.49 GPa and 13.12 GPa, respectively. The standard deviations in all the cases were found to be within 5 % of the average values. Thus, the flexural moduli of the PET/Vectra 30/70 and 20/80 blends are actually higher than that of pure Vectra alone. Furthermore, even the PET/Vectra 40/60 blend does not show any significant difference in the flexural modulus from pure Vectra.

The results of the dynamic mechanical analysis of the PET/Vectra A annealed plaques are shown in Fig. 39 where the torsional storage moduli (G′) have been plotted as a function of temperature. The torsional storage moduli of the above plaques at room temperature were observed to be 1.18 GPa, 1.60 GPa, 1.57 GPa, 1.54 GPa and 1.74 GPa for the PET/Vectra 100/0, 40/60, 30/70, 20/80 and 0/100 composition ratios, respectively. Furthermore, it can be observed that the value of G′ at elevated temperatures as well as the temperatures corresponding to the onset of flow for the blends are close to those for pure Vectra A. The glass transition (Tg) behavior of the as-molded and annealed blends was also examined. The Tg of the pure PET and pure Vectra as-molded samples were observed to be 87°C and 104°C, respectively. In comparison, the Tg's of the as-molded blends showed a peak at about 88°C and a shoulder in the peak at 104°C. This is clearly indicative of the fact that the two phases in the blends are distinct from one another and are in fact immiscible. The annealed samples showed different behavior in that now the Tg's of pure PET and Vectra A were seen to be 96°C and 106°C. The upward shift in the Tg of PET is due to the annealing effect. However, the blends now exhibit
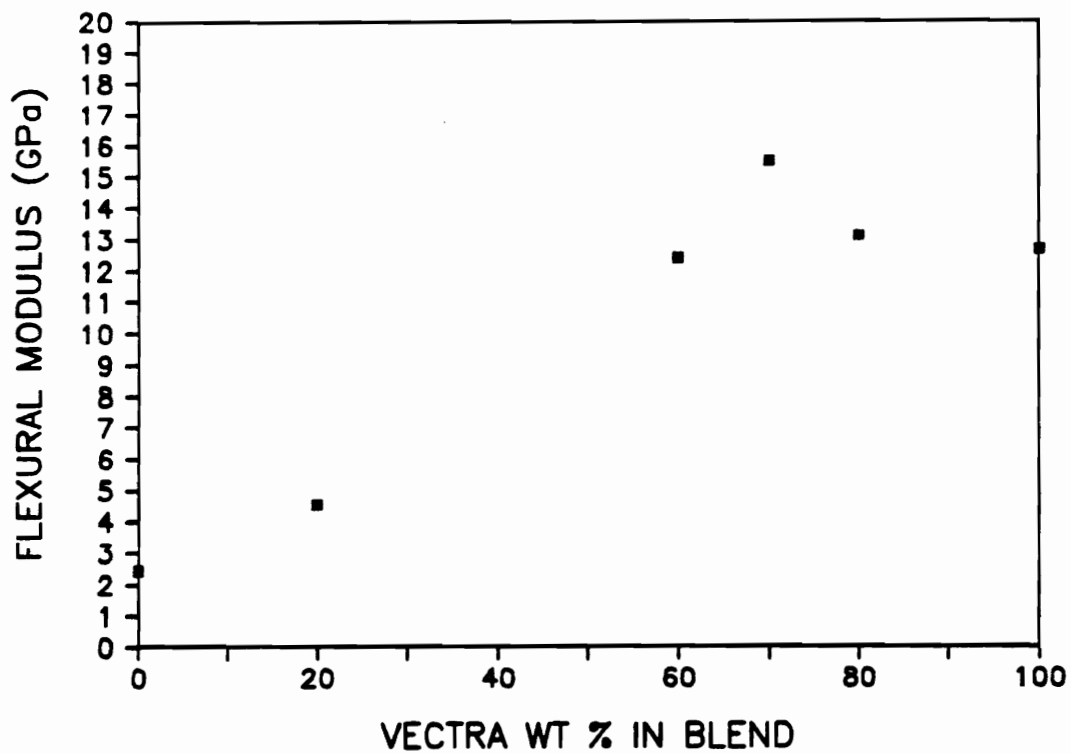
Figure 38. Flexural modulus vs LCP composition of injection-molded PET/Vectra A blends.

a single peak at about 99°C which is much broader. The Vectra peak is now subsumed by the broader peak of PET due to the annealing of the blends.

In Fig. 40 are shown the results of dynamic mechanical analyses of the PET/LCP60-80 injection molded plaques which were annealed at 120°C for one hour. The behavior of the torsional storage moduli, G', of the PET/LCP60- 80 blends appears to be quite different from the PET/Vectra A blends. First, it is clear that the pure LCP60-80 itself has a lower stiffness in the entire temperature range than pure PET as indicated by a lower value of G'. It should be noted here that the samples of LCP60-80 broke at about 200°C for three repeated tests which may be attributed to the brittleness of the LCP. Furthermore, the G' of the blends appear to lie in between the values of PET and LCP60-80 with the possible exception of the 90/10 blend where the G' is higher, though not significantly, than pure PET. The above results thus show that the reinforcing effect of Vectra is better than that of LCP60-80, as gaged by the higher stiffness of the blends, especially at elevated temperatures. This is interesting considering the fact that the glass transition temperature of the PHB units in LCP60-80 is reported to be between 140-180°C which is higher than the glass transition of the PHB/HNA chain units in Vectra A reported at about 104-110°C. Thus the incorporation of the flexible PET chains in the stiff PHB backbone reduces the overall chain stiffness considerably at elevated temperatures.

Much has been said earlier (6,116) regarding the possibility of partial miscibility between PET and LCP60. It was believed that the same possibility might hold true for the case of PET and LCP60-80 blends studied here due to the chemical similarities between LCP60 and LCP60-80. Thus the transition temperatures of the as-molded and annealed samples of the injection molded samples during the dynamic mechanical analyses were also monitored and are summarized in Table 5. In the case of the as-molded samples, three distinct transitions could be observed: a low temperature transition around 70°C, another transition around 86°C and a third one at about 122°C. Further, it can be seen from Table 5 that the low temperature transition decreases with increase in the PET (homopolymer) content from 76°C in pure LCP60-80 to 68°C in the 50/50 blend. In contrast, the transitions at roughly 86°C and 122°C remain largely independent of the blend composition. After annealing the blends at 120°C for one
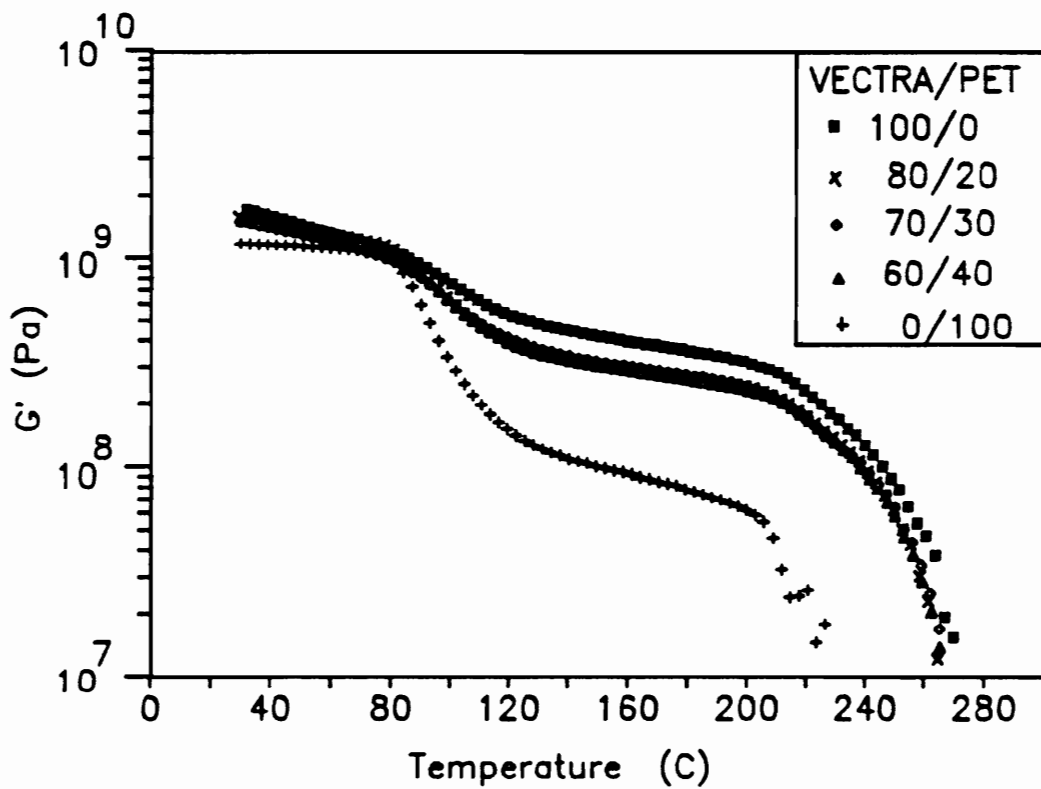
Figure 39. Torsional storage modulus as a function of temperature for injection molded PET/Vectra A blends annealed at 200°C for 30 minutes.
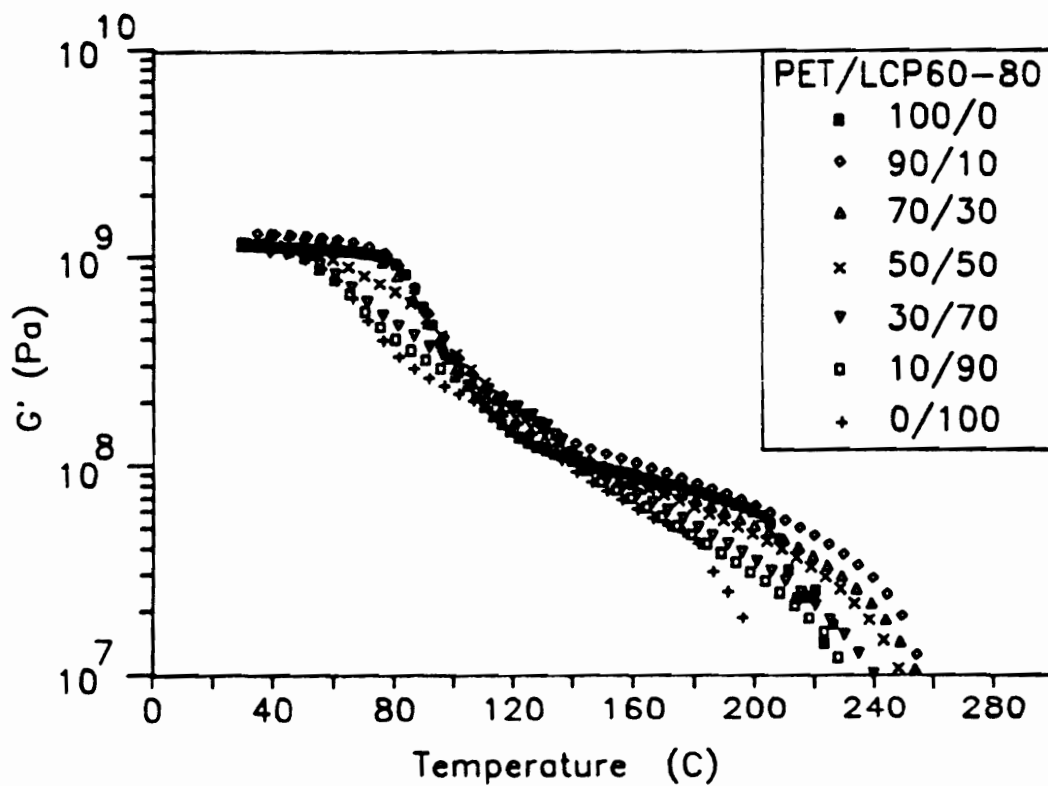
Figure 40. Torsional storage modulus as a function of temperature for injection molded PET/LCP60-80 blends annealed at 120°C for one hour.

hour, the low temperature transition for pure LCP60-80 and the 50/50 blend are lowered to 72 °C and 62°C. respectively. The middle transition increases slowly from 95°C for pure PET to about 103°C for the 90/10 blend. In the annealed samples, another transition at about 145°C is now seen in blends with 50 wt % and more of the LCP in the blend.

The above transitions may be explained as follows. In the case of the as-molded samples, the low temperature transition is attributed to the PET-rich phase of the LCP60-80. This transition, however, decreases with increase in matrix PET content and is believed to be due to the partial miscibility of the PET-rich phase with the matrix PET. Therefore as the matrix PET content increases, a greater percentage of the PET-rich phase is dissolved out by the matrix PET leaving a PET-rich phase which is poorer in PET content. It should be added here that the lowering of this low temperature transition with increasing matrix PET content cannot be attributed to a lower content of the PET-rich phase (due to lower LCP60- 80 in the blend) because if this was the case only a decrease in magnitude of the peak and not a change in where it occurs should be observed. The middle transition at about 86°C is due to the glass transition of the homopolymeric PET phase which remains unchanged with composition as expected. The third transition at roughly 122°C is due to the crystallization of PET which is probably amorphous in the as-molded samples. The transitions in the annealed samples may also be readily explained as follows. Again the low temperature transitions in the blends containing more than 50 wt % of the LCP60-80 are due to the PET-rich phase of the LCP. These temperatures are somewhat lower than in the as- molded samples which could be due to the fact that more of the PET-rich phase is dissolved out by the matrix PET during the annealing step due to the segmental mobility at the elevated temperature although this is not very clear. The middle transition is again due to the matrix PET which is now semicrystalline and thus exhibits a higher Tg than the as-molded samples. The higher Tg with higher LCP60-80 content in the blends could be due to the nucleating effect of the LCP60-80 resulting in increasing levels of crystallinity. Finally, the highest transition temperature is attributed to the glass transition of the PHB-rich phase which can only be observed in the blends with 50 wt % or more of the LCP60-80. It is probably worthwhile to mention here that Kimura and Porter (149) report similar

Table 5. Transition temperatures of injection molded PET/LCP60-80 blends resulting from dynamic mechanical analyses.

Sample PET/LCP60-80	Transition temperatures (°C)					
	As-molded			Annealed		
100/0		84			95	
90/10		86	122		93	
70/30		86	122		93	
50/50	68	84	122	62	100	145
30/70	71	87	122	68	102	145
10/90	73	87	122	71	97	145
0/100	77			78		137
Probable cause	(Tg) PET-rich domains	(Tg) PET matrix	(Tc) PET crystlzn.	(Tg) PET-rich domains	(Tg) PET matrix	(Tg) PHB-rich domains

results in their studies of blends of poly(butylene terephthalate) (PBT) with LCP60 wherein a drop in the Tg of the terephthalate-rich copolyester (i.e. the low temperature Tg) was observed with an increase in the PBT composition in the blends. Also, the higher transition (from the PHB-rich phase) was unchanged with composition suggesting partial miscibility of the PBT with only the PET-rich phase.

4.2   Blends via the Dual-Extruder Mixing Method

This section is devoted to the results and discussion of the blends processed via the mixing method developed in this study. For the sake of clarity this section will be broken up into several smaller sections. First, the rheology of the pure components, and in particular the various LCPs used in this study, will be thoroughly discussed. It is hoped that this discussion will give further insight into the philosophy and need for the development of the new mixing method. Following that, the generation of strands (or rods or filaments) of various thermoplastic/LCP blends will be discussed with respect to the processing conditions and the blend characterization. In the next section, comparison between the single-screw extrusion process and the mixing method will be made for one blend system with respect to the morphology and mechanical properties of the respective blends. Sheet extrusion of the blends via the mixing method will be presented next. One of the goals of this research was to be able to predict the feasibility of blending a given polymer pair a priori. Thus the next section will de devoted to results aimed at answering that question. The blends from the mixing method were also subjected to several post-processing studies and these results will follow. Lastly, some calculations aimed at predicting the pressure drop and shear rate in the mixer and heat transfer in the mixing process will be provided.

4.2.1   Rheology of Pure Components

The rheology of several of the matrix and LCP materials used in this study is discussed in this section. Specifically, the behavior of the melts upon cooling from the melt will be assessed. Then the viscosity (dynamic or steady mode) as a function of frequency (or shear rate) at different temperatures and with different histories will be discussed. Finally, the isothermal crystallization and solidification kinetics of the melts will be examined.

4.2.1.1   Supercooling Behavior

The importance of having a viscosity ratio of dispersed phase to matrix phase of less than one for successful fibril formation has been stressed numerous times in the previous chapters. Furthermore, it is quite clear from Table 3 that many of the thermotropic LCPs used today have high melting and processing temperatures. However, it was also shown in the literature review that the LCPs exhibit varying degrees of supercooling behavior. This behavior was examined first for the pure materials. In Fig. 41 is shown the cooling behavior of LCP60, LCP80, LCP60-80 and pure PET. These tests were performed as discussed in chapter 3. For direct comparison, all the materials were heated to 330°C and then cooled at a preprogrammed rate of 5°C/step (corresponding to a rate of about 3°C/min). The degree of supercooling as defined earlier is the difference between the nominal melting temperature and the temperature at which the material solidifies or crystallizes upon cooling from a temperature (higher than the melting temperature). Thus from Fig. 41, it can be seen that the degree of supercooling of LCP60, LCP80, LCP60-80 and pure PET are roughly 80°C, 20°C, 40°C and 100°C. It is important to point out here that this supercooling window also depends on the preheating temperature upto a limit. Specifically. as the preheating temperature is increased, the degree of supercooling also increases upto an upper limit of the preheating temperature after which the supercooling window remains unchanged. Two other points are also worth noting with regard

to Fig. 41. The way in which supercooling occurs is also important. For example, G' for LCP60 begins to rise gradually at 210°C and continues till about 150°C indicating very slow recovery. G' for LCP80, on the other hand, begins to rise at about 290°C and the recovery is essentially complete at 270°C. Thus a much larger processing window is available with LCP60 than LCP80. Furthermore, it may be observed from Fig. 41 that the magnitude of the complex viscosity of LCP60 is lower than pure PET in the entire temperature range. However, LCP80 has lower values of $\eta^\star$ than pure PET only above 285°C and they are higher than PET at temperatures below that. This crossover of viscosities is important since the viscosity ratio is reversed from less than to greater than unity.

A perhaps clearer picture of this may be seen in Fig. 42. The Vectra A has melting temperature of 283°C. However, when the material is cooled from 300°C it does not solidify (crystallize) until as low as 250°C which is again judged by a rapid rise is either $\eta^\star$ or G'. The actual solidification is in fact somewhat lower but the test is stopped here so as not to overload the transducer. Of further interest in Fig. 42 is the behavior of pure PET when cooled from 290°C and 330°C. In the former case the PET solidifies at about 200°C giving a processing window of ca. 65°C. When cooled from 330°C, the solidification is not complete until about 170°C giving a window of about 100°C. But of greater significance is the magnitude of the viscosity from the two cases. When the PET is cooled from 290°C, its viscosity is higher than that of Vectra in the entire temperature range of interest. If, however, it is cooled from 330°C, its viscosity is lower than that of the LCP in the entire temperature range. The viscosity ratio in the former case is thus favorable for fibril formation unlike the latter case. Furthermore, for processes such as sheet extrusion, film-blowing and blow-molding, where the melt emerging from the die is subject to further deformation, it is imperative that the melt have sufficient melt strength. Although no direct correlation between the viscosity and melt strength is known to exist, it has been observed that the lower the temperature the better is the melt strength. It is amply clear from the above results and discussion that being able to give independent thermal histories to the two polymers allows one to obtain the optimal processing conditions especially with regard to blending high melting LCPs with thermoplastics. As a final note, it ought to be
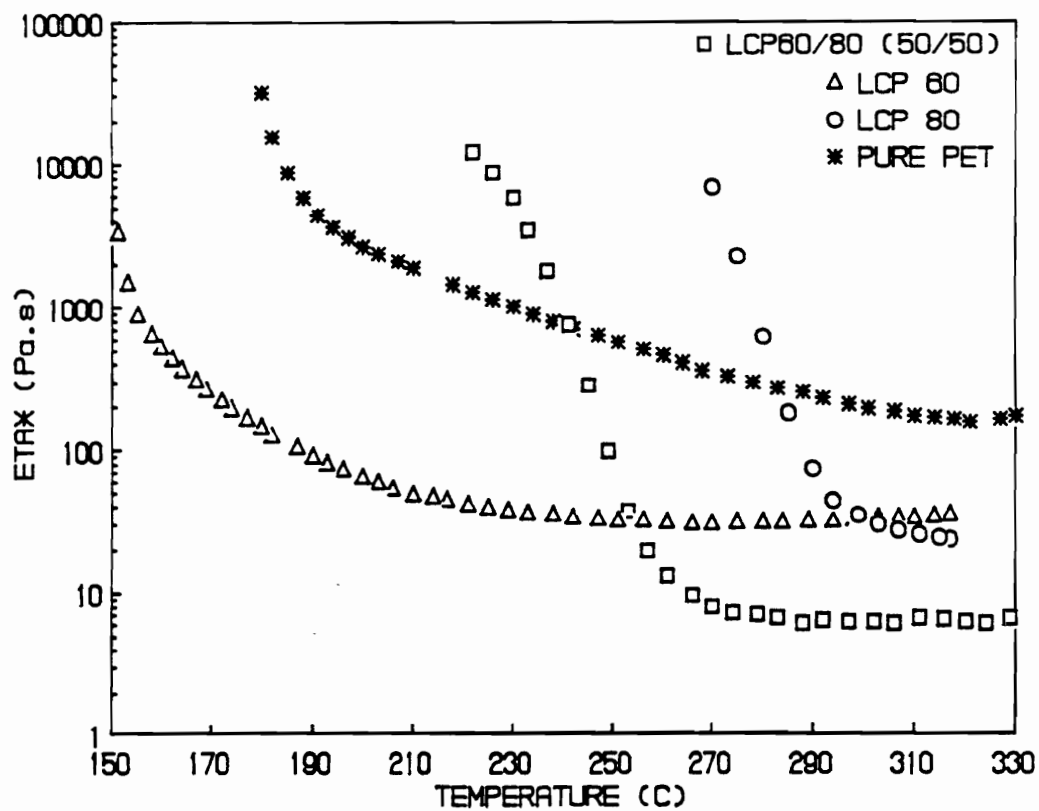
Figure 41. Complex viscosity as a function of temperature during cooling from temperatures higher than flow temperatures for LCP60, LCP80, LCP60-80 and PET.

RESULTS AND DISCUSSION

added here that for the processing of PET/Vectra A blends (to be discussed later), the thermal history given to the polymers during the tests above approximate fairly well the thermal history of the polymers during processing.

Another LCP used in this study was HX4000 which has a melting temperature of 314°C. The cooling behavior of HX4000 is shown in Fig. 43. It is clear from Fig. 43 that the material has a relatively small supercooling window of about 35°C with the recovery being almost complete at 280°C. Also, in this case there does not appear to be much of a difference in the degree of supercooling between the samples cooled from 340°C and 355°C. In light of the previous studies, this is probably indicative of the fact that complete melting of the crystallites is obtained at 340°C and thus no further changes in the supercooling are discerned by heating to higher temperatures.

As mentioned before, one of the other matrix polymers used in this study was polypropylene (PP). The melting temperature of the PP used in this study is 168°C. In Fig. 44 are shown the cooling curves of PP and Vectra B where the Vectra B is cooled from three different temperatures viz. 300°C, 310°C and 330°C. The PP is cooled from 260°C and 280°C. It is interesting to note the cooling behavior of Vectra B from Fig. 44. First, when preheated to only 300°C, the Vectra B solidifies at about 280°C. However, when preheated to 310°C and 330 °C, the solidification temperatures are roughly 250°C for both cases. It is important to note that only a 10°C difference in the preheating temperature (i.e. 300°C and 310°C) results in a 30°C increase in the supercooling window. This effect is most likely due to the melting of the residual crystallites above 300°C in a way similar to that seen for Vectra A900 (156,157). Thus preheating to higher temperatures aids in extending the supercooling and consequently the processing window of the LCPs as mentioned earlier. Also, it is observed from Fig. 44 that the cooling curves for PP cooled from 260°C and 280°C are not significantly different. Tests at higher temperatures were not done for fear of degrading the PP. Nevertheless, it is still clear that the viscosity of the PP is higher than Vectra B only above roughly 255°C and only if the Vectra B is cooled from 310°C or higher.
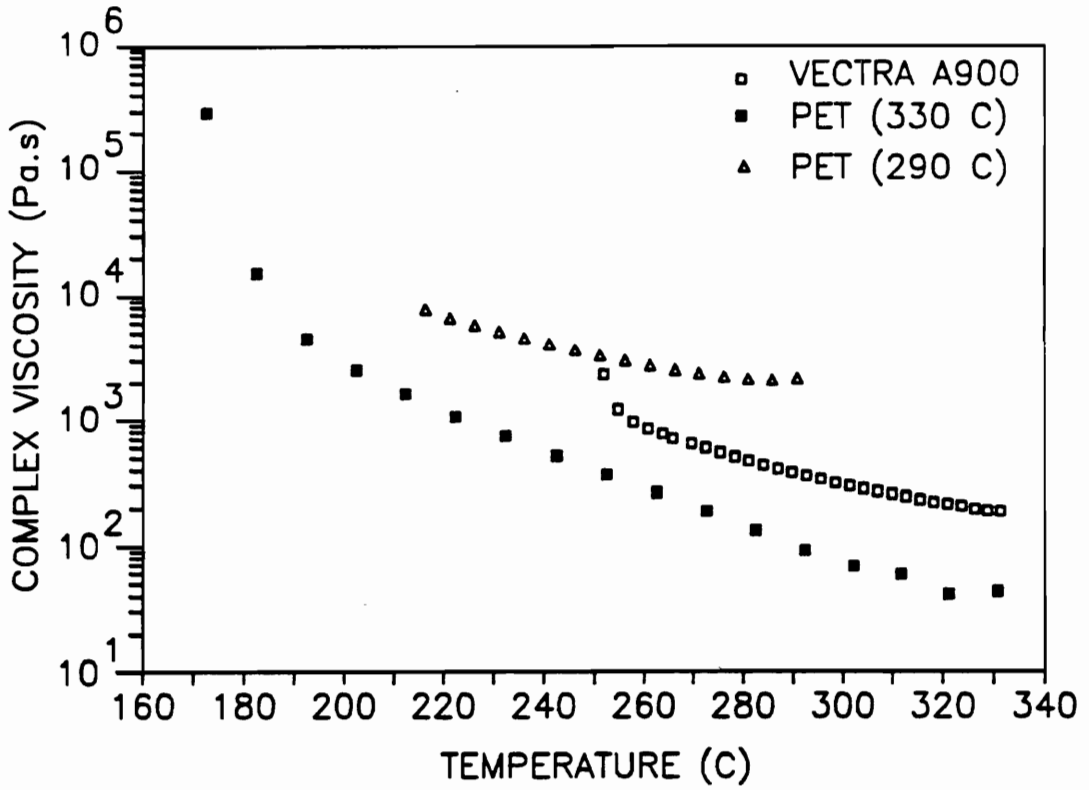
Figure 42. Complex viscosity as a function of temperature during cooling for PET and Vectra A900.
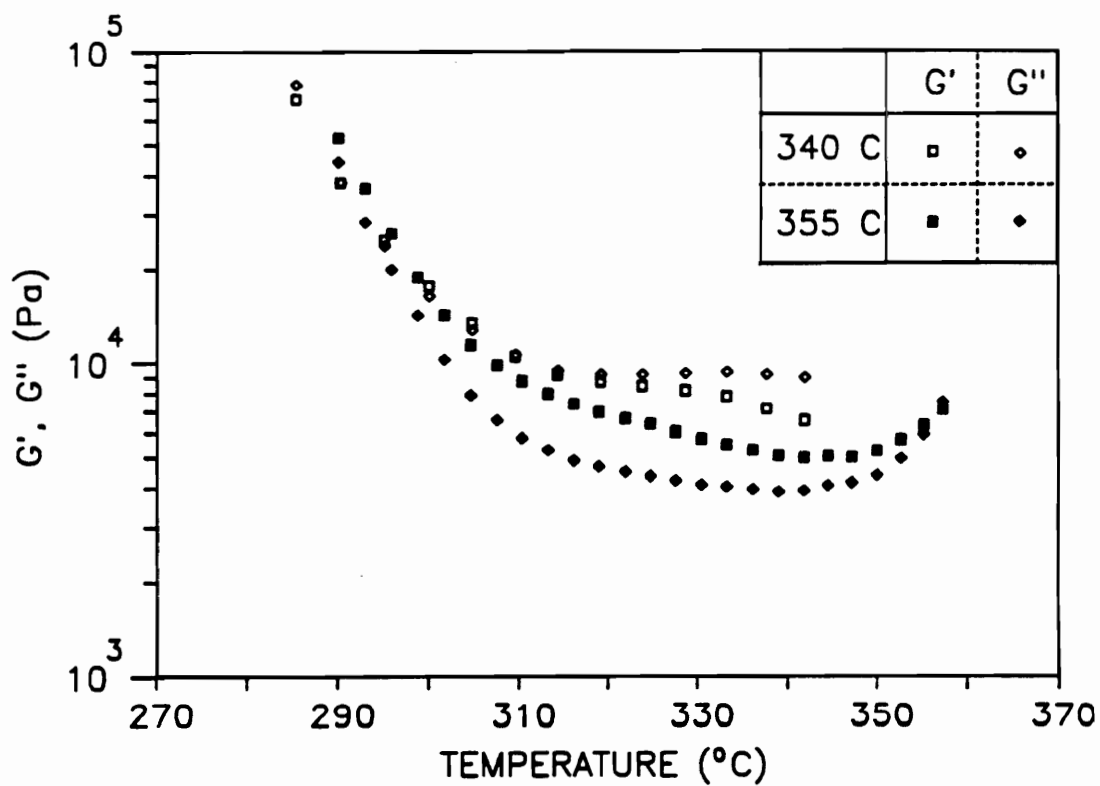
Figure 43. Shear storage moduli (G′) and shear loss moduli (G″) as a function of temperature during cooling for HX4000 cooled from 340°C and 355°C.
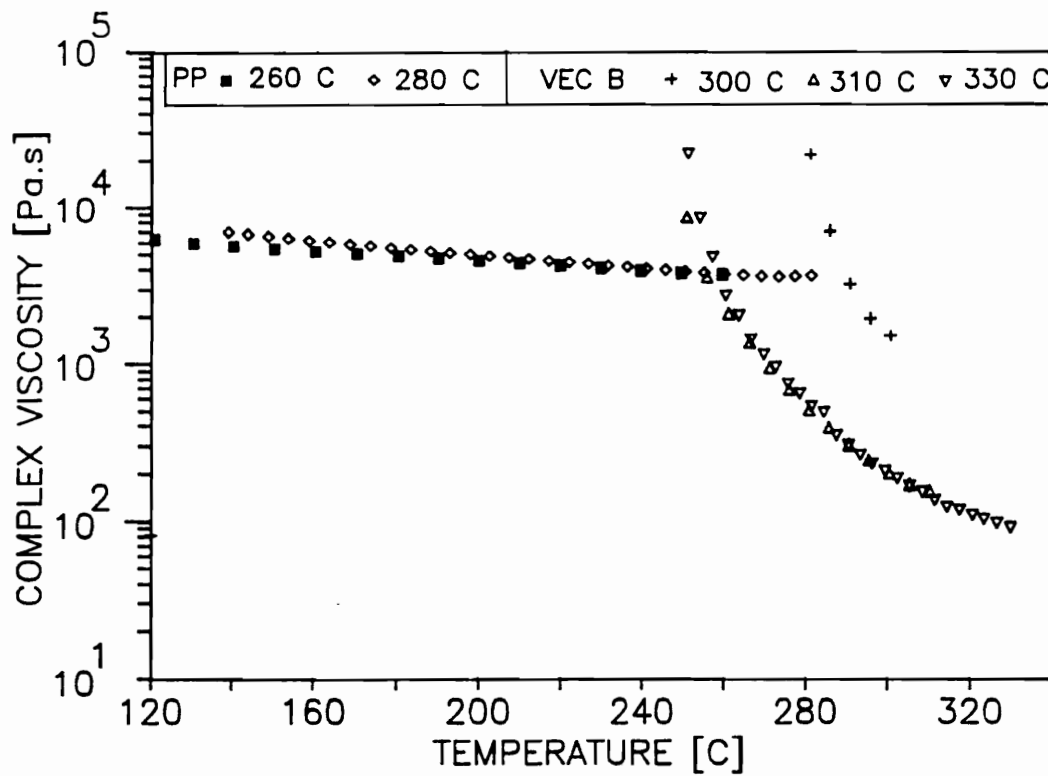
Figure 44. Complex viscosity as a function of temperature during cooling for PP and Vectra B950.

4.2.1.2 Viscosity-rate Behavior

Steady or dynamic rate sweeps of all the materials used in this study were also conducted. These studies were done so as to get better estimates of the magnitude of the viscosity of the different materials at different temperatures and having different thermal histories. Some mention of the viscosity ratio as estimated from the cooling curves was given earlier. However, a better way to determine this viscosity ratio is to conduct steady or dynamic rate sweeps at the temperatures of interest and then use that data to estimate the viscosity ratio at the desired rates. Results for some of these materials are discussed in the following section.

In Fig. 45 are shown the complex viscosity versus frequency behavior of Vectra A900 for three different temperatures 290°C, 300°C and 320°C. It is clear from Fig. 45 that there is indeed a significant dependence of the viscosity on temperature. For example, there is roughly a three fold decrease in viscosity at low frequencies between 290°C and 320°C. This effect as discussed earlier in the literature review is believed to be because of the melting of residual crystallites that remain unmelted below 320°C. Also, it can be seen that the Vectra A900 at 290 °C and 300°C exhibits highly shear thinning behavior with a two decade drop in the complex viscosity over the three decades of frequency tested. However, at 320°C, the material is less shear thinning.

In comparison, complex viscosity data for pure PET at 280°C, 290°C and 310°C is shown in Fig. 46. Two things are noteworthy from Fig. 46. The PET shows Newtonian behavior upto frequencies of about 10 sec^{-1} after which some shear thinning behavior is evident. Furthermore, the viscosity behavior appears anomalous at 310°C and is probably due to degradation of the material at this high a temperature. In fact, it is recommended that this PET not be subject to temperatures above 300°C for any period of time (130).

Perhaps the clearest idea regarding the effect of thermal history on the rheology of LCPs can be seen from Fig. 47. The complex viscosity of Vectra A900 shown in Fig. 45 is repeated on this plot for the sake of comparison. Also plotted in Fig. 47 are the complex viscosities of
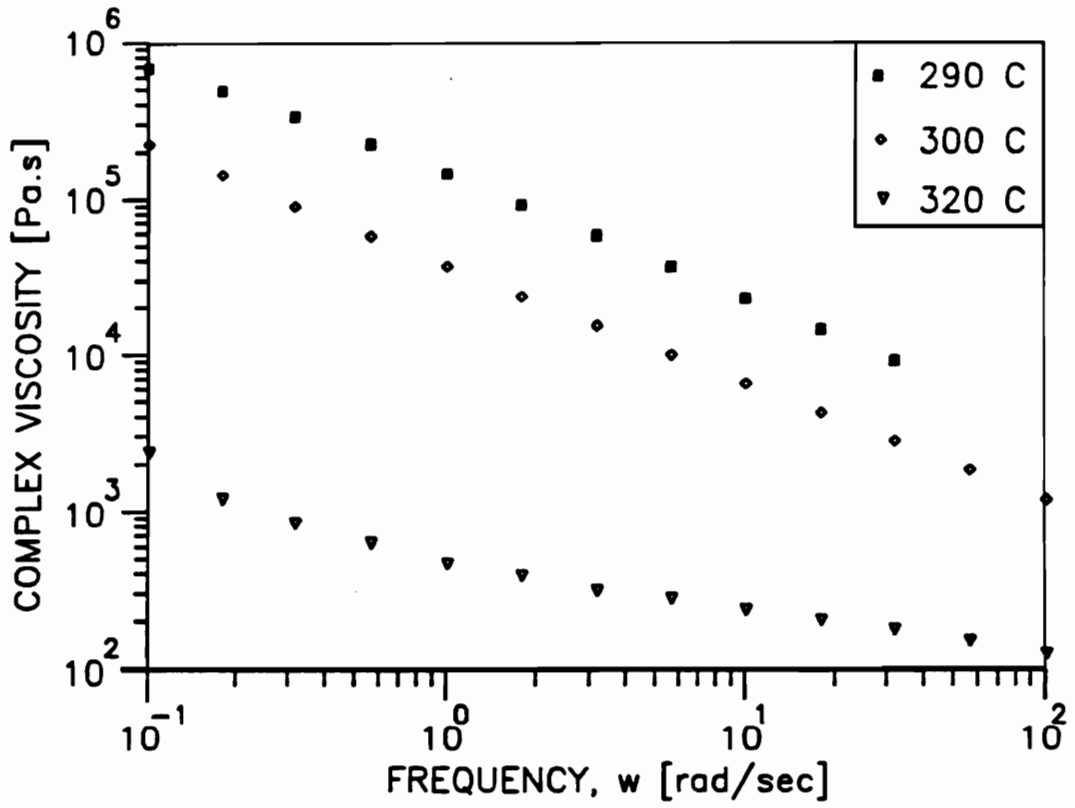
Figure 45. Dynamic frequency sweeps of Vectra A900 at 290°C, 300°C and 320°C
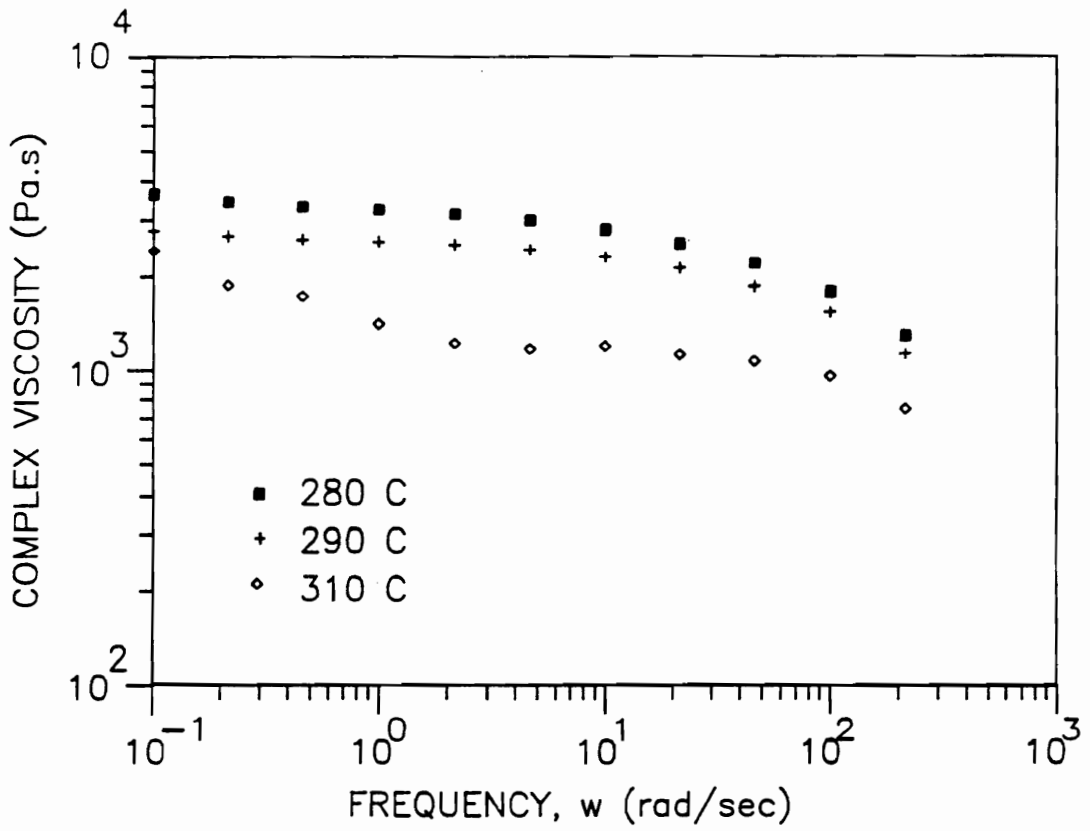
Figure 46.   Dynamic frequency sweeps of PET at 280°C, 290°C and 310°C

Vectra A at 265°C and 285°C *after preheating to 330°*C and the complex viscosity of PET at 265 °C *after preheating to 290°*C . What is observed now is that the viscosity of Vectra at both 265 °C and 285°C after being preheated to 330°C is lower than that of PET (at 265°C) in the entire frequency range. In fact, the viscosity of Vectra A at 285°C is almost the same as its viscosity when measured directly at 320°C.

For further comparison, the viscosity behavior of HX4000 is shown in Fig. 48. Here the viscosity measured directly at 340°C is shown along with viscosity-rate behavior at 290°C, 310 °C and 330°C *after preheating to 340°*C . It is observed that the viscosities at 310°C and 330°C after preheating are close to that measured directly at 340°C. However, at 290°C the viscosity increases above that at 340°C due to the combined effects of crystallization and solidification. In fact, it may recalled from Fig. 43 that upon cooling from 340°C, the G′ remains unchanged until about 310°C and then begins to rise very abruptly due to the crystallization. Thus the viscosity behavior shown in Fig. 48 is consistent with the supercooling behavior discussed earlier. Furthermore, a crossover in the viscosity of PET and HX4000 (except at 290°C) is observed at a frequency of about 5 sec^{-1}.

In Fig. 49, the viscosity of PP at several temperatures is plotted along with the data of Vectra A900 at 265°C and 285°C after preheating to 330°C discussed above. Once again by comparing the viscosity of Vectra A900 at 290°C, 300°C and 320°C (all without thermal history) from Fig. 45 along with the data presented in Fig.49, it is clear that the viscosity of PP would be lower than that of Vectra A900 in the entire frequency range tested. The other thing that needs to be pointed out is the fact that the PP exhibits shear thinning behavior in the entire frequency range at all the four temperatures tested. At the higher temperatures of 240°C and 260°C, there appears to be some tendency for the viscosity to level off at the lower frequency range. Thus due to this shear thinning of the PP, there is no crossover of the viscosities even at higher rates, and therefore the viscosity ratio of Vectra A/PP is greater than unity in the entire frequency range when the Vectra A does not undergo any thermal history i.e. preheating upto temperatures of about 330°C.
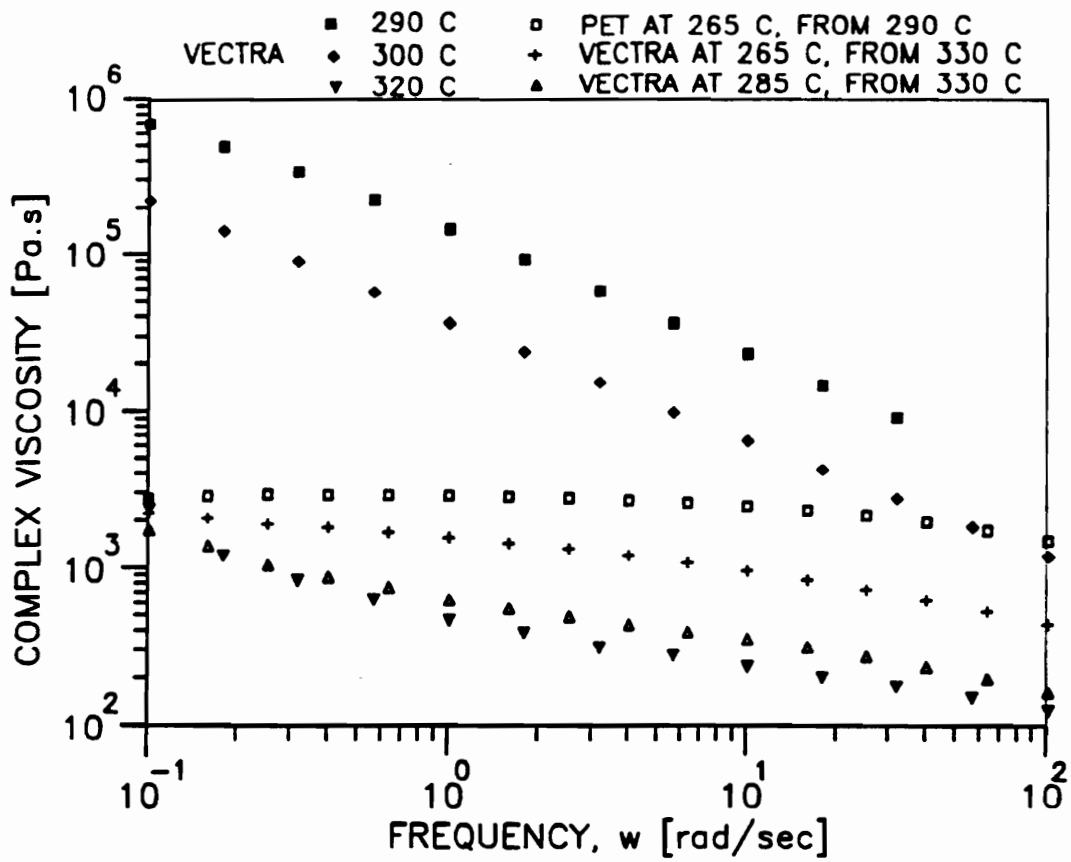
Figure 47. Dynamic frequency sweeps of PET and Vectra A (with and without thermal history).
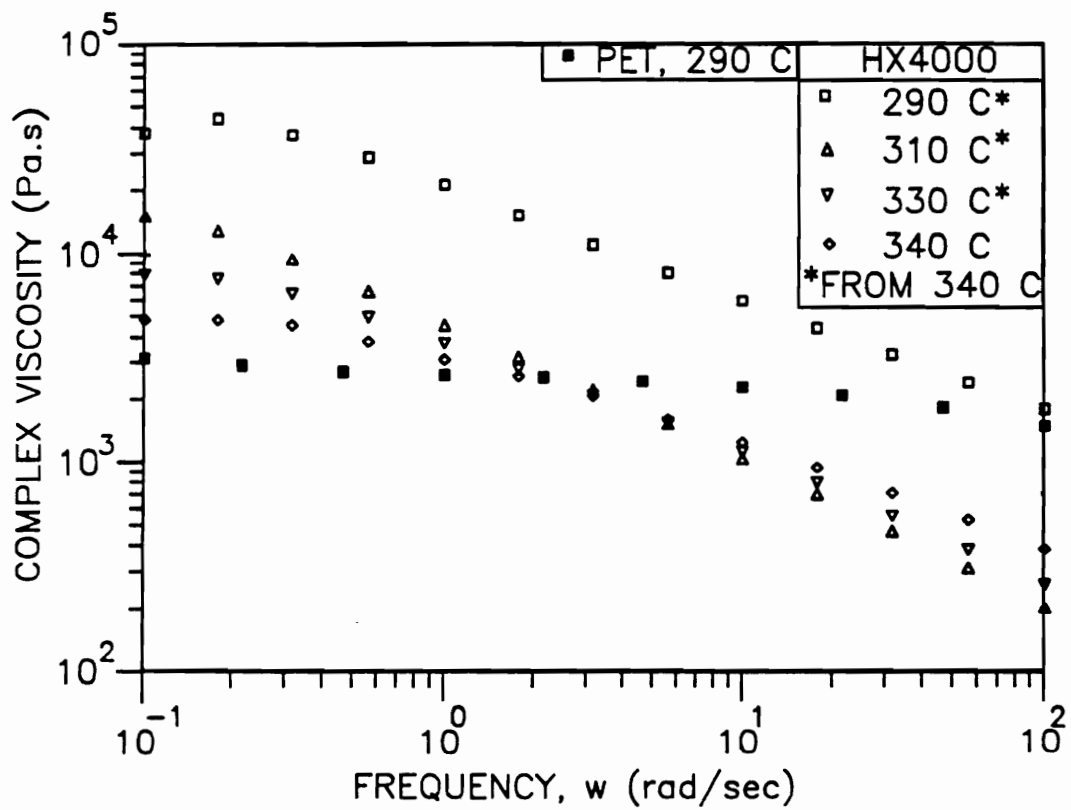
Figure 48. Dynamic frequency sweeps of PET and HX4000 (with and without thermal history).
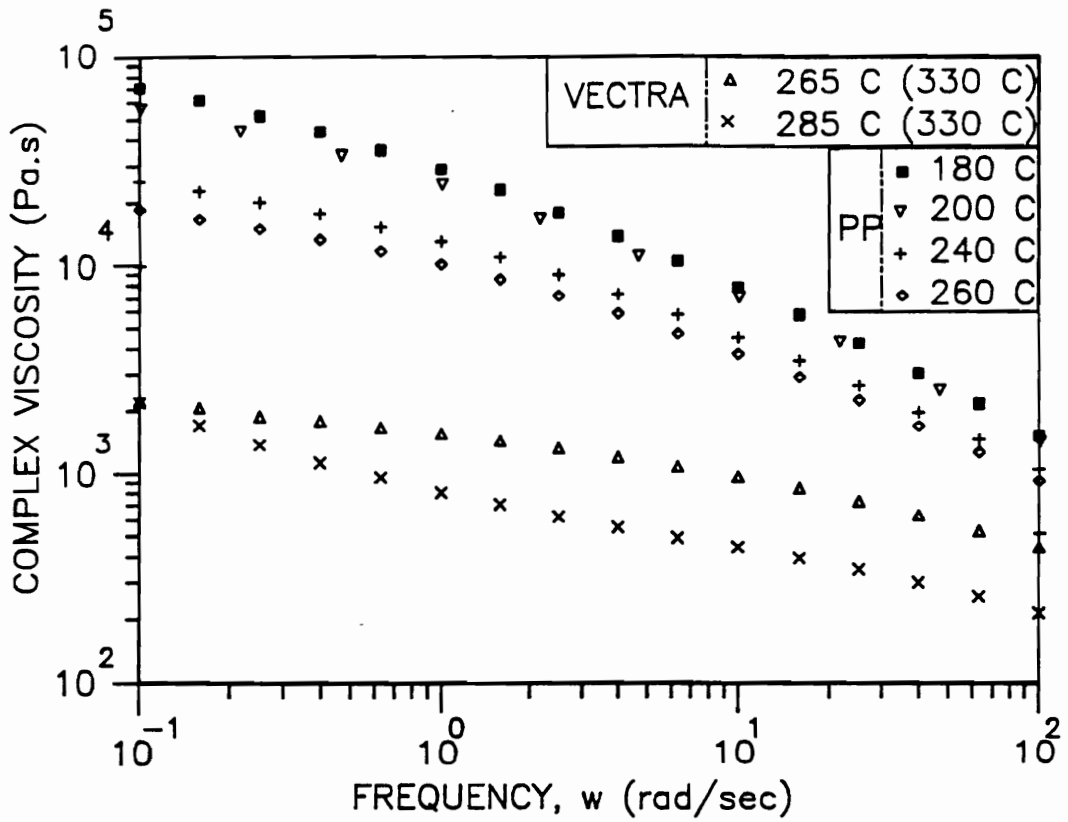
Figure 49. Dynamic frequency sweeps of PP and Vectra A (with and without thermal history).

4.2.1.3 Solidification Kinetics

One of the important objectives with regard to the rheological tests performed was to establish the length of time that any polymer could be processed before it solidified. In particular, it is obvious from some of the above discussions that the tests were also performed in order to examine the polymer melt behavior with respect to thermal history effects. Thus isothermal time sweeps were conducted by bringing the melt to a high temperature (above its melting or flow temperature), holding it there for 3-5 minutes and cooling rapidly by the forced convection mode available with the RMS-800 instrument to a lower test temperature and then starting the time sweep experiment isothermally. It is essential to realize that the results from such a test incorporate, inherently, a thermal history effect.

First in Fig. 50, the isothermal time sweeps of PET at 220°C and 240°C upon cooling from 290°C are shown. It is seen from here that the rheology of the PET at 240°C is quite stable for upto 20 minutes where the experiment was stopped. However, at 220°C, the materials response changes and an induction period of about 5 minutes can be observed before the complex viscosity appears to rise sharply. Even so, one observes that the material may be processed for about 6 minutes at 220°C before it may become too viscous to be deformed any further. It may be added here that similar time sweep experiments conducted on PET, but upon cooling from 330°C, showed that it takes about 5 minutes for the material to solidify at as low as 190°C. Thus by preheating to higher temperatures, it is possible to delay the onset of solidification to either lower temperatures or longer times at higher temperatures. However, there is of course an upper limit to which the material can be preheated as would be determined by either degradation or chemical reaction effects. This may be seen from the complex viscosity behavior of PET at 300°C and 330°C in Fig. 50. There appears to be some drop in the complex viscosity even at 300°C as the time increases. However at 330°C, the complex viscosity can be observed to reduce dramatically almost as soon as the experiment is begun. The drop in complex viscosity with increasing time at the elevated temperatures may be attributed to a drop in molecular weight due to degradation of the material. In the case of PET,

this degradation is likely due to hydrolysis reaction resulting in a decrease in molecular weight.

In Fig. 51 are shown the isothermal time sweeps of PP at temperatures of 280°C, 290°C, 305°C and 315°C. Again, it can be observed that the complex viscosity of the PP is relatively stable at 280°C and 290°C for upto 10 minutes where the test was terminated. However, at the higher temperatures of 305°C and 315°C, it can be seen that the complex viscosity begins to decrease quite rapidly almost as soon as the test is begun. This is again likely due to the degradation of PP at temperatures in excess of 300°C. These results are very important since they show that even short time exposure of the PP melt to temperatures above 300°C results in degradation of the polymer.

The kinetics of solidification of the LCPs used in this study are discussed in the following paragraphs. In Fig. 52 are shown the time sweep results of Vectra A900 at 240°C, 250°C and 260°C after cooling from 330°C. An induction period is seen for all the three temperatures which is approximately 2.5 min, 4.5 min and 8.0 min at 240°C, 250°C and 260°C, respectively. Thus it should be possible to process the Vectra A900 for a few minutes even at as low as 240°C as long as it has been provided the appropriate thermal history. Similar time sweeps conducted on Vectra B950 at 250°C, 260°C and 270°C after preheating to 330°C indicated induction times of 3 min, 7 min and 13 min. respectively.

In contrast to the behavior of Vectra A or Vectra B, the kinetics of LCP60-80 at 250°C, 260 °C and 270°C upon cooling from 330°C is quite different and is shown in Fig. 53. It can be seen that no induction time appears to be present and rapid solidification is seen for all the three temperatures. This is likely due to the crystallization of the PHB phase of the LCP which has been seen to crystallize rapidly for pure LCP60 and LCP80 (158). In terms of processing, the results imply that the residence times at these lower temperatures should not be too long (order of a 2-3 minutes) else deformation of the polymer becomes difficult.

Lastly, in Fig. 54 are shown time sweeps of HX4000 LCP at 290°C and 310°C after cooling from 355°C. Again these time sweep results are consistent with both the viscosity and cooling behavior of HX4000 discussed earlier. Specifically, the polymer melt is largely stable at 310°C
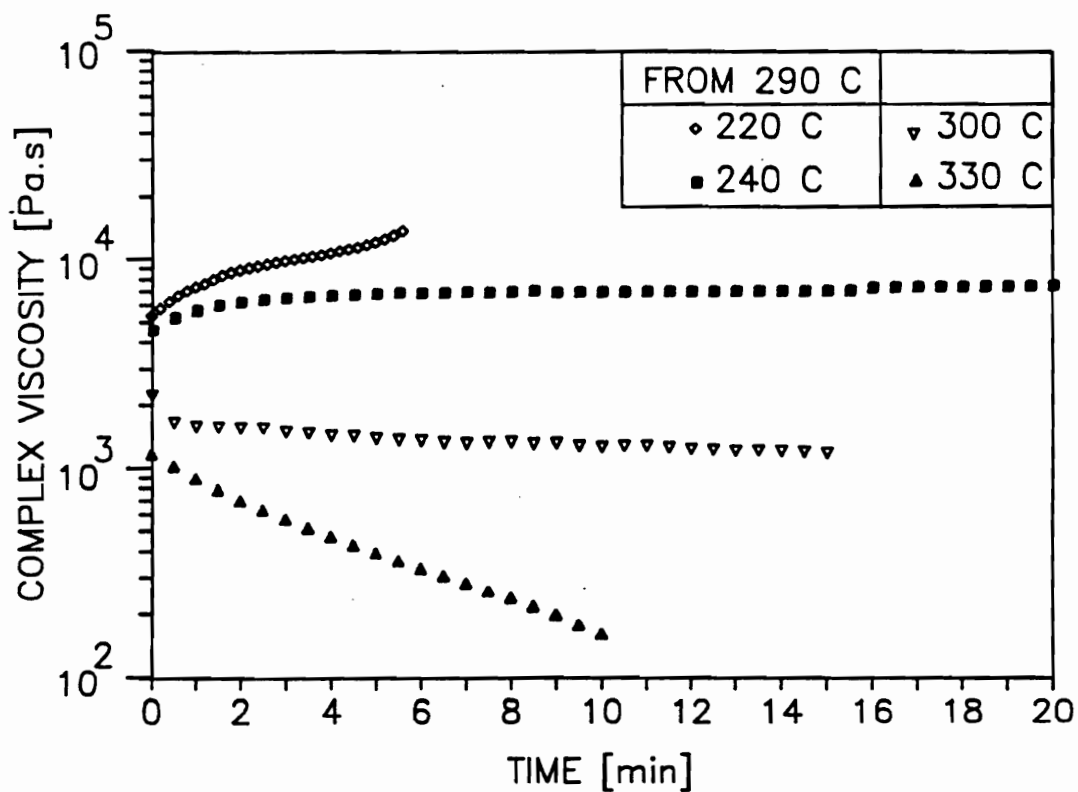
Figure 50. Isothermal time sweeps of PET at 220°C and 240°C (from 290°C) and at 300°C and 330°C.
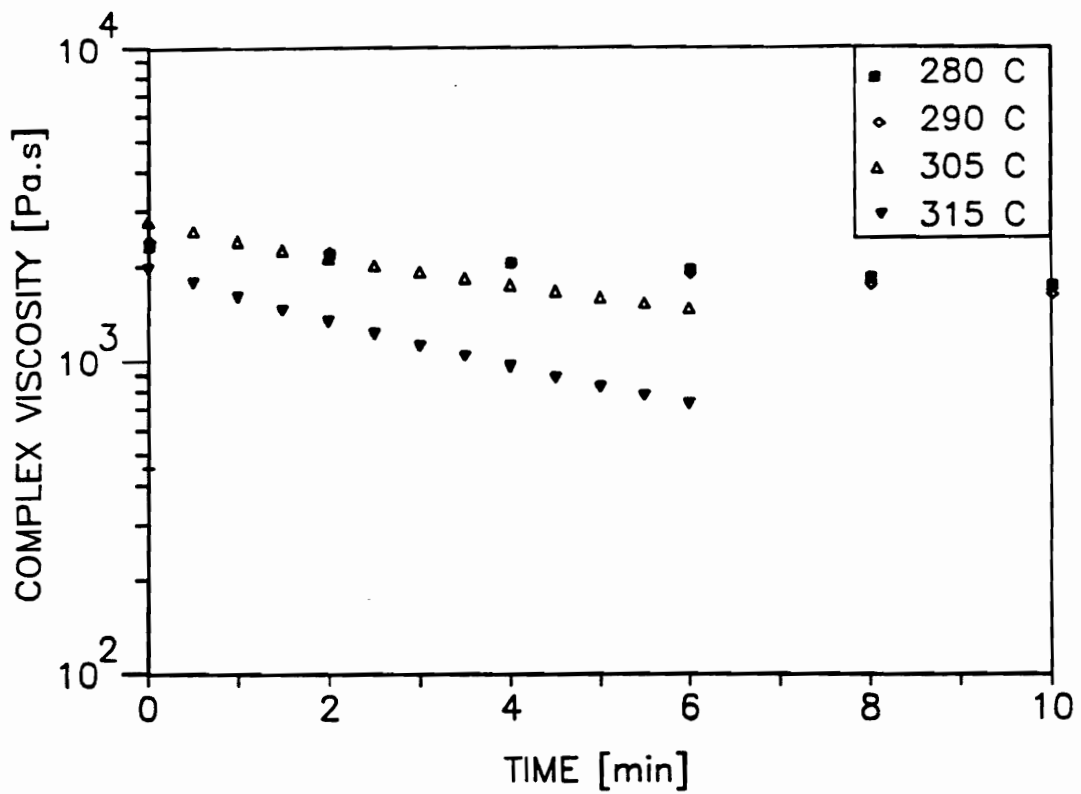
Figure 51. Isothermal time sweeps of PP at 280°C, 290°C, 305°C and 315°C.
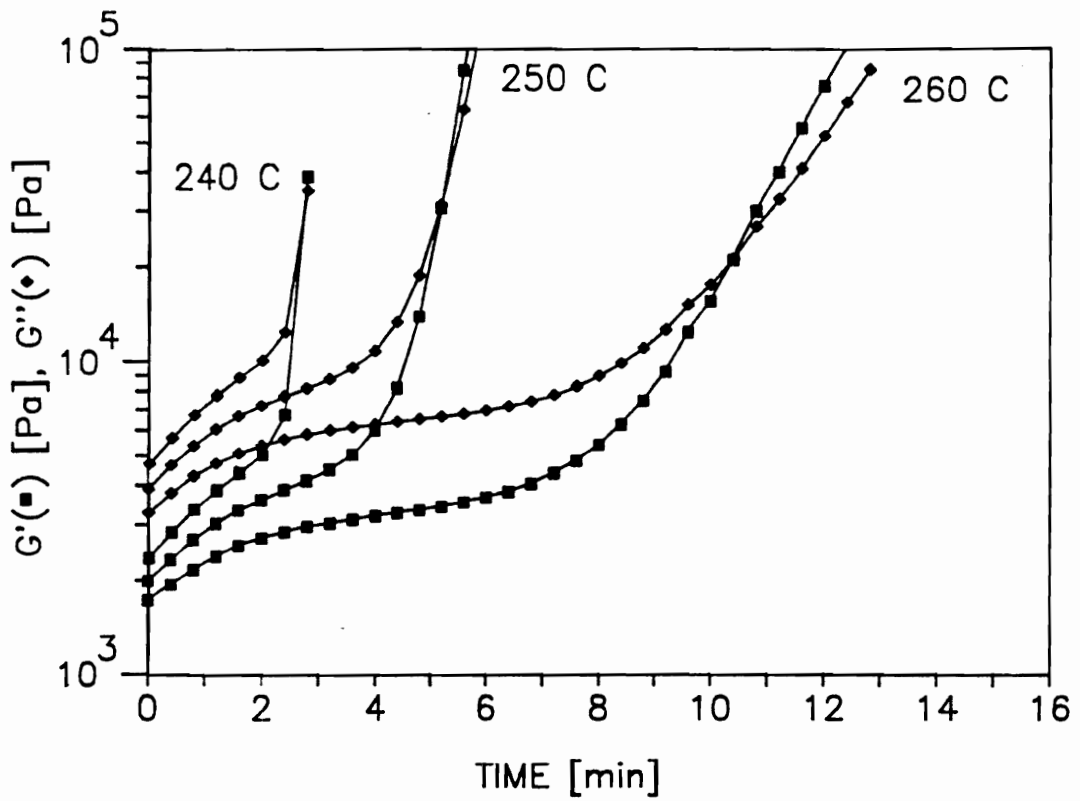
Figure 52. Isothermal time sweeps of Vectra A900 at 240°C, 250°C and 260°C upon cooling from 330°C.
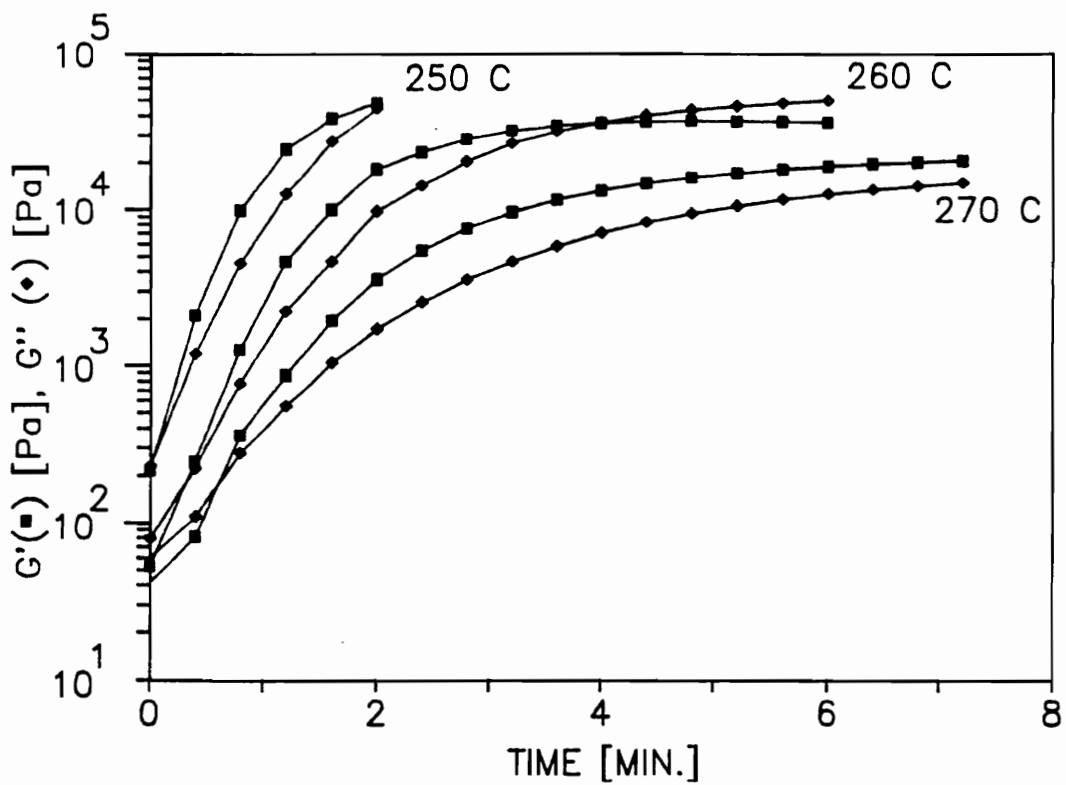
Figure 53. Isothermal time sweeps of LCP60-80 at 250°C, 260°C and 270°C upon cooling from 330°C.

for over 20 minutes. However, at 290°C, after an induction period of about 5 minutes, the polymer melt begins to solidify rapidly as seen by the upturn in G'. These results would imply that at lower temperatures than 290°C, for example at 270°C or 280°C, the time available for processing is probably only one or two minutes.

4.2.1.4   Discussion of Rheology Results

Several of the findings of the rheological tests performed on the pure polymers are of significant importance to the development of the following sections and warrant further discussion. In the above sections, an attempt was made to present data for a variety of polymers in order to establish the different kinds of rheological responses that might be encountered during processing. Furthermore, it will be shown in later sections that results from the rheological tests discussed above are imperative for design of the new mixing method and are necessary tools to predict a priori the feasibility of blending a given polymer pair.

From the results of the supercooling experiments, it was shown that the degree of supercooling or the supercooling window may be increased by preheating the polymer melts to temperatures much above their flow or nominal melting temperatures. Specifically, it was shown for PET that an increase in the preheating temperature from 290°C to 330°C increased the degree of supercooling from 65°C to over 100°C. Perhaps more importantly, it was shown in Fig. 44 that an increase in the preheating temperature of Vectra B from 300°C to 310°C increased the supercooling window from 20°C to 50°C, i.e. by 30°C. It is important to realize that this widening of the processing window offers significant advantages during processing. For example, as mentioned earlier, the melt strength of the polymer is enhanced when cooled to lower temperatures where deformation is still possible. With improved melt strength high draw can be imposed on the melt emerging from the die and thereby increase the level of molecular orientation and consequently the mechanical properties of the polymer or blend.
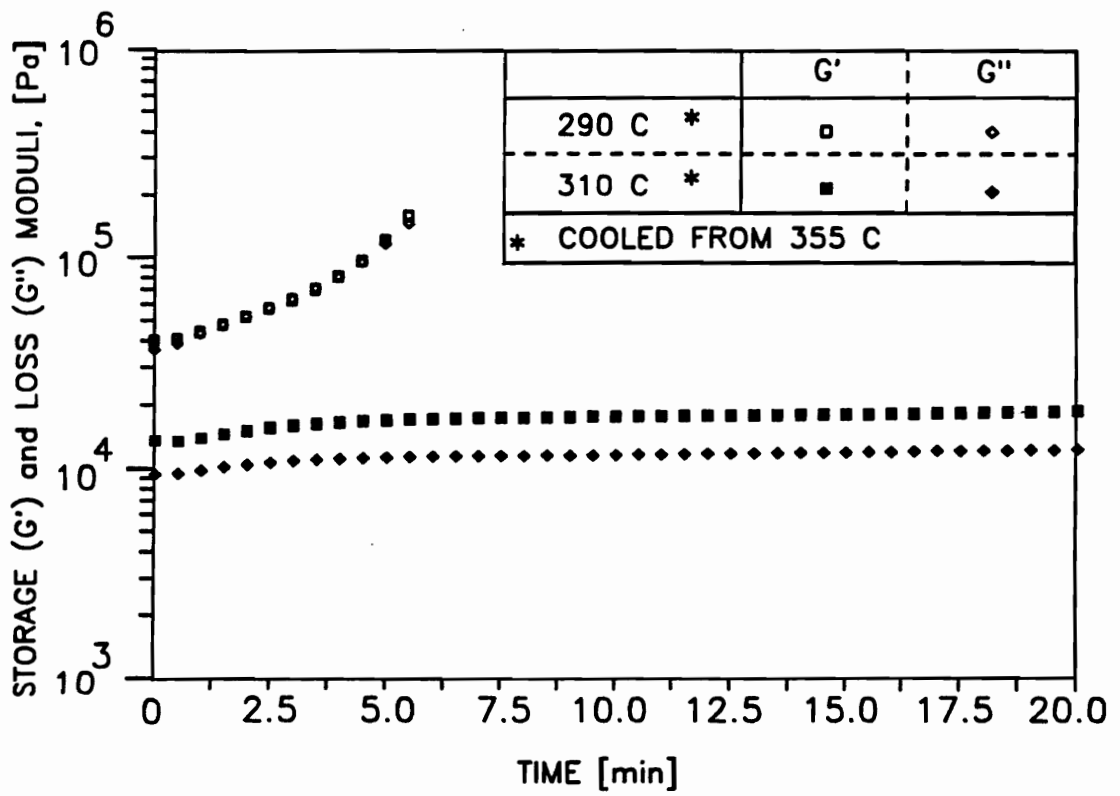
Figure 54. Isothermal time sweeps of HX4000 at 290°C and 310°C upon cooling from 355 °C.

From the viscosity-rate data, it is clear that independent control of the thermal history of the two polymers during blending offers a way by which a viscosity ratio of less than unity might be obtained. For example with the PET and Vectra A systems, it was observed that if the Vectra A was heated directly to 290°C and 300°C, its viscosity was higher than PET by two orders of magnitude. However, if the Vectra A was preheated to 330°C and then cooled to 265°C or 285°C, its viscosity was now lower than that of PET. Thus by giving the two polymers independent thermal history, two potential problems are avoided. First, a viscosity ratio greater than unity, which in the literature review has been shown to be unfavorable to fibril formation, is reversed. Secondly, once again the materials in the supercooled state tend to have better melt strength and therefore the problem of sagging melt emerging from the die is also avoided.

Lastly, from the solidification kinetics data, it was seen that supercooled melts exhibit widely different modes of recovery or solidification behavior. More importantly, it was shown that the matrix materials such as PET and PP begin to degrade quite rapidly at elevated temperatures. Specifically, the complex viscosities of PET and PP were observed to drop quite significantly at 330°C and at temperatures above 300°C, respectively, due most likely to degradation which would result in a loss in molecular weight. Therefore, one can easily envision that the blending of say PP with Vectra A or Vectra B in a single extruder at temperatures above 300°C is likely to cause significant degradation problems for PP and would thus make it impossible to do so. Further, in some melts such as Vectra A or Vectra B, an induction period of a few minutes can be observed before the kinetics become perhaps too rapid for successful deformation. LCP60-80 on the other hand did not show any induction period and begins to solidify almost as soon as it reaches the supercooled state. Therefore, in the design of any processing equipment, it is necessary to take into account the different residence times that the melts can undergo in the supercooled state before they become completely solid. Also, when the melts emerge from the die (either into a quench bath or air at room temperature), the solidification kinetics would be even more rapid due to the quenching of the melt. The ability to induce any further molecular orientation by drawing would then be inhibited by the

rapid crystallization and solidification process. These differences in the rheological response of the melts under processing condition are likely to have ramifications in the final mechanical properties.

4.2.2   Strand Extrusion

Strands of blends of PET and PP with several LCPs were extruded via the mixing process described in chapter 3. The processing conditions and in particular the temperature profiles employed in the extrusion process will be made with reference to the nomenclature of Figs. 27 and 28 throughout this manuscript. The extrusion of strands of the blends was done for several reasons. First, it is a relatively simple process and was therefore thought to be a suitable process to examine and understand the workings of the newly developed dual-extruder mixing method. Second, it was of interest to see what levels of enhancement in the mechanical properties, i.e. the tensile modulus and strength, of the blends could be obtained over the matrix polymer properties. Lastly, it was believed that it should be possible to further process a blend in which the LCP reinforcement has a higher melting temperature than the matrix polymer, by processing at temperatures above the melting temperature of the matrix but below the melting point of the LCP, without a significant loss of mechanical properties. Thus the strands were pelletized and reprocessed via injection-molding to test this hypothesis. In the following discussions, the blends made via the mixing method will be referred to as mixer blends or 'MB' while the single-screw extrusion blends will be referred to as physical blends or 'PB' for the sake of brevity. In the following experiments on strand extrusion, all the blends were extruded from a capillary die with L/D ratio of one and diameter 0.3175 cm (1/16") unless specified otherwise.

4.2.2.1 Blends of PET with LCPs

Blends of PET with several LCPs were extruded using the mixing method. First, the blends of PET/Vectra A900 are discussed. These blends were processed using the temperature profile shown below (see Figs. 27 and 28). Blends of PET/Vectra A in three different composition ratios of 96/4, 90/10 and 70/30 were extruded into strands via the mixing method. The PET was extruded at a constant 40 RPM for all the three blend compositions whereas the Vectra A was extruded at 4, 8 and 16 RPM for the three different runs. The mass flow rates were estimated, as mentioned in chapter 3, by timing the disappearance of known weights of the polymers. Thus the flow rates, in gms/min, for PET/Vectra A were determined to be 85.0/3.75, 77.71/9.31 and 67.02/28.28 for extrusion at 40/4, 40/8 and 40/16 RPM, respectively.

- PET extruder - 210°C, 295°C, 290°C and 240°C in Zones 1-3 and clamp ring, respectively
- Vectra A extruder - 265°C, 300°C, 330°C and 290°C in Zones 1- 3 and clamp ring, respectively
- Zones C1 and C2 were maintained at 240°C and 200°C, respectively
- Static mixer and capillary die were maintained at 225°C and 200°C, respectively.

A few comments regarding the particular temperature profile are necessary. The temperatures in the PET extruder were selected on the basis of the recommended processing temperatures for this particular grade (130). However, the temperature of the PET melt was decreased gradually in the clamp ring and Zone C2 to about 200°C so that at the 'T' junction where the two polymer melt streams meet, the temperature of the PET did not exceed 300°C. It is important to point out here that the temperatures selected are the wall temperatures and the actual melt temperatures are much higher. In fact, some simplified heat transfer analysis was done (to be discussed later) whereby it was seen that the PET melt exiting from the extruder at 295°C was cooled to 265°C at the 'T' junction. This will be discussed in more detail later but is nevertheless worth mentioning here so as to keep the processing aspects in proper perspective.

Results of tensile tests performed on the blends with different draw ratios are shown in Table 6. The tensile strengths for the strands could not be evaluated due to the tendency of the strands to break at the jaws of the instrument grips. As can be seen from Table 6, the tensile modulus of PET is 2.02 GPa at a draw ratio of 33. The samples of lower draw ratio i.e. 5.36 and 19.1 were in fact annealed at 120°C for 1 hour prior to testing and thus show higher moduli at lower draw ratios. However, with the addition of only 4 wt % of Vectra A to pure PET, it can be seen that the properties of PET are enhanced by a factor of almost 2.5 when compared at the draw ratio of 33. Even more significant enhancements are observed when the composition of the LCP is increased to 10 wt %. The modulus at the highest draw ratio of 156 is 12.57 GPa which is an increase of over 6 times that of pure PET. Even at a draw ratio of about 33, the increase is over 4 times that of pure PET. With a further increase to 30 wt % of the LCP in the blend, the modulus at even the lowest draw ratio of 2.36 is about 2 times that of pure PET. Further, at the highest draw ratio of 49, the modulus of the blend at 18.99 GPa is higher than pure PET by a factor of over 9.4. These are indeed very significant improvements in the properties.

In an effort to determine the reasons for these improvements, the morphology of the blends was examined using scanning electron microscopy (SEM). First in Fig. 55 are shown the SEMs of PET/Vectra 96/4 MB rods, fractured across the flow direction, of two different draw ratios, 2.77 and 26. The two SEMs are at approximately the same magnifications and therefore the effect of drawing may be interpreted as follows. In Fig. 55a the fibrils of the Vectra appear fewer in number and the diameters are roughly 4-6 μm. However, at the higher draw ratio of 26, there is an obvious increase in the number of fibrils and furthermore the diameters are now in the range of 1-3 μm. Thus the efficacy of the drawing is clear from the reduction in fibril diameter and increase in fibril number. One other point worth mentioning is that the presence of fibrils at this low LCP composition was not entirely expected. It was shown in the literature review that the presence of fibrils was typically seen at high LCP loadings of over 10-15 wt % in the blend (3, 6, 112, 125) with low draw. Thus the presence of fibrils at this low LCP content and low draw ratio was most encouraging and is believed to be a consequence of the

Table 6. Tensile modulus as a function of draw ratio of blends of PET/Vectra A 96/4, 90/10 and 70/30 composition ratios extruded from the mixing method.

Sample-#	Draw Ratio (D.R.) vs Young's Modulus (E)							
	PURE PET		96/4 (M)		90/10 (M)		70/30 (M)	
	D.R.	E [GPa]	D.R.	E [GPa]	D.R.	E [GPa]	D.R.	E [GPa]
1	5.36	2.86 (0.07)	5.0	3.11 (0.07)	2.89	4.49 (0.67)	2.36	5.45 (0.58)
2	19.1	2.51 (0.23)	10.4	3.37 (0.07)	7.67	6.05 (0.49)	3.25	6.97 (0.34)
3	33.4	2.02 (0.08)	17.3	3.45 (0.23)	12.4	7.91 (0.42)	3.80	8.93 (0.39)
4			26.04	4.97 (0.06)	35.5	8.82 (0.88)	39.0	13.31 (0.37)
5			45.28	4.86 (0.15)	69.0	9.60 (0.88)	43.2	17.21 (0.13)
6			67.0	5.15 (0.49)	156	12.57 (0.24)	49.7	18.99 (0.17)

Reported values are an average of at least four tests and standard deviations are given in parenthesis
(M) = Blends prepared by the mixing technique

particular flow-division and distribution mechanism of the static mixer. Further, no skin-core fibril-droplet type of structure was observed for even the low draw ratios examined. This is another advantage over the findings of some other researchers cited earlier (129, 151) where distinct skin-core structures were observed in extruded strands even with high LCP contents. The SEMs for the 90/10 MB blend were also similar showing good fibrillation and no skin-core structure. A further discussion of the PET/Vectra A 70/30 MB blend is deferred to a later section where it will be discussed and compared fully to the physical blend of equal composition.

Blends of PET with Ultrax (KR-4002) were extruded into strands. The PET was extruded at 40 RPM whereas the Ultrax was extruded at 8 RPM. The PET and Ultrax flow rates were estimated to be 64.07 gms/min and 16.1 gms/min, respectively, yielding a composition ratio of ca. 80/20. The temperature profile used in the extrusion of the PET/Ultrax MB blends is as follows.

- PET extruder - 175°C, 290°C, 290°C and 225°C in Zones 1-3 and clamp ring, respectively
- Ultrax extruder - 265°C, 325°C, 300°C and 275°C in Zones 1- 3 and clamp ring, respectively
- Zones C1 and C2 were maintained at 220°C and 190°C, respectively
- Static mixer and capillary die were maintained at 200°C and 180°C, respectively.

In Table 7 are shown the results of tensile tests of PET/Ultrax 80/20 MB composition. Once again an increase in the modulus with draw ratio is clearly observed. Also, the modulus of 8.28 GPa at the draw ratio of 28 represent a 4-fold improvement over pure PET. It is of interest to note here that the moduli of PET/Ultrax blend are lower than those of PET/Vectra A blends discussed earlier. SEMs of strands, fractured across the flow direction, of the PET/Ultrax 80/20 MB blend are shown in Fig. 56a and 56b where the samples shown are without drawing and draw ratio 13.7, respectively. Again the most distinct difference between the two micrographs is the fact that the sample drawn (Fig. 56b) has more fibrils which are smaller in diameter than the undrawn sample. However, it is even more interesting to note that the sample even without any draw has fibrils in the entire cross-section. The lower moduli of the PET/Ultrax system as compared to the PET/Vectra A system mentioned earlier are possibly due to the apparently
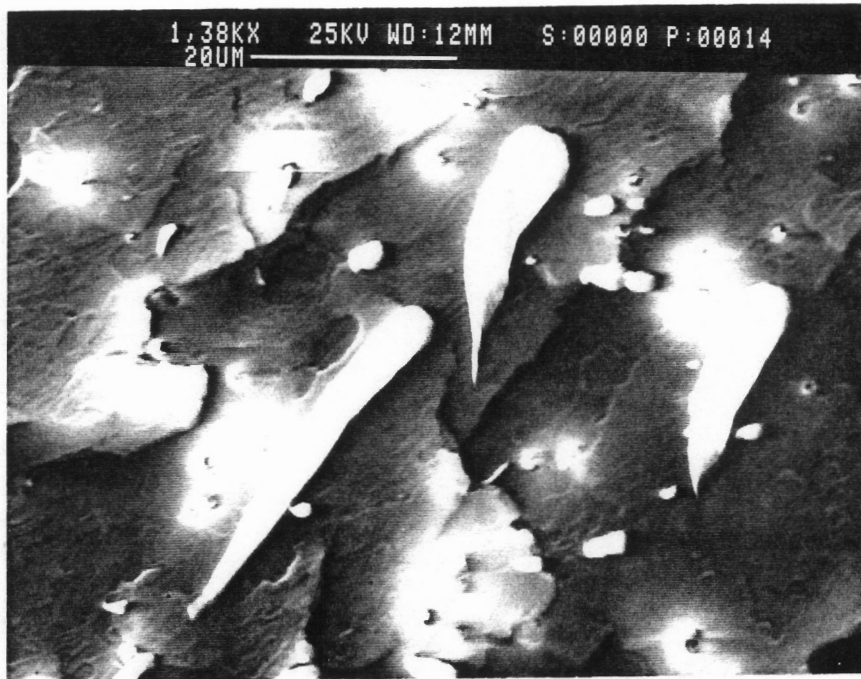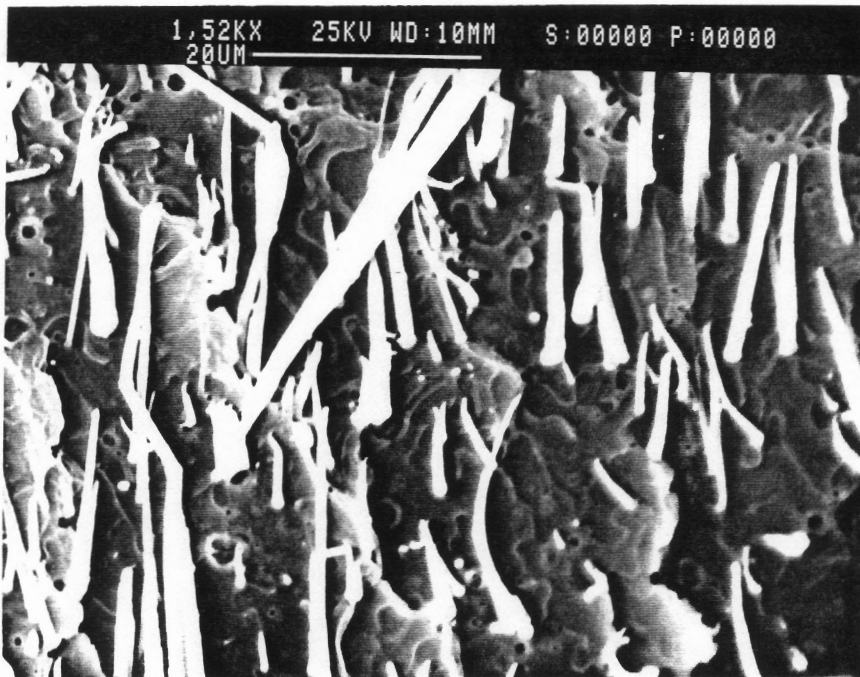
Figure 55. Scanning electron micrographs of fracture surfaces of PET/Vectra A900 96/4 MB blend strands at draw ratios of (a) 2.77 and (b) 26. Fracture is across the flow direction.

lower aspect ratio fibrils of the Ultrax than the Vectra A fibrils in the PET matrix as can be seen from the morphology.

The level of molecular orientation achieved in the above strands was also examined qualitatively using wide-angle x-ray scattering (WAXS). In Fig. 57 are shown WAXS patterns of (a) pure PET rod with draw ratio 40, (b) PET/Ultrax 80/20 MB rod with no draw and (c) draw ratio of 13.7. It is observed that the pure PET rod even at this high a draw ratio shows no azimuthal dependence in the scattering pattern which is indicative of no crystallization and no preferred direction of molecular orientation. Since the strands of PET were quenched in an ice-water bath upon exit from the die, it may not be very surprising that the sample did not crystallize. However, the lack of any preferred orientation direction implies that the relaxation of the PET is extremely rapid. For example, the distance between the exit of the die and the water bath is about 15 cm. On the basis of the flow rates in the extrusion process, it was estimated that the material takes about 1.3 seconds to traverse from the exit of the die to the water bath. Furthermore, even when the strand hits the water bath the solidification is not instantaneous due to obvious heat transfer effects within the strand. Therefore it would appear that any orientation induced during the drawing process is lost in a period of 1-2 seconds. Although this may seem surprising at first, if one takes a closer look at the viscosity-rate behavior of pure PET discussed earlier in Fig. 46, it is seen that the viscosity begins to shear-thin at about 10 sec^{-1}. It is known that the inverse of this shear rate or frequency at which a material begins to exhibit shear-thinning behavior is often equated to its longest relaxation time, λ. This would mean that the value of λ for PET is about 0.1 sec which is actually an order of magnitude faster than the time the material takes to traverse between the exit of the die and the quench bath. Therefore upon closer examination of the processing conditions the behavior of PET may be explained with some degree of satisfaction. On the other hand the PET/Ultrax 80/20 MB rod with no draw shows only a weak azimuthal dependence which was determined to be that from the Ultrax crystalline phase. However, the strand with a draw ratio of 13.7 (Fig. 57c) shows a distinct pair of arcs indicative of the high level of molecular orientation. The properties of the

Table 7. Tensile modulus as a function of draw ratio of blends of PET/Ultrax 80/20 MB strands extruded via the mixing method.

MATERIAL	DRAW RATIO	YOUNG'S MODULUS* [GPa]
PET	5.36 19.10 33.4	2.86 (0.07) 2.51 (0.23) 2.02 (0.08)
PET/Ultrax 80/20	1.93 2.40 10.20 13.70 28.4	2.34 (0.32) 3.15 (0.19) 4.33 (0.17) 5.30 (0.05) 8.28 (0.42)

*Standard deviations are given in parenthesis

Figure 56. Scanning electron micrographs of fracture surfaces of PET/Ultrax 80/20 MB blend strands at draw ratios of (a) 1 and (b) 13.7. Fracture is across the flow direction.

strands discussed earlier are in complete agreement with the observations of the morphology and molecular orientation.

Strands of PET/LCP60-80 blend were also extruded via the mixing method. Once again the PET was extruded at 40 RPM and the LCP60-80 at 10 RPM. The measured flow rates were 80.23 gms/min and 13.67 gms/min for PET and LCP60-80, respectively, yielding a composition ratio of PET/LCP60-80 85/15 wt %. The temperature profile for extrusion was as follows.

- PET extruder - 210°C, 295°C, 295°C and 240°C in Zones 1-3 and clamp ring, respectively
- LCP60-80 extruder - 240°C, 300°C, 330°C and 285°C in Zones 1- 3 and clamp ring, respectively
- Zones C1 and C2 were maintained at 225°C and 200°C, respectively
- Static mixer and capillary die were maintained at 225°C and 175°C, respectively.

Results of the tensile tests for the PET/LCP60-80 85/15 MB rods are shown in Table 8. Also included in this table are the properties of pure LCP60-80 strands which were extruded using only a single extruder. As can be seen from Table 8, the highest modulus of the pure LCP60-80 achieved was about 9.2 GPa. The properties of the 85/15 blend are somewhat higher than those of pure PET but not as high as those seen with either PET/Vectra A or PET/Ultrax. The reason for this may be quite simply that the properties of the base LCP are lower. For example, the modulus of a 30 mil (0.030″) rod of pure Vectra is reported to have a tensile modulus of 45 GPa. Therefore the comparatively lower properties of the PET/LCP60- 80 system are likely due to the lower modulus of the LCP60-80 itself. Nevertheless, the morphology of the strands was examined using SEM and is shown in Fig. 58. Fibrillar morphology of the LCP phase is clearly evident but does not appear to have as large aspect ratios as seen in the case of PET/Vectra A blends. Furthermore, it is also worth noting that even the undrawn sample (Fig. 58a, D.R. = 1) shows fibrillar morphology. The fibrils are about 2-3 μm in diameter.
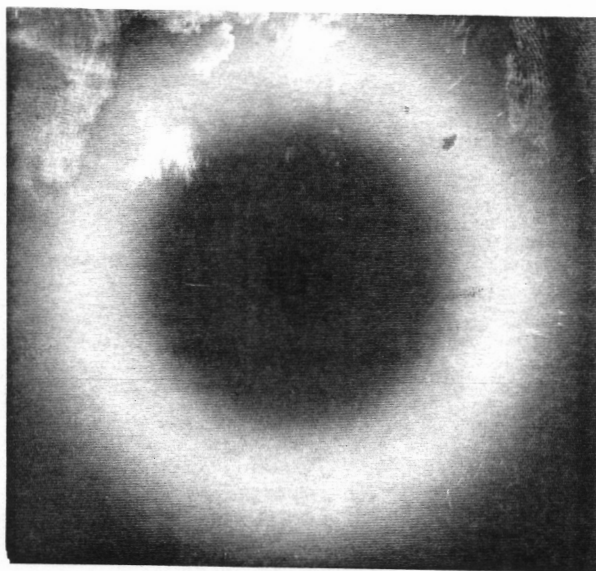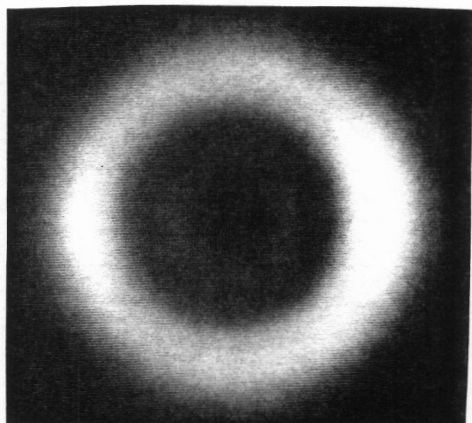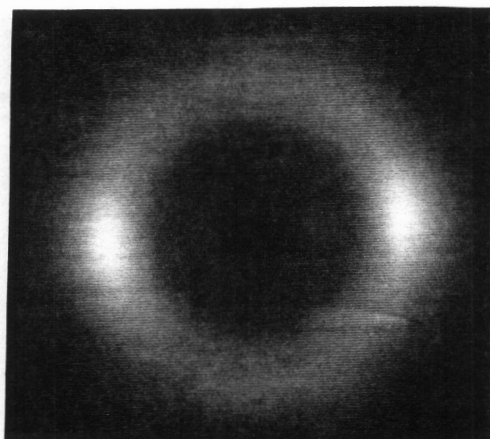
Figure 57. Wide-angle x-ray scattering patterns of extruded strands of (a) pure PET [D.R. = 40], (b) PET/Ultrax 80/20 MB [D.R. = 1], and (c) PET/Ultrax 80/20 MB [D.R. = 13.7].

Table 8. Tensile modulus as a function of draw ratio of blends of PET/LCP60-80 85/15 MB strands extruded via the mixing method.

MATERIAL	DRAW RATIO	YOUNG'S MODULUS* [GPa]
PET[1]	5.36 19.10 33.4	2.86 (0.07) 2.51 (0.23) 2.02 (0.08)
LCP60-80[2]	3.28 6.06 46.04	5.01 (0.31) 8.49 (0.25) 9.19 (0.38)
PET/LCP60-80 85/15	3.72 12.60	2.48 (0.12) 3.48 (0.24)

*Standard deviations are given in parenthesis
[1]denotes   poly(ethylene terephthalate)
[2]denotes   50/50 weight % blend of LCP60 and LCP80
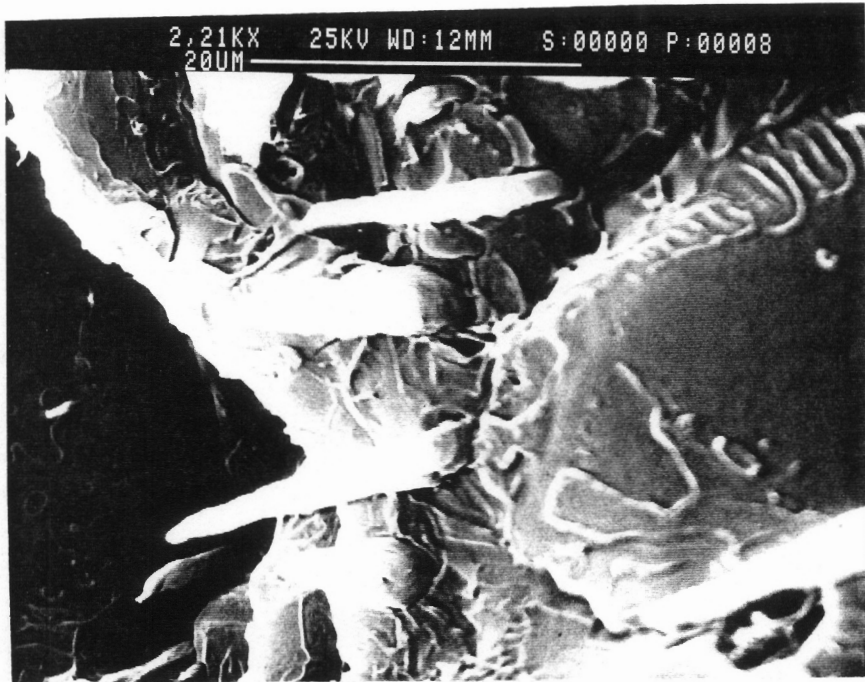
a
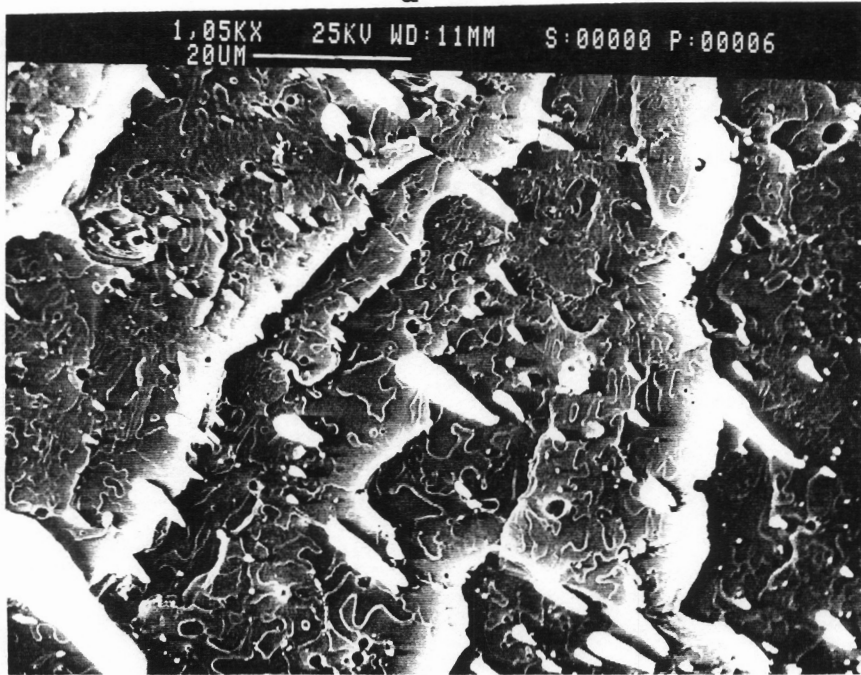
b

Figure 58. Scanning electron micrographs of fracture surfaces of PET/LCP60-80 85/15 MB blend strand with draw ratio (a) 1 and (b) 12.6. Fracture is across the flow direction.

4.2.2.2 Blends of PP with LCPs

The efficacy of the new mixing method is perhaps better demonstrated by the generation of blends of PP with several LCPs including Vectra A, Vectra B and LCP60. It may be recalled from Table 3 that the difference in the ordinary processing temperatures of the PP used in this study and LCPs such as Vectra A and Vectra B is about 110°C. Therefore, the successful blending of PP with these LCPs was a significant challenge to the limits of the blending method developed here. In the ensuing discussion, results from the above experiments are provided with appropriate details.

First, the blends of PP/Vectra A and PP/Vectra B are discussed. PP/Vectra A blend was extruded by operating the PP extruder at 40 RPM and the Vectra A extruder at 16 RPM to give PP and Vectra A flow rates of 25.10 and 9.50 gms/min, respectively, and a blend composition ratio of ca. 72/28 wt %. Two different compositions of PP/Vectra B blends were extruded. A PP/Vectra B 82/18 composition blend was obtained by operating PP at 40 RPM and Vectra B at 6 RPM, to give PP and Vectra B flow rates of 21.99 and 2.86 gms/min, respectively. A PP/Vectra B 74/26 composition blend was obtained by operating PP at 40 RPM and Vectra B at 16 RPM, to give PP and Vectra B flow rates of 28.51 and 10.25 gms/min, respectively. Further, due to the similarity in the processing temperatures of Vectra A and Vectra B. the PP/Vectra A and PP/Vectra B blend strands were extruded with the following temperature profile.

- PP extruder - 120°C, 190°C, 190°C and 200°C in Zones 1-3 and clamp ring, respectively
- Vectra A (or Vectra B) extruder - 265°C, 330°C, 300°C and 275°C in Zones 1-3 and clamp ring, respectively
- Zones C1 and C2 were maintained at 240°C and 200°C, respectively
- Static mixer and capillary die were maintained at 225°C and 175°C, respectively.

The Young's (tensile) modulus as a function of draw ratio for all the PP/LCP blends extruded are shown in Table 9 along with the data for pure PP strands. The modulus of PP strands is about 0.7 GPa. In comparison, the modulus of a PP/Vectra B 88/12 blend at the highest draw

ratio achieved is 2.75 GPa which is an increase of almost 4 times over pure PP. However, it is observed that when the Vectra B composition is increased to 26 wt % in the blend, there is a tremendous increase in the moduli over pure PP. Specifically, it can be seen that the modulus for the lowest draw ratio is 6.5 GPa which is already over 9 times pure PP. Furthermore, as the draw ratio is increased, the modulus of the blend also increases, and a peak value of 13.47 GPa is obtained at the highest draw ratio achieved. This is almost 20 times the value for pure PP. The moduli of the PET/Vectra A system are also increased from the pure PP values by a factor of over 6.5 at the highest draw ratio achieved. From the above, it is also clear that the properties of the PP/Vectra B strands are higher than PP/Vectra A strands by almost a factor of 3. Although it is not very clear why this is so, one of the reasons may be just the fact that the properties of Vectra B are higher than Vectra A. For example, the tensile modulus of pure Vectra A900 injection molded plaques is reported to be 9.6 GPa (148) as compared to a value of 19.3 GPa (159) for Vectra B according to Celanese specifications. Furthermore, the modulus of pure Vectra A rod is reported to be 45 GPa (160) compared to about 75 GPa for a pure Vectra B rod (159). Lastly, the moduli of the PP/LCP60 are somewhat higher than pure PP but the level of enhancement is only 2-3 times over pure PP.

The morphology of the above blends was examined using SEM and is discussed below. In Figs. 59a and 59b are shown the SEMs of PP/Vectra B 88/12 MB rods with draw ratios of 11 and 39, respectively. From Fig. 59a it is evident that there is no skin-core structure as the SEM scans from the outer edge of the rod through to the center. The fibrils of Vectra B are seen to be well distributed and from the pull-out of some of these fibrils, it appears that they have very high aspect ratios. The SEMs of a PP/Vectra B 74/26 MB rod with the entire strand cross-section and a higher magnification in the center are shown in Fig. 60. It can be seen clearly from Fig. 60a that the fibrils are present in the entire cross- section of the strand and high aspect ratios are visible from Fig. 60b. A similar morphology of the PP/Vectra A 72/28 MB blend strands can be observed from Fig. 61a. It is clear from Fig. 61a that the fibrils have quite uniform diameters and high aspect ratios. In contrast, the morphology of the PP/LCP60 strand fracture surface is shown in Fig. 61b from which it is clear that the LCP60 fibrils do not

Table 9. Tensile modulus as a function of draw ratio of blends of PP/LCP MB strands extruded via the mixing method.

MATERIAL	DRAW RATIO	YOUNG'S MODULUS★ (GPa)
Polypropylene (PP)	6.25 21.16	0.688 (0.047) 0.432 (0.066)
PP/Vectra B 88/12	3.11 6.26 13.97 40.85	1.59 (0.25) 2.07 (0.13) 2.09 (0.19) 2.73 (0.21)
PP/Vectra B 74/26	4.33 20.16 35.40	6.5 (1.25) 10.96 (1.14) 13.47 (1.78)
PP/Vectra A 72/28	3.80 8.07 39.06	3.837 (0.351) 4.211 (0.5) 4.711 (0.474)
PP/LCP60 76/24	5.70 18.16	1.66 (0.149 2.67 (0.49)

★Standard deviations are given in parenthesis

appear to have as high aspect ratios as seen with Vectra A or Vectra B and furthermore they appear fewer in number. This is possibly why the moduli of the PP/LCP60 strands were not as high as the PP/Vectra A or PP/Vectra B blends.

4.2.2.3   Comparison of the Mixing Method with Single-Screw Extrusion

In an effort to establish the differences, if any, in the properties of the blends generated by the mixing method discussed above and those generated by directly blending the two materials in a single-screw extruder, blends of PET/Vectra A 70/30 composition were extruded by the above two methods. In the case of the mixer blends, the processing conditions for extrusion were the same as outlined earlier in the section on strand extrusion. In the case of the blends generated by blending in a single-screw extruder, the temperature profile in the extruder was as follows: 240°C, 320°C, 300°C, 250°C and 220°C in Zones 1-3, clamp ring and capillary die, respectively. Although the temperatures in the extruder were higher than recommended for PET, they were intentionally chosen so as to ensure that the Vectra A900 had melted to a significant extent. The tensile modulus as a function of draw ratio for the PET/Vectra A 70/30 composition blends made by the two methods are shown in Table 10. The moduli of the blends processed via the mixing method were discussed earlier in this section and are repeated here for the sake of comparison.

As can be seen from Table 10, the tensile moduli of the blend from the mixing method are higher than those from the single screw extrusion at all the draw ratios measured. Furthermore, at the highest draw ratio of about 49, the MB blend has a modulus of 18.99 GPa as compared to 13.39 GPa for the blend processed in one extruder. Once again, it should be kept in mind that the modulus of the control PET rods was measured to be 2.02 GPa and was largely independent of the draw ratio.

The possible reasons for the above differences in the moduli were examined using WAXS and SEM. Thus the WAXS patterns of the rods with draw ratio of 49 are shown in Fig. 62. A
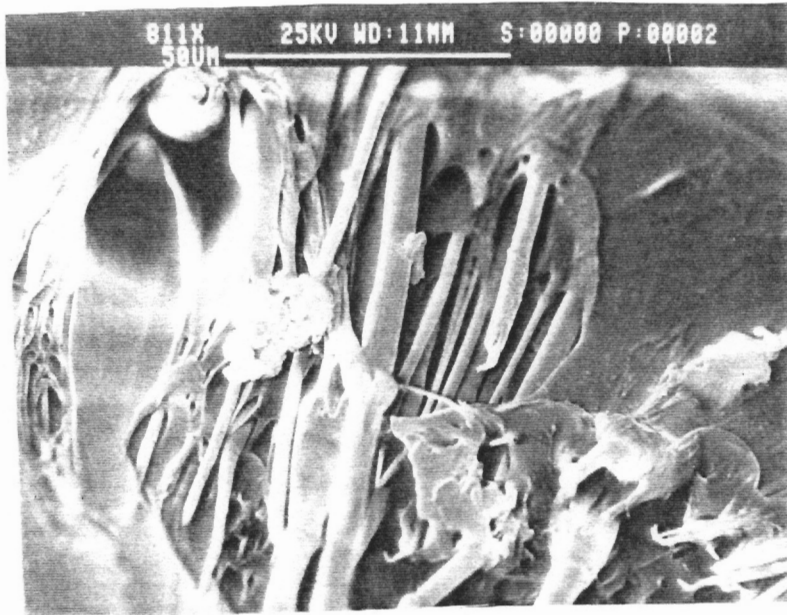
a
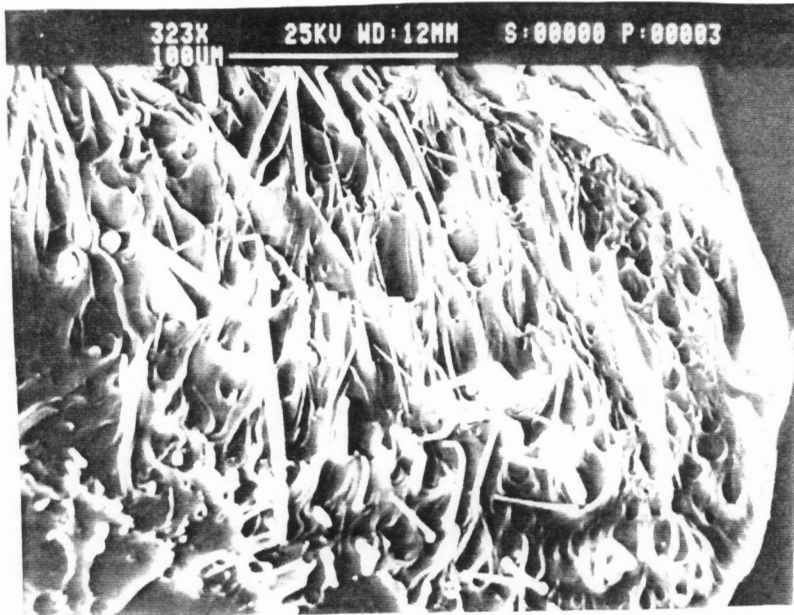
b

Figure 59. Scanning electron micrographs of fracture surfaces of PP/Vectra B 88/12 MB blend strand with draw ratio (a) 11 and (b) 39. Fracture is across the flow direction.
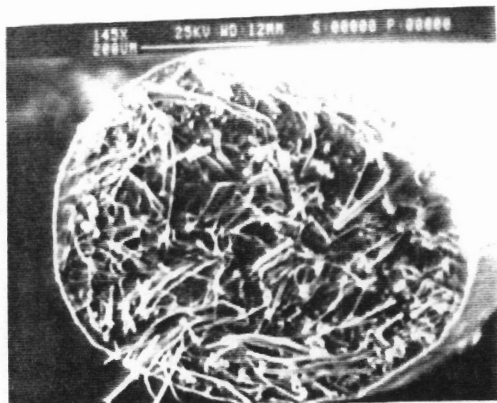
a
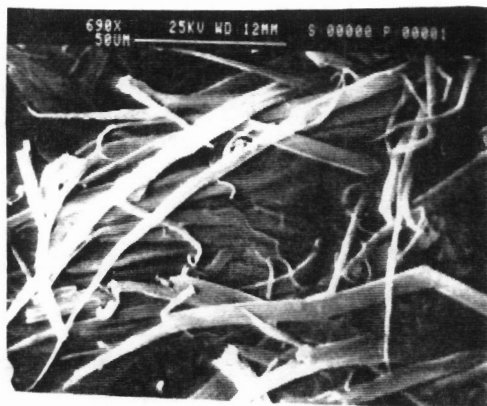
b

Figure 60.   SEMs of fracture surfaces of PP/Vectra B 74/26 MB blend strand with draw
ratio = 35; (a) low (145X) and (b) high (690X) magnifications. Fracture is
across the flow direction.
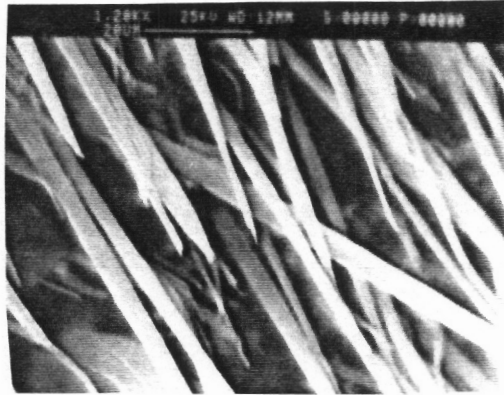
a
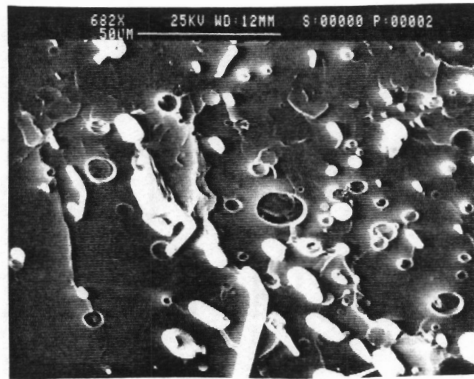
b

Figure 61. SEMs of fracture surfaces of (a) PP/Vectra A 72/28 MB blend strand with draw ratio = 39 and (b) PP/LCP60 76/24 MB blend strand with draw ratio = 39. Fracture is across the flow direction.

Table 10. Tensile modulus as a function of draw ratio of PET/Vectra A 70/30 blends processed via two methods.

Mixing Device Rods		Single-Screw Rods	
Draw Ratio	Young's Modulus [GPa]	Draw Ratio	Young's Modulus [GPa]
2.36	5.45 (0.58)	4.55	3.98 (0.23)
3.25	6.97 (0.34)	7.10	7.08 (0.82)
39.0	13.31 (0.37)	13.0	8.05 (0.09)
43.2	17.21 (0.13)	20.0	8.49 (0.54)
49.7	18.99 (0.17)	49	13.39 (0.45)

Reported values are an average of at least four tests and standard deviations are given in parenthesis
(M) = Blends prepared by the mixing technique

high level of molecular orientation, which was determined to be from the Vectra crystalline phase, can be seen in both the WAXS patterns. However, there is not any real qualitative difference between the orientation of the rods extruded by the two methods and certainly nothing that might account for the roughly 5.5 GPa difference in the tensile moduli of the two differently processed blends. The only thing that is clearly evident is that drawing is capable of producing high levels of molecular orientation in the LCP phase. One other point to be made is again the absence of any evidence of molecular orientation of the PET phase in either of the two blends.

It was clear from the above WAXS patterns that the differences in the properties of the blends from the two methods was not due to any significant differences in the level of molecular orientation. Thus the morphology of the two systems was examined in some detail to establish if the better properties of the mixer blend could be related to the morphology. In Fig. 63 are shown the SEMs of PET/Vectra A 70/30 PB rod of draw ratio 49. In Fig. 63a is shown the overall fracture surface of the extruded rod and in Fig. 63b is shown a high magnification in the core or center of the rod. A very distinct skin-core fibril-droplet structure is seen from this pair of micrographs. Furthermore. a very rough estimation from Fig. 63a indicates that the core region is 15 % of the total surface area of the rod fracture surface. Also, upon closer examination of Fig. 63a, it may be seen that the fibrils appear to get more evident and longer as one moves from the core to the skin region. In sharp contrast to this, the morphology of the rod extruded from the mixing method is shown in Fig. 64. From Fig. 64a, it is clear that the LCP phase is present in the form of very high aspect ratio fibrils and the morphology is devoid of any skin-core structure. The fibrils are seen in the entire cross-section and furthermore there does not appear to be any difference in the fibril shape or diameter along the radius of the rod i.e. the fibrils are quite uniform in size throughout the cross-section.

A small sample of strand of PET/Vectra A 70/30 from the mixing method was etched in n-propylamine for over 40 hours to remove much of the PET phase which is selectively dissolved out (the Vectra A900 was independently determined to be insoluble in the solvent over a period of 72 hours). The residue from the etching experiment was then carefully washed in
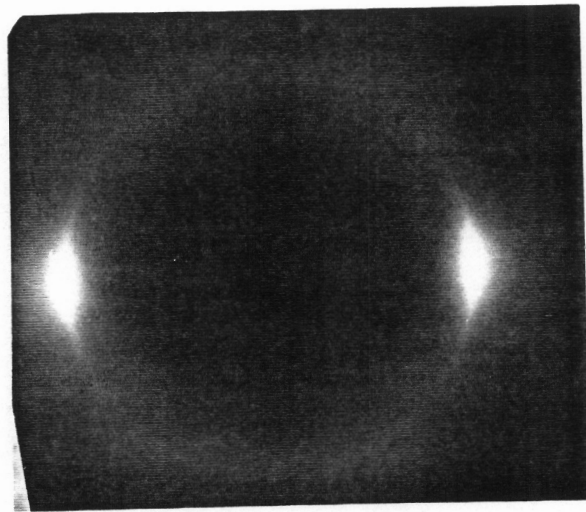
a
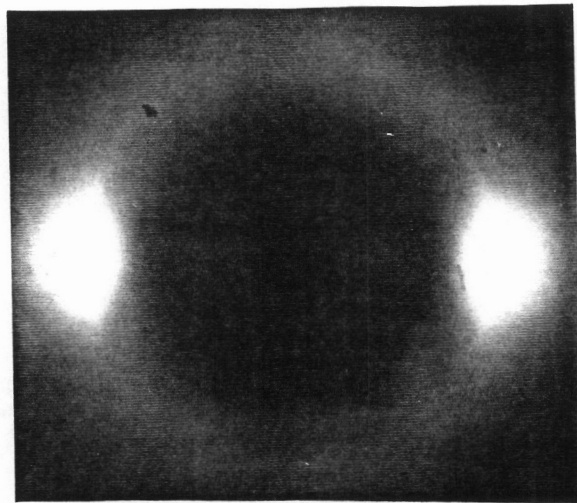
b

Figure 62. Wide-angle x-ray scattering patterns of PET/Vectra A900 70/30 blends gener-
ated from (a) single-screw extrusion and (b) mixing method.
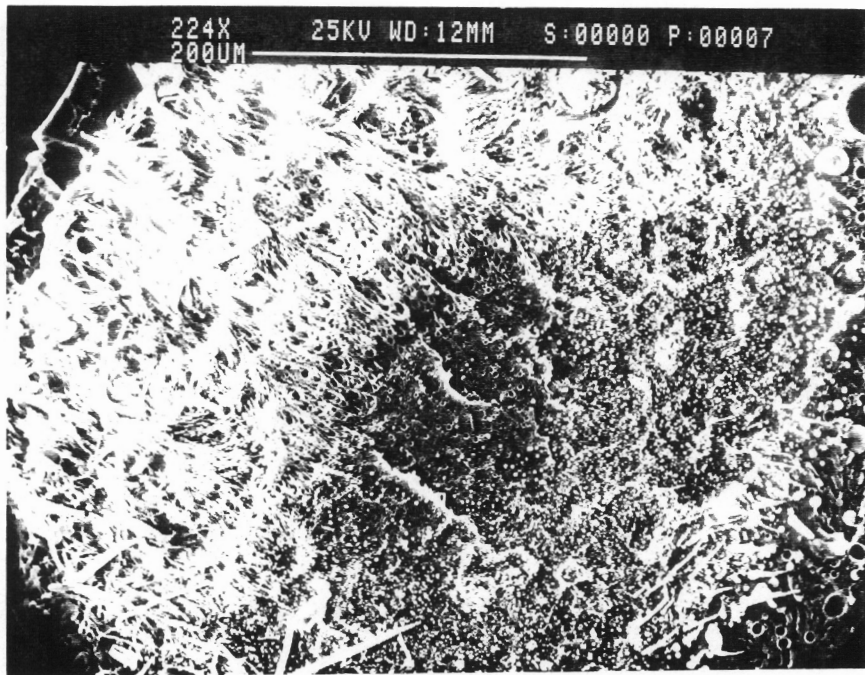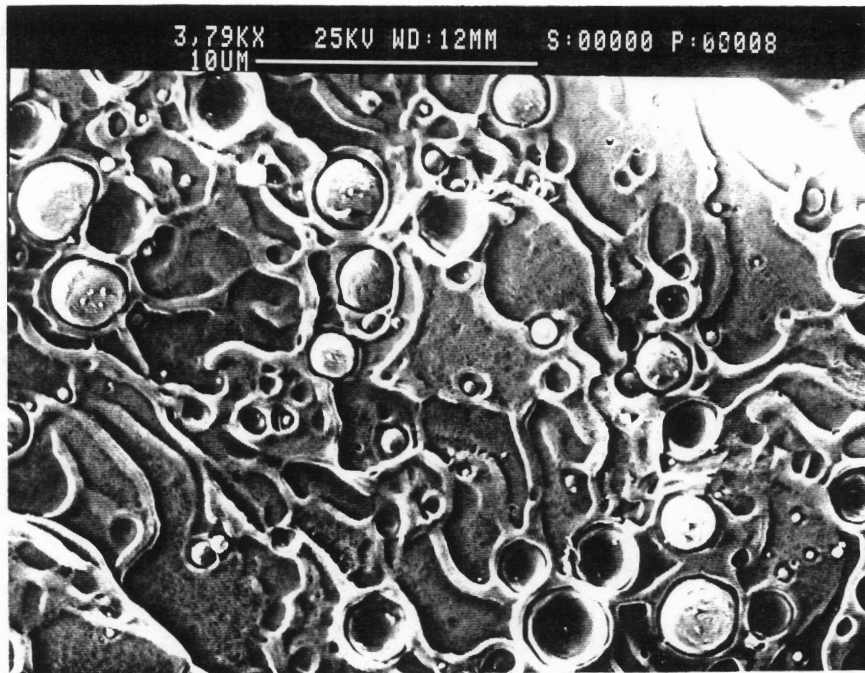
Figure 63. SEMs of transverse direction fracture surfaces of PET/Vectra A900 70/30 blend rod [D.R. = 49] generated from single-screw extrusion: (a) low and (b) high magnification in the center.
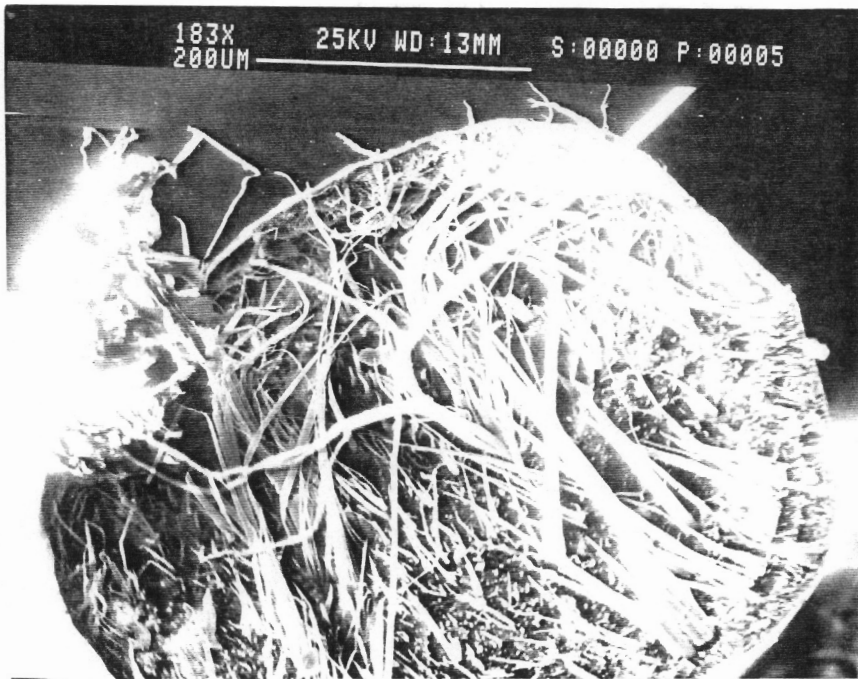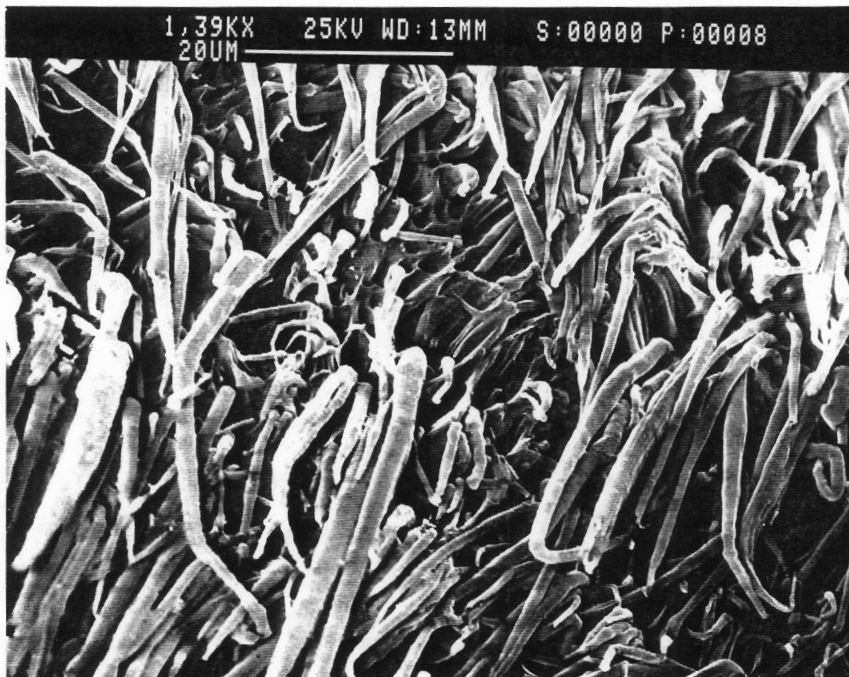
Figure 64. SEMs of transverse direction fracture surfaces of PET/Vectra A900 70/30 blend rod [D.R. = 49] generated from the mixing method: (a) low and (b) high magnification in the center of strand.

water and dried. A photograph of the resulting sample is shown in Fig. 65 wherein a rather dramatic morphology of the Vectra A900 phase in the form of continuous fibrils, infinite in aspect ratio can be seen. The fibrils were determined to be ranging from 0.5-2 μm in diameter and ran the length of the extrudate. The sample shown in Fig. 65 is about 5 cm in length and therefore the aspect ratio may be referred to as infinite for all intents and purposes. It may be added here that a strand from the physical blend of PET/Vectra A 70/30 was also etched for comparison. However, after etching for the same length of time, the fibrils that were left behind were not as continuous and thus could not be handled easily.

The observed differences in the moduli of the PET/Vectra A 70/30 blends discussed earlier (Table 10) may be better explained in light of the above morphology results. The significant increase in the properties of the mixer blend over pure PET and the physical blend can be attributed to the highly continuous LCP fibrillar morphology that is created in the blends during extrusion via the mixing method. In contrast, the morphology of the physical blend consists of smaller aspect ratio fibrils and are seen only in the skin region of the strand with only LCP droplets in the core. These droplets of the LCP do not contribute significantly to the property enhancement of the matrix and thus the properties are lower than those observed for the mixer blend.

The differences in the tensile moduli and the morphology of the blends from the two methods was discussed above. However, it is important to address also the possible reasons and mechanisms by which the morphology develops for the two blending cases. It is believed, largely on the basis of the work presented above and on the basis of some more experimental evidence to be discussed in a later section, that the formation of the LCP fibrils in the two blending methods, mixing method and physical blending, occurs by very different and distinct mechanisms. At the very outset, this belief should not be very surprising since in one case the mixing takes place in the extruder itself whereas in the mixing method all the mixing takes place in the static mixer alone. Therefore, the particular mixing mechanisms of the extruder and static mixer can be expected to influence the resultant morphology and properties quite significantly as observed. It is believed that the process of fibrillation in the single-screw
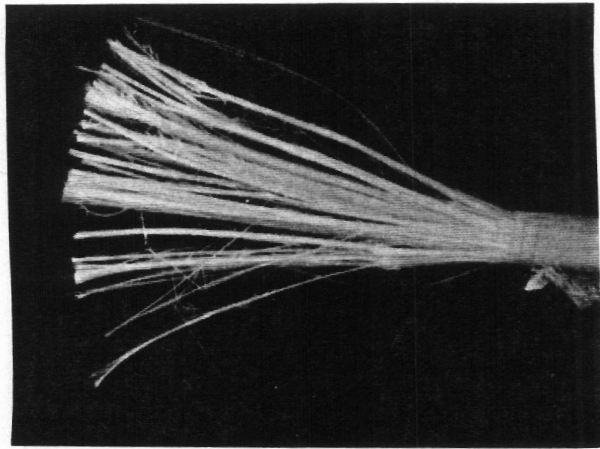
Figure 65. Photograph of the residue of a PET/Vectra A 70/30 MB strand etched in n-propylamine for 72 hours. Length of sample shown in about 5 cms.

extrusion process takes place in a fashion whereby first a dispersion of the LCP phase in the matrix is created by way of droplets and then these droplets are extended into fibrils. The droplets are extended into fibrils in cases where extensional forces are present, such as at the converging section of capillary dies or by drawing at the die exit. In fact, in an earlier study on the extrusion of PC/LCP60 blends through capillary dies it was concluded that the fibrous LCP morphology is created in the capillary die or at the entrance to the capillary die and not in the channel of the screw (162). Mixing in the static mixer, on the other hand, occurs by a rather complex combination of flow- division and distribution, flow-inversion and radial-mixing mechanisms (132, 142). The mixing in the static mixer is thus predominantly distributive rather than dispersive. The shear-rates in the static mixer are only about 1-10 sec^{-1} which are not significantly lower than the shear rate range of 15-25 sec^{-1} in the extruder channel, which were estimated for typical flow rates and processing conditions. Thus it is believed that the distributive mixing mechanism in the static mixer is responsible for creating continuous striations of the LCP phase in the matrix polymer. It is therefore believed that the LCP phase does not form droplets first which are then stretched into fibrils but rather forms continuous layers of the LCP in the matrix, which by using an appropriate number of elements, results in a more "homogeneous" blend. Experimental work, to be presented later, will further reinforce these ideas.

4.2.3 Sheet Extrusion

It is clear from the above results that the dual-extruder mixing method was quite successful in generating infinitely long and highly oriented LCP fibrils in the matrix of extruded rods. Further, the favorable fibrillar morphology and high orientation of the LCP phase was seen to result in blends with tensile moduli that were significantly higher than that of the respective matrix polymer. Having achieved this success with the strand extrusion, it was believed that if similar success could be obtained with sheet extrusion, then there was a

potential to treat these LCP blend sheets with continuous LCP reinforcements as prepregs. These prepreg sheets could then be subjected to post-processing options such as lamination to obtain unidirectional or cross-laminated composites. As mentioned before, it is strongly believed that a thermoplastic-LCP composite in which the LCP has a higher melting point than the matrix polymer, would offer the potential to further process these composites at elevated temperatures, but below the melting temperature of the LCP, without any significant loss in the mechanical properties. Thus sheets of PET and PP with several LCPs were extruded using the dual-extruder mixing method.

To reach the above objective, a sheet die with a simplified design was made. As may be recalled, sheets of PET/LCP60-80 were made using a 4" sheet die (Section 4.1.1), with a typical coat-hanger type of feed arrangement. However, on the basis of some experiments to be presented later, it appeared that the sheet die was possibly responsible for the break-up of LCP fibrils into droplets. In particular, the design of the abovementioned 4" sheet die seemed to have two main drawbacks. First, the land region of the sheet die was determined to be approximately 1.1" long. The die lips were typically set at between 30-40 mils (0.030- 0.040") which yielded a L/H ratio of between 27-37. This L/H ratio was seen to be too high (as will be shown later) for the LCP fibrils to remain stable. Secondly, the cross-section of the land region of the die was fairly irregular, incorporating towards the die exit an 'S'-shaped kink which served as a reservoir of polymer melt. It was mentioned earlier in Chapter 2 (Section 2.3) that a stretched liquid cylinder ($l/d > 4.5$) of a Newtonian fluid suspended in another Newtonian fluid is in a thermodynamically unstable state due to the unfavorable ratio of surface area to volume (45). This stretched liquid cylinder opposes a further increase in it's length, since it is energetically unfavorable, and consequently splits into droplets by interfacial tension driven Rayleigh disturbances (161). It has been observed that the liquid cylinder becomes varicose before fracture (45) and furthermore that the varicosity (capillary waves) may appear due to disturbances in the flow as may be caused by fluctuations in the density, viscosity and vibration of equipment (45). To eliminate possibilities for such a break-up of LCP fibrils due to the irregular die cross-section, a simplified die with an L/H ratio of about 10 and a step con-

traction at the exit was made. A schematic of the die is shown in Fig. 66. Due to the fact that the die was not equipped with a coat-hanger feed (which ensures an even flow rate along the width of the die), the width of the new die was limited to 2.5 inches. Details of the die dimensions and design are provided in the Appendix. The sheets in the discussions that follow were made using this new die attached to the exit of the static mixer.

4.2.3.1 PET/LCP Sheets

Sheets of PET with several LCPs, ranging from 20-40 mils in thickness and 0.75″ to 3.5″ in width, were made using the new die in conjunction with the mixing method. In addition to the processing details outlined in Chapter 3, some further details are discussed here. The polymer melt emerging from the die was either taken up on a pair of chill rolls or was passed through a calender. Calendering of the sheets was done for two reasons. First, it was hoped that the squeezing action of the nip rolls would tend to give some degree of biaxial properties to the sheets as compared to the largely uniaxial or unidirectional properties observed with simple drawing. Secondly, the surface of the sheets and the uniformity in thickness (along the sample width) with drawing were observed to be poor and it was believed that calendering would help alleviate these two problems to some extent. Thus the sheets will be referred to as 'NC' i.e. not calendered or 'C' i.e. calendered. Cooling water, at ambient temperature, was passed (not recirculated) through the chill rolls to quench the sheet and prevent it from being stuck on the roller surface. In the case of the calender rolls, the conduits or channels of the rollers were recirculated with oil at room temperature (which could also be heated up, if required) to remove the heat. In the case where the sheet was calendered, the rollers had to be cooled periodically by rubbing ice over the surface of the rollers due to the heating up of the recirculating oil.

The PET/Vectra A sheets were extruded using the following temperature profile:
- PET extruder - 225°C, 290°C, 290°C and 225°C in zones 1-3 and clamp ring, respectively
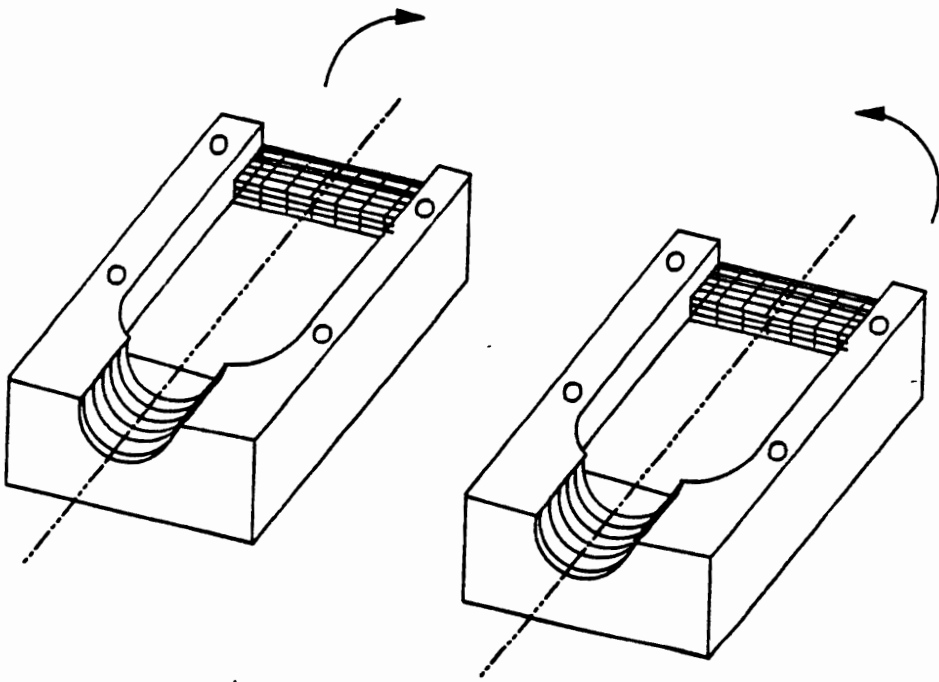
Figure 66. Schematic of the simplified sheet die used in conjunction with the mixing method to generate sheets of PET/LCP and PP/LCP blends.

- Vectra A extruder - 265°C, 330°C, 330°C and 290°C in zones 1- 3 and clamp ring, respectively

- Zones 'C1' and 'C2' were maintained at 220°C and 190°C, respectively

- Static mixer and sheet die at 225°C and 250°C, respectively

Three separate runs were made with the following extrusion conditions and resulting compositions. PET/Vectra extruders were run at 40/8, 40/13 and 40/18 RPM to yield flow rates, in gms/min, of 70/11.27, 83.54/17.55 and 63.5/32.4, respectively. The compositions for the three runs were calculated to be 15 %, 18 % and 35 wt % Vectra A in the blend.

Sheets of PET/HX4000, on the other hand, were made using the following temperature profile:

- PET extruder - 225°C, 290°C, 290°C and 225°C in zones 1-3 and clamp ring, respectively

- HX4000 extruder - 265°C, 340°C, 310°C and 300°C in zones 1- 3 and clamp ring, respectively

- Zones 'C1' and 'C2' were maintained at 225°C and 190°C, respectively

- Static mixer and sheet die at 225°C and 250°C, respectively

PET/HX4000 blend sheets of two composition ratios were made. One run was made at 40/10 RPM and the other at 40/18 RPM. The mass flow rates at these conditions were measured to be, in gms/min, 76/13.5 and 69.6/26.5, respectively, yielding composition ratios of ca. 85/15 and 72/28 wt %.

Results of tensile tests performed on the extruded PET/LCP sheets are shown in Table 11. The tensile modulus (TM) and tensile strength (TS) of pure PET sheet with a draw ratio of 5 were measured to be 2.2 GPa and 53.03 MPa, respectively. In comparison, it is quite clear from Table 11 that the TM of the several blends investigated are only slightly higher than that of pure PET and furthermore the TS is almost the same or even lower than pure PET. It can be further observed that the properties of the sheets that were drawn ('NC') are higher than the calendered sheets. Specifically, the highest properties, with the current set of experiments, were obtained with the PET/Vectra A 82/18 blend sheet that was drawn. However, even these properties represent only a very marginal increase in the TS and about a 34 % increase in the TM over pure PET values. Furthermore, the differences in properties of the sheets that were drawn and calendered are clear from the data on the PET/Vectra A 85/15

sheets. The drawn sheet is observed to have higher TS and TM than the calendered sheet of the same composition and in fact processed under identical conditions. As the composition is further increased to 35 wt % Vectra A, the TM and TS of the blend sheet are both seen to fall as compared to pure PET. Lastly. the PET/HX4000 72/28 sheet which was also calendered again has only marginally improved properties relative to PET. Therefore two things were clear from the above results. First, the extent of mechanical property enhancements, and in particular the TM, of the sheets are nowhere near those observed for the extruded strands discussed earlier. Second, the drawn sheets possess better properties than the calendered sheets.

Reasons for these were further investigated by SEM and WAXS characterization techniques. Scanning electron micrographs of fracture surfaces of PET/Vectra A 82/18 drawn sheet are shown in Fig. 67. From Fig. 67a. it can be seen that the Vectra A phase is present in the form of extended fibrils in the PET matrix. The fibril diameters are larger than those seen in the case of the extruded strands discussed earlier due most likely to the lower draw ratios involved and are of the order of 4-12 μm. The ends of the fibrils broken during the transverse fracture may be seen in Fig. 67b along with holes due to fibril pull-out.

SEMs of fracture surfaces of the PET/Vectra A 85/15 drawn and calendered sheets, fractured along the flow direction, are shown in Figs. 68a and 68b, respectively. It is quite clear from Fig. 68 that there does not appear to be any significant difference in the morphology of these sheets, one of which was drawn and the other calendered. Yet as seen from Table 11, the properties of the drawn sheet were higher than the calendered sheet. The fibril diameters are again of the order of 4-10 μm and there is no perceptible difference in fibril size either in the two micrographs.

The morphology of the PET/Vectra A 65/35 MB blend sheet was also examined and is shown in Fig. 69. Here, the fracture surface (a) along and (b) across the flow direction is shown. From both the micrographs in Fig. 69, it is quite clear that the LCP does form quite continuous fibrillar structures in the PET matrix. In fact, the transverse direction fracture surface in Fig. 69b shows clearly the fibrils that were pulled out during the fracture. Thus on the

Table 11. Tensile properties of PET/LCP sheets extruded from the mixing method.

MATERIAL	DRAW RATIO	TENSILE STRENGTH* [MPa]	YOUNG'S MODULUS* [GPa]
PET	5.0 (NC)	53.03 (2.86)	2.20 (0.18)
PET/Vectra A 82/18	6.0 (NC)	59.25 (2.61)	2.95 (0.42)
PET/Vectra A 85/15	6.2 (NC)	52.78 (3.23)	2.65 (0.28)
PET/Vectra A 85/15	5.8 (C)	45.97 (2.97)	2.19 (0.15)
PET/Vectra A 65/35	4.8 (C)	41.67 (3.96)	1.99 (0.11)
PET/HX4000 72/28	6.6 (C)	58.76 (3.71)	2.80 (0.16)

*Standard deviations are given in parenthesis
(NC) = Not calendered
(C) = Calendered
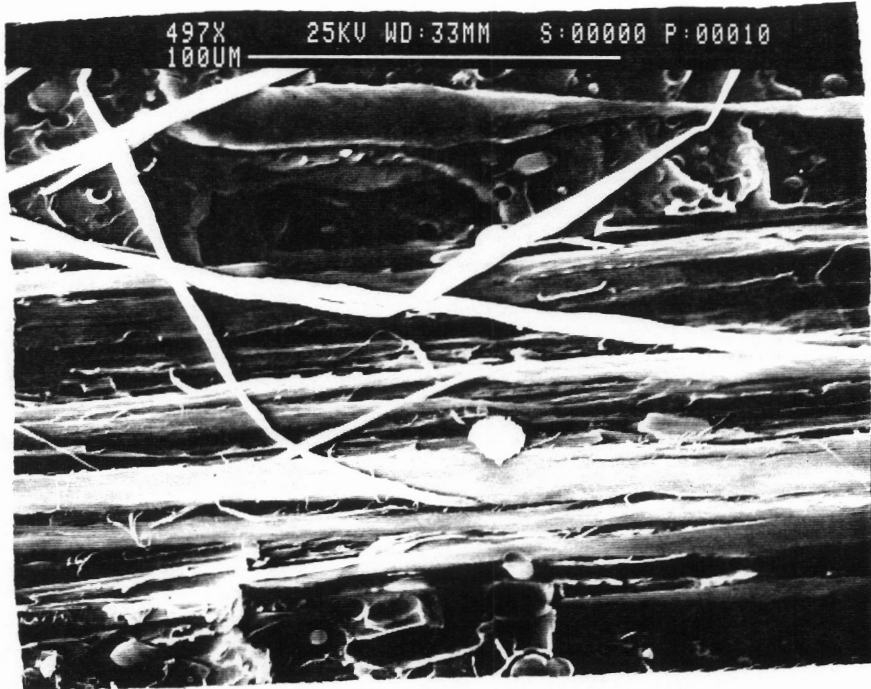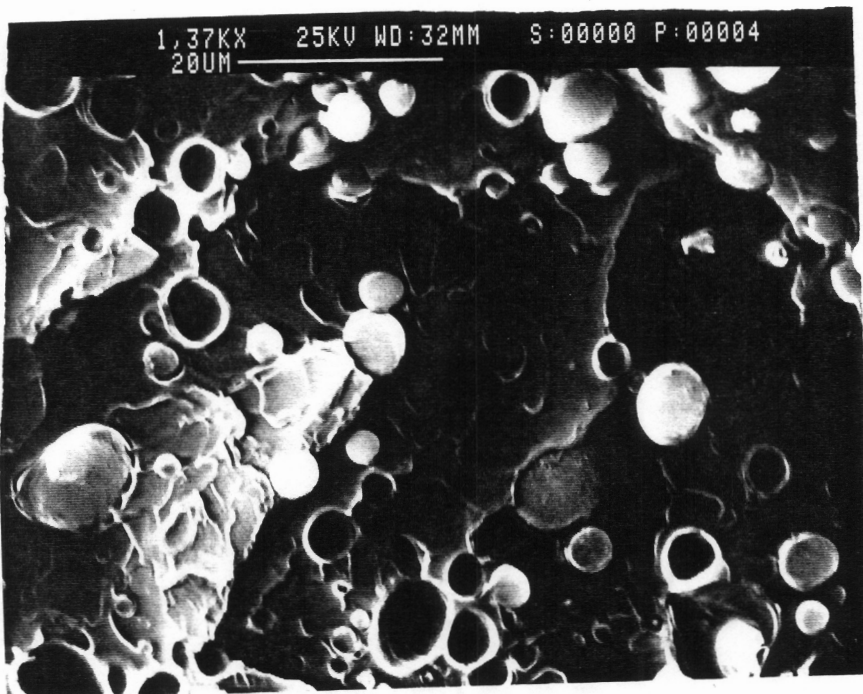
Figure 67. Scanning electron micrographs of fracture surfaces of extruded sheets of PET/Vectra A 82/18 MB blend with D.R.=6.0. Fracture is (a) along and (b) across the flow direction.
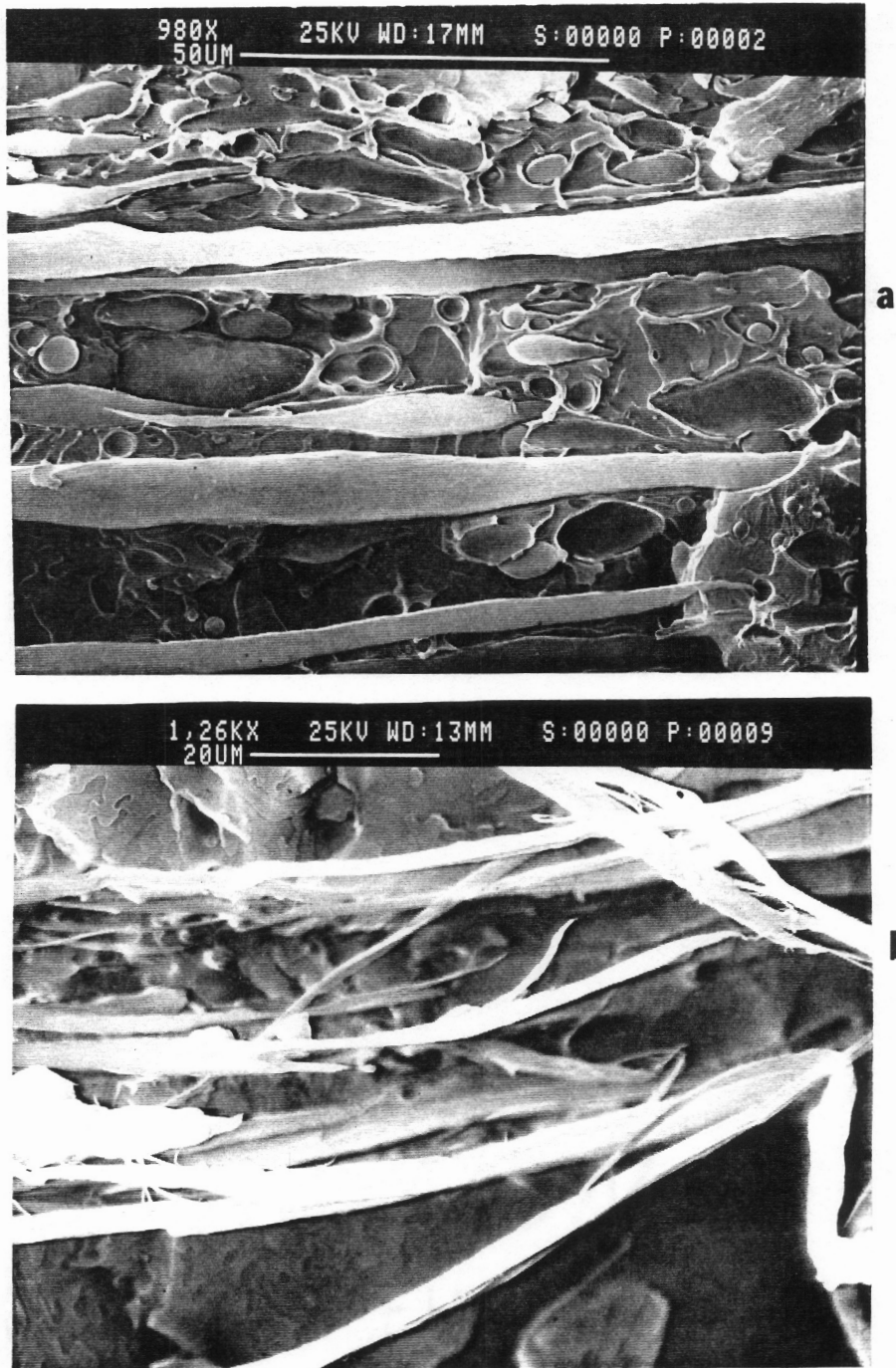
Figure 68. SEMs of fracture surfaces of extruded sheets of PET/Vectra A 85/15 MB blend which was (a) drawn [D.R. = 6.2] and (b) calendered [D.R. = 5.8]. Fracture is along the flow direction.

basis of the observed morphology, one would have expected better properties than observed in Table 11. Lastly, in Fig. 70 is shown the morphology of the PET/HX4000 72/28 MB extruded sheet. The HX4000 sheet does appear to have a somewhat different morphology than the PET/Vectra A sheets discussed earlier in that the size of the LCP phase is somewhat smaller, with the fibril diameters ranging from less than 1 to about 6 μm in diameter and further appear to be much smaller in length as well. However, from Table 11 it may be recalled that the properties of these sheets were better than the PET/Vectra A 65/35 and 85/15 blend sheets. These differences in the properties were thought to be a consequence of the differences in the level of molecular orientation and WAXS studies were done to confirm these ideas.

In Fig. 71 are shown the WAXS patterns of the as-extruded and annealed PET sheets a with draw ratio of 5. Clearly from Fig. 71a, there is no preferred direction of orientation and nor is there any developed crystallinity as evidenced by the diffuse halo characteristic of an amorphous phase. Upon annealing, however, three distinct rings due to the diffraction of the crystalline phase are now clearly visible. The d- spacings, d_s, of these rings were determined to be approximately 3.42, 4.20 and 5.03 °A. The fact that the as extruded PET sheet is amorphous and not oriented is not very surprising due to the fact that the PET did not crystallize very rapidly and further, as discussed earlier in the case of pure PET rods, the relaxation time of PET is much too rapid for any imparted orientation to be maintained. In contrast, the WAXS patterns of the PET/Vectra A 82/18 and PET/HX4000 72/28 sheets are shown in Fig. 72. In Fig. 72a, a pair of arcs, indicative of high molecular orientation and having $d_s = 4.68$ °A is clearly visible. This pair of arcs was determined to be from the crystalline Vectra A phase. Also, the three rings, determined to be from the PET crystalline phase, observed. These rings are seen possibly due to the nucleating effect of the Vectra A phase which enhance the crystallinity of the PET matrix. Such a nucleating effect of LCPs on PET has been observed before (120,121). Similarly, in Fig. 72b, a distinct pair of arcs is also seen with $d_s = 4.59$°A which was determined to arise from the HX4000 crystalline phase. Again a ring, just inside of the pair of arcs, is observed which arises due to the PET crystalline phase.

RESULTS AND DISCUSSION 208
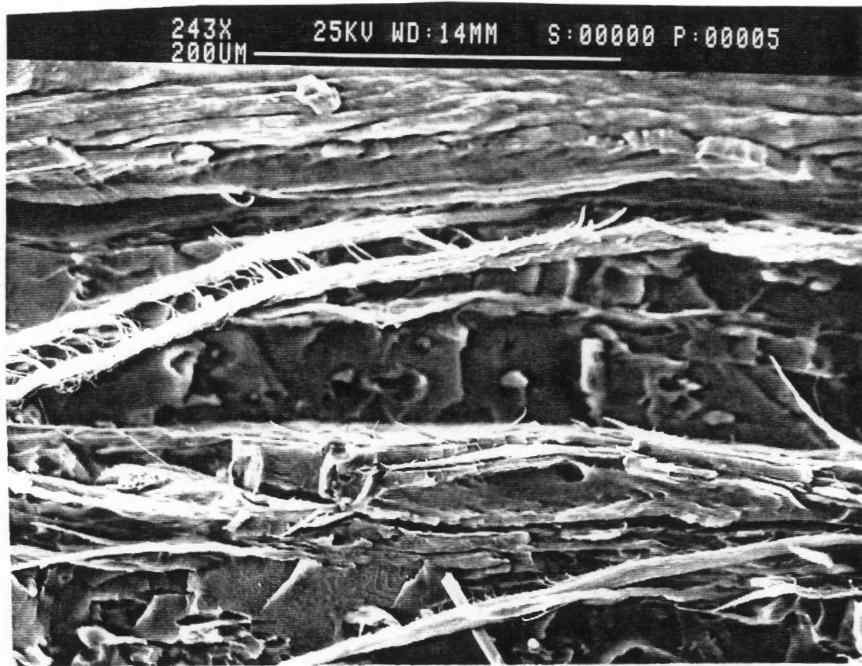
a
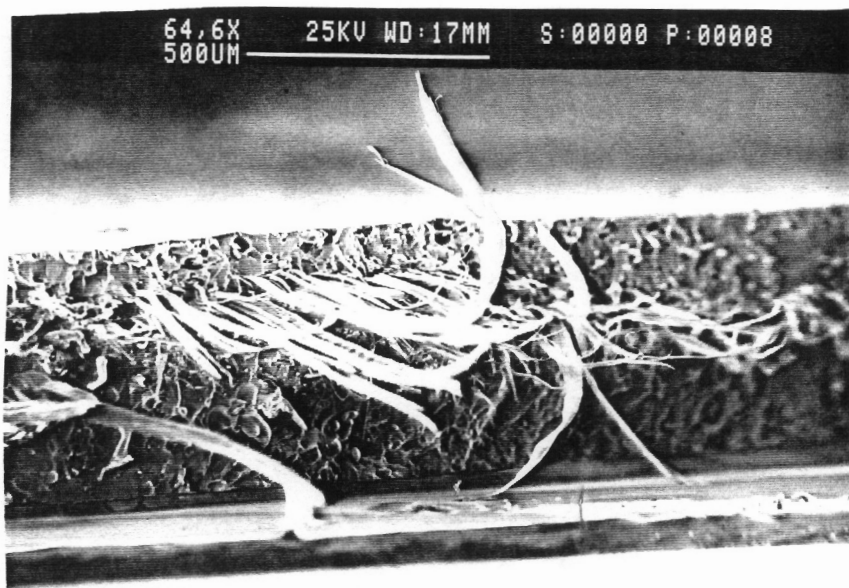
b

Figure 69.   Scanning electron micrographs of fracture surfaces of extruded sheets of PET/Vectra A 65/35 MB blend with D.R.=6. Fracture is (a) along and (b) across the flow direction.
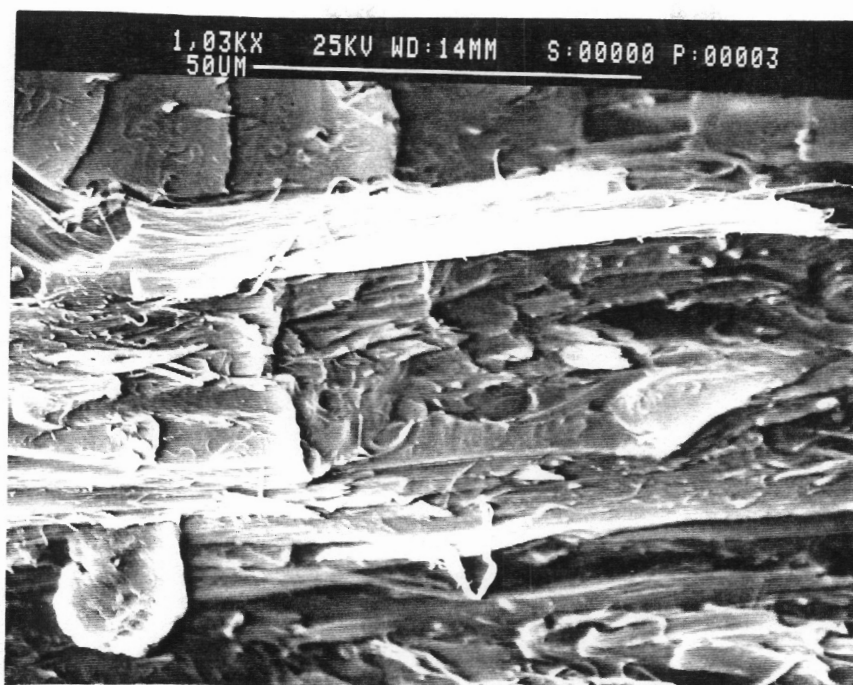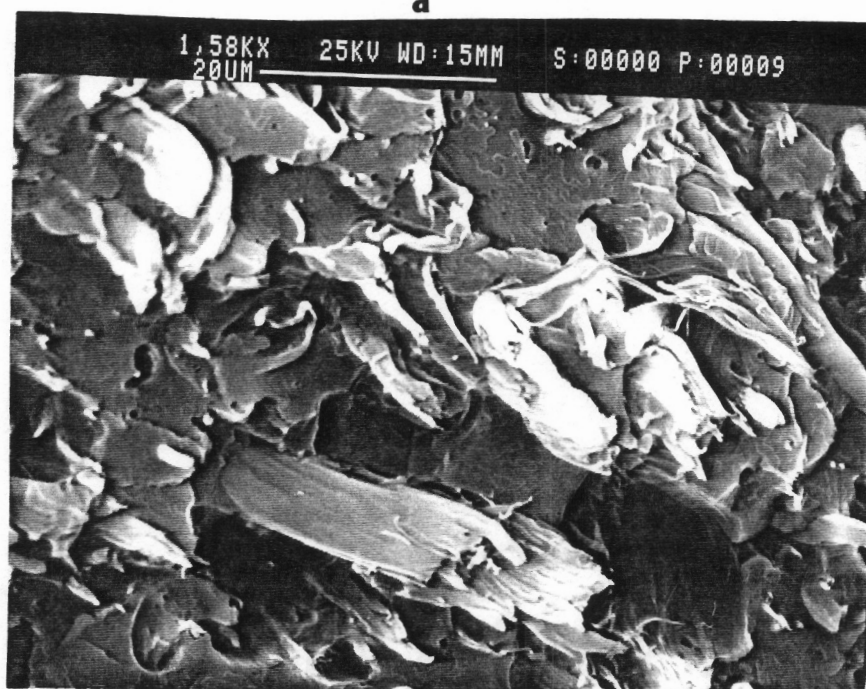
Figure 70. Scanning electron micrographs of fracture surfaces of extruded sheets of PET/HX4000 72/28 MB blend with D.R.=6.6. Fracture is (a) along and (b) across the flow direction.
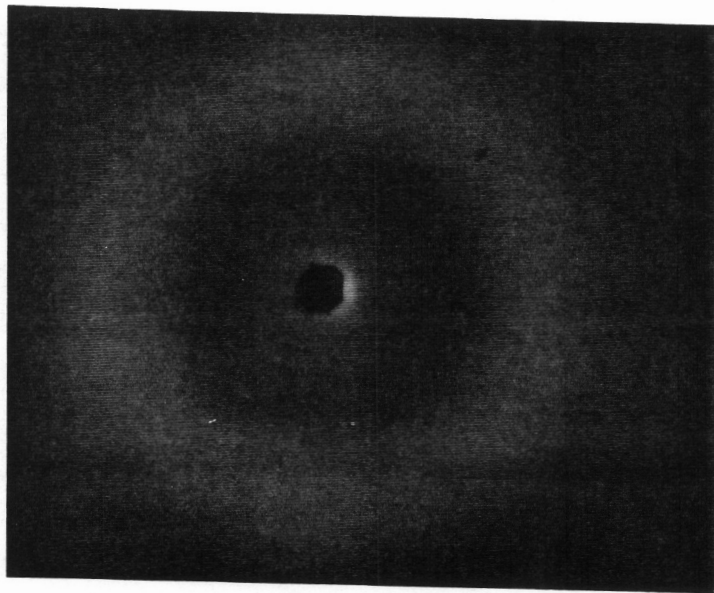
a
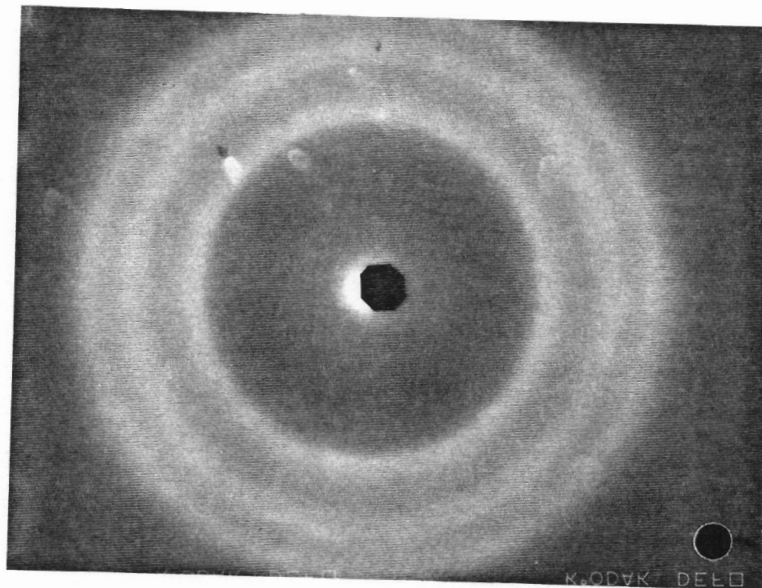
b

Figure 71. Wide-angle x-ray diffraction patterns of pure PET sheet with D.R. = 5: (a) as extruded and (b) annealed at 120°C for 1 hour. Flow direction is vertical.
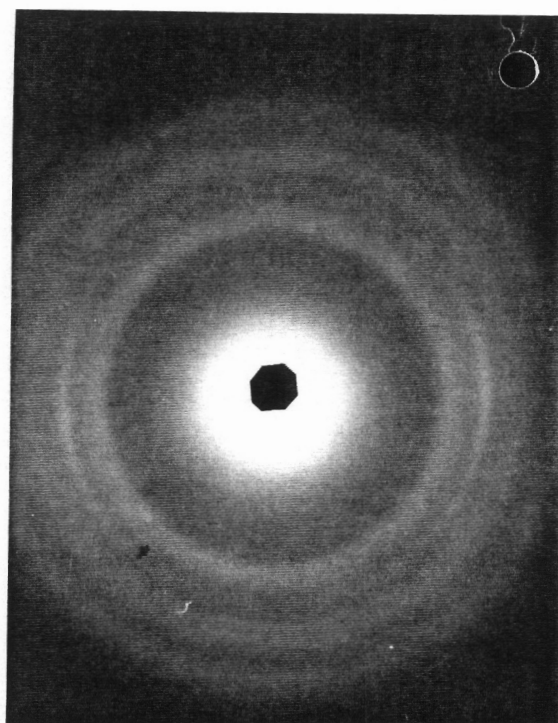
a
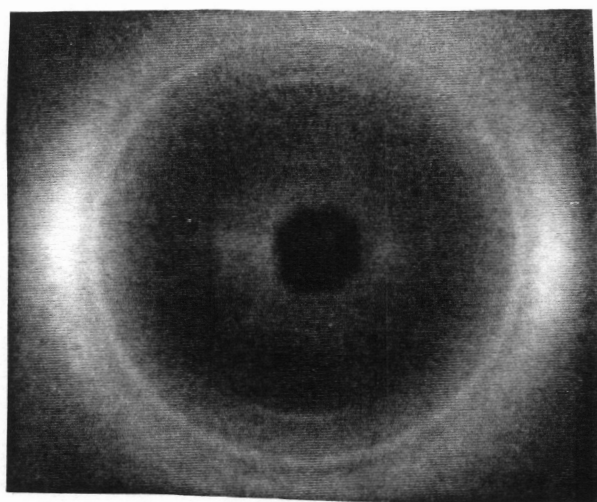
b

Figure 72.   Wide-angle x-ray diffraction patterns of (a) PET/Vectra A 82/18 sheet
[D.R. = 6.0] and (b) PET/HX4000 72/28 sheet [D.R. = 6.6]. Flow direction is vertical.

In Fig. 73 are shown the WAXS patterns of the PET/Vectra A 85/15 sheets which were (a) drawn and (b) calendered, respectively. The flow direction is vertical for both the diffraction patterns. The two patterns are quite different from each other. In the case of the drawn sheet (Fig. 73a), a pair of sharp arcs are observed due to the induced molecular orientation in the LCP phase. However, in the calendered sheet (Fig. 73b), the level of induced orientation appears to much lower than in the drawn sheet as evidenced by a relatively lower azimuthal dependence of the diffraction pattern resulting in an almost complete ring. Furthermore, upon closer examination of Fig. 73b, it appears that this slight orientation is offset from the horizontal indicating that the direction of preferred orientation is not the flow direction but at some small angle (roughly 15-20°) to the flow direction. This is most likely due to the squeezing action between the calender rolls. Thus it appears that the calender rolls do not induce the same levels of orientation in the LCP as direct drawing resulting in lower properties.

4.2.3.2 PP/LCP Sheets

Sheets of PP with several LCPs were also extruded using the same process as described earlier for PET/LCP sheet extrusion. Specifically, PP blends with LCP60, Vectra A and Vectra B were extruded. The extrusion conditions for sheet extrusion are described first. The temperature profile for the extrusion of PP/LCP60 sheets was as follows:

- PP extruder - 120°C, 190°C, 190°C and 200°C in zones 1-3 and clamp ring, respectively
- LCP60 extruder - 200°C, 265°C, 290°C and 290°C in zones 1- 3 and clamp ring, respectively
- Zones 'C1' and 'C2' were maintained at 225°C and 200°C, respectively
- Static mixer and sheet die at 225°C and 240°C, respectively

The PP and LCP60 extruders were operated at 40 and 7 RPM, and the resulting mass flow rates were measured to be 24.26 and 9.28 gms/min, respectively, giving a composition ratio of ca. 73/27. The PP/Vectra A and PP/Vectra B sheets were extruded using the same temperature profiles used for strand extrusion with the exception that the die was now maintained at a higher temperature viz. 240°C. The PP and Vectra A were extruded at 40 and 12 RPM, and
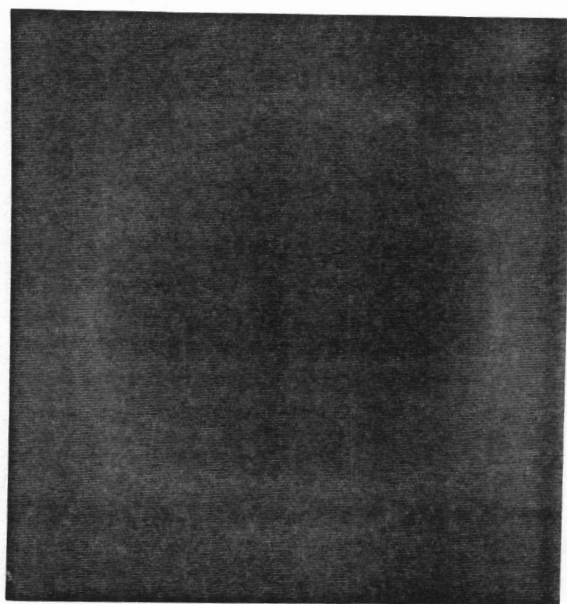
a
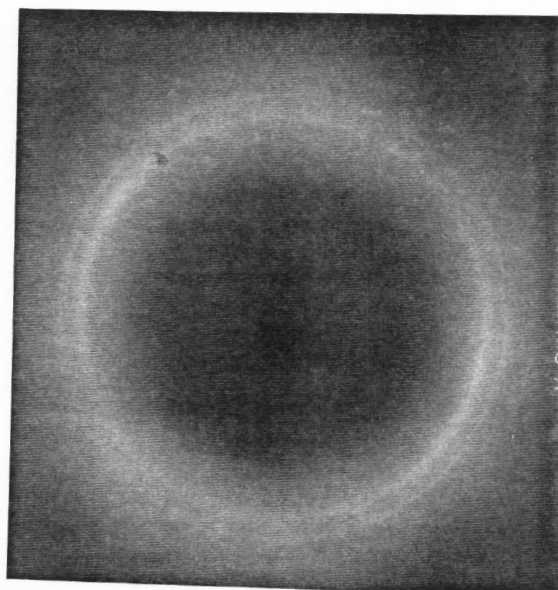
b

Figure 73. Wide-angle x-ray diffraction patterns of PET/Vectra A 85/15 sheets: (a) drawn [D.R. = 6.2] and (b) calendered [D.R. = 5.8]. Flow direction is vertical.

the respective flow rates were measured to be 28.53 and 7.31 gms/min yielding a composition ratio of about 81/19. Two compositions ratios of PP/Vectra B sheets were extruded. In the first run, the PP and Vectra B extruders were operated at 40 and 11 RPM, whereas in the second experiment they were operated at 40 and 16 RPM, respectively. The PP and Vectra B flow rates were estimated to be 27.98 and 6.09, and 30.07 and 12.31 gms/min, for the first and second runs. respectively, yielding sheets of composition ratios 82/18 and 70/30.

Results from tensile tests on the above blends are shown in Table 12. The modulus of pure PP sheet at a draw ratio of 4 is 0.56 GPa and the tensile strength is 15.73 MPa. In comparison, the TM and TS of the PP/LCP60 73/27 sheet with draw ratio 5.6 were measured to be 2.11 and 28.85 MPa. Thus the modulus is enhanced by almost 4 times whereas the strength is almost doubled. It should be noted here that these properties are for sheets that were drawn and not calendered. The TM of PP/Vectra A 81/19 sheets is also enhanced by almost four times that of pure PP and the tensile strength increases about 2.5 times. In contrast, the TM of PP/Vectra B 82/18 sheets at draw ratios of 3.2 and 6.8 were measured to be 0.96 GPa and 1.54 GPa, respectively. These results are surprising in view of the fact that the TM of Vectra B is almost twice that of Vectra A, as discussed earlier in the section on strand extrusion. However, it is worth noting that these sheets were calendered and not drawn. Furthermore, the PP/Vectra B 70/30 composition sheet with a draw ratio of only 2 is 2.33 GPa whereas the strength is 25.78 MPa. Thus it is clear that while 2-4 fold increase in the TM is achieved even for these low draw ratios, the TS is not increased to the same extent.

The morphology of the fracture surface of these sheets is shown in Figs. 74 and 75. In Fig. 74a is shown the fracture surface of PP/LCP60 73/27 sheet with draw ratio 5.6 whereas the fracture surface of PP/Vectra A 81/19 sheet with draw ratio 4.4 is shown in Fig. 74b. Fracture surfaces of PP/Vectra B 70/30 sheet along and across the flow direction are shown in Fig. 75. The presence of fibrillar LCP morphologies is evident in all the three cases. However, there is a very significant difference in the size scale of these LCP structures. In the case of the drawn PP/LCP60 and PP/Vectra A sheets, the LCP fibrils are of the order of 5-15 μm in diameter. However, in the calendered sheet of PP/Vectra B, the fibril are much larger being in the

Table 12. Tensile properties of PP/LCP sheets extruded from the mixing method.

MATERIAL	DRAW RATIO	TENSILE STRENGTH* [MPa]	YOUNG'S MODULUS* [GPa]
Polypropylene (PP)	4.0 (NC) 10.0 (NC)	15.73 (3.11) 21.95 (3.42)	0.56 (0.098) 0.615 (0.047)
PP/LCP60 73/27	4.8 (NC) 5.6 (NC)	26.45 (1.81) 28.85 (1.25)	1.57 (0.156) 2.11 (0.121)
PP/Vectra A 81/19	4.4 (NC)	39.42 (4.19)	2.10 (0.170)
PP/Vectra B 82/18	3.2 (C) 6.8 (C)	27.55 (2.16) 31.45 (2.54)	0.96 (0.07) 1.54 (0.08)
PP/Vectra B 70/30	2.0 (C)	25.78 (2.06)	2.33 (0.30)

*Standard deviations are given in parenthesis
(NC) = Not calendered
(C) = Calendered

range of 30-60 μm. This difference is believed to be a direct consequence of the fact that the PP/Vectra B sheet was calendered and thus the additional driving force for reducing the fibril diameter at the die exit, by way of extensional drawing, was largely absent.

The degree of molecular orientation achieved in the PP/LCP sheets was also examined. Thus the WAXS patterns of pure PP sheet with a draw ratio of 10, PP/LCP60 73/27 sheet with draw ratio 5.6 and PP/Vectra A 81/19 sheet with draw ratio 4.4 are shown in Fig. 76. The WAXS pattern for pure PP indicates that although the sheet is crystalline, there is no preferred orientation present even at this high draw ratio. In contrast, both the blend sheets show a sharp pair of arcs which correspond to high orientation arising from the respective LCP phase. The fibrillar morphology and the high level of orientation enhance the mechanical properties of pure PP as observed.

From the above results on both PET/LCP and PP/LCP blend sheets extruded using the mixing method, some important conclusions can be made. First, it is evident that the properties of the blend sheets are not enhanced to the same extents as were seen with the extruded rods. This is attributed to the low draw ratios attained in the sheet extrusion process due to processing limitations. Specifically, the extruder throughputs are not sufficient to feed dies of larger widths, which would then make it possible to draw sheets further without tearing or reduction down to sizes (widths) which make mechanical property testing difficult. Second, it is also clear that the direct drawing process results in marginally higher properties than obtained with the calendering due to the higher levels of molecular orientation of the LCP phase reached. In particular, the difference in mechanical properties as well as orientation levels was shown for the PET/Vectra A 85/15 sheets which were drawn and calendered. Further, it is observed that the mechanical properties of the sheets are more dependent on the level of orientation rather than on the composition of the blend. For example, the PET/Vectra A 65/35 composition blend sheet which was calendered [D.R. = 2] had lower properties than a PET/Vectra A 82/18 sheet [D.R. = 6] which was drawn as shown in Table 11. Despite the lack of significant enhancements in the mechanical properties of extruded sheets, it is nevertheless important to recognize that the extrusion of both the PET/LCP and PP/LCP blend sheets
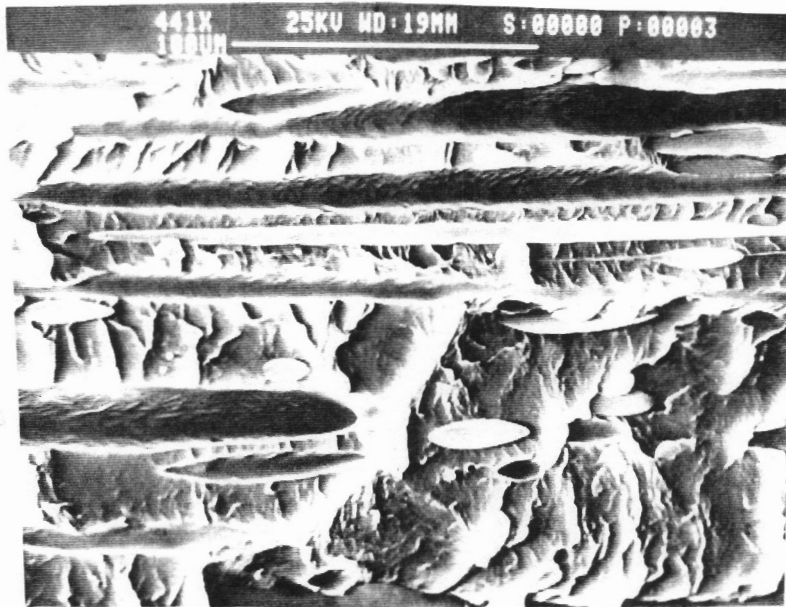
a

b

Figure 74. Scanning electron micrographs of fracture surfaces of extruded sheets of (a) PP/LCP60 73/27 [D.R. = 5.6] and (b) PP/Vectra A 81/19 [D.R. = 4.4]. Fracture is along the flow direction.
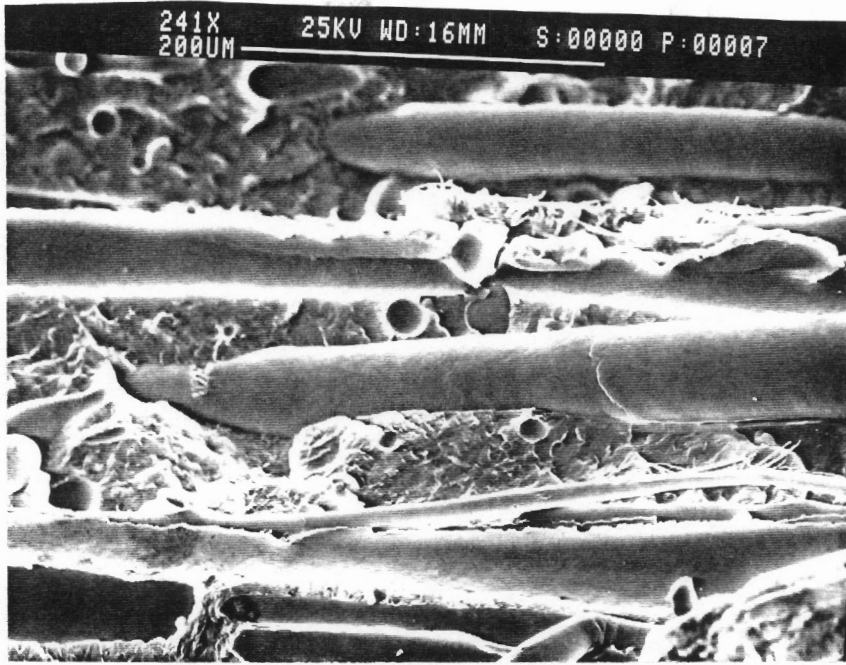
a
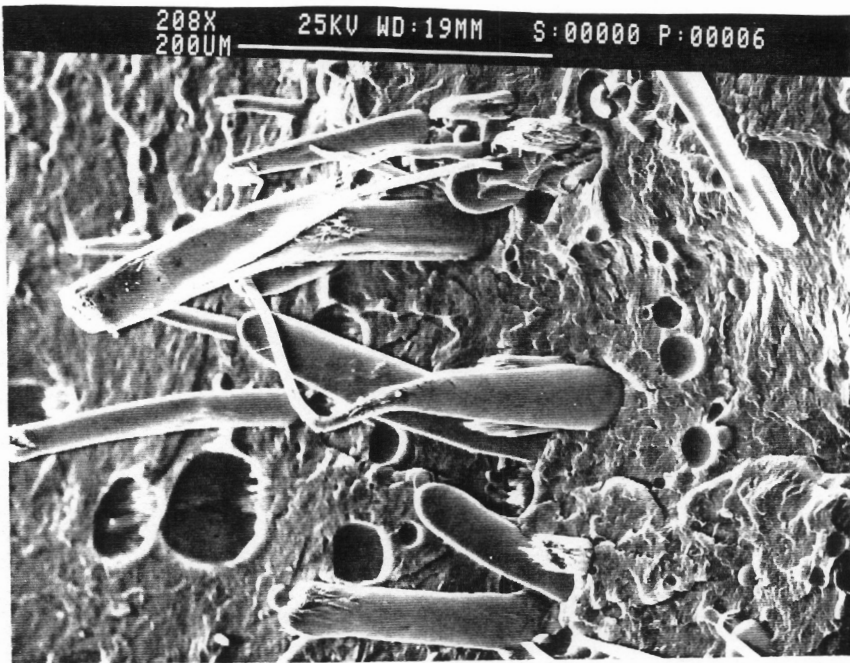
b

Figure 75. Scanning electron micrographs of fracture surfaces of extruded sheets of PP/Vectra B 70/30 [D.R. = 2] (a) along and (b) across the flow direction.
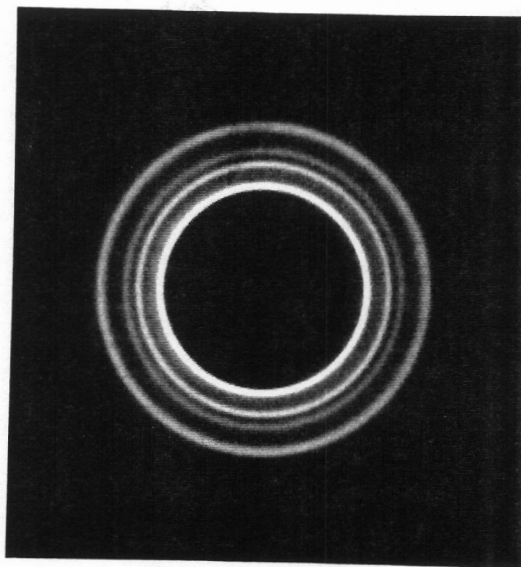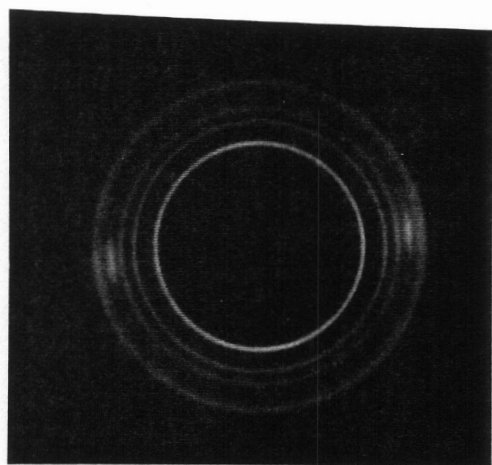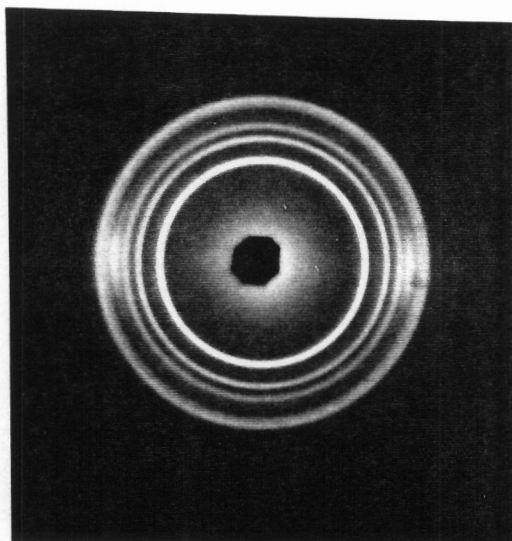
Figure 76. WAXS patterns of (a) pure PP sheet [D.R.=10], (b) PP/LCP60 73/27 sheet [D.R.=5.6] and (c) PP/Vectra A 81/19 sheet [D.R.=4.4]. Flow direction is vertical.

is possible due to the mixing method developed. In fact, attempts to make sheets of blends of PP/Vectra A and PET/HX4000 using only a single extruder were unsuccessful due to the extremely poor melt strength of the extrudate. The emerging melt was observed to sag under its own weight and thus could not be handled or taken up on the chill rolls for drawing. Therefore. it is clear that the dual-extruder mixing method is critical for processes such as sheet extrusion, where good melt strength is required, since the melts can be processed in the supercooled state. It may be recalled from Fig. 20 that the melt strength of Vectra B950 was observed to fall about 10 fold as the melt temperature was increased from below 290°C to above 290°C (107). Lastly, it was shown in Section 4.2.1 that it was impossible to obtain a viscosity ratio less than or even equal to unity for several of these blend systems e.g. PET/Vectra A, PET/HX4000, PP/Vectra A etc. while processing in a single extruder, at the temperatures and shear rates of interest. The importance of having a favorable viscosity ratio was demonstrated with the PET/LCP60 and PET/LCP60-80 blend sheets discussed earlier in Section 4.1.1.

4.2.4 Design Considerations and Calculations

As mentioned earlier during the statement of research objectives, one of the goals after the design and development of the dual-extruder mixing method was to provide further information about the feasibility of blending a given polymer pair based on the rheology of the pure materials, the heat-transfer and residence time considerations and the degree of mixing achieved. To fulfill this objective, a detailed study of the rheology of several LCPs along with pure PET and PP rheology was discussed in section 4.2.1. However, the goal there was to establish some of the more fundamental aspects involved with blending LCPs with thermoplastics such as the importance of the viscosity ratio, the thermal history effects on LCP rheology and the solidification and crystallization kinetics of the melts in the supercooled state as well as at elevated temperatures. An attempt will be made now in the forthcoming dis-

cussions to connect the important results from that section with particular reference to the design and operation of the dual-extruder mixing method. Details of the calculations will be given either by way of appropriate references or provided in the appendix. It should also be added here that the goal of this section was not to model the flow in the dual-extruder apparatus or in the static mixer itself, but rather to conduct relatively simple macroscopic heat and mass transfer balances so as to provide some basis for the design of the apparatus. References to different parts of the dual-extruder mixing method and the various heating zones will be made with respect to the nomenclatures discussed in chapter 3 (see Figs. 27 and 28).

4.2.4.1   Degree of Mixing

As mentioned in chapter 3, all of the preceding blending operations using the dual-extruder mixing method were performed using 18 static mixer elements. The reasons for the prior selection of 18 mixing elements, as discussed in chapter 3, were based on estimations of the residence times, pressure drop and efficiency of mixing. Also, mixing in the Kenics Static Mixer (KSM) occurs by the division of flow at the leading edge of each element and follows the channel created by the element shape, thereby resulting in an exponential increase in stratification as shown schematically in Fig. 77 (165). The thickness of the striations produced is given by $D/2^n$, where D is the inside diameter of the KSM and 'n' is the number of elements. Furthermore, the smaller the striation thickness, the larger is the interfacial area and hence the better the mixing. However, in actual practice the number of mixing elements that can be used is limited by residence time and pressure drop constraints.

To examine how the mixing is affected by reducing the number of mixing elements and also to assess the minimum number of elements that could yield a "homogeneous" blend, experiments were conducted using the same dual-extruder setup but with only 3 or 9 elements and using the same capillary die as used before for strand extrusion i.e. with diameter $= 0.125''$ and $L/D = 1$. For these studies, the static mixer was replaced by stainless steel pipe sections
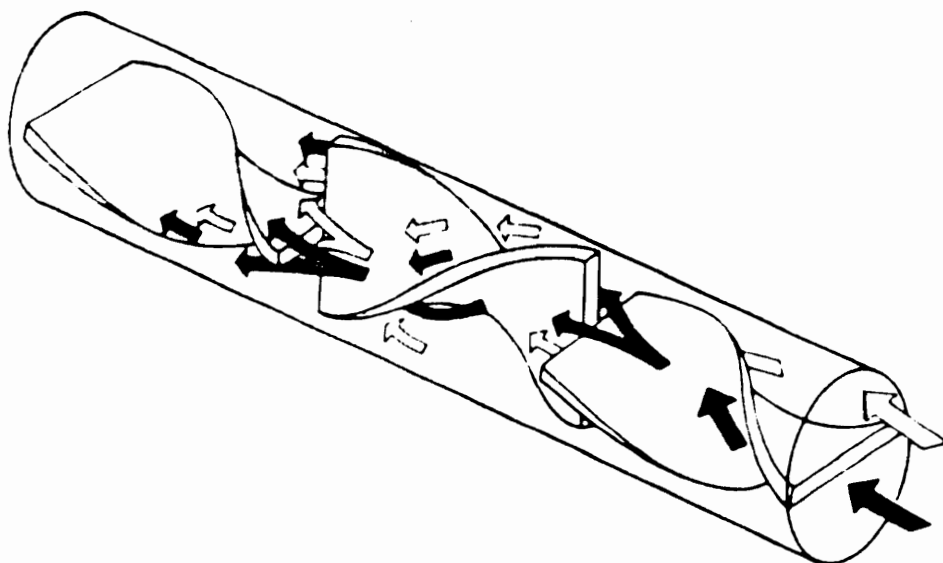
Figure 77. Schematic of the mixing mechanism in a Kenics Static Mixer (165).

that were just adequate in length to house either 3 or 9 elements as the case may be. Blends of PET/Vectra A and PET/HX4000 were extruded using only 3 elements. It is of interest to add here that the extrusion temperature profile of the dual- extruder mixing method had to be changed quite substantially due to the reduced residence time in the mixer. Specifically, the temperatures in several of the zones were reduced from those used earlier in the extrusion of the corresponding blend strands or sheets. Thus PET/Vectra A 94/6 composition ratio blend was extruded with the following temperature profile:

- PET extruder - 225°C, 275°C, 270°C and 210°C in zones 1-3 and clamp ring, respectively
- Vectra A extruder - 265°C, 320°C, 275°C and 275°C in zones 1-3 and clamp ring, respectively
- Zones 'C1' and 'C2' were maintained at 175°C each
- the mixer (now pipe section) and capillary die were maintained at 180°C and 160°C

PET/HX4000 85/15 ratio blend was extruded with the following profile:

- PET extruder - 225°C, 275°C, 270°C and 210°C in zones 1-3 and clamp ring, respectively
- HX4000 extruder - 280°C, 340°C, 315°C and 300°C in zones 1-3 and clamp ring, respectively
- Zones 'C1' and 'C2' were maintained at 160°C and 175°C
- the mixer (now pipe section) and capillary die were maintained at 180°C and 160°C

Also, four other blends viz. PET/Vectra A 96/4, PET/Vectra 85/15, PET/HX4000 85/15 and PET/HX4000 72/28 were extruded using 9 mixing elements and the same temperature profile as above. Results of these experiments are discussed below.

SEM micrographs of the PET/Vectra A 94/6 and PET/HX4000 85/15 blends extruded using 3 mixing elements are shown in Figs. 78 and 79, respectively. Clearly, the two phases in each case exist as very distinct phases with very little mixing having taken place. Essentially, two separate bundles of Vectra A in the PET matrix can be seen from Fig. 78a. Also, a close-up of the development of striations can be seen from Fig 79b. It is interesting to note that one should theoretically observe $2^n = 2^3 = 8$ striations. This does not seem very obvious from the above SEM micrographs. However, two other important comments need to be made. First, since the PET matrix was transparent, it was possible to see the dispersed LCP phase running the entire length of the extrudate in a distinct cocontinuous manner. Secondly, and more im-

portantly, it is clear that the LCP does not get dispersed into droplets but is simply redivided at each element to yield continuous fibrils of infinite length as seen earlier for the extruded strands in section 4.2.2.

SEM micrographs of the PET/Vectra A and PET/HX4000 blends extruded using 9 mixing elements are shown in Figs. 80 and 81, respectively. It can be seen from both these figures that although a greater percentage of the cross- section is now occupied by the dispersed LCP phase, it is still clear to distinguish between "pockets" or areas of the LCP and the matrix. Again it is important to emphasize the resultant morphology of Vectra A from Figs. 80a and 80b. The highly fibrillar nature of the Vectra A is evident from Fig. 80b. Furthermore, these SEM micrographs give further insight into the mixing mechanisms of the static mixer and in es- sence reinforce the conclusions discussed in section 4.2.2.3 that the KSM does not disperse the LCP phase but rather distributes it to give continuous fibrillar LCP structures. It should also be added here that two different compositions with each system were tested to see if there was any composition dependence on the degree of mixing. None is certainly expected, since the degree of mixing depends only on the number of mixing elements and visual comparison of Figs. 81a and 81b indeed show no perceptible difference in the degree of mixing achieved for the two compositions.

It is clear from all of the above results that in the blending of high viscosity polymer melts using a Kenics Static Mixer, after the two streams are fed as separate streams to the mixer and consequently where all the mixing takes place in the static mixer alone, more than 9 mixing elements are required for adequate mixing. It is important to distinguish where the mixing occurs since other researchers have used various static mixers with 6-9 elements at- tached to the exit of single extruder and found the mixing to be very good (56,111).
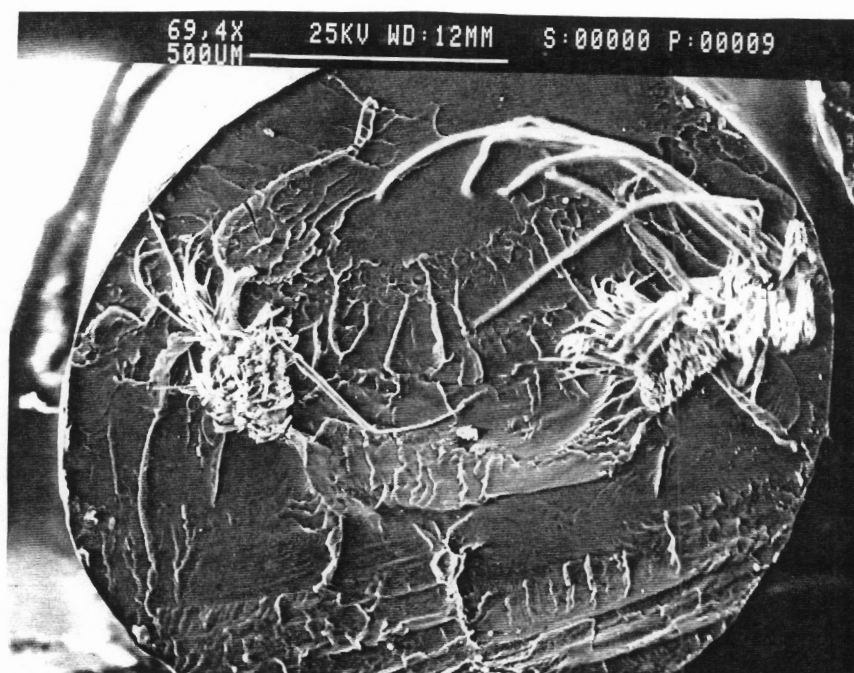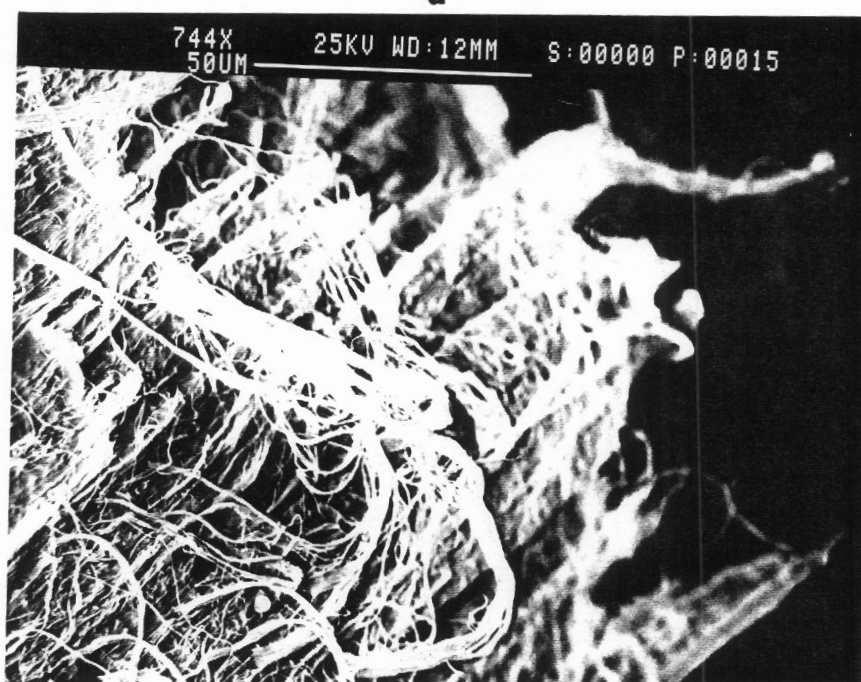
Figure 78. SEM micrographs of PET/Vectra A 94/6 mixer blend extruded using 3 mixing elements: (a) overall fracture surface and (b) PET-Vectra A interface. Fracture is across the flow direction.
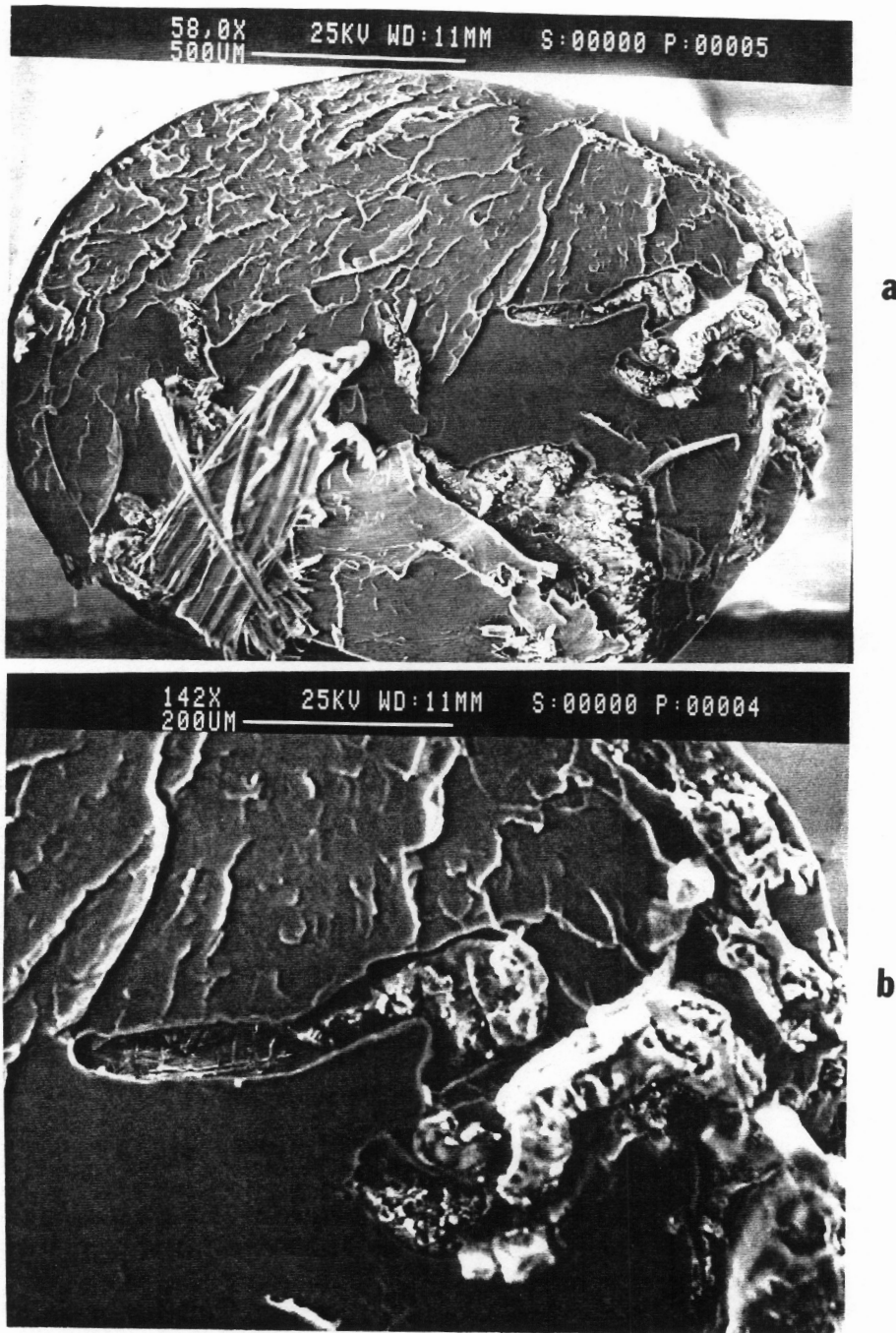
Figure 79. SEM micrographs of PET/HX4000 85/15 mixer blend extruded using 3 mixing elements: (a) overall fracture surface and (b) close-up of interface. Fracture is across the flow direction.
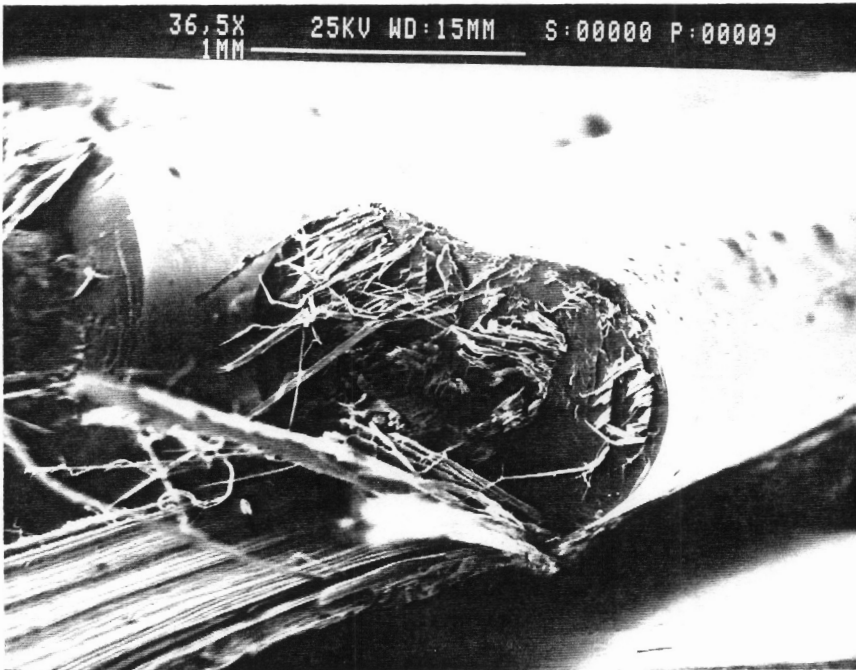
Figure 80. SEM micrographs of PET/Vectra A blends extruded using 9 mixing elements: (a) 96/4 and (b) 85/15 composition ratios. Fracture is across the flow direction.
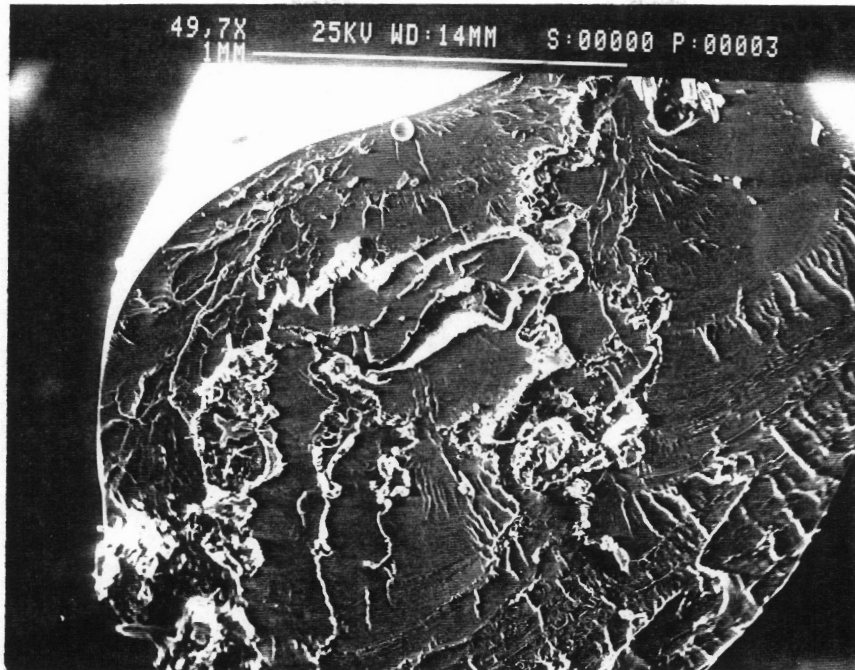
a
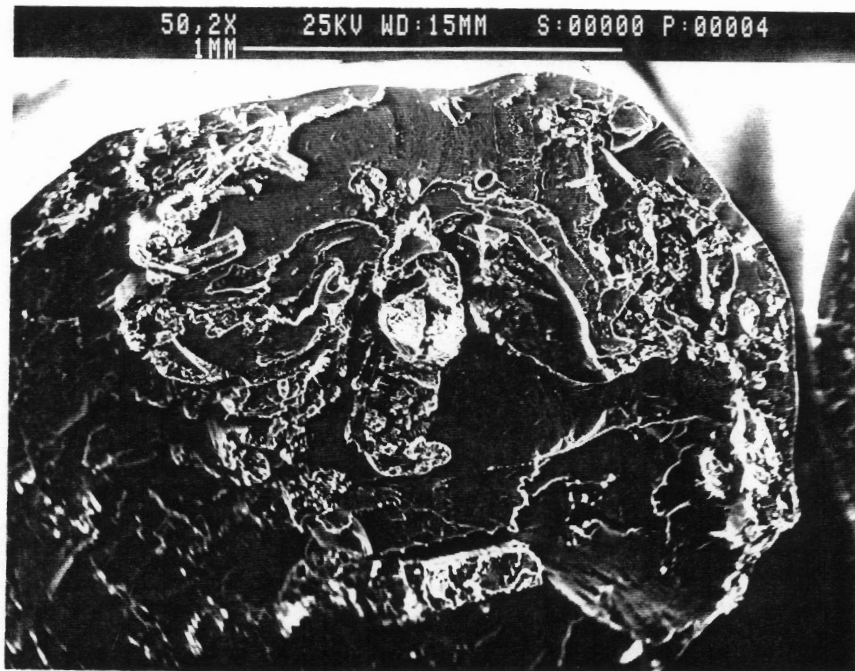
b

Figure 81.   SEM micrographs of PET/HX4000 blends extruded using 9 mixing elements: (a) 85/15 and (b) 72/28 composition ratios. Fracture is across the flow direction.

4.2.4.2 Heat and Mass Transfer

A knowledge of the temperature profile of the melts as they flow through the dual-extruder mixing apparatus is important from several perspectives. One of the first concerns in the development of this method was that the matrix material not be exposed to temperatures where it may degrade while the LCP is not cooled to temperatures below which no more deformation of the melt is possible due to solidification. It is easy to see that with the several different heating zones in the apparatus coupled with the complexities involved with the melts entering at different temperatures and flow rates into the static mixer, the problem does not lend itself to any easy analytical solution. However, as mentioned earlier, the objective was to get some basis for the design of the apparatus as well as to make it possible to predict a priori the feasibility of blending certain polymer pairs.

The heat transfer problem was defined as follows (see Figs. 27 and 28). All the major assumptions made in solving this problem will also be stated later. The matrix material which is melted in extruder E1 flows through pipe sections 1, 2 and 3 which may be simply treated as the steady-state forced convection of a fluid in laminar flow in a circular tube. At the 'T' junction, the matrix and dispersed (LCP) phases are combined and the melt mix then flows through the pipe sections 5, 6 (static mixer), 7 and 8 (die). All the pipe elements are maintained at some constant temperatures. The heat transfer problem to be solved was the determination of the matrix melt temperature as it approaches the 'T' junction, the temperature of the melt mix just before entry into the static mixer and the temperature of the mixed stream at the exit of the die. The overall assumptions were as follows: (1) steady state (2) incompressible fluids (3) no heat source (4) no viscous heating (5) physical properties of the fluids are independent of temperature (6) axial conduction in the tube is neglected (7) fully developed parabolic velocity profile for a Newtonian fluid. In addition, the flow in the static mixer was treated as being essentially plug flow.

It is appropriate to pause here and address the above assumptions. Viscous heating is neglected on the basis of estimates of the Brinkman number (Br) which is the ratio of the heat

generated due to melt viscosity to the heat conducted due to the imposed temperature differ-
ence. It has been noted that the average temperature is not affected much if Br < 1.0 (165).
The Brinkman number was estimated in various sections of the pipe and found to be much
less than unity. The Reynolds numbers (based on the apparent viscosities) in the different
sections were found to be of the order of 1E-4 and thus laminar flow may be assumed. The
shear rates in the various sections were estimated to be between 1-10 sec^{-1} where the melts
may be considered to be Newtonian. However, this assumption may be readily relaxed to ac-
commodate a power-law fluid with the form of the equation and the solution remaining the
same except for different constants (see below). Lastly, the flow in the static mixer has been
shown to be relatively close to that for plug flow behavior (142,146,165).

The resulting equation to be solved is then

$$V_z \rho C_v \frac{\partial T}{\partial z} = \frac{k}{r} \frac{\partial}{\partial r} \left(r \frac{\partial T}{\partial r} \right)$$
[4.1]

with the boundary conditions

$$T(z,R) = T_w$$
[4.2a]

$$T(0,r) = T_i$$
[4.2b]

$$\left(\frac{\partial T}{\partial r} \right)_{r=0} = 0$$
[4.2c]

where V_z is the axial velocity, ρ is the density, k is the thermal conductivity, C_v is the heat
capacity, T is the temperature and r and z are the radial and axial variables, T_w is the wall
temperature and T_i is the inlet temperature. The above equation is then solved for the tem-
perature of the fluid in each section and the temperature at the exit of each section is then
used as the inlet temperature for the following pipe section. This problem has been solved
by Graetz for a Newtonian fluid and the solution in the form of an infinite series is as follows
(166):

$$\frac{T_{cup} - T_W}{T_i - T_W} = \sum_{n=1}^{\infty} Dn\,(e)^{B_n Z} \qquad [4.3]$$

where Z is the dimensionless axial distance given by

$$Z = \frac{k z}{\rho\, C_v R^2 <V_z>} \qquad [4.4]$$

and where z is the axial distance downstream, R is the pipe inner diameter and $<V_z>$ is the average velocity = volumetric flow rate/cross- sectional area. The first three terms of the series are usually sufficient (166) and the Dn's and Bn's are constants whose values are (166): $D_1 = 0.82$, $D_2 = 0.10$, $D_3 = 0.014$, $B_1 = -3.7$, $B_2 = -22$ and $B_3 = -53$. T_{cup} is the mean or average temperature that a cup of fluid scooped out of the stream (at any axial distance z) and thoroughly mixed would attain (167). Also, the problem as defined by equations 4.1 and 4.2 has been solved for the plug flow velocity case and this solution was used to solve the temperature profile in the static mixer with the difference that diameter was replaced by 4 times the hydraulic radius due to the non-circular cross-section in the static mixer. Again, details of this are shown in the Appendix. The plug flow solution can be found in its entirety in ref. (168) and thus will not be repeated here.

The temperature profile for one test case is discussed here. PET melt from the matrix extruder was extruded at 300°C The temperatures of the walls of the different piping sections were as follows: 225°C, 200°C, 200°C, 240°C, 240°C, 225°C, 200°C and 200°C for pipe sections 1 to 8, respectively. The PET was extruded at 40 RPM and the mass flow rate was estimated to be 72 gms/min. Vectra A was extruded at 12 RPM and its flow rate was estimated to be 16 gms/min. At the 'T' junction the melts were assumed to be completely mixed and the temperature of the resulting blend stream was calculated using a simple enthalpy balance based on the weight fractions of the two melts. The physical properties of PET and Vectra were obtained from the suppliers and are provided in the Appendix and these were weighted according to the mass fractions (law of mixtures) to calculate the physical properties of the blend

stream. The resulting calculated temperature profile of the polymer melts at various locations in the apparatus is shown in Fig. 82. The actual temperature could be measured at only two locations, one just prior to the entry to the static mixer and the other at the exit of the capillary die. A pressure transducer equipped with a thermocouple was placed flush with the inside of part # 5 and another thin wire thermocouple was inserted 1 cm (from the exit) inside the capillary die and was manually kept roughly in the center. It should therefore be noted that the measured temperature prior to the static mixer was at the wall whereas the measured temperature at the die exit was roughly in the center.

Two sets of experiments were run. First, only PET was extruded at 40 RPM through the whole system and after those measurements were completed, then Vectra A was extruded through 'E2' at 12 RPM. The PET and Vectra A extruder temperature profiles were the same as for extrusion of strands discussed earlier. The different pipe sections were maintained at temperatures given in the preceding paragraph. When PET was extruded alone, the T_{cup} temperature was calculated to be 259.94 °C at the point just before the entrance to the mixer. The temperature measured here by the thermocouple was found to be 267°C. Also, the T_{cup} temperature at the exit of the die was calculated to be 233.82 °C whereas the actual measured temperature was between 275-280°C. The Vectra A was now extruded with its exit temperature from the extruder at 300°C. The temperature of the blend stream just before entry to the static mixer as measured by the thermocouple (after steady state) was observed to be 270°C whereas the exit temperature was measured to be between 287-290°C. In comparison, the calculated temperature at the entrance to the static mixer was 268.82°C and the T_{cup} temperature at the die exit was estimated to be 238.83°C. The difference between the estimated and measured temperatures, especially at the exit of the die, appear to be quite large. However, it is important to point out that the estimated temperature, i.e. T_{cup}, is in a sense related to the total heat content or enthalpy of the system at any 'z' and hence one cannot expect a direct equality between the measured temperature (which is really a function of the radial distance as well) and the estimated cup-mixing temperature. Nevertheless, estimation of the T_{cup} gives an idea of the mean temperature of the fluid stream at any given axial distance. On the basis
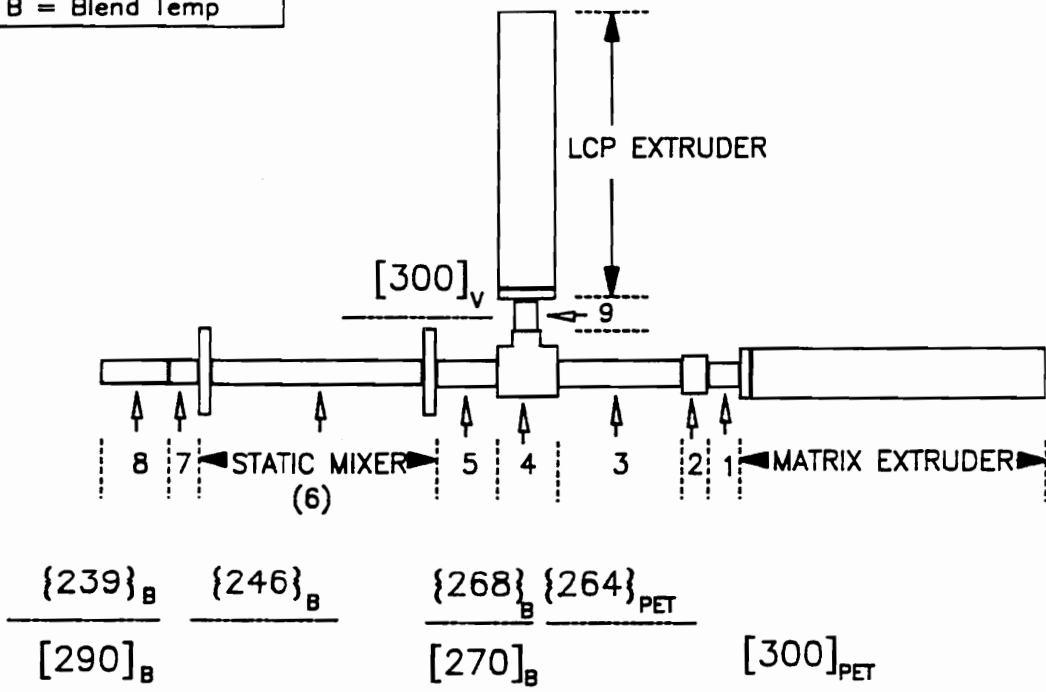
Figure 82.   Estimation of the temperature profile for the dual-extruder mixing method.

of further calculations, it was also observed that the T_{cup} temperature is roughly an arithmetic average of the temperatures of the fluid in the centerline ($r=0$) and at the walls ($r=R$). Therefore, one can still get an idea of the maximum temperature of the fluid on the basis of T_{cup}. Therefore although the above estimates have obvious limitations, the predictions are still somewhat useful in the absence of actual temperature measurements at several locations without interrupting the flow.

4.2.4.3   Residence Time

The average residence time of the melts in the various sections of the piping were also estimated by simply taking the ratio of the internal volume of the pipe section to the volumetric flow through that section. Again two experiments were run: one with pure PET and the other with pure PP. These results were compared to the estimated average residence times. For the experiments, an average of two different readings was taken. Colored high density polyethylene was used as a tracer. The matrix material was allowed to run through till steady state was achieved. Then a few pellets of the colored HDPE were introduced into the hopper and a stopwatch was started. The time of the first appearance of dyed fluid was noted. Also, the same method was used to determine independently the residence time of the melt in the extruder alone. The results are discussed below.

Again with reference to Figs. 27 and 28, PET was extruded through the system alone at 40 RPM and the residence time between the feed end of the matrix extruder 'E1' to the exit of part # 7 (adaptor, no die) was experimentally determined to be 188 seconds. The flow rate was measured to be 72 gms/min. On the basis of the internal volumes of the different pipe sections (given in the appendix), the average residence time through the piping sections alone was calculated to be 131.07 seconds and that through the extruder (by the method outlined in ref. (169)) to be 152.93, giving a total combined average residence time of 283.95 seconds. It may be noted that for the static mixer, the void volume was used as the internal free volume.

Similar experiments and calculations with pure PP alone gave an experimentally determined

residence time (in 'E1' + parts 1-8) of 365 seconds at a measured flow rate of 31 gms/min.

The estimated average residence time through the piping alone (i.e. parts 1-8 only) was 263.75

seconds whereas that through the extruder alone to be 266.42, giving a total average resi-

dence time of 530.17 seconds.

Thus for pure PET the measured residence time of 188 seconds may be compared with

an estimated time of ca. 284 seconds, while the same for pure PP are 365 seconds and 530

seconds. Although these differences appear to be quite large, it should be realized that the

measured times are not truly the "average residence time" but in fact the shortest or minimum

residence times since the first appearance of dyed fluid were timed. It is well known that the

average residence time in flow through a circular tube is twice the minimum residence time

whereas the average residence time in the extruder is approximately 1.33 times the minimum

residence time. Therefore the true average residence times are likely to be much closer to the

calculated values. These studies again give at least some idea of the residence times that

may be expected at the flow rates of interest.

Of greater interest from the above estimations is the time that the dispersed phase viz.

the LCP takes to traverse from the exit of the extruder 'E2' to the die exit. This residence time

is of more importance since the LCP is being slowly cooled during this time and as discussed

earlier in section 4.2.1, the solidification kinetics become important. In fact, it is really a

combination of the temperature history of the LCP as it passes through the static mixer and

die and the residence time it takes to do so that will finally determine the "state" of the LCP

phase at the die exit. An estimate of the residence time from the point of entry into the 'T' to

the die exit is about 65 seconds for PET/LCP blends and 139 seconds for PP/LCP blends based

on typical total flow rates of about 88 gms/min and 37 gms/min for the two cases. respectively.

4.2.4.4 Estimation of the Shear-Rate and Pressure Drop in the Static Mixer

As mentioned in chapter 3, the Kenics Static Mixer or KSM has no moving parts and consequently the energy required for the mixer is that required to overcome the pressure drop. Typically, the pressure drop in the mixer is estimated by multiplying the calculated pressure drop in an empty pipe of the same length and diameter as the mixer by an experimentally determined factor, 'K', which is a function of the geometry of the mixer elements and the Reynolds number (142). For highly viscous fluids and in flows where the Reynolds number is less than 10, the value of 'K' has been observed to be between 3-6 (142,165), i.e. the pressure drop through the mixer is 3-6 times that observed in an empty pipe of same dimensions. The exact 'K' value for the static mixer used here was not known and hence the pressure drop was estimated on the basis of equations derived for the flow of a power-law fluid through a packed tube. The equations and derivations were taken largely from ref. (170) and thus will not be repeated here. It is probably suffice to mention that the derivations in ref. (170) are based on the modification of the Hagan- Poiseuille equation for a power-law fluid. Specifically, the velocity in the Hagan-Poiseuille equation is replaced by the superficial velocity, V_o, with the two velocities being related through the bed void fraction. Also, the diameter of the pipe or tube is replaced by the equivalent diameter for a non-circular cross-section which is equal to 4 times the hydraulic radius. Finally, the length of the tube, L, is replaced by a multiplicative factor of 25L/12, which is an experimentally determined factor which accounts for the tortuosity. The final equation for the pressure drop takes the form

$$V_o = \frac{n\,\varepsilon}{3n + 1}\left(\frac{D_p\,\varepsilon}{3(1 - \varepsilon)}\right)^{1 + 1/n}\left(\frac{6\,\Delta P}{25\,K\,L}\right)^{1/n} \qquad [4.5]$$

and the shear rate at the wall $\dot{\gamma}_W$ (nominal shear rate) is given by

$$\dot{\gamma}_W = \frac{3n + 1}{4n}\frac{12\,V_o\,(1 - \varepsilon)}{D_p\,\varepsilon^2} \qquad [4.6]$$

where V_o is the superficial velocity $= <V>.\varepsilon$, ε is the void fraction in the bed $=$ volume of voids/volume of bed, n is the power- law flow index, K is the power-law consistency index, D_p is the mean particle diameter $= 6$ (volume of the particle)/(total particle surface), L is the tube length and ΔP is the pressure drop.

In using the above equations for determining the pressure drop and shear-rate in the static mixer, each element of the mixer was treated as one particle. The calculations for the estimation of pressure drop for one case are shown in some detail below. An experiment with PET/Vectra 82/18 blend was conducted and the pressure was measured just prior to the entrance of the mixer using a pressure transducer. An adaptor and capillary die were attached to the exit of the mixer and the total pressure drop over the mixer, adaptor and die combined was measured to be 255 psi ($\pm$ 12 psi). The measured pressure is an average of 6 readings taken over a period of about 30 minutes during a single experiment. It was not feasible to take averages from different experiments due to the difficulties in reproducing the compositions exactly as mentioned earlier. The relevant quantities used in the calculations are as follows:

- Length of each element $=$ Le $= 0.87''$
- Element diameter $=$ De $= 0.494''$
- Wall thickness of each element $=$ Te $= 0.075''$
- Pipe inner diameter $=$ D $= 0.546''$
- Mass flow rate for test experiment $= 88$ gms/min
- Average melt density $= 1.24$ gms/cm^3

Using the above quantities, the calculated values for the variables of equations 4.5 and 4.6 are as follows:

- $V_o = 0.7831$ cm/sec
- $D_p = 0.4615$ cms
- $\varepsilon = 0.8417$
- $K = 1674.16$ Pa sec^n

RESULTS AND DISCUSSION 238

- $n = 0.8690$

The power-law parameters were determined using a regression analysis for the data points of a dynamic frequency sweep test for a PET/Vectra A 80/20 blend at 290 °C. The selection of this set of data will be discussed shortly. Using the values of the variables as shown above, the pressure drop in the mixer was estimated using equation 4.5 to be 189.64 psi. Furthermore, the pressure drops in the adaptor and die were also estimated using Darcy's law for flow in an empty pipe (142) and using the same power-law parameters. Thus the pressure drop in the adaptor was calculated to be 29.62 psi and that in the die to be 31.97 psi. Thus the total estimated pressure drop is $189.64 + 29.62 + 31.97 = 251.23$ psi. This compares surprisingly well with the experimental value of 255 psi. Furthermore. the shear-rate estimated using equation 4.6 was calculated to be 4.72 sec^{-1}.

The pressure drop in the static mixer (plus adaptor and die) was found to be usually within 200-350 psi for most blends. Therefore the estimated values are of some merit. However, as is clear from equation 4.5, the estimated pressure drop depends (for a fixed geometry) on the choice of the power-law parameters. Since the materials in the actual process enter the mixer with largely different thermal histories there is no way to simulate that in a rheological test using the available resources. The average temperature in the mixer was estimated to be about 260°C (obtained by averaging the inlet and outlet T_{cup}). Therefore frequency sweeps on PET heated to 290°C and then cooled to 260°C and Vectra A preheated to 330°C and then cooled to 260°C were conducted. Also, several rheological tests on a PET/Vectra A 80/20 blend were performed at different temperatures and/or with thermal histories. For example, tests were performed on the blend at 290°C, 300°C, 330°C and at 265°C (the average temperature in the mixer) upon cooling from 290°C, 300°C and 330°C. It was observed that only the data at 290°C lay between the curves of pure PET and pure Vectra A with the appropriate thermal history. The other curves were either too high or too low and thus the data at 290°C was selected with the presumption that the blend viscosity would lie somewhere in between. The use of an average viscosity of the blend (based on the law of mixtures),

calculated by weighting the viscosity of each component at a shear-rate of 5 sec^{-1} gave a pressure drop that was higher than the experimental value by a factor of over 3 times. Thus it is clear that any accurate prediction of both the shear-rate and pressure drop in the static mixer are largely dependent on obtaining accurate values of the viscosity (power-law parameters). Furthermore, although the estimated pressure drop using the power-law parameters from the other tests on the blend as described above in equation 4.6 was either higher or lower than the experimental value, the range of estimated pressure drops was between 200-400 psi. Furthermore, it was also observed that the power-law flow index, n, was between 0.8 and 0.9 for all these tests whereas the consistency index, K, varied from 1000 Pa sec^n to 3500 Pa sec^n. Therefore it appears that within the range of power-law parameters of interest for the PET/Vectra A 80/20 system, the pressure drop was more sensitive to the consistency index than the flow index. As a final note, it may be added here that the viscosity behavior of LCP blends, even without the different thermal history aspect included, has been observed to be quite anomalous in that minima in the viscosity of the blends or significant reductions therein have been observed with LCP levels varying from as low as 2 wt % to 30 wt % (109,110,112,129,136). Thus even under ordinary situations, the viscosity behavior of LCP blends is quite complex and largely unexplained making predictions on the basis of known theories or empiricisms all the more difficult.

4.2.4.5 Discussion of Design Studies

From the studies conducted on PET/Vectra A and PET/HX4000 blends with 3 and 9 elements, it is clear that the degree of mixing is largely insufficient. Also from previous studies on the strands and sheets, it was observed that 18 mixing elements provided quite adequate mixing based on the morphological results. Thus although the exact number of mixing elements that can provide sufficient mixing is not known, it is known that it is between 9 and 18 elements. This number being fixed, the average residence times are also known, particularly

for the LCP phase between the 'T' and the exit of the die wherein all the cooling and gradual solidification takes place. A knowledge of the cooling behavior as well as the solidification kinetics as discussed in section 4.2.1 for the pure melts and particularly the LCPs would then help determine what temperatures need to be used (i.e. wall temperatures) in the various sections of piping and the static mixer in particular and the extrusion speeds or flow rates, to ensure that the LCP phase was still deformable and yet the matrix polymer is not above its degradation temperature. However, it is important to remember here that the flow rates of the two materials in the dual-extruder mixing method cannot be changed independently of one another since this would obviously affect the final composition. It is quite clear that the dual-extruder blending method is quite complex and thus no "formula" for blending can be established. However, a knowledge of the main factors involved in the processing of the blends such as melt rheology, solidification kinetics, residence times etc. and some reasonably accurate data on the same can all be combined together to establish the suitability of blending certain polymers.

4.2.4.6 Effect of Capillary L/D Ratio on Blend Morphology

The objective of these studies was to determine the effects, if any, of increasing the L/D (Length/Diameter) ratio (constant D) of capillary dies on the morphology of the blends. It was mentioned earlier that the fibrils in the case of the mixer blend appeared to be formed inside the static mixer itself in comparison to the single-screw extrusion process where they seemed to formed either in the converging section of the die or by drawing at the exit of the die. Thus it was also of interest to see if the mechanism of the fibril formation had any perceptible effect on the fibril stability and break-up. The following studies were conducted with the aim of examining these ideas.

Blends of PET/Vectra A 70/30 (PB) were extruded through a single extruder using a temperature profile as follows: 225°C, 295°C, 295°C, 225°C and 175°C in zones 1-3, clamp ring and

capillary die, respectively. The blends were extruded with no die (no converging section be-tween the exit of extruder and die exit) and from dies with L/D ratios of 1, 10 and 55 (D = 0.125"). Also, a blend of PET/Vectra A 70/30 composition ratio was extruded using the dual-extruder mixing method and the same temperature profile as used for the extrusion of strands described earlier. These blends were also extruded with no die and from the same L/D ratio dies mentioned above. The results of the above experiments are described as fol-lows. First the physical blend is discussed and then the mixer blend.

In Fig. 83 are shown the SEM micrographs of the fracture surface of strands of PET/Vectra A 70/30 (PB) blend extruded without any die. The SEM micrographs in the skin and core re-gions are shown. The strand upon exiting the die was not drawn. It can be seen that the bulk of the core region contains no LCP fibrils and even in the skin region the level of fibrillation is small. The morphology of the physical blends extruded from capillary dies of 1, 10 and 55 showed a much higher level of fibrillation in the skin region but no fibrils in the core could be seen even for those sample that were drawn. The morphology of all these blends was in fact quite similar to that shown in Fig. 63 for the PET/Vectra A 70/30 physical blend rod and hence will not be shown here. However, it is important to point out that fibrils of the Vectra A could be seen in the blends extruded with the die with an L/D ratio of 55 die even for the undrawn samples but these fibrils were of very small aspect ratio and limited to positions near the skin region only.

The morphology of the blends extruded through the mixing apparatus was quite different. In Fig. 84 are shown the SEM micrographs of the fracture surfaces of the PET/Vectra A 70/30 (MB) blends extruded with (a) no die and (b) from a capillary die with L/D = 1. The sample extruded without a die was not drawn and in fact exhibited some die swell. Its draw ratio was consequently less than unity. As is clear from Fig. 84a, the blend contains fibrils of the LCP even in the sample that was not drawn and in fact did not pass through any converging section between the exit of the static mixer and the die exit. Therefore this is very clear evidence that the fibrillar morphology of the LCP is in fact being generated in the static mixer itself. From Fig. 84b it can be seen that no skin-core structure is present as seen with the physical blend
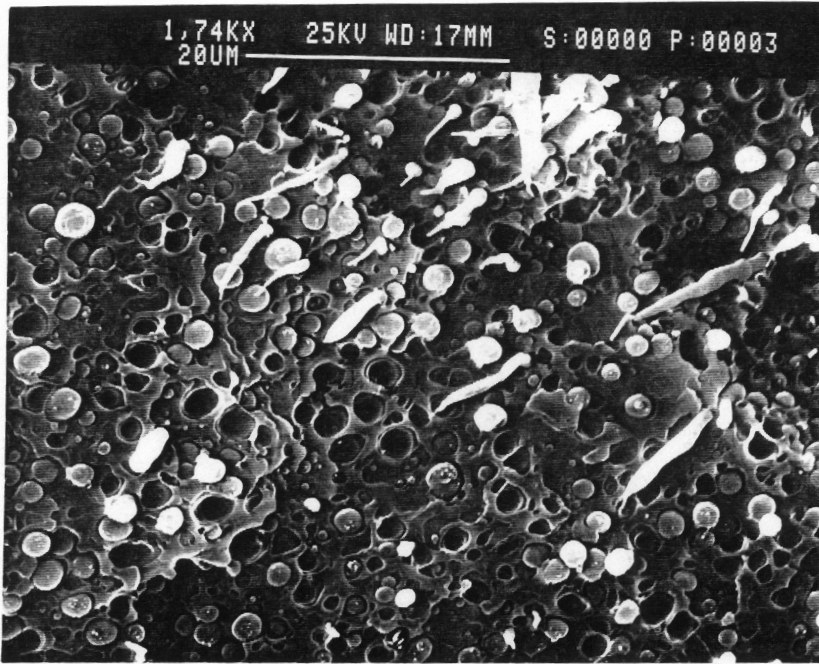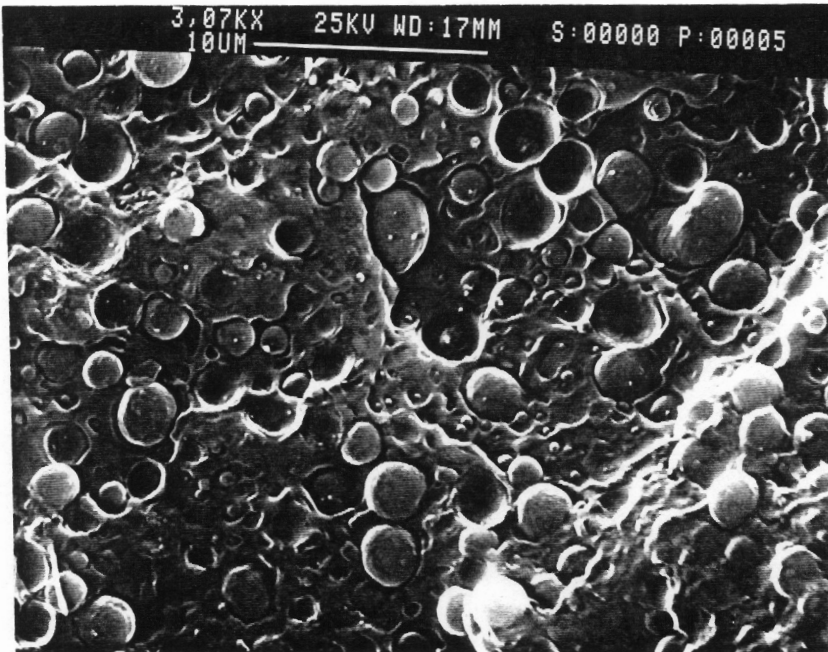
Figure 83. SEMs of the fracture surface of PET/Vectra A 70/30 (PB) strand extruded from a single extruder with no die: (a) skin region and (b) core region. Fracture is across the flow direction.

case. Furthermore, the blends extruded through the capillary dies with L/D = 10 and L/D = 55 showed similar morphology.

Before the above results are discussed further, the morphology of a PET/LCP60 80/20 blend extruded from a single extruder using capillary dies with L/D ratios of 16 and 40 are shown in Figs. 85 and 86, respectively. The two SEM micrographs in each figure are from samples with different draw ratios. It can be seen from Fig. 85 that the fibrils of the LCP60 get larger in number and smaller in diameter as the draw ratio is increased from 1.9 to 24. However, as the blend is extruded from a die with essentially a longer land region the morphology is drastically changed from fibrillar to droplet structure for both the corresponding draw ratios as can be seen from Fig. 86.

The above results are believed to be important for the following reasons. First it is confirmed that the morphology of the LCP blends evolving from the extruder is largely in the form of a dispersion of LCP droplets in the matrix and that some extensional flows, such as are present at the converging section of the die or drawing at the die exit, are necessary to extend these droplets into fibrils. Furthermore, the single extruder blends have a persistent problem with a skin-core fibril-droplet structure and in the course of this study it has been difficult to avoid this problem even by drawing at the die exit. Also, as mentioned earlier, the PET/Vectra blends did not show any perceptible difference in the morphology from those extruded with L/D = 1 and those with L/D = 55 for either the physical or mixer blend case. In other words, the physical blends showed a fibril-droplet structure and the mixer blends showed a completely fibrillar structure of the LCP phase in the PET matrix. This is in sharp contrast to the PET/LCP60 blends discussed above where the morphology of the LCP changed from fibrillar to droplet as the L/D ratio of the die was increased from 16 to 40. (It should be added here that a skin-core structure was seen even with this system). Therefore, the stability of the fibrils once formed is of great importance to the final morphology and hence mechanical properties. The factors that are believed to govern the stability of these liquid cylinders were discussed in chapter 2 and will not be repeated here. It is clear however that the Vectra A fibrils seem to have a much longer lifetime in the PET matrix than the LCP60 fibrils. The breakup phe-

a
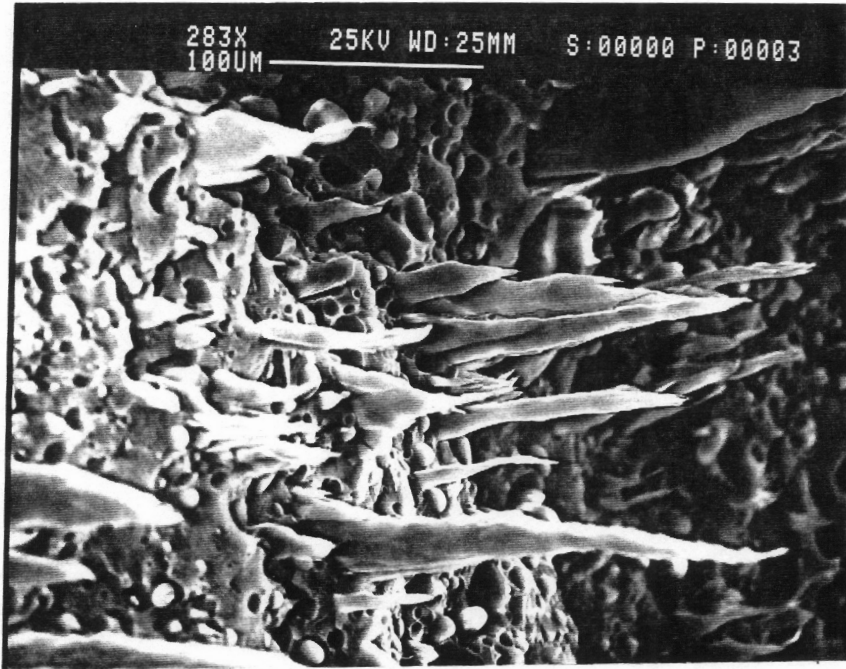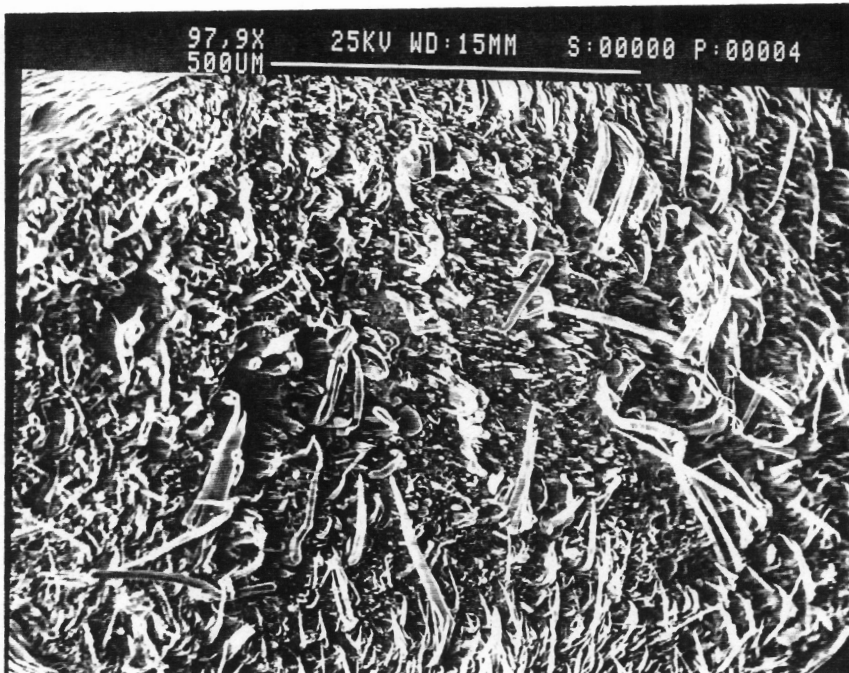
b

Figure 84. SEM micrographs of the fracture surfaces of PET/Vectra A 70/30 (MB) strand extruded from the dual-extruder mixing method: (a) no die [D.R. = 0.85] and (b) L/D = 1 [D.R. = 5].

RESULTS AND DISCUSSION
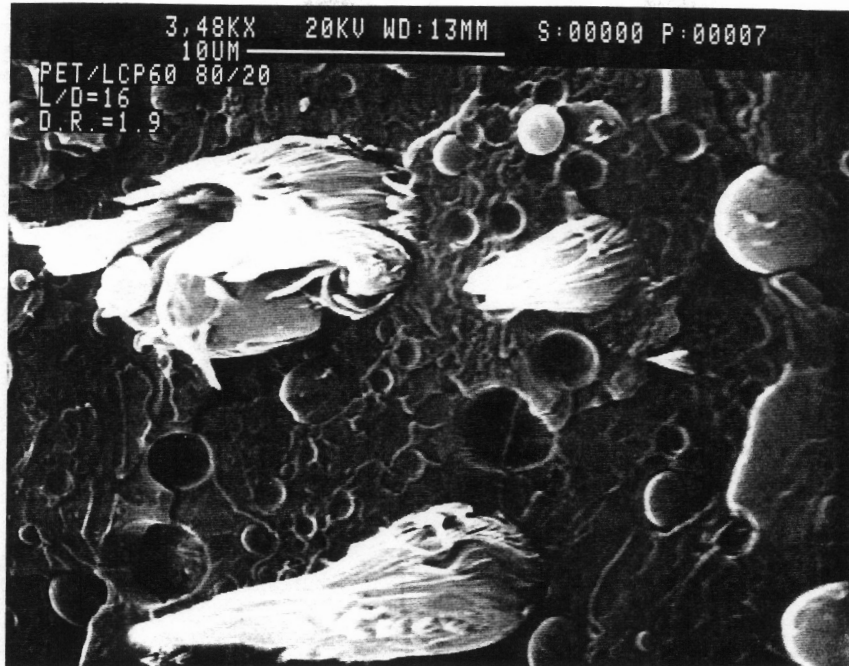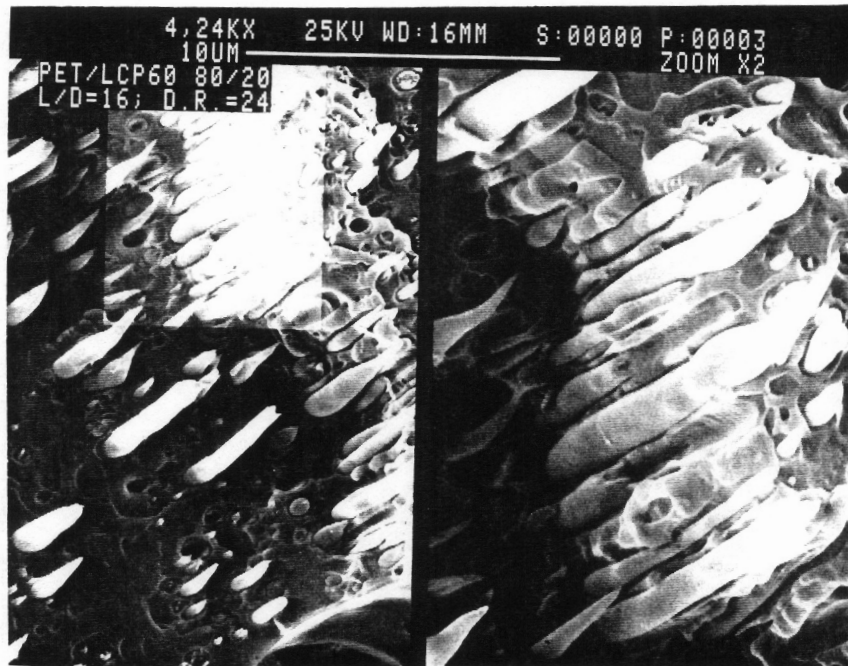
Figure 85. SEM micrographs of the fracture surfaces of PET/LCP60 80/20 (PB) strands extruded using a single extruder with L/D = 16: (a) D.R. = 1.9 and (b) D.R. = 24.
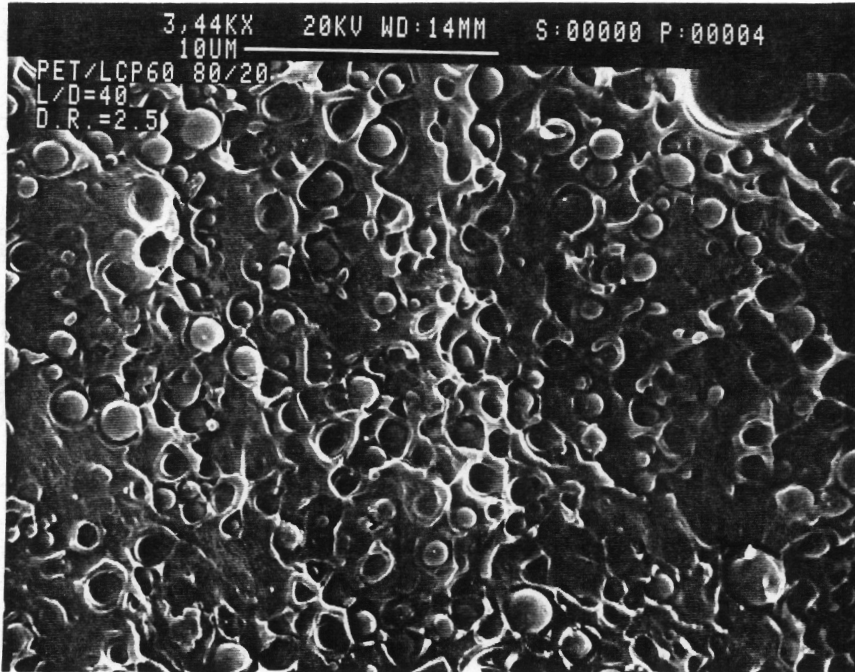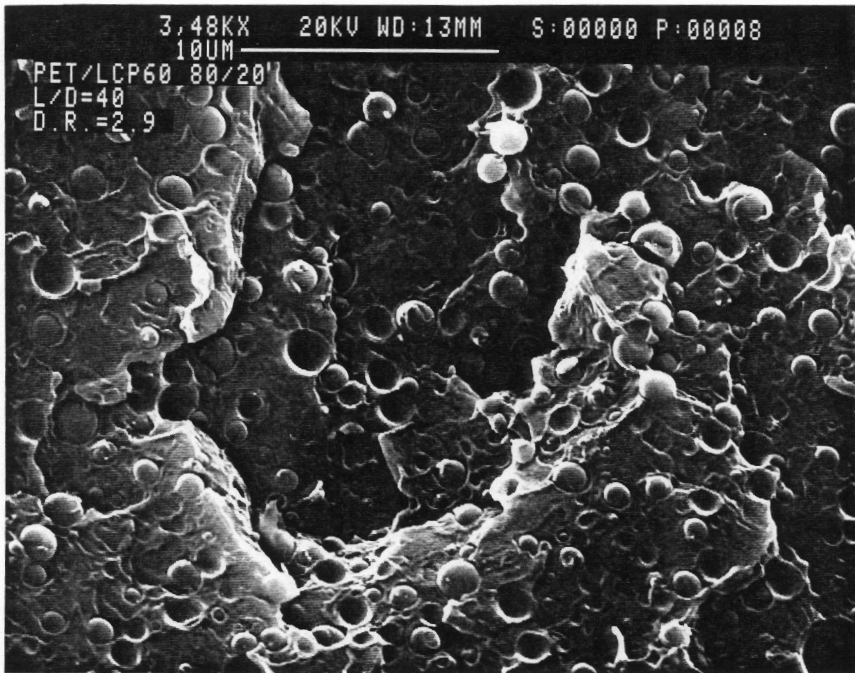
Figure 86. SEM micrographs of the fracture surfaces of PET/LCP60 80/20 (PB) strands extruded using a single extruder with L/D = 40: (a) D.R. = 2.5 and (b) D.R. = 29.

nomena of these fibrils is itself quite complex and it was shown in chapter 2 (section 2.3) that studies aimed at quantifying the lifetime of the cylinders under static conditions (without flow) have been done. However, the equations involve quantities such as interfacial tension, wavelength of the disturbance, amplitude of the disturbance etc. which are all quantities that are either difficult to measure or really unknown. Nevertheless, it is clear from the present studies that the faster the obtained morphology can be frozen in, the better are the chances for obtaining a fibrillar LCP morphology.

4.3 Post-Processing of the Blends

In this section, results from post-processing studies on the blends viz. injection-molding, solid phase forming and thermoforming are presented. Specifically, injection-molding was done using pellets of blends extruded via the dual-extruder mixing method and solid phase forming and thermoforming of extruded blend sheets was carried out.

4.3.1 Injection Molding

These studies were conducted for several reasons. First, it was of importance to ascertain if blends of both PET/LCP and PP/LCP extruded via the dual-extruder mixing method could be further processed without a loss of the LCP reinforcement. The objective here was to conduct the injection molding experiments at temperatures where the matrix material could be processed with relative ease, while ensuring that the temperatures did not exceed the melting point of the LCP. If it was possible to do this, i.e. process the blends at temperatures below the melting point of the respective LCP, then it was believed that the LCP phase would behave as a solid reinforcement in these situations, similar to glass or carbon fibers in thermoplastic

matrices. It was of further interest to learn if the properties of blends post-processed as described above were any different from the blends directly blended in the injection molder (physical blends), and if so, in what way and why. The properties of some of the injection molded plaques of physical blends (i.e. from pellets of the two materials tumbled in a container and fed to the hopper) were presented in section 4.1.2 and will be repeated here for comparison.

The injection molding conditions for the different systems for the direct injection molded or physical blends (PB) and those from the mixing method (MB) were as shown below. The mold was held at room temperature for all cases.

- PET/Vectra A

    Temperature profile (PB): 200°C, 290°C, 310°C and 290°C in zones 1-3 and nozzle, respectively

    Temperature profile (MB): 250°C, 280°C, 280°C and 280°C in zones 1-3 and nozzle, respectively

- PET/HX4000

    Temperature profile (PB): 245°C, 290°C, 310°C and 290°C in zones 1-3 and nozzle, respectively

    Temperature profile (MB): 245°C, 280°C, 280°C and 290°C in zones 1-3 and nozzle, respectively

- PP/Vectra A

    Temperature profile (PB): 220°C, 290°C, 290°C and 230°C in zones 1-3 and nozzle, respectively

    Temperature profile (MB): 245°C, 250°C, 250°C and 230°C in zones 1-3 and nozzle, respectively

The morphology and orientation of PET/Vectra A 80/20 (PB) injection molded plaques was discussed earlier and shown in Figs. 34-46. The morphology of a PET/Vectra A 82/18 (MB) blend plaque is shown in Figs. 87 and 88. The fracture surface (a) along and (b) across the flow direction in the skin region (Fig. 87) and the core region (Fig. 88) of the plaque are shown. These figures may be compared with Figs. 34 and 35 shown earlier. Several observations from these micrographs can be made. The first and most evident is the fact that the Vectra A fibrils can be seen in both the skin and core regions of the plaque and furthermore appear to be well

aligned in the flow direction, as seen in Figs. 87a and 88a. The fibrils appear to range from 0.5-2 μm in diameter and the aspect ratio, though quite high, cannot be more accurately quantified from the SEM micrographs.

To examine the differences, if any, in the level of orientation in the skin and core regions of the injection molded plaque of the PET/Vectra A 82/18 (MB) mixer blend, thin sections (ca.100 μm in thickness) of the plaque were microtomed along the machine direction from the skin and the core and WAXS patterns of these samples are shown in Fig. 89. Clearly, there is a distinct orientation in the flow direction arising from the Vectra phase in both the skin and core of the plaque. It may be recalled that the PET/Vectra A 80/20 physical blend plaque, in contrast, did not show any preferred orientation in the core region (Fig. 36). Also, the WAXS pattern of the PET/Vectra A 82/18 (MB) blend strands (which were subsequently pelletized and injection molded) is shown in Fig. 90a (flow direction is vertical) along with the SEM of the transverse fracture surface of the extruded strand in Fig. 90b. It is clear from the distinct pair of arcs seen in Fig. 90a that the extruded strands (or pellets) possess a high degree of molecular orientation arising from the Vectra A phase.

The results of the injection molded PET/Vectra A 82/18 MB plaque shown in Figs. 87-89 may be interpreted as follows. The extruded strands (or pellets) of the mixer blend possess fibrils of the Vectra A phase which are highly oriented in the flow direction as seen from Fig. 90a. These Vectra A fibrils are not remelted to any significant extent in the subsequent injection molding step due to the fact that the maximum temperature used was below the melting point of Vectra A viz. 283°C. Furthermore, it is also clear from Figs. 87 and 88 that the Vectra A fibrils are well aligned in the flow direction in both the skin and core regions of the plaque. Therefore the high levels of orientation in the skin and core regions as seen from the WAXS patterns in Fig. 89 can be attributed to a combination of two factors. First, the orientation in the Vectra A fibrils that was achieved in the pelletizing or strand extrusion step is not lost or relaxed during injection molding. Secondly, the fibrils of the Vectra A are in fact aligned in the flow direction during injection molding thus leading to a high level of overall orientation in both the skin and the core regions. Once again, these results are in contrast to the physical

a
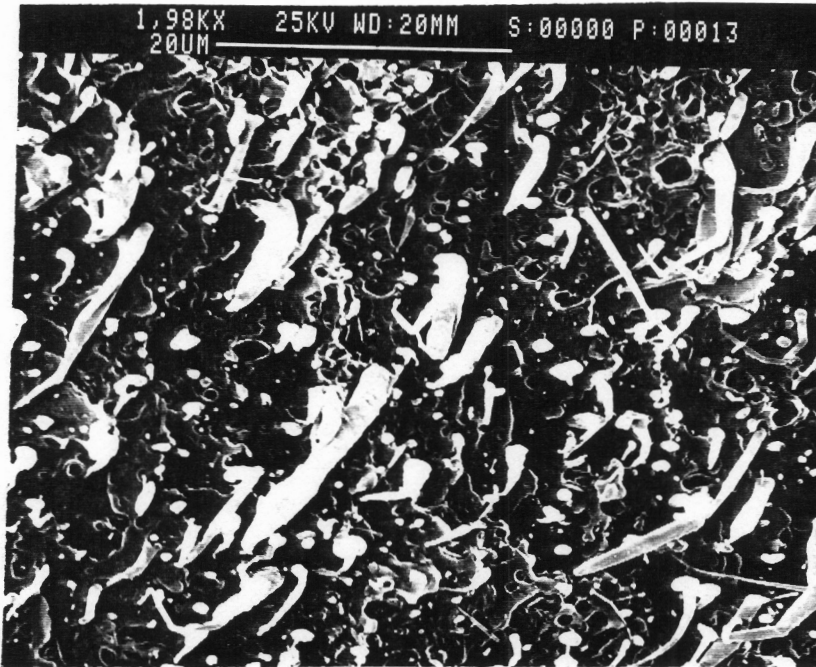
b

Figure 87. SEM micrographs of fracture surfaces of PET/Vectra A 82/18 (MB) blend injection molded plaque in the skin region: fracture is (a) along and (b) across the flow direction.
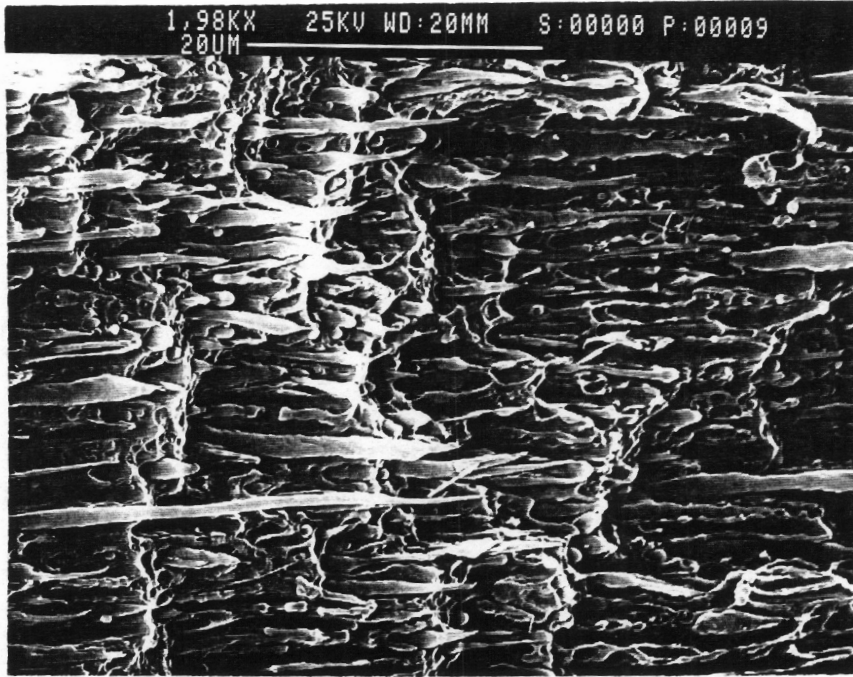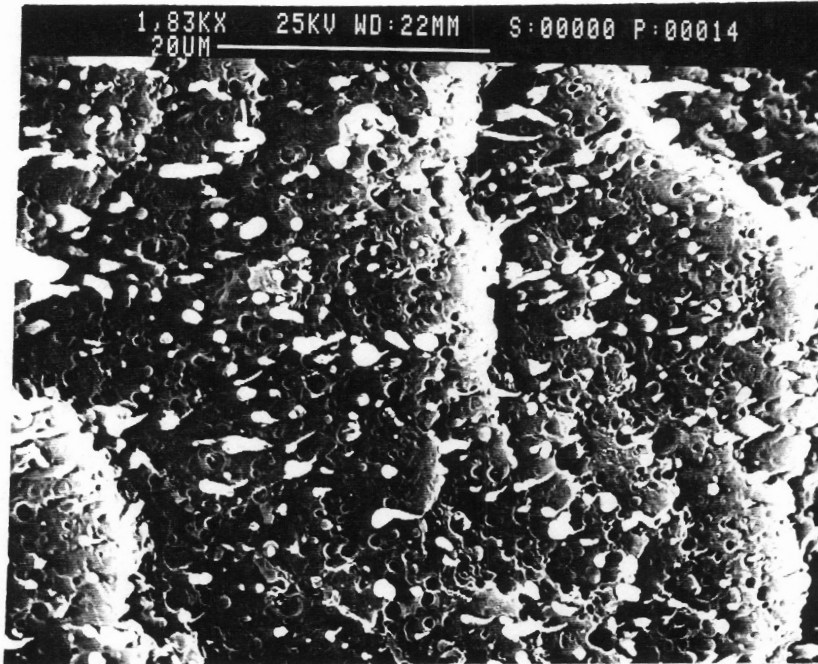
Figure 88. SEM micrographs of fracture surfaces of PET/Vectra A 82/18 (MB) blend injection molded plaque in the core region: fracture is (a) along and (b) across the flow direction.
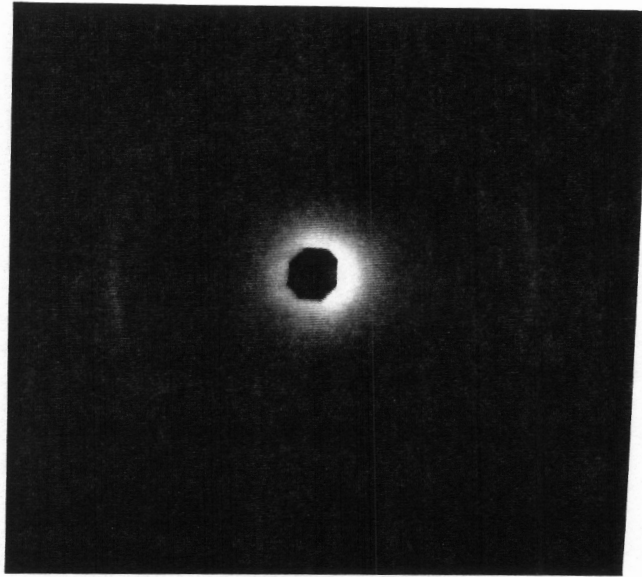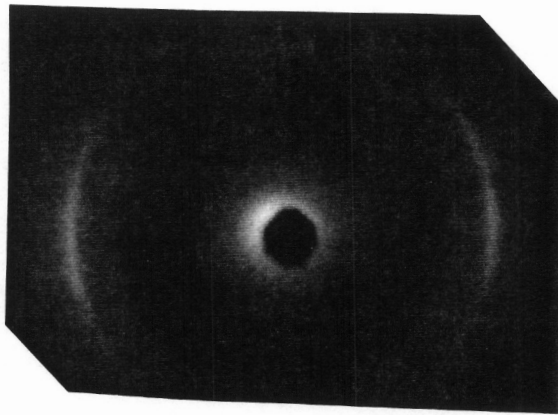
Figure 89. WAXS patterns of PET/Vectra A 82/18 (MB) blend injection molded plaque in the (a) skin and (b) core. Flow direction is vertical.
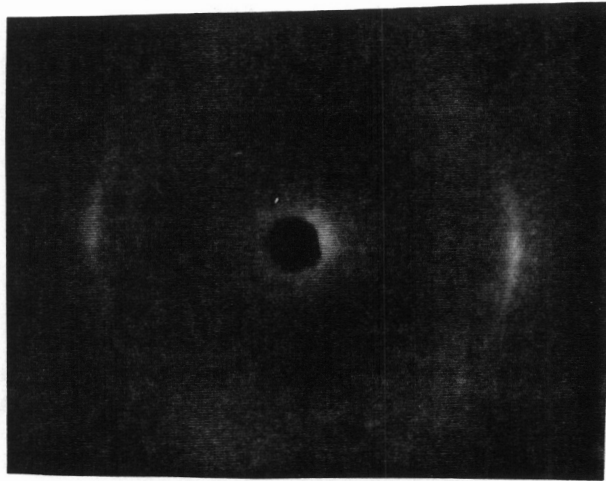
a
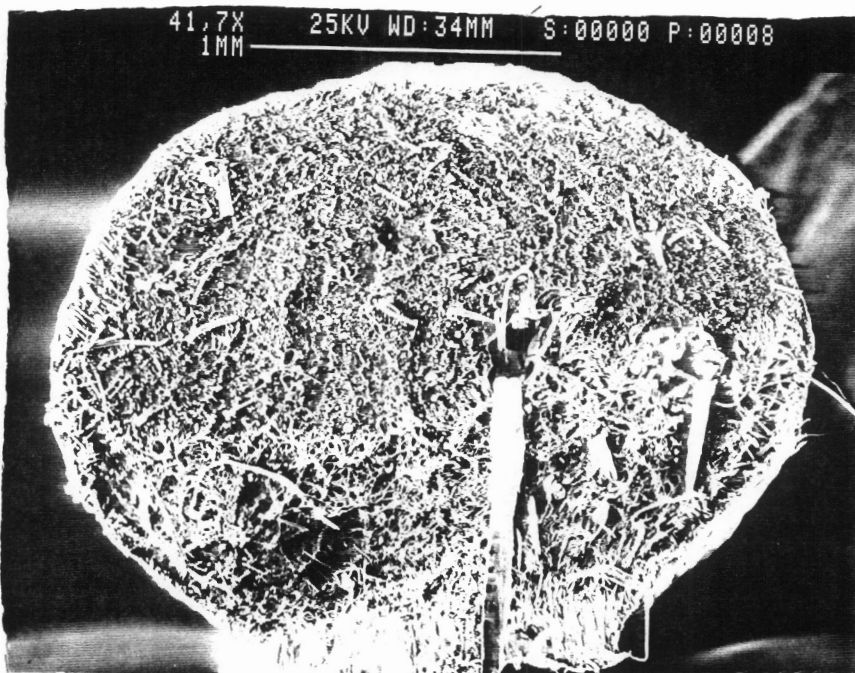
b

Figure 90. (a) WAXS pattern and (b) fracture surface of PET/Vectra A 82/18 extruded strands.

blend plaques shown in Fig. 36 where orientation of the Vectra A was observed in the skin region only.

The mechanical properties of these PET/Vectra A 82/18 mixer blend plaques were determined to see if the differences in the molecular orientation between the physical and mixer blend plaques, as discussed above, had any effect on these properties. One would expect that the mixer blend plaques might have higher properties on the basis of the fact that the core region was also highly oriented and would therefore contribute more to the mechanical properties than the core region of the corresponding physical blend plaque. The mechanical properties are thus shown in Table 13 along with the data for pure PET and PET/Vectra A 80/20 PB plaques discussed earlier in section 4.1.1. Two main points need to be made with reference to Table 13. The mechanical properties of both the blends i.e. PET/Vectra A 80/20 (PB) and PET/Vectra A 82/18 (MB) are higher than pure PET by a factor of roughly 1.8. Further, the tensile and flex moduli of the two blends are the same, within the limits of experimental error. However, the tensile strength of the physical blend plaque is in fact higher than the mixer blend plaque. These results are a little surprising in view of the discussion and WAXS results above. The tensile strength of the mixer blend plaques is possibly lower than the physical blend due to poorer adhesion between the LCP fibrils and the PET matrix, although this is not very evident from the SEM micrographs shown in Figs. 87 and 88. These results then suggest that although there may be no advantage in preblending materials that have some overlap of processing temperatures via the dual-extruder mixing method, there is also no significant loss in doing so. Also, one other important point needs to be mentioned here. The physical blend plaques were injection molded with a maximum barrel temperature of 310°C. It was shown in Fig. 45 that significant melting of the Vectra A occurs at temperatures above 300°C. Thus the thermal history undergone by the Vectra A in the two cases, i.e. physical blending and mixer blending, though not identical is still largely similar which may also partly account for the properties not being much different.

In sharp contrast to the PET/Vectra A results above, the PET/HX4000 (MB) 80/20 blend plaques had lower tensile and flex moduli than the corresponding physical blend plaques as

Table 13. Comparison of the mechanical properties of injection molded plaques of PET/Vectra A 80/20 physical blend and PET/Vectra A 82/18 mixer blend.

MATERIAL	FLEXURAL MODULUS (GPa)	YOUNG'S MODULUS (GPa)	TENSILE STRENGTH (MPa)
PET	2.44 (0.25)	1.87 (0.02)	66.0 (0.74)
PET/VECTRA 80/20 PHYSICAL BLEND	4.55 (0.25)	3.42 (0.19)	103.66 (4.57)
PET/VECTRA 82/18 MIXER BLEND	4.46 (0.30)	2.90 (0.27)	83.64 (3.95)

can be seen from Table 14. The WAXS patterns from both these plaques were examined, and it was observed that there was no preferred orientation in either of the two cases. Also, some crystallization of the HX4000 was seen in both cases as evidenced by a complete ring corresponding to a d-spacing of roughly 4.67 °A. However, the morphology of the two differently processed blends was quite different and the flow direction fracture surfaces of both these plaques are shown in Fig. 91. It is observed that the HX4000 domains in the physical blend case (Fig. 91a) are much smaller than those seen in the mixer blend plaque (Fig. 91b). The fracture surface of the extruded strands of the mixer blend exhibited fibrils of HX4000 in the PET matrix that ranged from about 0.1-1.5 μm in diameter and did not appear to have very long aspect ratios. The HX4000 domains are even smaller in the physical blend case. However, the mechanical properties observed in Table 14 do not appear to have any satisfactory explanation on the basis of either the WAXS or SEM results and nor is any explanation forthcoming on the basis of the processing conditions.

As mentioned earlier, a PP/Vectra A system was also examined in order to study the property differences, if any, as a consequence of the two different processes. It should be noted here that this system is different from the PET/LCP systems in that the maximum temperature in the injection molder (for the physical blend case) was limited to 290°C due to the degradation of PP at higher temperatures. Therefore, the thermal history effects, if any, of preheating Vectra A to 330°C (in the mixer blend case) and to only 290°C (in the physical blend) are likely to be manifested in these results to a greater extent than seen in the PET/Vectra case where the maximum temperature was 310°C for the physical blend.

A blend of PP/Vectra A 75/25 was extruded using the dual-extruder mixing method with the same processing temperature profiles discussed earlier in the strand extrusion section. SEM micrographs of the fracture surface of the extruded strands are shown in Fig. 92 wherein an overall view of the cross-section and a higher magnification of the strand are shown. It is clear from Fig. 92 that the Vectra A is present in the form of infinitely long aspect ratio fibrils with the diameters ranging from 0.5- 2 μm. Pellets of these strands were subsequently injection molded using the conditions discussed above. The resulting mechanical properties of

Table 14. Comparison of the mechanical properties of injection molded plaques of PET/HX4000 80/20 physical blend and PET/HX4000 80/20 mixer blend.

MATERIAL	TENSILE STRENGTH (MPa)	TENSILE MODULUS (GPa)	FLEX MODULUS (GPa)
PET	66.0 (0.74)	1.87 (0.28)	2.44 (0.25)
PET/HX4000 80/20 (PB)	56.99 (2.18)	4.71 (0.43)	4.21 (0.52)
PET/HX4000 80/20 (MB)	51.86 (0.99)	2.90 (0.21)	2.76 (0.18)
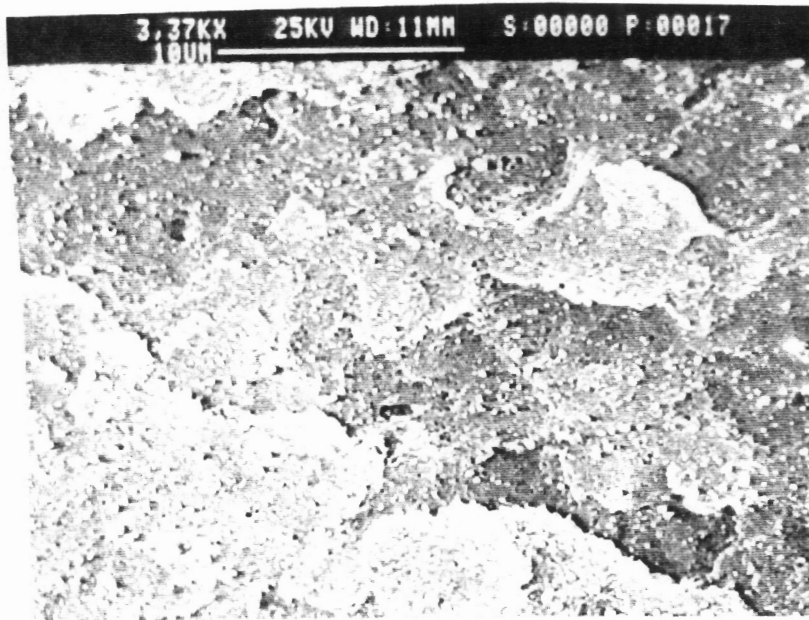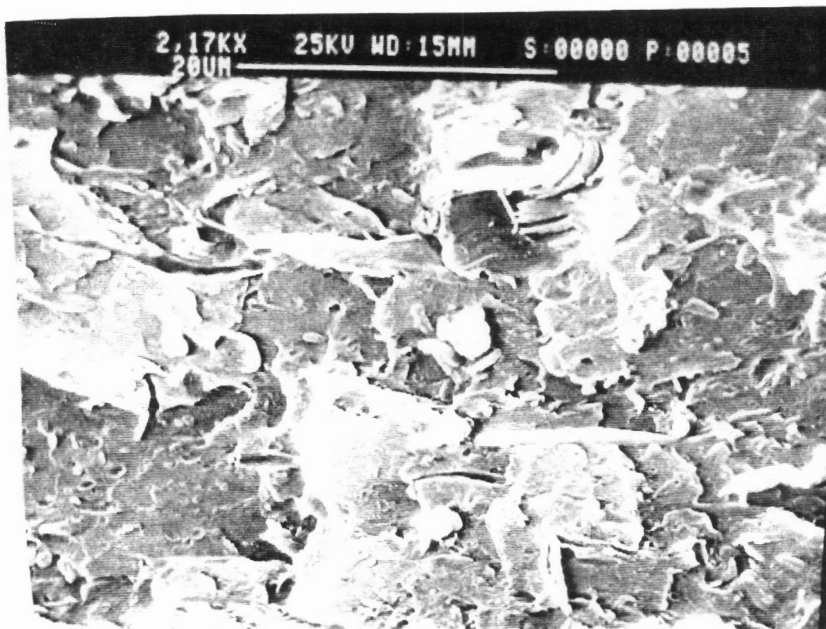
Figure 91. SEM micrographs of fracture surfaces of PET/HX4000 80/20 injection molded (a) physical blend and (b) mixer blend plaques. Fracture is along the flow direction.

these plaques are shown in Table 15 along with data for pure PP and PP/Vectra A 80/20 (PB) and PP/Vectra A 70/30 (PB) plaques. It can be seen that the tensile and flex moduli of all the blends are higher than those of pure PP. However, the tensile strengths are not much different from the pure PP value for any of the blends. The tensile moduli are higher by 2-3.5 fold whereas the flex moduli are higher by roughly 2-2.5 fold. Furthermore, the properties of the mixer blend plaques are higher than both the 20 and 30 wt % physical blend plaques (keeping in mind that the mixer blend composition is 25 wt % Vectra A). This set of data indicates that there appears to be an advantage with preblending via the dual- extruder mixing method over direct physical blending. As mentioned before, one of the more significant differences in the two processes is the fact that the Vectra A underwent largely different thermal histories and it is seems very likely that the higher mixer blend properties are due to the higher preheating temperature (viz. 330°C) possible during pelletizing.

SEM micrographs of the fracture surfaces of PP/Vectra A 75/25 mixer blend plaque along and across the flow direction are shown in Fig. 93. The Vectra A fibrils are visible more clearly from Fig. 93b wherein the fibrils have been pulled out during the fracture. The morphology of the physical blend plaques was also examined and there did not appear to be much of a qualitative difference in the morphology of the physical and mixer blend plaques. It is important to note, however, that the morphology of the physical blends also exhibited Vectra A fibrillar structures. It is believed that these fibrils are formed due to a combination of the high shear rates in the injection molder (which effectively reduce the LCP viscosity) and the elongational flow at the advancing melt front.

The level of molecular orientation achieved in the physical blend and mixer blend plaques was also examined. First in Fig. 94 are shown the WAXS patterns of the PP/Vectra A 80/20 and 70/30 composition ratio physical blend plaques. In Fig. 95 are shown the WAXS patterns of the PP/Vectra A 75/25 mixer blend plaque wherein the diffraction patterns from (a) the overall plaque, (b) skin region and (c) core region are shown. The high level of molecular orientation in both Figs. 94a and 94b, as evidenced by three distinct pairs of arcs, were determined to arise from crystalline regions with d-spacings of 5.26 °A, 4.85°A and 4.68°A (going from inner-

a

b

Figure 92. SEM micrographs of fracture surface of PP/Vectra A 75/25 (MB) strand at magnifications of (a) 120X and (b) 196X. Fracture is across the flow direction.

Table 15. Comparison of the mechanical properties of injection molded plaques of PP/Vectra A made from physical and mixer blends.

MATERIAL	TENSILE STRENGTH (MPa)	TENSILE MODULUS (GPa)	FLEX MODULUS (GPa)
PP	26.89 (1.2)	0.89 (0.03)	1.27 (0.07)
PP/VECTRA A 80/20 (PB)	27.44 (1.62)	2.31 (0.24)	2.49 (0.09)
PP/VECTRA A 70/30 (PB)	27.75 (1.11)	2.93 (0.07)	2.46 (0.09)
PP/VECTRA A 75/25 (MB)	30.75 (1.84)	3.46 (0.13)	3.24 (0.19)

(PB) = Physical Blend
(MB) = Mixer Blend
Standard deviations are given in parenthesis
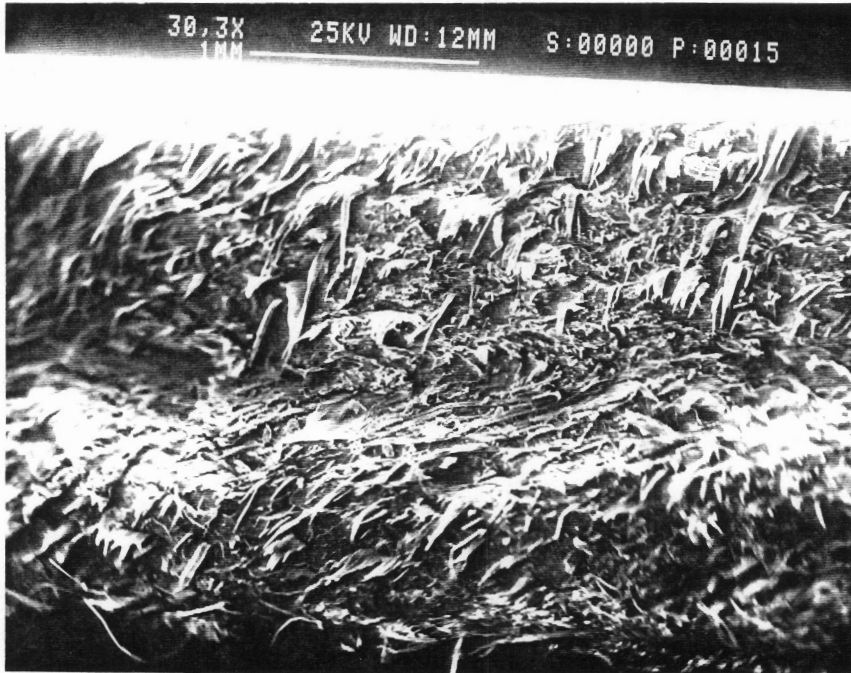
Figure 93. SEM micrographs of fracture surfaces of PP/Vectra A 75/25 (MB) injection molded plaques made from the mixer blend. Fracture is (a) along and (b) across the flow direction.

RESULTS AND DISCUSSION

most to outermost pair of arcs). The inner two were determined to be from the PP phase whereas the arcs with $d_s = 4.68°A$ were determined to be from the Vectra A phase. Thus in the direct injection molded plaques, there is evidence of a high level of orientation even in the PP matrix. It is of interest to note that no orientation in the PET phase was observed in either the physical or mixer blend plaques (or rods or sheets) discussed earlier. This difference between the PET and PP behavior is believed to be a consequence of the longer relaxation time of PP as compared to PET. The onset of shear- thinning for PP at a temperature of 260°C was observed to occur at a frequency of about 0.1 sec^{-1} which would imply a relaxation time of roughly 10 seconds as compared to a relaxation time of 0.1 second for PET. In contrast to the WAXS patterns shown in Fig. 94, the WAXS patterns of the mixer blend plaque shown in Fig. 95 show quite unexpected results. The overall plaque (Fig. 95a) shows a pair of arcs which arise from the PP crystalline phase and a much weaker pair of arcs with $&ds = 4.68 °A$ due to the Vectra A orientation. The skin layer of the plaque shows a high level of orientation arising from both the PP and Vectra A phases as expected. However, the core region of the plaque also shows a high level of orientation from both the PP and Vectra A phases. These results are similar to those for the PET/Vectra A 82/18 MB plaques discussed earlier (Fig. 89) where orientation in both the skin and the core regions of the plaques were observed. The presence of orientation in the core is once again believed to be a result of the Vectra A fibrils which are oriented in the pelletizing step and are not remelted and further are well aligned in the flow direction during injection molding. The high degree of orientation in the core region leads to better properties as observed.

Some additional comments regarding the above results are warranted in view of the varied results observed. The results show that equal (PET/Vectra A system), lower (PET/HX4000 system) or higher (PP/Vectra A system) properties may be obtained by injection molding of the mixer blend pellets as compared to direct injection molding. Thus although no single conclusion regarding the trend may be possible, it is still worthwhile to make some appropriate observations that might render the above results more meaningful. It is worth repeating the results of Isayev and Modic (111) here who conducted studies on blends of
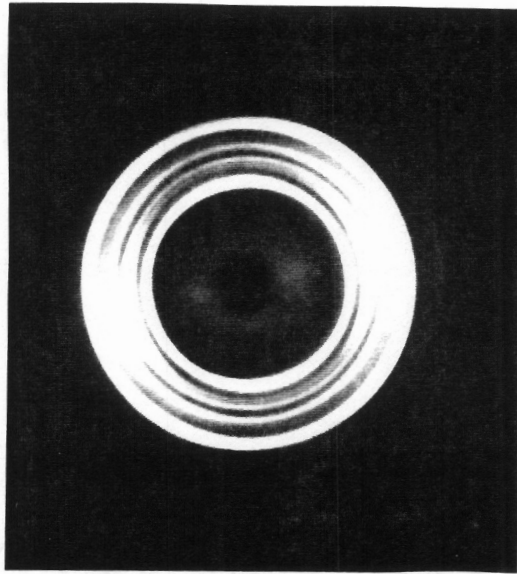
a
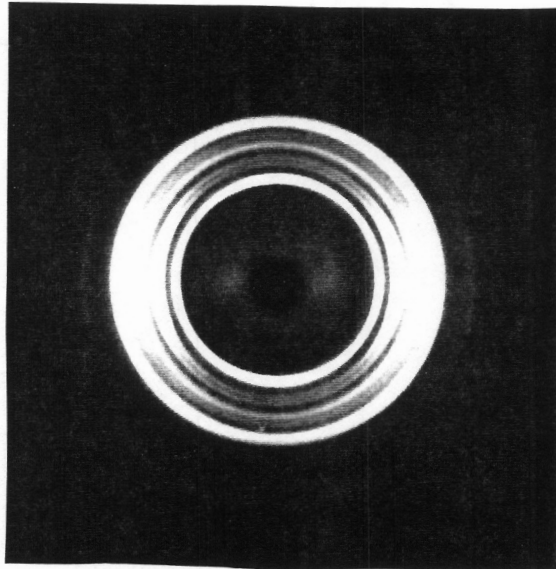
b

Figure 94.   WAXS patterns of injection molded plaques of physical blends of PP/Vectra A (a) 80/20 and (b) 70/30 composition ratios. Flow direction is vertical.
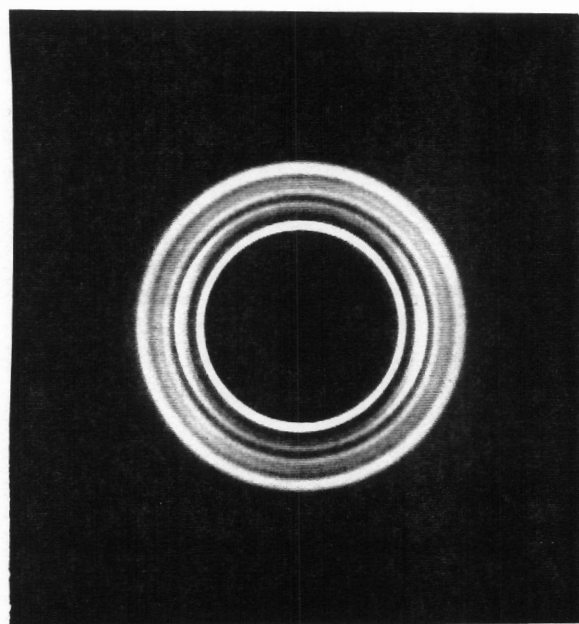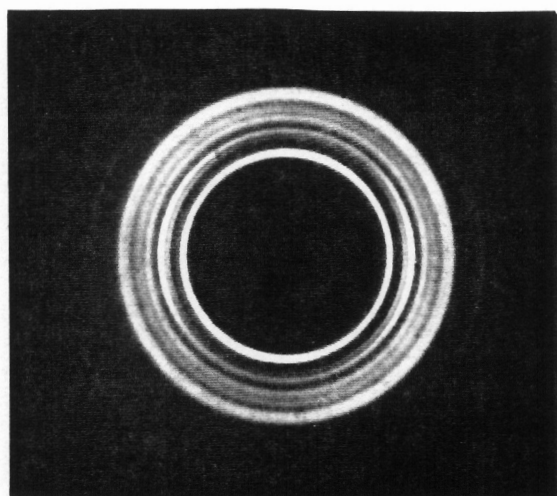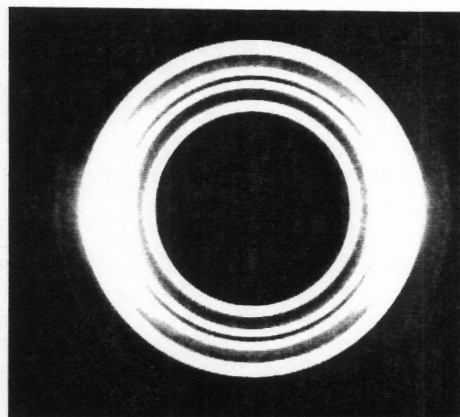
Figure 95. WAXS patterns of a mixer blend PP/Vectra A 75/25 injection molded plaque: (a) overall, (b) skin and (c) core regions of the plaque. Flow direction is vertical.

PC/Vectra A950 processed in two different ways. Injection molded disks of PC/Vectra A950 90/10 composition ratio were made either by direct tumbling of the pellet mixture in the molder (physical blend) or were molded using pellets of the blend which were extruded through a Koch six-element static mixer connected to single extruder (mixer blend). The results of their mechanical property tests showed that both the tensile modulus as well as tensile strength of the mixer blend were higher than the corresponding physical blend. An examination of the morphology revealed that the disks contained larger, more continuous LCP fibrils in the mixer blend case whereas the physical blend disks had thinner and shorter fibrils. Thus it is clear that the static mixer does result in higher aspect ratio fibrils which reinforce the matrix material better. Furthermore, more recent studies conducted at the present author's laboratory with PP/Vectra B blends also showed that the properties of the mixer blend plaques were slightly higher or at worst equal to the physical blend plaques. Therefore it is important to realize that the dual-extruder mixing method provides an effective way to make blends (pellets) of materials otherwise considered incompatible (by virtue of different processing temperatures), which can be further processed by injection molding with, in general, no loss or even a gain in the mechanical properties.

4.3.2 Solid Phase Forming

Extruded sheets of some PET/LCP and PP/LCP blends made via the dual- extruder mixing method were further processed by solid phase forming to examine the effects on the mechanical properties, morphology and orientation. As was shown earlier in section 4.2.3 on sheet extrusion (of mixer blends), the tensile moduli of the sheets were only marginally higher than the modulus of the pure matrix polymer. Furthermore, the tensile strengths of the blend sheets were sometimes even less than that of the matrix material. Thus one of the objectives of this study was to improve the mechanical properties of the as-extruded sheets. Also, since the extruded sheets are oriented in one direction only, the properties of the sheets are rela-

tively poor in the transverse direction. Therefore composites of the extruded sheets were made using the procedures described in chapter 3. The results that follow are all for 4-ply, alternate cross stack composites. It should be added here that the reported results are an average of 3 tests for each system due to the limited samples available. The samples were pressed with a maximum of 15000 pounds force (about 2500 psi pressure based on the surface area of the sample) and the temperatures at which the consolidation was done were 280°C for PET blends and 240°C for PP blends. The temperatures were selected to ensure that the matrix material was sufficiently fluid and yet the temperature was below the melting point of the respective LCP.

Four different systems were studied. The draw ratios in the following discussion refer to those of the as-extruded blend sheets. The thickness (T) and draw ratio of the as-extruded sheets, the thickness of the composite (Tc) and the percentage reduction in thickness for the composites were as follows:

- PP/Vectra B 82/18 sheet [D.R. = 2.8], T = 0.021"; Tc = 0.0685"; thickness reduction = 22.6 %

- PP/Vectra B 70/30 sheet [D.R. = 2.0], T = 0.026"; Tc = 0.0920"; thickness reduction = 11.5 %

- PET/Vectra A 65/35 sheet [D.R. = 3.0], T = 0.034"; Tc = 0.1125"; thickness reduction = 17.3 %

- PET/HX4000 72/28 sheet [D.R. = 6.6], T = 0.028"; Tc = 0.0980"; thickness reduction = 12.5 %

The PET/HX4000 blend sheets did not consolidate very well and the composite was extremely brittle which made the cutting of samples for mechanical property testing difficult. Hence these results will not be included here. The results of the mechanical properties of the other composites are shown in Table 16. The tensile modulus and tensile strength of the PP/Vectra B 82/18 composite were measured to be 3.42 GPa and 15.81 MPa, respectively. The TM and TS of the as-extruded sheet were measured to be 0.96 GPa and 27.55 MPa. Thus there appears to be an enhancement of over three fold in the modulus while the strength is reduced by a factor of ca. 0.8. The PP/Vectra B 70/30 composite has TM and TS of 3.74 GPa and 25.79 MPa as compared to the as-extruded sheet properties of 2.33 GPa and 25.78 MPa, respectively.

Lastly, the TM of the PET/Vectra 65/35 composite is 2.49 GPa while the TS is 10.37 MPa as compared to the as-extruded sheet properties of 1.99 GPa and 41.67 MPa.

The morphology of the above composites made by solid phase forming was also examined and the fracture surfaces of the PET/Vectra A 65/35 composite are shown in Fig. 96. The four layers are quite clearly visible from Fig. 96a where the layers have orientation, from top to bottom, in the transverse/machine/transverse/machine direction. Furthermore, it is also clear from Fig. 96b that the interface between two layers (transverse/machine top/bottom) appears to be have consolidated very well with no voids or clear interface evident. In fact, the different layers are only easy to tell due to the different Vectra A fibril orientations. The micrographs of the other composites were also very similar in appearance and hence will not be shown here.

The increase in the moduli of the composites made above is surprising since the as-extruded sheets were cross-stacked which effectively increases the thickness of the composite and hence would be expected to reduce the moduli. However, it is important to note that very high pressures were employed in the consolidation process. Furthermore, the plaques were pressed non-isothermally since they were rapidly cooled to room temperature, under pressure, after consolidation at high temperatures. The non-isothermal solid phase forming technique has been observed to improve the tensile modulus of injection molded plaques (163,164), although to a lesser extent than observed here. Furthermore, the decrease in the tensile strength of the composite observed here could possibly be due to a lack of adhesion between the different sheet layers although this did not appear to be evident from the SEM micrographs. It is also possible that the composites failed prematurely due to slight surface imperfections that come about as a result of the consolidation. Nevertheless, the above solid phase forming studies indeed show a potential for LCP blend sheets to be further processed and also show a new avenue whereby improvements in properties in more than one direction may be achieved.

Table 16. Mechanical properties of composites made by solid phase forming of extruded blend sheets.

MATERIAL	DRAW RATIO	TENSILE STRENGTH* [MPa]	YOUNG'S MODULUS* [GPa]
PP/Vectra B 82/18	2.8	15.81 (1.70)	3.42 (0.03)
PP/Vectra B 70/30	2.0	25.79 (4.70)	3.74 (0.21)
PET/Vectra A 65/35	3.0	10.37 (1.40)	2.49 (0.15)

*Standard deviations are given in parenthesis

All the composites are 4-ply alternate cross (90°) stack

a
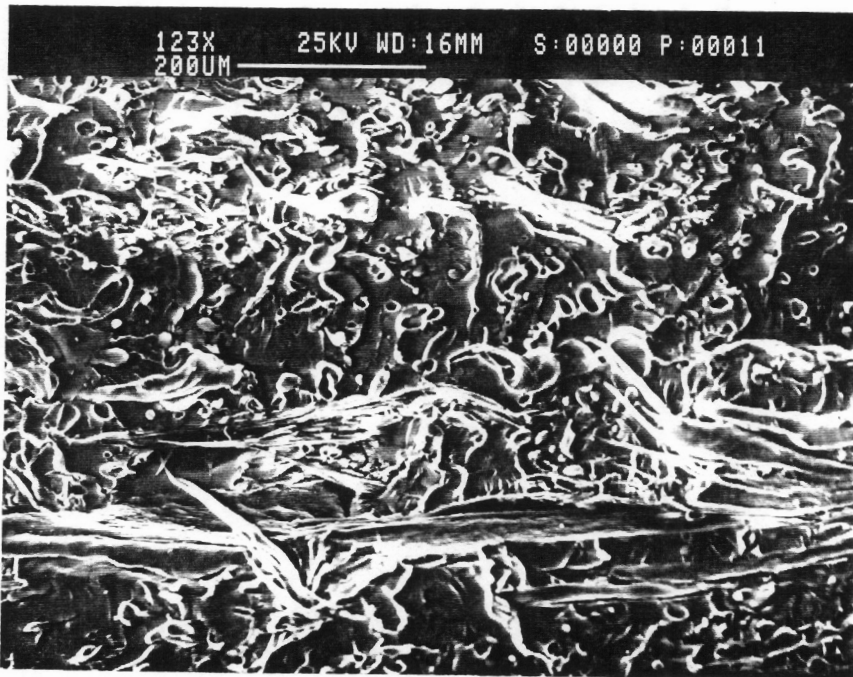
b

Figure 96. SEMs of the fracture surface of a 4-ply, cross-stack PET/Vectra A 65/35 composite: (a) view of entire cross-section (b) higher magnification at the interface between two layers.

RESULTS AND DISCUSSION   271

4.3.3 Thermoforming

To further examine the post-processing of LCP blends, thermoforming experiments were conducted. The objectives here were two-fold. The first was to qualitatively assess if the blend sheets and injection molded plaques could in fact be thermoformed and if so to determine at what thermoforming conditions viz. thermoforming temperature and preheating time. The second objective was to study the changes in the morphology and orientation that were associated with the thermoforming of thermoplastic/LCP blends.

The experimental details and mold dimensions have been provided in chapter 3 and thus will not be repeated here. The holding time for all the tests was 15 seconds. Also, both the male and female molds were kept at room temperature for all the experiments. Most of the studies conducted were with PET/LCP blends and thus only these results will be presented here. Also, as mentioned earlier in chapter 3, the size of the thermoformed parts were quite small and thus no mechanical properties could be tested. A schematic of the thermoformed cup showing the placement of the sample and the different zones as they will be referred to in the following discussions is shown in Fig. 97.

Thermoforming experiments were conducted with PET/LCP60-80 70/30, PET/Vectra A 85/15 and PET/HX4000 sheets. A range of experiments was conducted with the above three systems where essentially the preheating temperature was varied from 60°C to 220°C and the preheating time from 30 to 99 seconds. The findings of these experiments may be summarized as follows. A temperature of about 120°C was found to best suited for all the PET/LCP blends in terms of obtaining a "good" thermoformed part without tearing and also in terms of where the draw occurred. At higher temperatures such as 175 °C, 190°C and 220°C the drawing appeared to take place primarily in zone 1 with little or no draw taking place in the sides or the base of the part. Ideally, it is desirable to get the drawing to occur in the base and sides of the sample so that the thermoformed part will have good properties despite a reduction in thick-
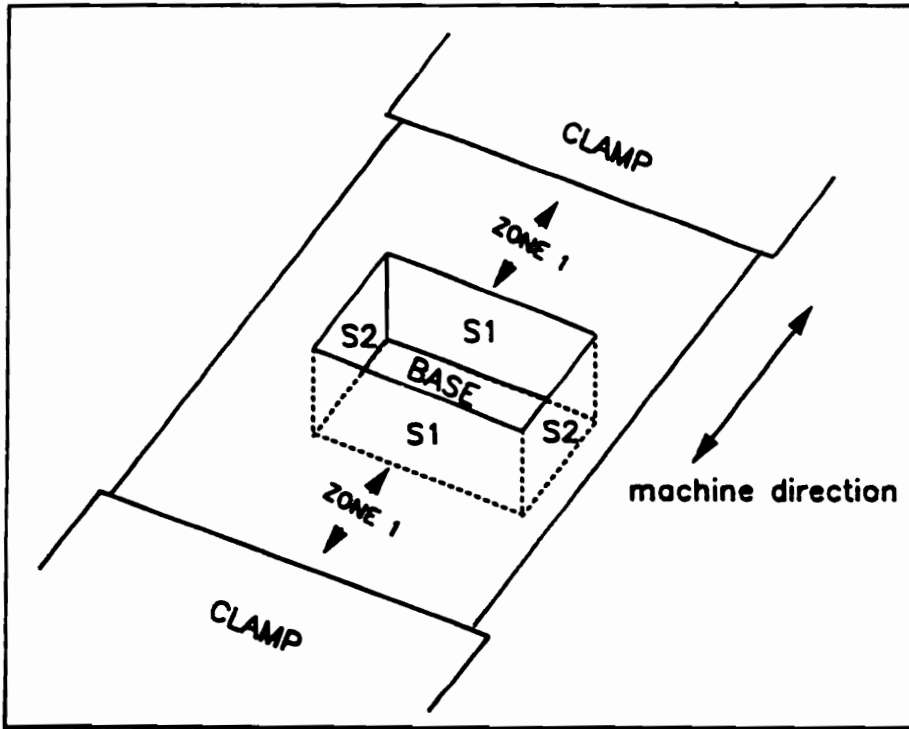
Figure 97.   Schematic of thermoformed cup showing the different zones.

ness. The drawing results in significant stretching which induces a high level of orientation in the base and walls of the part.

In Fig. 99 and 100 are shown SEM micrographs of a PET/LCP60-80 70/30 blend sheet that was thermoformed by preheating to 120°C for 99 seconds. For comparison the SEM micrographs of the as-extruded sheet prior to thermoforming are shown in Fig. 98 where the fracture surface along and across the flow direction are shown. It is very clear from Figs. 99 and 100 that the thermoforming process stretches the LCP phase into very highly elongated domains. In fact, it can be seen from Fig. 100a that the LCP60-80 fibrils have a very uniform diameter and high aspect ratios of the order of 40-50. At the same time, it can be seen from the transverse direction fracture surfaces that larger holes or voids are also present. These voids may possibly be due to the reduction of the fibril diameters during thermoforming which leaves open spaces in the surrounding matrix. If this was in fact true, then the adhesion and hence tensile strength are likely to be diminished to some extent.

WAXS patterns of the as-extruded PET/Vectra A 85/15 sheet, along with those from the thermoformed cup base and side walls are shown in Fig. 101. The film was thermoformed by preheating to 120°C for 99 seconds. The change in thickness was also measured and it was found that the side walls reduced in thickness by 62 % whereas the base of the cup was reduced by 39 % as compared to the original sheet thickness. Furthermore, the as- extruded sheet shows a relatively faint pair of arcs (Fig. 101a) which were determined to be from the Vectra A orientation that was developed during the sheet extrusion process. The WAXS pattern from the base of the formed part (Fig. 101b) show that the arcs are much more distinct indicating a more enhanced level of LCP orientation. Furthermore, an additional, much weaker pair of arcs were also observed which were determined to be from the PET matrix phase. Finally, the side walls of the cup show extremely high orientation from both the PET (inner arcs) and Vectra A (outer arcs) phases. This is not surprising considering that the thickness of the sides was reduced by 62 %. Also, since the molds were kept at room temperature, all the orientation that is developed during the forming step is locked in due to the quenching of the sheet as it is being formed. In fact, it was mentioned earlier while discussing the formation

RESULTS AND DISCUSSION
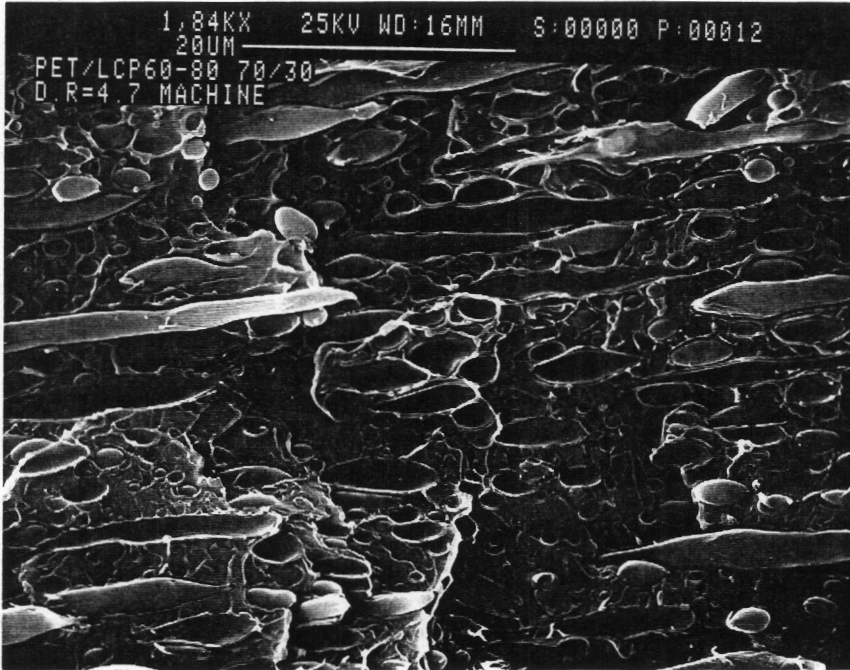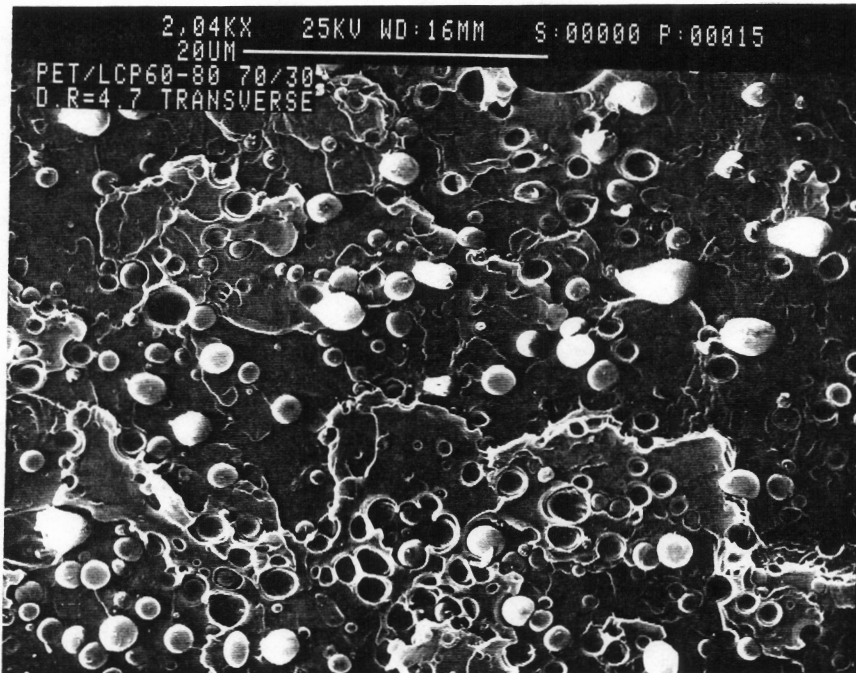
Figure 98. SEM micrographs of PET/LCP60-80 extruded sheet fractured (a) along and (b) across the flow direction.
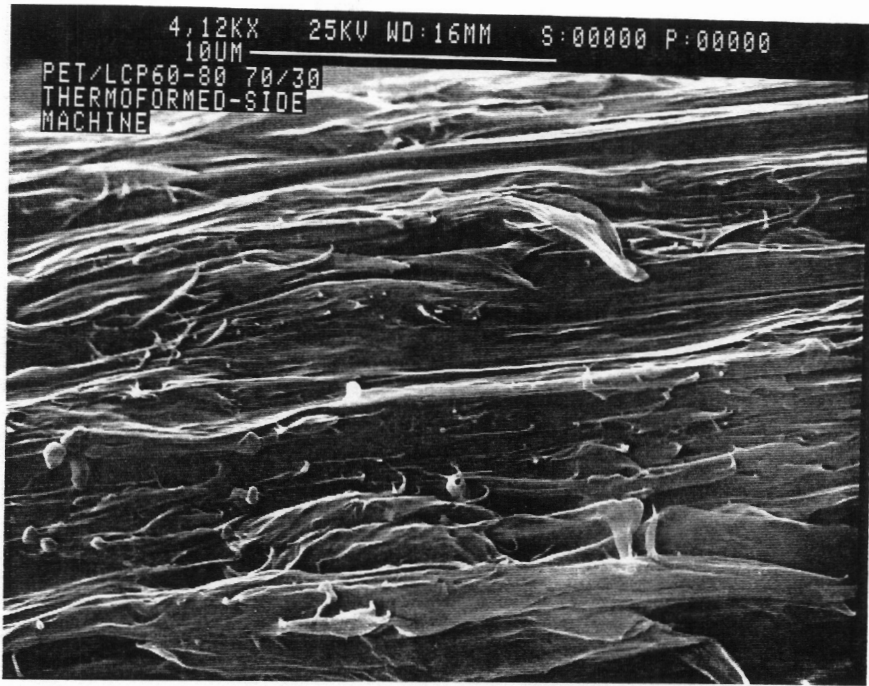
a
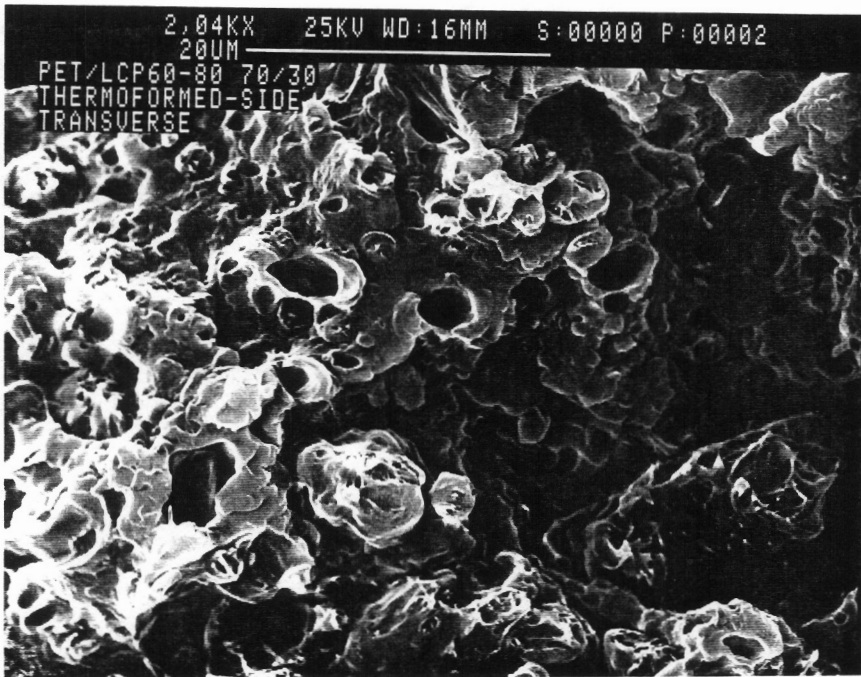
b

Figure 99.   SEM micrographs of fracture surfaces (a) along and (b) across the flow di-
rection of the base of a PET/LCP60-80 thermoformed cup.
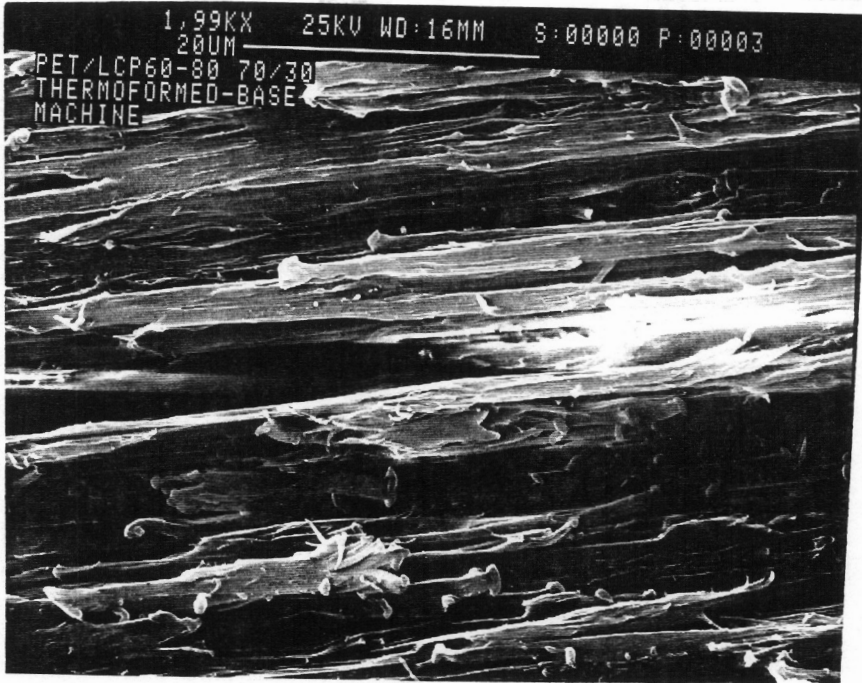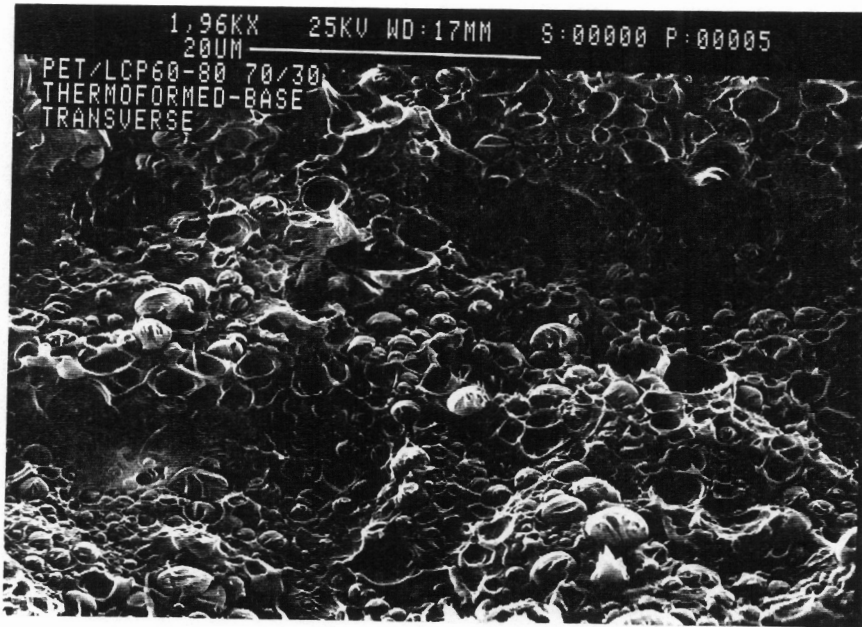
Figure 100. SEM micrographs of fracture surfaces (a) along and (b) across the flow direction of the side walls of a PET/LCP60-80 thermoformed cup.

of sheet composites that deformation while cooling i.e. non-isothermal processes resulted in a higher degree of orientation and hence improved properties over isothermal processes. As a final note, it should also be pointed out that it would appear, on the basis of the discussions above and those in earlier sections, that inducing orientation in materials such as PET which have very rapid relaxation times is easier by processing in the solid state (above the Tg) than from the melt state. The above results show the potential, once more, of these LCP reinforced thermoplastic blends to be further processed with possible gains in the mechanical properties.

4.4   In Situ (LCP) Composites vs Inorganic Filler Composites

It is the objective of this section to briefly compare the properties and processing of in situ LCP reinforced composites generated in this study with the data available in the literature on thermoplastic composites containing inorganic fibers (172) (typically glass, asbestos, carbon etc.) and/or particulate (mineral) fillers (172) (eg. mica, talc, calcium carbonate etc.) as the reinforcements. For the sake of brevity, all the above types of composites will be referred to from hereon as simply inorganic filler composites. However, any comprehensive or detailed comparison of these types of composites is well beyond the purview of this section and in fact this work. The intention is merely to show, from the data gathered on LCP composites during the course of this study, that the range of the mechanical properties that have been achieved using LCPs as reinforcements are of comparable magnitude to those typically achieved with thermoplastic inorganic filler composites. The variation in the exact processing methods, processing conditions, filler type, filler geometry etc. in the LCP composites of this study and the inorganic filler composites data that they will be compared with is indeed of such magni-
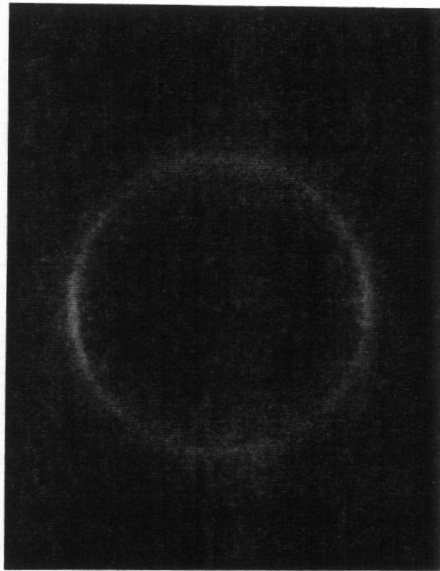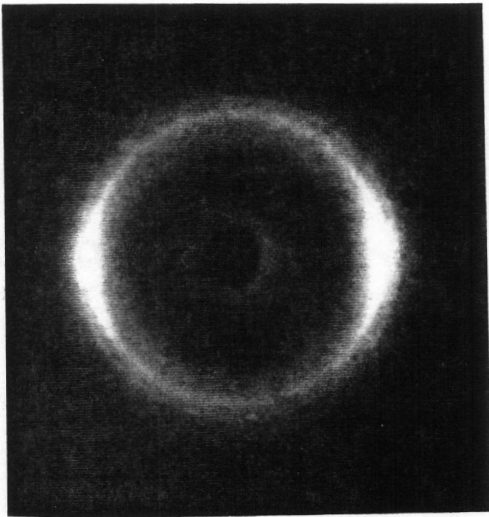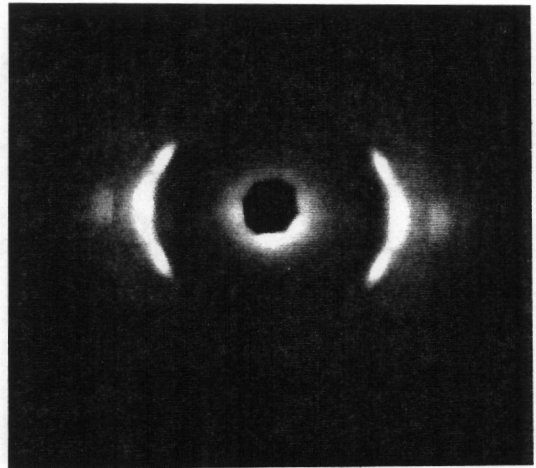
Figure 101.   WAXS patterns of: (a) PET/Vectra A 85/15 sheet; samples from the (b) base and (c) side walls of the thermoformed cup.

tude that any direct comparison is impossible. Nevertheless, it is felt that such a comparison is still helpful in establishing the value of in situ generated LCP composites and is therefore presented briefly in the coming paragraphs. To keep the results in proper perspective, an attempt will be made to choose equal wt % of the filler as a basis for the following comparisons.

The properties of some of the inorganic filler composites along with data for the LCP blends generated in this study are shown in Table 17. It may be observed that the tensile strength (TS) of pure PP injection molded plaques is about 27 MPa whereas the tensile modulus (TM) and flexural modulus (FM) are 0.89 GPa and 1.27 GPa, respectively. In comparison, it can be seen that the TM, TS and FM of the PP/Vectra A 75/25 injection molded plaque are very comparable to those for the inorganically filled composites, keeping in mind that the inorganic composites all contain higher amounts of the filler or reinforcement. It of further interest to note that densities of most inorganic fillers are roughly between 2-3.2 gms/cm^3 (171) and with the densities of the LCPs being in the range of 1.2-1.4 gms/cm^3, the properties of the LCP composites would be somewhat higher on a specific weight basis. The properties of the PET/LCP composites can also be seen to quite comparable with the corresponding PET/inorganic filler composites shown in Table 17. In particular, the TS of the PET/Vectra A 80/20 (PB) plaque is almost twice that of pure PET and close to the value for the 35 wt % continuous glass filled composite. The TM and FM appear to be somewhat lower than the inorganic filler composites but the loading of the LCP is also lower for the blends made in this study. It may be recalled that the PET/Vectra 40/60 injection molded plaque (discussed in section 4.1) had a flexural modulus of 12.41 GPa whereas the 80/20 blend shown in Table 17 has a FM value of 4.55 GPa. Therefore, at the intermediate composition of about 40 wt % of the LCP, the LCP blend may be expected to have properties similar to those of the PET filled with glass. It is important to reiterate that the above comparisons should be regarded as qualitative only due to the reasons mentioned earlier. Nevertheless, it is clear from the above discussion that the some of the mechanical properties viz. TM, TS and FM of the LCP blends made in the course of this study are very comparable to the properties that are achieved with inorganic filler composites.

Table 17. Comparison of the mechanical properties of LCP composites with inorganic filler composites.

MATERIAL	TENSILE MODULUS* (GPa)	FLEX MODULUS* (GPa)	TENSILE STRENGTH* (MPa)
Polypropylene (PP)	0.89 (0.027)	1.27 (0.068)	26.89 (1.20)
PET	1.87 (0.275)	2.44 (0.251)	66.0 (0.74)
PP/30 WT % Glass Fiber [1]	4.14	3.59	63
PP/40 WT % Talc [2]	-	3.45	27.58
PP/40 WT % Asbestos Fiber [2]	-	5.03	38.61
PP/Vectra A 75/25 MB plaque	3.46 (0.13)	3.24 (0.19)	30.75 (1.84)
PET/30 WT % Glass Fiber [3]	-	8.96	158
PET/35 WT % Cont. Glass [1]	7.83	7.73	120
PET/45 WT % Glass-Mica [4]	-	9.65	-
PET/Vectra A 80/20 (PB)	3.42 (0.19)	4.55 (0.25)	103.66 (4.57)
PET/HX4000 80/20 (MB)	2.90 (0.27)	4.46 (0.30)	83.64 (3.95)

★Standard deviations are given in parenthesis
(PB) = Physical Blends; (MB) = Mixer Blends
[1] = Azdel, Inc
[2] = J.T. Lutz (ed.), *Thermoplastic Polymer Additives*, Marcel Dekker, Inc. N. Y., 1989.
[3] = Encyclopaedia of Polymer Science and Technology, Vol. 12.
[4] = D.G. Baird and G.L. Wilkes, *Polym. Eng. Sci.*, 23(11), 632 (1983).

RESULTS AND DISCUSSION

Furthermore, the LCP blends offer certain processing advantages which deserve brief mention and are as follows. It has been shown earlier in the literature review that the viscosity of the LCP blends at elevated temperatures (during processing) is often decreased from that of the pure matrix polymer. In contrast, the viscosity of thermoplastic melts containing inorganic fillers under typical processing conditions is in fact higher than that of the pure matrix polymer and thus more energy intensive. Injection pressures are roughly 10-40 % higher than those for nonreinforced compounds (172). Another disadvantage with inorganic fillers is their abrasiveness (especially inorganic fibers such as glass, carbon) which cause significant wear on extrusion and injection molding equipment (172). One other problem encountered with inorganic fillers, especially glass, is the inability to obtain a high gloss finish (172). Although the status of this problem with LCP composites is not known, the surface of most of the LCP composites made in the course of this study did appear to have a smoother finish as compared to glass filled composites.

LCP blends also offer some processing advantages over inorganic filler composites, particularly short fiber composites, in processes such as film-blowing and blow-molding wherein the processing of the thermoplastic matrix containing the inorganic filler becomes difficult. In fact, there do not appear to be any established film-blowing or blow-molding processes currently known using inorganic fillers as the reinforcements. Therefore the option to obtain reinforced thermoplastics by using LCPs as the reinforcements is a significant advantage over inorganic fillers. Lastly, in processes such as thermoforming, significant problems exist with thermoforming inorganic continuous fiber filled sheets (173), e.g. buckling of fibers under compressive strains, limited extensional deformations due to the low ultimate tensile strains in fibers, low applicable load due to interply slip and transverse flow and long reconsolidation times and pressures after forming (173). In contrast, the LCP sheets (and plaques) that were thermoformed in this study did not, in general, appear to be associated with these problems. In fact, since the reinforcement (LCP) is itself deformable, parts with sharp corners can be made more easily by forming at temperatures above the glass transition temperature

of the LCP. As mentioned in section 4.3, the thermoformability of the LCP composites was very good.

In conclusion, it is clear that the mechanical properties of thermoplastics reinforced with liquid crystalline polymers are very similar to those obtained with conventional inorganic fillers. Furthermore, as discussed earlier, the thermoplastic/LCP systems offer certain processing avenues that are currently difficult or not available with thermoplastic/inorganic systems such as film-blowing and blow-molding operations. However, the big disadvantage of using LCPs at the present time is their extremely high cost. To give some perspective about this, Vectra A900 is about $15-16/lb compared with short glass fibers which cost between &2-3/lb. Thus although the properties of LCP blends are comparable, they are not yet cost effective enough for large volume applications. There are predictions, however, that the cost of LCPs will drop to within $5/lb in the next 2-3 years (175). It is believed that the full potential of thermoplastic/LCP blends will then be better appreciated and realized.

5.0   Conclusions and Recommendations

Results and discussions of the experimental work along with the appropriate calculations have been presented in the previous chapter. In this chapter, the main conclusions from this study are provided along with recommendations for future work. In section 5.1, the main conclusions are given followed by recommendations in section 5.2.

5.1   Conclusions

1. **Studies on blends of PET with LCPs (LCP60, LCP60-80, HX4000 and Vectra A900) indicate that significant enhancements (50-350%) in the mechanical properties of PET can be achieved by blending with relatively small amounts (0-50 wt %) of LCPs. Furthermore, the properties of these blends are between 40-90 % of those of inorganic fiber- filled composites when compared on the basis of equal wt % of the reinforcement.** With only 10 wt % LCP60-80 in the blend, the properties (both tensile modulus and strength) of the extruded sheets were increased by roughly 1.6 times that of pure PET. Further, the tensile modulus (TM), tensile strength (TS) and flexural modulus (FM) of pure PET injection

molded plaques were measured to be 1.87 GPa, 66.0 MPa and 2.44 GPa, respectively. In comparison. the injection molded plaques of PET/LCP60-80 showed even more significant enhancements over pure PET plaques with the TM and Ts of the 90/10, 70/30 and 50/50 composition ratios being 3.21 GPa and 60.95 MPa, 4.9 GPa and 67.19 MPa and 6.4 GPa and 72.45 MPa, respectively. Injection-molded plaques of PET/Vectra 80/20 (PB) showed roughly a doubling of the mechanical properties viz., TM. TS and FM to 3.42 GPa, 103.66 MPa and 4.55 GPA, respectively. With 20 % HX4000 in the blend the TM, TS and FM increased to 4.71 GPa, 56.99 MPa and 4.2 GPa, respectively. These values may be compared with 7.7 GPa, 7.8 GPa and 120 MPa for a 35 wt % continuous strand glass fiber reinforced PET sheet (Azmet, Azdel Inc.) and a 9.64 GPa flexural modulus of PET with 45 wt % glass-mica reinforcement (Rynite).

2. **A mixing method which can blend high melting liquid crystalline polymers with lower melting thermoplastics has been successfully designed and developed.** The success of this method is gaged by the fact that highly oriented LCP fibrillar structures with extremely high aspect ratios (and in some cases even infinite length) were observed in most of the blends processed by this method. Further, materials with over a 100°C difference in their processing temperature regimes were successfully blended together using this method.

3. **Blends of PET/Vectra A and PET/HX4000 extruded through the dual-extruder mixing method using 3 and 9 mixing elements (with respect to the Kenics Static Mixer), showed inadequate mixing based on the observed morphology. However, the mixing was observed to be adequate, again on the basis of the observed morphology, when 18 mixing elements were used. Thus it is concluded that for the blending of polymer melts (where all the blending takes place in the mixer only), more than 9 mixing elements are needed for satisfactory mixing.** All the blends in this study were extruded using 18 mixing elements.

4. **The blending method developed here offers significant advantages over the single-screw extrusion process in terms of the enhancing the mechanical properties of the blends.** The tensile moduli of PET/Vectra 70/30 blend rods made using the mixing method were seen to be higher by a factor of about 1.5 than those of the same composition made using a single-screw extrusion process in the entire range of draw ratios studied. At the highest draw ratio of 49. the MB rod had a modulus of 18.99 GPa compared to 13.39 GPa for the PB rod. This difference is believed to be a consequence of the enhanced distributive mixing action of the static mixer which is responsible for the infinitely long LCP fibrillar morphology observed and the absence of any skin-core type structure as seen in the physical blend.

5. **In contrast to the single-screw extrusion process where the LCP fibrils are generated in the die and/or by drawing at the exit of the die, the LCP fibrils in the case of the dual-extruder blending method developed here are formed in the static mixer itself.** SEMs of PET/Vectra 70/30 MB blend show clearly the presence of fibrils in samples taken imme-diately upstream of the mixer without any converging section or extensional drawing at the exit of the die. In sharp contrast, a blend of the same composition extruded through a single extruder without drawing showed droplets in much of the cross-section. It seems likely that these differences are due to the pre-heating of Vectra to 330°C in combination with the enhanced distributive flow-division mechanism of the mixer.

6. **Significant enhancement in the tensile modulus of extruded rods was observed in all the PET blends studied.** In the case of PET/Vectra 70/30 blend, the tensile modulus of the rod, extruded using the dual-extruder mixing method described earlier, at the highest draw ratio of 49 (18.99 GPa) was higher than that of pure PET (2.5 GPa) by a factor of over 7. Even with as little as 4 wt % of Vectra A in the blend the TM of the blend was observed to be over 2 times that of pure PET at high draw ratios.

7. **Significant enhancement in the tensile modulus of extruded rods was also observed in all the PP blends studied.** PP/Vectra 72/28 exhibited a tensile modulus (4.71 GPa) over 7 times that of pure PP (0.69 GPa). In case of PP/Vectra B (13.47 GPa), the enhancement was over 19 times that of pure PP.

8. **Significant enhancements in the tensile and flex moduli of the various blends made by strand extrusion, sheet extrusion, injection molding and the dual-extruder mixing method were obtained as shown above. However, the tensile strengths of all these differently processed blends were consistently poor being, in general, only marginally better or sometimes even lower than that of the respective matrix.** The poor adhesion and wetting between the LCP and matrix polymers is believed to be responsible for the poor tensile strengths and SEMs of fracture surfaces support this idea.

9. **The properties of the extruded sheets of PET/LCP and PP/LCP blends were more dependent on the level of molecular orientation achieved than on the composition or morphology.** The tensile modulus (TM) and tensile strength (TS) of pure PET sheet were observed to be 2.2 GPa and 53.03 MPa whereas the values for PP sheet were measured to be 0.62 GPa and 21.95 MPa, respectively. In comparison, PET/Vectra A 82/18 sheet which was drawn exhibited TM and TS of 2.95 GPa and 59.25 MPa. Furthermore, the TM and TS of PET/Vectra A 85/15 sheets with and without calendering were measured to be 2.65 GPa and 52.78 MPa, and 2.19 GPa and 45.97 MPa, respectively. Also, PET/Vectra A 65/35 sheets which were calendered exhibited TM and TS of 1.99 GPa and 41.67 MPa, respectively. In the case of PP/LCP sheets, the PP/LCP60 73/17 and PP/Vectra A 81/19 sheets which were drawn exhibited TM and TS values of 2.11 GPa and 28.85 MPa and 2.1 GPa and 39.42 MPa, respectively. In contrast, PP/Vectra B 82/18 and PP/Vectra B 70/30 sheets which were calendered exhibited TM and TS values of 1.54 GPa and 31.45 MPa and 2.33 GPa and 25.78 MPa, respectively. The morphology was largely indistinguishable between the calendered and non-calendered (i.e. drawn) sheets but the WAXS patterns showed much higher levels of orientation in the latter than in the former.

10. **Break-up of the LCP fibrillar morphology into droplets was observed in some cases with an increase in the L/D or (L/H) ratio of the die.** For example, the morphology of a PET/LCP60 80/20 blend was observed to change from fibrillar to droplet morphology when the L/D ratio of the capillary die (constant D) was increased from 16 to 40. However, with PET/Vectra 70/30 (PB), a skin-core fibril-droplet type of morphology was observed to be essentially unchanged from L/D = 1 to L/D = 51. Also, a simplified sheet die with an L/H of 10 was seen to create a much better fibrillar morphology in terms of the seemingly larger proportion and higher aspect ratio of the LCP fibrils than a sheet die with an L/H of roughly 40 for several blend systems.

11. **Studies on the further processing of the mixer blends by injection-molding resulted in plaques with lower (PET/HX4000), equal (PET/Vectra 80/20) or better (PP/Vectra A 75/25) tensile properties than the corresponding physical blend plaques.** The decrease in the PET/HX4000 case is attributed to the fact that the HX4000 does not form highly fibrillar structures during the strand extrusion step and upon injection-molding there is no pre-ferred orientation. The LCP orientation levels in the core of the PET/Vectra and PP/Vectra MB plaques were observed to be much higher than in the core of the physical blends. These results suggest that the LCP fibrils do indeed behave as an inorganic fibers in this situation.

12. **Preliminary studies show that significant enhancements in the tensile modulus of the LCP blends can be achieved by post-processing the extruded sheets via solid phase forming wherein the sheets (4-ply, cross-stacking) are consolidated at high temperatures and un-der significant pressure. These results suggest a potential to treat the LCP blend sheets and plaques as prepregs.** For example, the tensile modulus of a PP/Vectra B 82/18 blend sheet which was laminated (4-ply, alternate cross-stack) increased from 0.96 GPa to 3.42 GPa. Also, the tensile modulus and tensile strength of of a PP/Vectra B 70/30 laminate were observed to be 3.74 GPa and 25.89 MPa, respectively. These properties are very comparable to a continuous glass fiber reinforced PP containing 30 % glass (Azdel sheet

SM 10300) which exhibits a tensile modulus of 4.14 GPa and tensile strength of 63 MPa. A further comparison of the laminate with a PP/Vectra B 70/30 injection molded plaque with modulus and strength of 3.1 GPa and 17.31 MPa, respectively, shows that higher properties are obtained by solid phase forming of the sheets as compared to injection-molding in this case. Lastly, the modulus of a PET/Vectra A laminate also increased from 1.99 GPa to 2.49 GPa although the strength of the laminate decreased from 41.67 MPa to 10.37 MPa.

13. **The use of the concepts of flow of a power-law fluid through a packed bed gives reasonably good estimates of the pressure drop in the static mixer.** The range of the pressure drop estimates in the static mixer compare quite well with the experimentally observed pressure drop range. However, the estimated pressure drop was largely dependent on the accurate measurement of the power-law parameters and was further seen to be more sensitive to the consistency (K) than the power-law index (n) in the range of flow rates and pressure-drops of interest here.

14. **Mixing in the static mixer occurs in the laminar flow region based upon the estimated value of the prevalent Reynolds numbers which were determined to be in the range of 1E-6 to 1E-3 for typical flow conditions.** These estimates were based on the typical flow rates encountered in this study and by using the concepts of flow of a power-law fluid through packed beds. The mixing mechanism in the static mixer is thus primarily distributive as compared to the dispersive mode in single-screw extruders.

5.2 Recommendations

In view of the above conclusions and also keeping in mind the results and discussions of chapter 4, the following recommendations may be made for future work.

1. It was shown through several experiments that the static mixer was responsible for the generation of continuous LCP fibrillar morphology in the respective matrix material when blends were extruded via the dual-extruder mixing method. However, the viscosity ratio during the extrusion of all the blends presented in this study was less than unity which is known to be favorable for fibril formation. It is recommended that further studies be carried out where the viscosity ratio is greater than unity to see if the static mixer is capable of forming LCP fibrils even when the viscosity ratio is unfavorable for the formation of fibrils.

2. In conjunction with the above recommendation, it is also of importance to establish if blends extruded using a single extruder and static mixer attached to it's exit will have similar morphology and properties as those extruded here via the dual-extruder mixing method. If the morphology and properties are comparable to the blends from the dual-extruder technique, then in cases where the two materials have some overlap of processing temperatures. the blends may be made without the inherent processing complications of the dual-extruder method.

3. In the dual-extruder mixing method, the two streams were joined in a 'T' and then fed into a static mixer. It may be worthwhile to examine what would happen if the minor phase (LCP) was injected into the barrel of the matrix extruder and the emerging melt blend then fed into the static mixer. On the basis of the studies conducted here, it is believed that the minor phase would be dispersed into droplets in the matrix extruder and may not result in highly continuous fibrils as seen with the dual-extruder mixing method.

4. The degree of mixing attained by lowering the number of mixing elements (3 and 9 elements) in the dual-extruder mixing method were performed during the course of this work. However, it is a matter of interest to see what happens if the number of mixing elements is increased from 18 to say 24 or 30 mixing elements. It is expected that the size scale of the LCP fibrils will level off at some point but this is something that is best established experimentally. Also, the effects of enhanced mixing on the resultant properties should also be monitored so that a pattern of morphology, mixing and mechanical properties may be established.

5. The properties of the extruded blend sheets were not significantly enhanced over the pure matrix material properties and possible reasons for this have been outlined in chapter 4. It is believed that the use of larger extruders would translate into larger throughputs which would allow the use of a sheet die which is wider than the 2.5" and 4" wide sheet dies used in this study. It is then possible to achieve higher draw ratios which are expected to lead to better sheet properties than obtained here due to the limited draw possible. Another advantage of wider sheets would be the possibility of post-processing by transverse stretching (using perhaps a tenter) to obtain more biaxial properties.

6. The potential of the dual-extruder mixing method in generating continuous LCP fibrils has been established. It is believed that film-blowing or blow-molding operations, if carried out in a single unified step in conjunction with the dual-extruder mixing method, may then be able to take advantage of the high fibril continuity and possibly result in significant mechanical property enhancements. The operation of the dual-extruder mixing method is itself quite complex and thus the film-blowing and blow-molding operations are likely to increase the level of complexity of the process. Adjustments to the temperature profiles are also likely to be necessary to accommodate the increased residence times and thus some more calculations may be required in combination with the rheological data of the pure melts to reduce the trial and error involved with direct experimentation.

7. In view of the apparent success of the solid phase forming experiments performed on extruded sheets. more direct studies aimed at looking into the reasons and mode of the property enhancements is recommended. It the mechanisms of property enhancements can be better established, the use of the blend sheets as prepregs would be a strong possibility.

8. The tensile strength of the LCP blends, in general, was not significantly higher than that of the matrix material. Studies aimed at improving the adhesion of the polymers are recommended to improve this situation. Compatibilization of the polymer pairs by addition of a third component to the polymer blend is one suggested avenue in overcoming the problem. For example, there are several documented polymer-polymer pairs that are believed to be compatible. One might take this as a starting point in finding polymers that are compatible with both the matrix and dispersed phases in question. Some preliminary estimates of compatibility can also be made using equations outlined in Chapter 2.

9. Synergism of properties of certain blends at certain compositions was observed in this study and reasons for this are not fully understood. However, if further insights into the reasons for this behavior can be assessed then it may be possible to channel further efforts in obtaining high mechanical properties in appropriate directions.

10. Only a limited set of properties of the LCP blends could be tested in this work. To realize the full potential of thermoplastic/LCP composites, it is highly recommended that other properties of the blends such as heat distortion temperature (HDT), impact strength, gas permeability, solvent resistance etc. also be tested.

11. Last, it is clear that the dual-extruder mixing method offers some advantages in processing as outlined earlier. Although all the work in this study was done with LCP blends, it is believed that the mixing method may be used to blend any two polymers with (or even without) a processing temperature mismatch with some potential advantages in the

morphology and properties and this conjecture needs to be tested using different polymer pairs.

References

1. Isayev and Modic, *SPE, ANTEC* , 573(1986).

2. G. Kiss, *Polym. Eng. Sci.* , 27(6), 410(1987).

3. Sharma, Tendolkar, and Mishra, *Mol. Cryst. Liq. Cryst. Inc. Nonlin. Opt.*, 157, 597(1988).

4. W. Huh, R. Weiss, and L. Nicolais, *SPE, ANTEC* , 306(1986).

5. Siegmann, Dagan, and S. Kenig, *Polym.* , 26, 1325(1985).

6. W. Brostow et. al., *Polym. Eng. Sci.* , 28(12), 785(1988).

7. K.G. Blizard and D.G. Baird, SPE 44th ANTEC, Conf. Proc., Boston, 311(1986).

8. J.A. Manson and L. Sperling, *"Polymer Blends and Composites"* , Plenum Press, 1976.

9. O. Olabisi, L.M. Robeson, and M.T. Shaw, *"Polymer-Polymer Miscibility"* , Academic Press, 1979.

10. K. Solc (ed.), *"Polymer Compatibility and Incompatibility,- Principles and Practices"* , Harwood Academic Publishers, 1982.

11. R.L. Scott, *J. Chem. Physics* , 17, 279(1949).

12. J.H. Hilderbrand and R.L. Scott, *"The Solubility of Noneletrolites"* , 3rd. edn., Van Nostrand-Reinhold, Princeton, N.J., 1950.

13. J.H. Hilderbrand and R.L. Scott, *"Regular Solutions"* , Prentice Hall, Englewood Cliffs, N.J., 1962.

14. D.R. Paul and S. Newman, *"Polymer Blends-I"* , Academic Press, 1978.

15. K.C. Hoy, *J. Paint Technol.* , 42, 76(1970).

16. G.I. Taylor, *Proc. Roy. Soc.* , A146, 501(1934).

17. S. Wu, *Polym. Eng. Sci.* , 27(5), 335(1987).

18. B.J. Bentley and L.G. Leal, *J. Fluid Mech.*, 167, 241(1986).

19. C.E. Chaffey and H. Brenner, *J. Coll. Sci.* , 24, 258(1967).

20. D. Barthe's -Biesel and A. Acrivos, *J. Fluid Mech.*, 61, 1(1973).

21. R.G. Cox, *J. Fluid Mech.*, 37(3), 601(1969).

22. H.J. Karam and J.C. Bellinger, *Ind. Eng. Chem. Fundam.* , 7(4), 576(1968).

23. R.W. Flumerfelt, *Ind. End. Chem. Fumdam.* , 11(3), 312(1972).

24. S. Torza, R.G. Cox, and S.G. Mason, *J. Colloid Interface Sci.* , 23(2), 395(1972).

25. H. Vanoene, *J. Colloid Interface Sci.* , 40(3), 448(1972).

26. Han and Funatsu, *J. Rheo.* , 22(2), 113(1978).

27. Han and Chin, *J. Rheo.* , 23(5), 557(1979).

28. Han and Chin, *J. Rheo.* , 24(1), 1(1980).

29. J.J. Elmendorp and R.J. Maalke, *Polym. Eng. Sci.* , 25, 1041(1985).

30. J.J. Elmendorp, *Polym. Eng. Sci.* , 26, 418(1986).

31. G.I. Taylor, *Proc. 11th Int. Cong. of Applied Mech.* , 1964.

32. J. Buckmaster, *J. Fluid Mech.*, 55, 385(1972).

33. J. Buckmaster, *J. Appl. Mech.* , E40, 18(1973).

34. A. Acrivos and T.S. Lo, *J. Fluid Mech.*, 86, 641(1978).

35. F.D. Rumsheidt and S.G. Mason, *J. Coll. Sci.* , 16, 238(1981).

36. T. Tavgac, Ph.D Thesis, Univ. of Houston, Houston, TX, 1972.

37. W.K. Lee, Ph.D Thesis, Univ. of Houston, Houston, Tx, 1972.

38. S. Wu, *Polym. Eng. Sci.* , 27(5), 335(1987).

39. B.D. Favis and J.P. Chalfoux, *Polym. Eng. Sci.* , 27(20), 1591(1987).

40. S. Tomotika, *Proc. Roy. Soc.* , A150, 322(1935).

41. S. Tomotika, *Proc. Roy. Soc.* , A153, 302(1936).

42. A.P. Plochocki, *Adv. Polym. Tech.* , 2(4), 267(19).

43. M.V. Tsebrenko et. al., *Polym.* , 17, 831(1976).

44. M.V. Tsebrenko et. al., *Polym. Eng. Sci.* , 20(15), 1023(1980).

45. M.V. Tsebrenko et. al., *J. Non-Newt. Fluid Mech.* , 31, 1(1989).

46. G.V. Vinogradov et. al., *Polym.* , 16, 613(1975).

47. T.I. Ablazova et. al., *J. Appl. Polym. Sci.*, 19, 1781(1975).

48. V.E. Dreval et. al., *Rheol. Acta* , 22, 102(1983).

49. M.P. Zabugina et. al., *Int. J. Polym. Mater.* , 10, 1(1983).

50. S. Danesi and R.S. Porter, *Polym.* , 19, 448(1978).

References 295

51. D. Heikens and W. Barenstein, *Polym.* , 18, 69(1977).

52. Y.P. Miroshnikov and H.L. Williams, *Polym. Sci. U.S.S.R.* , 24(8), 1811(1982).

53. K. Min., J.L. White, and J.F. Fellers, *Polym. Eng. Sci.* , 24(17), 1327(1984).

54. W. Berger, H.W. Kammer, and C. Kummerlowe, *Macromol. Chem., Suppl.* , 8, 107(1984).

55. N.P. Kransnikova et.al., *J. Appl. Polym. Sci.*, 22, 2081(1978).

56. C.D. Han, Y.W. Kim, and S.J. Chen, *J. Appl. Polym. Sci.*, 19,2831(1975).

57. D.A. Tree and A.J. McHugh, *Int. Polym. Proc. II* , 3/4, 223(1988).

58. S.L. Sakellarides and A.J. McHugh, *Polym. Eng. Sci.* , 25(18), 1179(1985).

59. S.L. Sakellarides and A.J. McHugh, *Polym. Eng. Sci.* , 27(22), 1662(1987).

60. B.L. Lee and J.L. White, *Transc. Soc. Rheo.* , 19(3), 481(1975).

61. C.D. Han, *"Multiphase Flow in Polym. Process."* , Academic Publ., 1981.

62. S.Y. Hobbs, M.E.J. Dekkers, and V.H. Watkins, *Polym.* , 29, 1598(1988).

63. Ph. Teyessie, *Macromol. ol. Chem., Macromol. Symp.* , 22, 83(1988).

64. Ph. Teyessie, R. Fayt, and R. Jerome, *Macromol. Chem., Macromol. Symp.* , 16, 41(1988).

65. A.K. Van Der Vegt and J.J. Elmendorp in, *Integ. Funda. Polym. Sci. Tech.* , P.J. Lemstra (ed.),

66. J. Lyngaae-Jorgensen, *Org. Coat. Plast. Chem.* , 45, 174(1981).

67. N. Alle and J. Lyngaae-Jorgensen, *Rheo. [Proc. Int. Congr.]* , 8th, vol. 2, G. Astarita (ed.), ,1980.

68. J.L.-Jorgensen, F.E. Andersen, and N. Alle in, *"Polymer Alloys"* , D. Klempner and K.C. Frisch (eds.), Plenum Press, N.Y., 1983.

69. E.B. Priestly, P.J. Wojtowicz, and P. Sheng (eds.), *"Introduction to Liquid Crystals"* , Plenum Press, N.Y., 1974.

70. S. Chandrashekhr, *"Liquid Crystals"* , Cambridge University Press, Cambridge, 1977.

71. K.F. Wissburn, *J. Rheo.*, 25(6), 619(1981).

72. G.V. Vinogradov et al., *Inter. J. Polym. Mater.*, 9, 187(1982).

73. J.R. Tuttle, H.E. Bartony Jr., and R.W. Lenz, *Polym. Eng. Sci.*, 27(15), 1156(1987).

74. S. Onagi and T. Asada, *"Rheolog"* , Vol. I, G. Astarita, G. Marrucc and L. Nicolais (eds.), Plenum Press, N.Y., 1980.

75. D.G. Baird in *"Polymeric Liquid Crystals"* , A. Blumstein (ed.), Plenum Press, N.Y., 1985.

76. K.F. Wissburn, G. Kiss, and F.N. Cogswell. *Chem. Eng. Commu.*, 53, 149(1987).

77. H. Sugiyama et al., *J. Appl. Polym. Sci.*, 30, 2329(1985).

78. K.F. Wissburn, *Brit. Polym. J.*. December, 163(1980).

79. D.G. Baird, *J. Rheo.*, 24(4), 465(1980).

80. R.K. Mishra, *Mol. Cryst. Liq. Cryst.*, 29, 201(1975).

81. R.B. Bird, R.C. Armstrong, and L. Hassager, *"Dynamics of Polymeric Liquids"* , Vol. I, John Wiley Publications, N.Y., 1977.

82. K.F. Wissburn and A.C. Griffin, *J. Polym. Sci., Polym. Phys. Edn.*, 20, 1835(1982).

83. A. Blumstein, O. Thomas, and S. Kumar, *J. Polym. Sci., Polym. Phys. Edn.*, 24, 27(1986).

84. G. Kiss, *J. Rheo.*, 30(3), 585(1986).

85. A. Bickel, M.T. Shaw, and E.T. Samulski, *J. Rheo.*, 28, 647(1984).

86. S. Suto, J.L. White, and J.F. Fellers, *Rheol. Acta.*, 21, 62(1982).

87. D.A. Simoff and R.S. Porter, *Mol. Cryst. Liq. Cryst.*, 110, 1(1984).

88. D. Done, Ph.D. Dissertation, Virginia Polytechnic Institute and State University, 1986.

89. D. Done and D.G. Baird, *Polym. Eng. Sci.*, 27(11), 816(1987).

90. F.N. Cogswell, *The Brit. Polym. J.*, December, 170(1980).

91. G.G. Viola, D. Done and D.G. Baird, 619, SPE, ANTEC 1985.

92. Y.G. Lin and H.H. Winter, *Macromol.*, 21, 2439 (1988).

93. F.N. Cogswell in *"Recent Advances in Liquid Crystal Polymers"* , L.L. Chapoy (ed.), Elsevier, London, 1985.

94. G. Menges and G. Hahn, *Mod. Plast.*, 56, October, (1981).

95. D. Acierno et al., *Macromol.*, 15(6), 1455(1982).

96. E. Suokas, *Polym.*, 30, 1105(1989).

97. Z. Ophir and Y. Ide, *Polym. Eng. Sci.*, 23(14), 792(1983).

98. Y. Ide and Z. Ophir, *Polym. Eng. Sci.*, 23(5), 261(1983).

99. W.J. Jackson Jr. and H.F. Kuhfuss, *J. Polym. Sci., Polym. Chem. Ed.*, 14, 2043(1976).

100. M.K. Cox, *Mol. Cryst. Liq. Cryst.*, 153, 415(1987).

101. T.S. Chung, *J. Polym. Sci. Lett.*, 24, 299(1986).

102. H. Muramatsu and W.R. Krigbaum, *J. Polym. Sci., Polym. Phys.*, B-24, 1695(1986).

103. H. Muramatsu and W.R. Krigbaum, *J. Polym. Sci., Polym. Phys.*, B-25, 803(1987).

104. D.N. Lewis and J.F. Fellers, *"Processing of Polymer Liquid Crystals"*, PATRA Report no. 233, April 1986.

105. T.Y. Tam, M.B. Boone and G.C. Weedon, *Polym. Eng. Sci.* 28(13), 871(1988).

106. A.E. Zachariades and J.A. Logan, *Polym. Eng. Sci.* 23, 797(1983).

107. F.P. La Mantia and A. Valenza, *Polym. Eng. Sci.* 29(10), 625(1989).

108. T.S. Chung, *Polym. Eng. Sci.*, 26(13), 901(1986).

109. A. Siegmann, A. Dagan and S. Kenig, *Polym.*, 26, 1325(1985).

110. T.S. Chung, SPE 45th ANTEC, Conf. Proc., Los Angeles, 1404(1987).

111. A.I. Isayev and M. Modic, *Polym. Compos.*, 8(3), 158(1987).

112. K.G. Blizard and D.G. Baird, *Polym. Eng. Sci.* , 27(9), 653(1987).

113. Y. Ide, U.S. Patent-4,468,364 to Celanese Corporation, 1984.

114. R. Ramanathan, K.G. Blizard and D.G. Baird, SPE 45th ANTEC, Conf. Proc., Los Angeles, 1399(1987).

115. R. Ramanathan, K.G. Blizard and D.G. Baird, SPE 46th ANTEC, Conf. Proc., Atlanta, 1123(1988).

116. P. Zhuang, T. Kyu and J.L. White, *Polym. Eng. Sci.* 28(17), 1095(1988).

117. E. Amendola, C. Carfugna, L. Nicodemo and M.R. Nobile, *Macromol. Chem., Macromol. Symp.* , 23, 253(1989).

118. K. Friedrich, M. Hess and R. Kosfeld *Macromol. Chem., Macromol. Symp.* , 16, 251(1988).

119. T. Kyu and P. Zhuang, *Polym. Commu.*, 29, 99(1988).

120. E.G. Joseph, G.L. Wilkes and D.G. Baird in *"Polymeric Liquid Crystals"*, A. Blumstein (ed.), Plenum Press, New York, 1985.

121. A.M. Sukhadia, D. Done and D.G. Baird, SPE 47th ANTEC, Conf. Proc., New York, 1847(1989).

122. S.H. Jung and S.C. Kim, *Polym. Jour.*, 20(1), 73(1988).

123. M.R. Nobile et al., *Polym. Eng. Sci.* 29(4), 244(1989).

124. S.K. Bhattacharya, A. Tendolkar and A. Misra, *Mol. Cryst. Liq. Cryst.*, 153, 501(1987).

125. S Swaminathan and A.I. Isayev, *Poly. Mater. Sci. Eng.*, 57, 330(1987).

126. D. Beery, A. Siegmann and S. Kenig, *Jour. Mater. Sci. Lett.* , 7, 1071(1988).

127. R.A. Weiss, W. Huh and L. Nicolais, *Polym. Eng. Sci.*, 27(9), 684(1987).

128. T.M. Malik, P.J. Carreau and N. Chapleau, *Polym. Eng. Sci.*, 29(29), 600(1989).

129. S.G. James, A.M. Donald and W.A. MacDonald, *Mol. Cryst. Liq. Cryst.*, 153, 491(1987).

130. PET Product Manual- Cleartuff, Goodyear Tire and Rubber Company, Akron, Ohio, 1989.

131. G.W. Calundahn and M. Jaffe, *Proc. Robert A. Welch Fond. Conf. Chem. Res., Res. Conf. XXVI*, Synthetic Polymers, 1982.

132. S.J. Chen and W.E. Segl, SPE 32nd ANTEC, May, 1974.

133. Chemineer, Inc., Bulletin #806.

134. J.W. Barlow and D.R. Paul, *Polym. Eng. Sci.*, 21(15), 985(1981).

135. D.B. Baird in *"Polymeric Liquid Crystals"*, A. Blumstein (ed.), Plenum Press, New York, 1985.

136. F.N. Cogswell, U.S. Patent-4.433,083, submitted to ICI, London, England, 1984.

137. L.E. Nielsen, *"Predicting the properties of Mixtures"*, Marcel Dekker, Inc., New York, 1978.

138. R. Mehta, Masters Thesis, Virginia Polytechnic Institute and State University, 1989.

139. Rheometrics Inc., *Rheometrics Mechanical Spectrometer Operations Manual*, Union, New Jersey (1989).

140. D. Done and D.G. Baird, ***Polym. Eng. Sci.***, 30 (16), 989 (1990).

141. L.E. Alexander, *X-Ray Diffraction Methods in Polymer Science* , Wiley-Interscience, New York, 1969.

142. Chemineer Inc., Kenics Static Mixer, KTEK Series, May, 1988.

143. M.H. Paul and E. Muschelknautz, ***Inter. Chem. Engg.***, 22 (2), 197 (1982).

144. V. Novak, V. Jandourek and F. Rieger, ***5th European Conference on Mixing***, West Germany, Poster # 23, June, 1985.

145. S.J. Chen, SPE ANTEC, Conf. Proc., Montreal, 258 (1973).

146. T.S. Tung, Ph.D. Dissertation, Univ. of Massachusetts, 1976.

147. HX-4000 Series. Products and Properties Guide. DuPont Nemours & Company.

148. C.E. McChesney and J.R. Dole, ***Modern Plastics***, January, 112 (1988).

149. M. Kimura and R.S. Porter, ***J. Polym. Sci., Polym. Phys. Ed.***, 22, 1697 (1984).

150. B.R. Bassett and A.F. Yee, ***Polym. Compos.***, 11(1), 10 (1990).

151. T. Katoh and N.R. Schott, ***SPE (ANTEC), Conf. Proc.***, 1861 (1990).

152. F.P. La Mantia, A. Valenza, M. Paci and P.L. Magagnini, ***Polym. Eng. Sci.***, 30(1), 7 (1990).

153. P.R. Subramaniam and A.I. Isayev, ***SPE (ANTEC), Conf. Proc.***, 489 (1990).

154. K.G. Blizard, C. Federici, O. Federico and L.L Chapoy, ***Polym. Eng. Sci.***, 30(22), 1442 (1990).

155. D.S. Kalika, D.W. Giles and M.M. Denn, ***J. Rheol.***, 34(2), 139 (1990).

156. Y.G. Lin and H.H. Winter, ***Liq. Cryst.***, 3(5), 593 (1988).

157. Y.G. Lin and H.H. Winter, ***Liq. Cryst.***, 3(4), 519 (1988).

158. D. Done and D.G. Baird, ***Polym. Eng. Sci.***, 30(16), 989 (1990).

159. G. Crevecoeur and G. Groeninckx, ***Polym. Eng. Sci.***, 30(9), 532 (1990)

160. Vectra A900 Data Sheet, Publication # 113, Celanese Specialty Operations, Celanese Corporation, 1989.

161. H.E.H. Meijer, P.J. Lemstra and P.H.M. Elemans, ***Macromol. Chem., Macromol. Symp.***, 16, 113 (1988).

162. K.G. Blizard, Masters Thesis, Virginia Polytechnic Institute and State University, 1986.

163. K.G. Blizard, Ph.D. Dissertation, Virginia Polytechnic Institute and State University, 1988.

164. A. Datta et al., ***SPE (ANTEC), Conf. Proc.***, 1991.

165. S. Middleman, *Fundamentals of Polymer Processing*, McGraw Hill, Inc., pg. 429. N.Y., 1977

166. E.C. Bernhardt (ed.), *Processing of Thermoplastic Materials* , Reinhold Publishers, N.Y., 1959.

167. L.C. Burmeister. *Convective Heat Transfer* , John Wiley & Sons, N.Y., 1983.

168. W.L. Wilkinson. *Non-Newtonian Fluids: Fluid Mechanics, Mixing and Heat Transfer* , Chapter 4, Pergamon Press, N.Y., 1960.

169. D. Bigg and S. Middleman, *Ind. Eng. Chem. Fundam.*, 13(1), 66 (1974).

170. R.H. Christopher and S. Middleman, *Ind. Eng. Chem. Fundam.*, 4(4), 422 (1965).

171. L. Mascia, *Thermoplastics Materials Engineering*. Elsevier, New York, 1989.

172. J.T. Lutz (ed.), *Thermoplastic Polymers and Additives: Theory and Practice*, Marcel Dekker, Inc., New York, 1989.

173. J.D. Muzzy. X. Wu and J.S. Colton, *Polym. Compos.*, 11(5), 280 (1990).

174. Z. Tadmor and C.G. Gogos, *Principles of Polymer Processing*, John Wiley & Sons, New York, 1979.

175. M.C. Gabriele. *Plast. Technol.* , April. 92 (1990).

Appendix A. Design Data

Table 18. Summary of dimensions of the different piping sections used in the dual-extruder mixing method.

Part No. {1}	Length (inch)	Diameter (inch)	Internal Volume Inch³	Residence Time {2} seconds
1	2.0	0.375	0.2208	3.83
2	2.0	0.75	0.8836	15.33
3	6.5	0.5625	1.6153	28.03
4	3.5	0.5625	0.8697	15.09
5	3.5	0.5625	0.8697	15.09
6	17.0	0.494	3.4	58.99
7	1.25	0.375	0.138	2.39
8	5	0.5625	1.2425	21.56

{1} = See Figs. 27 and 28
{2} = Sample calculation for pure PET run through the system at a flow rate of 0.0576 inch³/sec.

TOP VIEW

4.0

2.5

4.0

SIDE VIEW

1.0

0.75

1.0

0.3125

0.1875

L=0.585

H=0.060

4.0

ALL DIMENSIONS IN INCHES
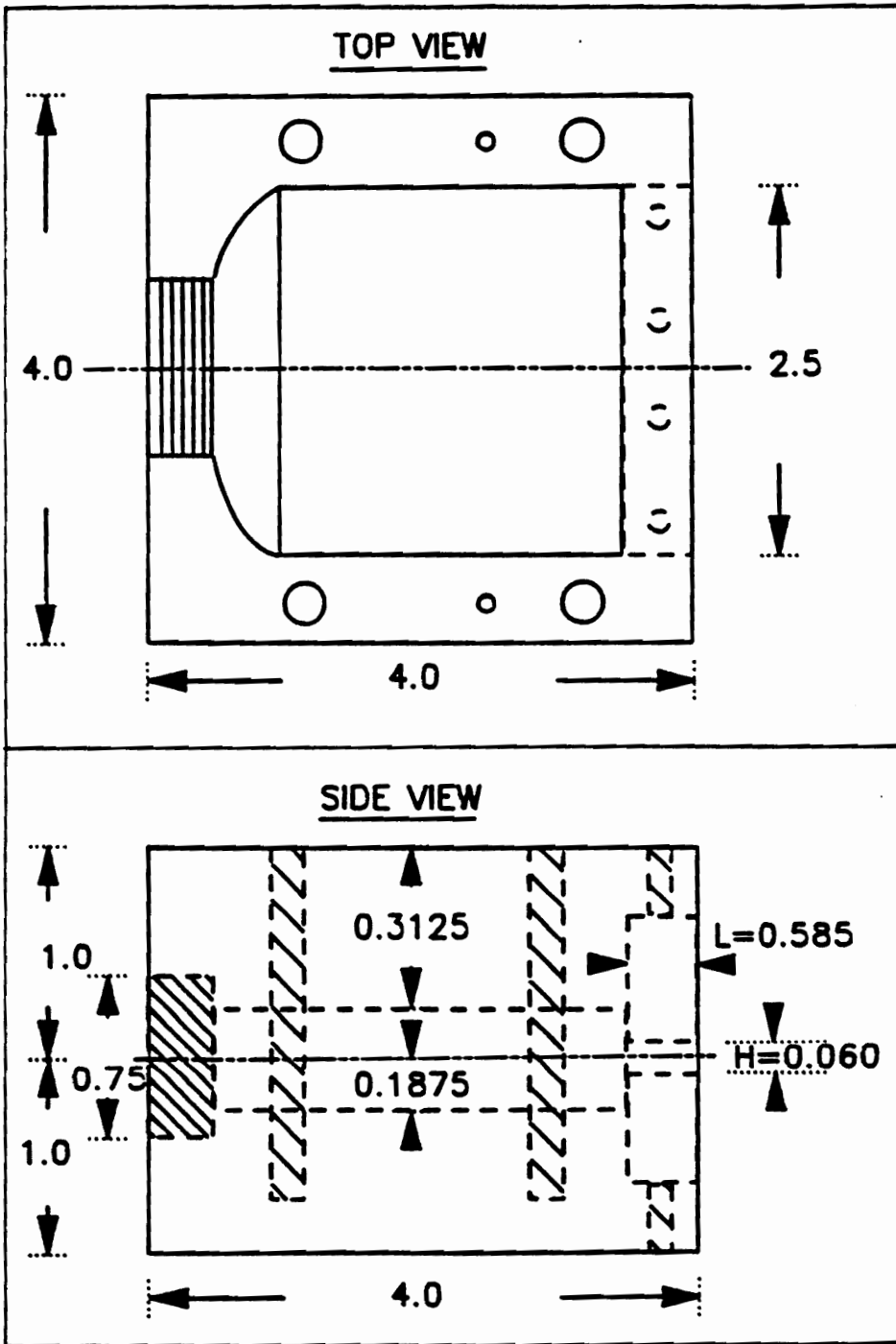
Figure 102.   Dimensions of the 2.5″ sheet die.
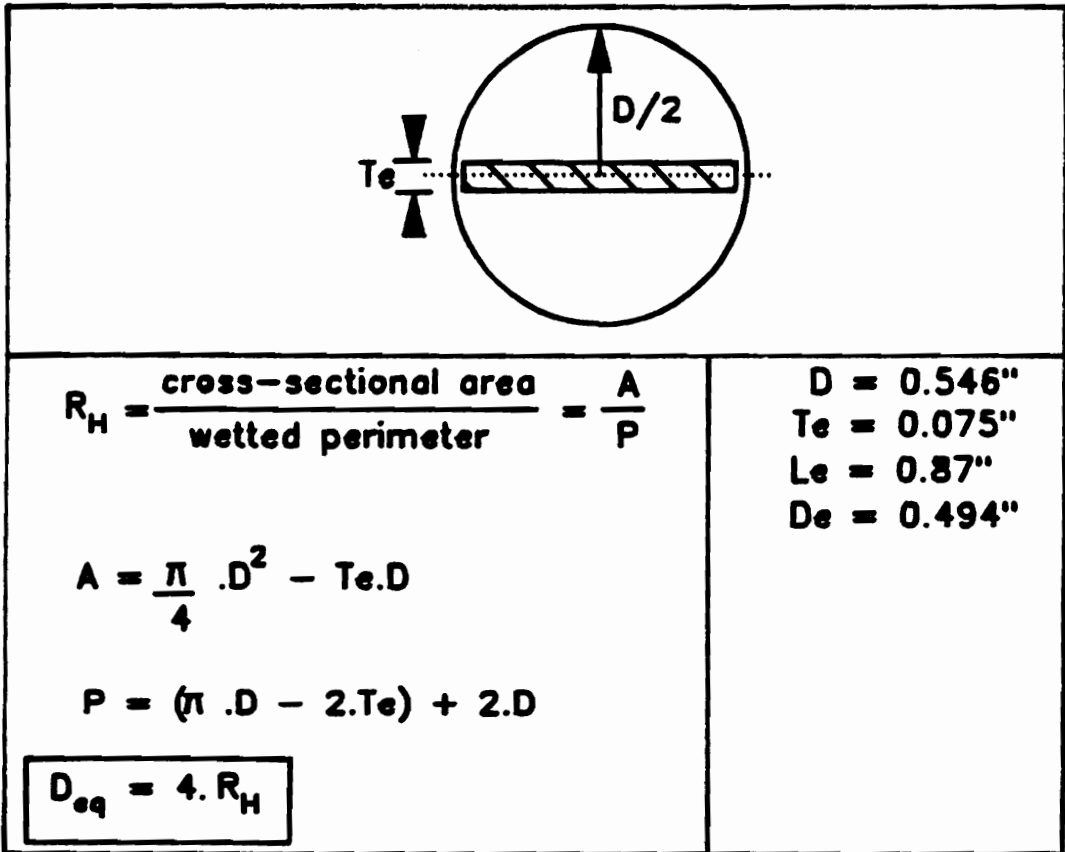
Figure 103. Calculation of the hydraulic radius of the static mixer.

Table 19. Physical properites of PET and Vectra A900.

Poly(ethylene terephthalate) (PET) [1]

- Thermal conductivity. $k = 3.36$ E-4 cal/(gm sec °C)
- Heat capacity for molten polymer (270-290°C). $Cp = 0.3243 + 0.000565T$ cal/(gm °C): $(T = °C)$
- Melt density, $\rho = 1.2$ gms/cm^3

Vectra A900 [2],[3]

- Thermal conductivity at 250°C, $k = 4.20$ E-4 cal/(gm sec °C)
- Heat capacity at 300°C, $Cp = 0.45$ cal/(gm °C)
- Melt density at 300°C, $\rho = 1.27$ gms/cm^3

[1] = Cleartuf Polyester Product Manual, Goodyear Polyesters.
[2] = Vectra LCP Technical Data Sheet, Engineering Plastics Division, Hoechst Celanese Corporation.
[3] = K.F. Wissburn, G. Kiss and F.N. Cogswell, **Chem. Eng. Comm.**, 53. 149 (1987).
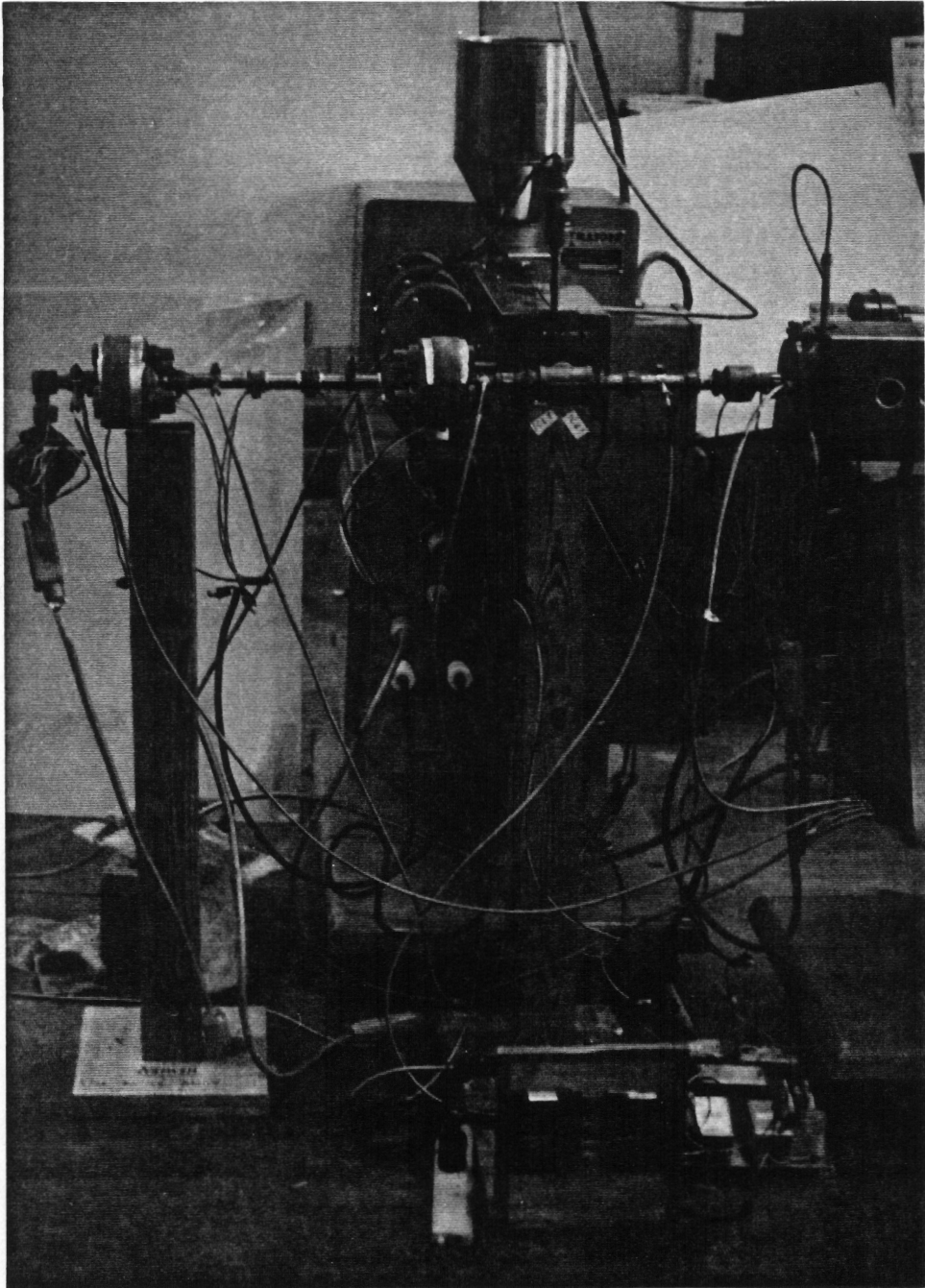
Figure 104.   Photograph of the dual-extruder mixing method: side view.
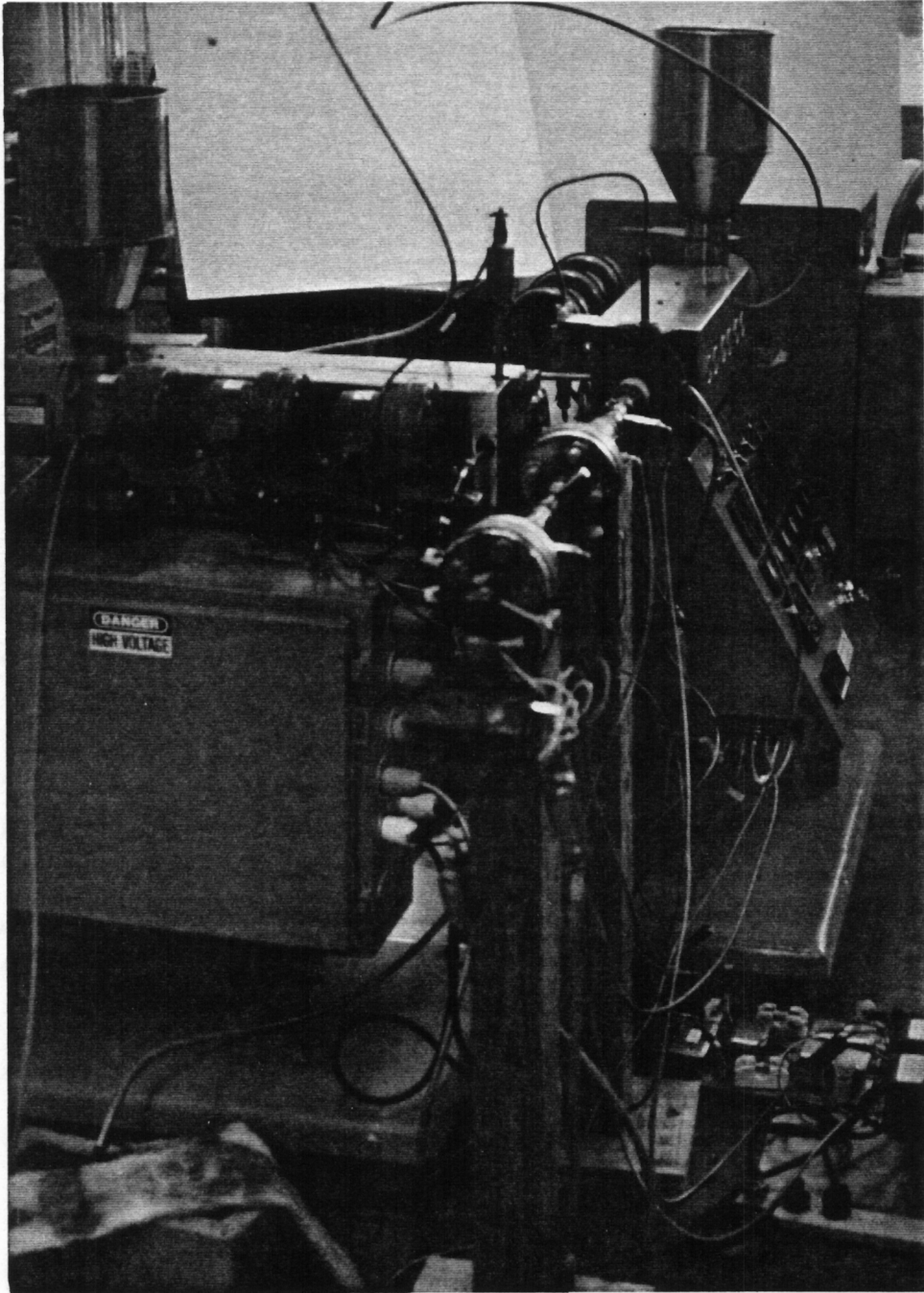
Figure 105. Photograph of the dual-extruder mixing method: front view.

Appendix B. Tensile Test Data

Table 20. Tensile properties of PET/LCP60-80 and PET/LCP60 blend sheets.

MATERIAL	TENSILE MODULUS* [GPa]	TENSILE STRENGTH* [MPa]
PET	2.80 (0.18)	71.22 (2.86)
PET/LCP60-80 98/2	2.50 (0.14)	61.74 (5.88)
PET/LCP60-80 95/5	3.04 (0.05)	81.90 (4.82)
PET/LCP60-80 90/10	4.41 (0.37)	104.38 (4.35)
PET/LCP60-80 80/20	2.87 (0.12)	82.78 (4.74)
PET/LCP60-80 70/30	2.45 (0.14)	41.37 (3.19)
PET/LCP60 80/20	3.20 (0.17)	63.72 (2.12)
PET/LCP60 70/30	4.08 (0.28)	58.98 (4.21)

*Standard deviations are given in parenthesis

Table 21.   Flexural moduli of injection molded plaques of PET/Vectra A blends.

MATERIAL	FLEXURAL MODULUS★ [GPa]
PET/Vectra A 100/0	2.20 (0.25)
PET/Vectra A 80/20	4.55 (0.25)
PET/Vectra A 40/60	12.41 (0.43)
PET/Vectra A 30/70	15.49 (0.67)
PET/Vectra A 20/80	13.12 (0.66)
PET/Vectra A 0/100	12.66 (0.63)

★Standard deviations are given in parenthesis

Appendix C. Rheological Data

NO.	G′ (Pa)	G″ (Pa)	ETA* (Pa.s)	TORQUE (g.cm)	TEMP (°C)	FREQ (rad/s)
			Table 22. Dynamic frequency sweep data for pure PET at 280°C.			

NO.	G′ (Pa)	G″ (Pa)	ETA* (Pa.s)	TORQUE (g.cm)	TEMP (°C)	FREQ (rad/s)
1	2.246e+00	3.646e+02	3.646e+03	1.065e+00	278.9	1.000e-01
2	2.425e+01	7.410e+02	3.441e+03	2.166e+00	280.1	2.154e-01
3	5.968e+01	1.547e+03	3.334e+03	4.522e+00	280.4	4.642e-01
4	1.822e+02	3.245e+03	3.250e+03	9.499e+00	280.1	1.000e+00
5	5.714e+02	6.758e+03	3.148e+03	1.984e+01	280.2	2.154e+00
6	1.731e+03	1.382e+04	3.000e+03	4.080e+01	280.2	4.641e+00
7	5.026e+03	2.755e+04	2.800e+03	8.228e+01	280.1	1.000e+01
8	1.368e+04	5.291e+04	2.537e+03	1.612e+02	280.2	2.154e+01
9	3.409e+04	9.607e+04	2.196e+03	2.996e+02	280.3	4.641e+01
10	7.579e+04	1.617e+05	1.786e+03	4.857e+02	280.2	9.999e+01
11	1.407e+05	2.396e+05	1.290e+03	5.521e+02	280.1	2.154e+02
12	1.152e+05	1.584e+05	4.221e+02	2.090e+02	280.1	4.641e+02

NO.	G′ (Pa)	G″ (Pa)	ETA* (Pa.s)	TORQUE (g.cm)	TEMP (°C)	FREQ (rad/s)
1	6.427e+00	2.771e+02	2.772e+03	8.096e-01	290.3	1.000e-01
2	7.036e+00	5.765e+02	2.676e+03	1.684e+00	289.8	2.154e-01
3	2.343e+01	1.211e+03	2.610e+03	3.539e+00	289.9	4.642e-01
4	9.747e+01	2.571e+03	2.573e+03	7.515e+00	289.8	1.000e+00
5	3.629e+02	5.407e+03	2.515e+03	1.583e+01	289.8	2.154e+00
6	1.168e+03	1.118e+04	2.421e+03	3.285e+01	289.8	4.641e+00
7	3.549e+03	2.258e+04	2.286e+03	6.681e+01	289.8	1.000e+01
8	1.008e+04	4.409e+04	2.099e+03	1.319e+02	289.7	2.154e+01
9	2.612e+04	8.163e+04	1.847e+03	2.468e+02	289.7	4.641e+01
10	6.032e+04	1.402e+05	1.526e+03	4.105e+02	289.8	9.999e+01
11	1.161e+05	2.115e+05	1.120e+03	5.167e+02	289.7	2.154e+02
12	9.853e+04	1.395e+05	3.681e+02	2.821e+02	289.7	4.641e+02

Table 23. Dynamic frequency sweep data for pure PET at 290°C.

NO.	G' (Pa)	G" (Pa)	ETA* (Pa.s)	TORQUE (g.cm)	TEMP (°C)	FREQ (rad/s)
Table 24. Dynamic frequency sweep data for pure PET at 265°C, upon cooling from 290 °C.						
1	9.136e+00	3.099e+02	3.100e+03	9.694e-01	264.7	1.000e-01
2	2.410e+01	7.114e+02	3.304e+03	2.226e+00	265.4	2.154e-01
3	7.551e+01	1.524e+03	3.288e+03	4.773e+00	265.5	4.642e-01
4	2.349e+02	3.281e+03	3.289e+03	1.029e+01	265.5	1.000e+00
5	6.939e+02	6.905e+03	3.221e+03	2.171e+01	265.5	2.154e+00
6	2.070e+03	1.421e+04	3.094e+03	4.491e+01	265.5	4.641e+00
7	5.914e+03	2.832e+04	2.893e+03	9.045e+01	265.5	1.000e+01
8	1.583e+04	5.389e+04	2.607e+03	1.751e+02	265.5	2.154e+01
9	3.855e+04	9.605e+04	2.230e+03	3.177e+02	265.5	4.641e+01
10	8.346e+04	1.571e+05	1.779e+03	5.091e+02	265.5	1.000e+02

NO.	G′ (Pa)	G″ (Pa)	ETA* (Pa.s)	TORQUE (g.cm)	TEMP (°C)	FREQ (rad/s)
1	5.347e+04	4.584e+04	7.043e+05	1.072e+02	289.8	1.000e-01
2	7.066e+04	5.459e+04	5.021e+05	1.346e+02	289.8	1.778e-01
3	9.002e+04	6.132e+04	3.444e+05	1.625e+02	289.8	3.162e-01
4	1.119e+05	6.452e+04	2.297e+05	1.907e+02	289.8	5.623e-01
5	1.326e+05	6.630e+04	1.483e+05	2.167e+02	289.9	1.000e+00
6	1.550e+05	6.683e+04	9.493e+04	2.439e+02	289.9	1.778e+00
7	1.763e+05	6.860e+04	5.982e+04	2.708e+02	290.0	3.162e+00
8	1.990e+05	7.184e+04	3.763e+04	3.000e+02	290.1	5.623e+00
9	2.238e+05	7.733e+04	2.368e+04	3.324e+02	290.2	9.999e+00
10	2.517e+05	8.529e+04	1.495e+04	3.689e+02	290.1	1.778e+01
11	2.823e+05	9.641e+04	9.434e+03	4.077e+02	290.1	3.162e+01

Table 25. Dynamic frequency sweep data for pure Vectra A900 at 290°C.

NO.	G′ (Pa)	G″ (Pa)	ETA* (Pa.s)	TORQUE (g.cm)	TEMP (°C)	FREQ (rad/s)
Table 26.	Dynamic frequency sweep data for pure Vectra A900 at 300°C.					
1	1.716e+04	1.458e+04	2.252e+05	3.493e+01	299.0	1.000e-01
2	2.101e+04	1.465e+04	1.440e+05	3.965e+01	299.4	1.778e-01
3	2.461e+04	1.515e+04	9.140e+04	4.466e+01	299.3	3.162e-01
4	2.893e+04	1.602e+04	5.881e+04	5.099e+01	299.4	5.623e-01
5	3.321e+04	1.738e+04	3.749e+04	5.768e+01	299.4	1.000e+00
6	3.863e+04	1.899e+04	2.421e+04	6.606e+01	299.4	1.778e+00
7	4.451e+04	2.131e+04	1.561e+04	7.557e+01	299.4	3.162e+00
8	5.151e+04	2.425e+04	1.012e+04	8.698e+01	299.4	5.623e+00
9	5.975e+04	2.800e+04	6.599e+03	1.006e+02	299.4	9.999e+00
10	6.954e+04	3.262e+04	4.320e+03	1.167e+02	299.4	1.778e+01
11	8.086e+04	3.841e+04	2.831e+03	1.353e+02	299.4	3.162e+01
12	9.398e+04	4.538e+04	1.856e+03	1.549e+02	299.4	5.623e+01
13	1.089e+05	5.365e+04	1.214e+03	1.704e+02	299.4	1.000e+02

NO.	G' (Pa)	G" (Pa)	ETA* (Pa.s)	TORQUE (g.cm)	TEMP (°C)	FREQ (rad/s)
Table 27.	Dynamic frequency sweep data for pure Vectra A900 at 320°C.					
1	2.155e+02	1.026e+02	2.387e+03	3.727e-01	320.0	1.000e-01
2	1.603e+02	1.453e+02	1.217e+03	3.379e-01	320.6	1.778e-01
3	2.176e+02	1.555e+02	8.458e+02	4.177e-01	320.8	3.162e-01
4	2.596e+02	2.504e+02	6.415e+02	5.634e-01	320.8	5.623e-01
5	2.945e+02	3.690e+02	4.721e+02	7.376e-01	320.9	1.000e+00
6	3.793e+02	5.913e+02	3.951e+02	1.098e+00	320.9	1.778e+00
7	4.791e+02	8.822e+02	3.175e+02	1.572e+00	320.9	3.162e+00
8	7.253e+02	1.414e+03	2.827e+02	2.493e+00	320.9	5.623e+00
9	9.888e+02	2.178e+03	2.392e+02	3.764e+00	321.0	9.999e+00
10	1.541e+03	3.316e+03	2.056e+02	5.788e+00	320.9	1.778e+01
11	2.497e+03	5.108e+03	1.798e+02	9.031e+00	321.0	3.162e+01
12	3.947e+03	7.589e+03	1.521e+02	1.346e+01	321.0	5.623e+01
13	6.146e+03	1.093e+04	1.254e+02	1.855e+01	320.9	1.000e+02

NO.	G′ (Pa)	G″ (Pa)	ETA* (Pa.s)	TORQUE (g.cm)	TEMP (°C)	FREQ (rad/s)
1	1.009e+02	6.697e+01	1.211e+03	3.783e-01	330.1	1.000e-01
2	1.271e+02	9.273e+01	7.303e+02	4.914e-01	330.2	2.154e-01
3	1.613e+02	1.468e+02	4.699e+02	6.813e-01	330.2	4.642e-01
4	2.142e+02	2.354e+02	3.183e+02	9.942e-01	330.2	1.000e+00
5	2.968e+02	3.955e+02	2.295e+02	1.545e+00	330.2	2.154e+00
6	4.261e+02	6.680e+02	1.707e+02	2.478e+00	330.2	4.641e+00
7	6.464e+02	1.138e+03	1.309e+02	4.098e+00	330.3	1.000e+01
8	1.059e+03	1.977e+03	1.041e+02	7.031e+00	330.2	2.154e+01
9	1.786e+03	3.329e+03	8.140e+01	1.178e+01	330.2	4.641e+01
10	3.054e+03	5.335e+03	6.148e+01	1.846e+01	330.2	9.999e+01
11	4.917e+03	7.579e+03	4.194e+01	2.526e+01	330.3	2.154e+02
12	3.476e+03	3.678e+03	1.090e+01	1.824e+01	330.3	4.641e+02

Table 28. Dynamic frequency sweep data for pure Vectra A900 at 330°C.

NO.	G′ (Pa)	G″ (Pa)	ETA* (Pa.s)	TORQUE (g.cm)	TEMP (°C)	FREQ (rad/s)
1	1.787e+02	1.376e+02	2.255e+03	3.520e-01	264.9	1.000e-01
2	2.306e+02	2.374e+02	2.088e+03	5.165e-01	264.9	1.585e-01
3	3.024e+02	3.726e+02	1.911e+03	7.490e-01	264.7	2.512e-01
4	4.561e+02	5.653e+02	1.824e+03	1.134e+00	264.7	3.981e-01
5	6.152e+02	8.716e+02	1.691e+03	1.665e+00	264.7	6.310e-01
6	8.768e+02	1.315e+03	1.580e+03	2.466e+00	264.1	1.000e+00
7	1.226e+03	1.949e+03	1.453e+03	3.592e+00	264.6	1.585e+00
8	1.762e+03	2.868e+03	1.340e+03	5.256e+00	264.6	2.512e+00
9	2.532e+03	4.138e+03	1.218e+03	7.575e+00	264.6	3.981e+00
10	3.684e+03	5.859e+03	1.097e+03	1.081e+01	264.6	6.310e+00
11	5.268e+03	8.230e+03	9.771e+02	1.528e+01	264.6	1.000e+01
12	7.414e+03	1.138e+04	8.569e+02	2.125e+01	264.6	1.585e+01
13	1.033e+04	1.552e+04	7.420e+02	2.915e+01	264.6	2.512e+01
14	1.418e+04	2.089e+04	6.342e+02	3.933e+01	264.6	3.981e+01
15	1.920e+04	2.778e+04	5.351e+02	5.181e+01	264.6	6.310e+01
16	2.569e+04	3.651e+04	4.465e+02	6.580e+01	264.5	1.000e+02

Table 29. Dynamic frequency sweep data for pure Vectra A900 at 265°C, upon cooling from 330°C.

NO.	G′ (Pa)	G″ (Pa)	ETA* (Pa.s)	TORQUE (g.cm)	TEMP (°C)	FREQ (rad/s)
1	1.490e+02	9.739e+01	1.780e+03	5.565e-01	284.5	1.000e-01
2	1.735e+02	1.401e+02	1.407e+03	6.972e-01	284.6	1.585e-01
3	1.839e+02	1.945e+02	1.066e+03	8.370e-01	284.7	2.512e-01
4	2.282e+02	2.732e+02	8.941e+02	1.113e+00	284.6	3.981e-01
5	2.626e+02	4.065e+02	7.670e+02	1.513e+00	284.6	6.310e-01
6	3.229e+02	5.509e+02	6.385e+02	1.997e+00	284.7	1.000e+00
7	4.143e+02	7.915e+02	5.636e+02	2.793e+00	284.6	1.585e+00
8	5.452e+02	1.129e+03	4.991e+02	3.921e+00	284.6	2.512e+00
9	7.150e+02	1.622e+03	4.452e+02	5.546e+00	284.6	3.981e+00
10	9.863e+02	2.332e+03	4.012e+02	7.926e+00	284.6	6.310e+00
11	1.401e+03	3.327e+03	3.610e+02	1.131e+01	284.5	1.000e+01
12	2.029e+03	4.660e+03	3.206e+02	1.593e+01	284.7	1.585e+01
13	2.915e+03	6.417e+03	2.806e+02	2.207e+01	284.6	2.512e+01
14	4.154e+03	8.614e+03	2.402e+02	2.983e+01	284.6	3.981e+01
15	5.804e+03	1.128e+04	2.011e+02	3.904e+01	284.6	6.310e+01
16	7.900e+03	1.437e+04	1.640e+02	4.881e+01	284.6	1.000e+02

Table 30. Dynamic frequency sweep data for pure Vectra A900 at 285°C, upon cooling from 330°C.

NO.	G′ (Pa)	G″ (Pa)	ETA* (Pa.s)	TORQUE (g.cm)	TEMP (°C)	FREQ (rad/s)
1	3.100e+03	6.382e+03	7.095e+04	2.214e+01	179.6	1.000e-01
2	5.003e+03	8.485e+03	6.215e+04	3.071e+01	179.7	1.585e-01
3	7.340e+03	1.094e+04	5.246e+04	4.102e+01	179.8	2.512e-01
4	1.057e+04	1.397e+04	4.401e+04	5.444e+01	179.8	3.981e-01
5	1.459e+04	1.747e+04	3.607e+04	7.056e+01	179.8	6.310e-01
6	1.988e+04	2.138e+04	2.920e+04	9.022e+01	179.8	1.000e+00
7	2.659e+04	2.549e+04	2.324e+04	1.133e+02	179.7	1.585e+00
8	3.447e+04	2.989e+04	1.816e+04	1.399e+02	179.8	2.512e+00
9	4.387e+04	3.437e+04	1.400e+04	1.700e+02	179.7	3.981e+00
10	5.471e+04	3.879e+04	1.063e+04	2.034e+02	179.7	6.310e+00
11	6.694e+04	4.304e+04	7.958e+03	2.399e+02	179.7	1.000e+01
12	8.034e+04	4.698e+04	5.872e+03	2.787e+02	179.8	1.585e+01
13	9.495e+04	5.057e+04	4.283e+03	3.195e+02	179.8	2.512e+01
14	1.104e+05	5.370e+04	3.085e+03	3.600e+02	179.7	3.981e+01
15	1.264e+05	5.630e+04	2.193e+03	3.950e+02	179.8	6.310e+01
16	1.418e+05	5.794e+04	1.532e+03	4.145e+02	179.7	1.000e+02

Table 31. Dynamic frequency sweep data for pure PP at 180°C.

NO.	G′ (Pa)	G″ (Pa)	ETA* (Pa.s)	TORQUE (g.cm)	TEMP (C)	FREQ (rad/s)
1	2.284e+03	5.103e+03	5.591e+04	3.484e+00	199.8	1.000e-01
2	4.728e+03	8.232e+03	4.406e+04	5.909e+00	200.1	2.154e-01
3	9.165e+03	1.267e+04	3.370e+04	9.704e+00	200.1	4.642e-01
4	1.591e+04	1.850e+04	2.441e+04	1.507e+01	200.1	1.000e+00
5	2.619e+04	2.521e+04	1.687e+04	2.231e+01	200.0	2.154e+00
6	4.022e+04	3.266e+04	1.116e+04	3.156e+01	200.0	4.641e+00
7	5.844e+04	4.014e+04	7.090e+03	4.278e+01	200.1	1.000e+01
8	8.036e+04	4.704e+04	4.323e+03	5.551e+01	200.0	2.154e+01
9	1.052e+05	5.282e+04	2.536e+03	6.810e+01	200.0	4.641e+01
10	1.307e+05	5.694e+04	1.426e+03	7.440e+01	200.0	1.000e+02

Table 32. Dynamic frequency sweep data for pure PP at 200°C.

NO.	G′ (Pa)	G″ (Pa)	ETA* (Pa.s)	TORQUE (g.cm)	TEMP (°C)	FREQ (rad/s)
			Table 33. Dynamic frequency sweep data for pure PP at 240°C.			

NO.	G′ (Pa)	G″ (Pa)	ETA* (Pa.s)	TORQUE (g.cm)	TEMP (°C)	FREQ (rad/s)
1	8.013e+02	2.401e+03	2.531e+04	7.912e+00	239.3	1.000e-01
2	1.280e+03	3.360e+03	2.269e+04	1.124e+01	239.6	1.585e-01
3	2.061e+03	4.651e+03	2.025e+04	1.589e+01	239.7	2.512e-01
4	3.204e+03	6.334e+03	1.783e+04	2.216e+01	239.6	3.981e-01
5	4.863e+03	8.437e+03	1.543e+04	3.037e+01	239.5	6.310e-01
6	7.151e+03	1.105e+04	1.316e+04	4.100e+01	239.6	1.000e+00
7	1.034e+04	1.408e+04	1.102e+04	5.430e+01	239.6	1.585e+00
8	1.450e+04	1.758e+04	9.073e+03	7.071e+01	239.5	2.512e+00
9	1.983e+04	2.147e+04	7.341e+03	9.043e+01	239.6	3.981e+00
10	2.648e+04	2.566e+04	5.843e+03	1.137e+02	239.6	6.310e+00
11	3.447e+04	3.004e+04	4.572e+03	1.405e+02	239.6	1.000e+01
12	4.384e+04	3.444e+04	3.517e+03	1.705e+02	239.6	1.585e+01
13	5.462e+04	3.880e+04	2.667e+03	2.037e+02	239.6	2.512e+01
14	6.665e+04	4.293e+04	1.991e+03	2.384e+02	239.5	3.981e+01
15	7.963e+04	4.663e+04	1.462e+03	2.713e+02	239.5	6.310e+01
16	9.297e+04	4.960e+04	1.054e+03	2.952e+02	239.6	1.000e+02

Table 33. Dynamic frequency sweep data for pure PP at 240°C.

NO.	G′ (Pa)	G″ (Pa)	ETA* (Pa.s)	TORQUE (g.cm)	TEMP (°C)	FREQ (rad/s)
1	5.036e+02	1.794e+03	1.863e+04	5.826e+00	258.9	1.000e-01
2	8.552e+02	2.521e+03	1.680e+04	8.322e+00	259.2	1.585e-01
3	1.374e+03	3.535e+03	1.510e+04	1.185e+01	259.2	2.512e-01
4	2.185e+03	4.880e+03	1.343e+04	1.670e+01	259.2	3.981e-01
5	3.417e+03	6.620e+03	1.181e+04	2.325e+01	259.3	6.310e-01
6	5.141e+03	8.808e+03	1.020e+04	3.180e+01	259.4	1.000e+00
7	7.602e+03	1.143e+04	8.659e+03	4.273e+01	259.4	1.585e+00
8	1.088e+04	1.453e+04	7.227e+03	5.644e+01	259.3	2.512e+00
9	1.519e+04	1.805e+04	5.924e+03	7.318e+01	259.3	3.981e+00
10	2.070e+04	2.198e+04	4.785e+03	9.343e+01	259.3	6.310e+00
11	2.749e+04	2.617e+04	3.795e+03	1.171e+02	259.3	1.000e+01
12	3.561e+04	3.053e+04	2.959e+03	1.442e+02	259.3	1.585e+01
13	4.511e+04	3.494e+04	2.272e+03	1.744e+02	259.4	2.512e+01
14	5.593e+04	3.925e+04	1.716e+03	2.068e+02	259.4	3.981e+01
15	6.788e+04	4.328e+04	1.276e+03	2.384e+02	259.4	6.310e+01
16	8.028e+04	4.660e+04	9.282e+02	2.624e+02	259.4	1.000e+02

Table 34.   Dynamic frequency sweep data for pure PP at 260°C.

Vita

The author was born in Surat, India on August 22, 1962. He moved with his family to Bombay in 1969 and completed his schooling at the Greenlawns High School in 1979. He then completed his H.S.C. in Science from K.C. College in Bombay in 1981. Having wanted to be a chemical engineer ever since his childhood days, he joined the Maharaja Sayajirao University of Baroda, Baroda in August, 1981. He graduated with a B.E. degree in chemical engineering in December, 1985. He started his M.S. in chemical engineering at the University of Louisville, KY in January of 1986 and graduated in July, 1987. In August, 1987 he began his Ph.D. at Virginia Tech under the guidance of Prof. D.G. Baird and graduated in April, 1991. In March of 1991 he was offered, and accepted, a research engineer's position with Philips Petroleum Company in Bartlesville, OK.